Vaporisation and Thermodynamic studies on systems of relevance to nuclear technology

By

P. MANIKANDAN

(Enrolment No: CHEM02200904003)

Indira Gandhi Centre for Atomic Research, Kalpakkam

A thesis submitted to the

Board of Studies in Chemical Sciences

In partial fulfillment of requirements

for the Degree of

DOCTOR OF PHILOSOPHY

of

HOMI BHABHA NATIONAL INSTITUTE

Aug, 2017

Homi Bhabha National Institute

Recommendations of the Viva Voce Committee

As members of the Viva Voce Committee, we certify that we have read the dissertation prepared by P. Manikandan entitled 'Vaporisation and Thermodynamic studies on systems of relevance to nuclear technology' and recommend that it may be accepted as fulfilling the thesis requirement for the award of Degree of Doctor of Philosophy.

Chairman - Dr. K.Ananthasivan	Date: 6/4/18
Guide / Convener - Dr. M.Joseph	Date: 6/4/18
Examiner	Date: 6.4.2018
Member 1- Dr. Lakshmi Narasimhan	Date: 06/04/18
Member 2- Dr.D. Ponraju	Date: 6/4/2018

Final approval and acceptance of this thesis is contingent upon the candidate's submission of the final copies of the thesis to HBNI.

I/We hereby certify that I/we have read this thesis prepared under my/our direction and recommend that it may be accepted as fulfilling the thesis requirement.

Date: 6/4/2018

Place: Kalpakkam

Guide

STATEMENT BY AUTHOR

This dissertation has been submitted in partial fulfillment of requirements for an advanced degree at Homi Bhabha National Institute (HBNI) and is deposited in the Library to be made available to borrowers under rules of the HBNI.

Brief quotations from this dissertation are allowable without special permission, provided that accurate acknowledgement of source is made. Requests for permission for extended quotation from or reproduction of this manuscript in whole or in part may be granted by the Competent Authority of HBNI when in his or her judgment the proposed use of the material is in the interests of scholarship. In all other instances, however, permission must be obtained from the author.

P. Manikandan

DECLARATION

I, hereby declare that the investigation presented in the thesis has been carried out by me. The work is original and has not been submitted earlier as a whole or in part for a degree / diploma at this or any other Institution / University.

P. Manikandan

Publications in refereed journals

a. Published:

1. "High Temperature Mass Spectrometric studies on U-Ga system: Thermodynamic properties over (U_3Ga_5+UGa_2) and (UGa_2+UGa_3) phase regions", **P. Manikandan**, V. V. Trinadh, Suranjan bera,T.S. Lakshmi Narasimhan, M. Joseph**,** J. Nucl. Mater. 475 (2016) 87.
2. "Thermodynamic data of U_3Ga_5(s) from calorimetric measurements", **P. Manikandan**, R. Kandan, T. S. Lakshmi Narasimhan, B. Prabhakara Reddy, M. Joseph, J. Therm. Anal. Calorim, 129 (2017) 241.
3. "The Design, Construction, and Testing of a Knudsen Effusion Mass Spectrometric System Suitable for Studies of Nuclear Fuel Materials", D. Darwin Albert Raj, R. Viswanathan, and **P. Manikandan,** The Electrochemical Society Transactions, 46(1) (2013) 77-97.
4. A vporisation study of Ru-Te binary system by Knudsen effusion mass spectrometry, T.S.Lakshmi Narasimhan, R.Balasubramanian, **P. Manikandan**, R. Viswanathan, J.Alloys.Comp, 581(2013) 435-445.

b. Proceeding and presentation at national/international conference:

1. **"**Recommissioning of the high temperature mass spectrometric facility with a new QMS", D. Darwin Albert Raj, **P. Manikandan**, R. Viswanathan, presented at Eleventh ISMAS Triennial International Conference on Mass Spectrometry - TRICON 2009**,** Hyderabad, Nov 24-28, 2009, PP. 380-382
2. "Vaporisation Studies on MnO(s) by High Temperature Mass Spectrometry", **P. Manikandan**, R. Viswanathan, T.S.Lakshmi Narasimhan and D. Darwin Albert Raj, presented at International Conference on Vistas in Chemistry, ICVC-2011, P-224
3. "High Temperature Mass Spectrometric Studies on U-Ga system", **P. Manikandan**,

T. S.Lakshmi Narasimhan, M. Joseph, K. Nagarajan, presented at Thermans-2013 held at BARC, Mumbai

4. “Vaporisation studies on U-Pu-Zr”, **P. Manikandan,** V. V. Trinadh, T. S. Lakshmi Narasimhan and M. Joseph, presented at theme meeting (CHEMNUT) held at IGCAR, Kalpakkam. (July 30-31,2015)

5. ”Thermodynamic data of U_3Ga_5 from calorimetric measurements”, **P. Manikandan**, R. Kandan, B. Prabhakara Reddy, T. S. Lakshmi Narasimhan, M. Joseph, presented at NUCAR-17, 2017 held at KIIT University, Bhubaneswar.

6. “High Temperature Mass Spectrometric Studies on U-19Pu-6Zr”, **P. Manikandan**, V. V. Trinadh, M. Prasad, T. S. Lakshmi Narasimhan, M. Joseph, presented at ISMC-2016 held at BARC, Mumbai

Contents

DEDICATION

Dedicated to my mother tongue, TAMIL and Mr. K. KAMARAJ (Indian freedom fighter, former Tamilnadu Chief Minister and my inspiration)

ACKNOWLEDGEMENTS

I am highly indebted to Dr. M. Joseph, my guide for each and every help provided by him during my Ph.D period as well as during the preparation of the dissertation. I am extremely thankful to Dr. T.S. Lakshmi Narasimhan, one of the members of my doctoral committee (dc) for his immense support during my Ph.D period. I am deeply grateful to Dr. D. Darwin albert raj, my former colleague for having taught me the operation of the KEMS instrument and having shared some fruitful discussions with me. I thank my present and former doctoral committee chairmans, namely, Dr. K. Ananthasivan and Dr. T.G. Srinivasan & Dr. K. Nagarajan, respectively, for their valuable suggestions during the dc meetings. I thank Dr. C. Mallika (my former dc member) for having given some valuable suggestions during the dc meetings and my other present member, Dr. D.Ponraju. I express my heartfelt thanks to Mr. V.V. Trinadh, my colleague, for having helped me enormously in Knudsen effusion mass spectrometric measurements on U-Ga and U-Pu-Zr systems. His help is timely and of great worth in nature as far as my Ph.D is concerned. I express my sincere and heartfelt gratitude to Dr.R. Kandan for having helped me in the determination of enthalpy increments on a U-Ga intermetallic compound and the preparation of the manuscript for that work.

I express my sincere thanks to Dr. Rajesh ganesan, Dr. G. Panneerselvam, Dr. K. Chandran, Mr. S. Nedumaran, Mr. S. Shyam kumar, Mr. R. Raja madhavan, Mr. Sanjay kumar parida and T. Muthu ambika for their valuable help in preparation and characterisation of the U-Ga samples. These people's contribution is hugely valuable to my Ph.D studies. I thank my colleague, Mrs. S. Nalini for having given me the motivation whenever required and other colleague, Mr. S. Suranjan bera for having given some valuable suggestions. I thank Dr. S. Balakrishnan also for having given me the motivation.

Ultimately I thank my wife (M. Mari selvi) and my daughter (M. Arthi) for having helped me personally during my Ph.D period. **It will not look good if I thank my mother, who is everything to me. My thanks are of no value in front of her. What I am today is entirely due to my mother.**

SYNOPSIS

Per capita energy consumption is an index of standard of living. Various means of energy production are available. Some of the energy generating methods like fossil fuel burning results in release of huge amounts of carbon dioxide, a potential green house gas, thereby, leading to global warming. Nuclear energy, which is devoid of emission of any green house gas, is considered to be the best alternative for producing the electricity. At present, in India, the share of electricity generated through nuclear energy amounts to ~ 3%. India has limited reserves of uranium whereas thorium is abundantly available. Hence, India follows a three stage program proposed by H.J. Bhabha, the pioneer of Indian atomic energy program [1]. Accordingly, our county has embraced a closed fuel cycle to effectively utilise limited uranium reserves and abundant thorium resources. In the three stage nuclear program, the first stage reactors uses natural uranium dioxide as the fuel (Pressurised Heavy Water Reactor) or uranium dioxide enriched in U-235 to the extent of ~2-3% (Pressurised Water Reactor and Boiling Water Reactors). In addition to the generation of electricity, U-238 is transmuted into Pu-239, which is a man made and highly useful fissile element. The second stage reactor employs this ^{239}Pu based systems (uranium plutonium mixed oxide or carbide or nitride or alloy with zirconium) as the fuel in the Fast Breeder Reactors (FBRs). Thorium dioxide kept in the blanket, upon capture of the escaping neutrons, transforms into ^{233}U, another man made fissile nucleus. The third stage reactor (Advanced Heavy Water Reactor) uses (^{233}U-Th) or (Pu-Th) mixed oxide as the fuel. This stage requires a small fraction of fissile nuclei (^{233}U or ^{239}Pu) to start the fission as thorium is a non-fissile element.

India follows PUREX (Plutonium Uranium REdox Extraction), a well established aqueous process for reprocessing the spent fuel discharged from the reactors. Tri n-butyl

phosphate (TBP) is employed as the extractant for extracting uranium and plutonium (by forming the complexes with their nitrates) from the dissolver solution prepared by dissolving the spent fuel in Conc. HNO_3. For future Indian fast reactors, U-Pu-Zr alloy has been envisaged to be the driver fuel due to high breeding ratio and shorter doubling time. Plutonium in the alloy fuel to be used in fast reactors will range upto 20 wt.% and this fuel will undergo high burn up. The fuel irradiated to high burnup is an intense source of radiation. In order to multiply the fissile value rapidly, the out of pile storage of the spent fuel should be kept as minimum as possible. TBP used in aqueous process is prone to decomposition by radiation, whereas the chloride salts in molten medium are used as the solvent in non-aqueous process such as electrorefining to separate uranium and plutonium from the spent fuel. These salts possess high temperature and radiation stabilities. This non-aqueous process is capable of handling highly irradiated and short cooled fuels. The spent molten salt remnant after the electrorefining contains valuable actinides. This is treated with suitable non-aqueous solvents to recover the actinides.

The present thesis describes the commissioning of an active Knudsen effusion Mass Spectrometer (KEMS) inside an inert atmosphere glove box and the thermochemical studies carried out on U-Ga and U-Pu-Zr systems using the same. Similar KEMS studies done on Ru-Te system (employing an earlier existing facility) and the enthalpy increment measurements carried out on U_3Ga_5 using an inverse drop calorimeter are also discussed.

The thesis is divided into six chapters. A brief description of the chapters is given below:

Chapter 1: Introduction

This introduction chapter discusses about the nuclear energy as the alternative to meet the rising energy demand of our country. It gives a brief account of various types of nuclear reactors, nuclear fuels employed in them and various methods of reprocessing of spent fuel. The literature

survey of the systems (U-Ga, U-Pu-Zr and Ru-Te) investigated in the present study is also covered in this chapter. Thermodynamic properties of U-Pu-Zr system are important to understand the fuel behaviour during the irradiation under normal and off-normal conditions ; that of Ru-Te is required to understand the interaction among these fission products; whereas those of intermetallic compounds of U-Ga system is of interest for the separation of uranium from spent molten (chloride) salt obtained from electrorefining

Chapter 2: Measurement of vapour pressure and derivation of thermodynamic properties

This chapter gives a brief account of experimental methods. This chapter is divided into two sections. In the first section, various methods of vapour pressure measurements are discussed. Essentially, KEMS method is explained elaborately. The second section deals with the calorimetric and EMF methods. It gives a special emphasis on the drop calorimetric method. In the present study, the Knudsen effusion mass spectrometry (KEMS) also known as High temperature mass spectrometry (HTMS) was employed to generate the data like vapour pressure, the Gibbs energy of formation and the enthalpy of formation. Then the inverse drop calorimetric method was employed to measure the enthalpy increments of $U_3Ga_5(s)$, one of the intermetallic compounds of U-Ga system.

Chapter 3: Commissioning of Knudsen Effusion Mass Spectrometer (KEMS) inside the glove box

This chapter discusses about the exploratory experiments carried out with Knudsen effusion mass spectrometer (Quadrupole Mass Spectrometer [QMS] supplied by M/S Hiden Analyticals, UK) erected inside the glove box and commissioning of high purity inert atmosphere glove box towards carrying out high temperature mass spectrometric studies on U-Pu-Zr alloys. KEMS housed inside the glove box consists of two chambers positioned one over another. The bottom

chamber is called the cell chamber, since the Knudsen cell furnace assembly is kept inside this chamber. It is used for heating the sample taken in a Knudsen cell fitted with a lid having a tiny orifice parallel to the axis of the cell. The cell is placed inside an outer cup made of tantalum closed with tantalum lid. The outer cup is heated by bombarding it with the electrons released from the two filaments, one of which is located just below the top of the outer cup lid and other one lies just above the bottom of the cup. The sample was heated by electron bombardment. The cup is provided with a black body hole at the bottom. The temperatures are measured by the disappearing filament pyrometer focused onto the hole at the bottom of the cup. The equilibrium vapour established over the sample inside the cell effuses through the orifice. The upper chamber is the source chamber, which houses the QMS, to analyse the molecular beam reaching the ion source. The ion source entrance orifice is located parallel to the axis of the orifice. The vapour species in the molecular beam arriving at the ion source are ionised by electrons of suitable energy. The positive ions produced are mass analysed by QMS. The ions emerging out of the MS are detected by Secondary Electron Multiplier (SEM) operating in pulse mode. A mechanical shutter located inside the source chamber just above the ion source entrance orifice is used to discriminate the ions formed from the molecular beam from those produced from the residual gases in the ion source region. In the shutter open condition (when the shutter is pulled out), the total ion intensity (sample vapour + residual gases) is recorded whereas in the shutter closed conditions (when the shutter is pushed in) the ion intensity due to residual gases is measured. Net ion intensity corresponds to the ion intensity due to the sample vapour.

Preliminary vaporisation studies were carried out with the elements, namely, Cr, Ni and Zr to test the reliability of the instrument. These experiments generally helped us to know the sensitivity of the KEMS and to examine whether the enthalpies of sublimation or vaporisation of

these elements derived experimentally are in agreement with those reported in the literature and whether the instrument is capable of providing the temperature independent pressure calibration constant values. Subsequently, KEMS studies on Fe-40 at.% Al were taken up. Dr. Darwin [2] had previously measured and reported $I(Al^+)/I(Fe^+)$ using an Extrel QMS which, on becoming defective, was replaced by a QMS from M/s Hiden Analyticals, UK. The above experiment was carried out by Darwin [2] to address the discrepancy between the isotope composition of xenon obtained using Extrel QMS and that obtained employing the Micromass 30 BK magnetic sector mass spectrometer available in our lab. Having an apprehension that the mass dependent transmission of the QMS may influence the vaporisation results, he had carried out the vaporisation studies on the above alloy and found out that the ratio $I(Al^+)/I(Fe^+)$ obtained using Extrel QMS was in agreement with the literature data. Similar type of experiment using QMS from M/S Hiden Analyticals, UK was carried out in the present work and good agreement was found between the ratio reported by Darwin and present data. The results indicated that this HTMS facility is well suited to conduct the vaporisation studies on such metal alloy system. These were followed by the KEMS investigation on MnO, a congruently vaporising system, the aim was to gain experience with an oxide system. A question arose about the congruently vaporising nature of MnO(s) when the partial pressure data for MnO(g), Mn(g) and O_2(g) reported by Matraszek et al. [3] were analysed by us. The values of O-Mn ratio calculated using these data were found to be not close to one, a necessary condition for congruent vaporsiation. Four different Knudsen cell combinations were used to contain the sample, each placed in a tantalum outer cup and heated by electron bombardment. Totally, four series of vaporisation experiments were performed with the sample contained in an alumina Knudsen cell (series 1), in an alumina cell with a platinum liner (series 2), in a Platinum Knudsen cell (series 3) and in a

tantalum Knudsen cell (series 4). In the first three series of experiments, O_2^+ was the principal shutterable ion to begin with, as the samples were heated from room temperature, but its variation with time as well as temperature was different in each series. This was the case with other ions Mn^+ and MnO^+ as well. During the first series of experiments, O_2^+ disappeared completely at temperature above 1700 K. In the second series of experiments conducted with platinum liner, O_2^+ intensity did not disappear even at temperature above 1700 K. Inference from series 2 was that, while the Pt liner did help in prevention of disappearance of O_2^+ and also of reaction with alumina crucible, the orifice clogging did occur which was attributed to reaction of the condensate (or its liquid form) with alumina lid. In third series, a platinum Knudsen cell was used and the results that decrease in O-Mn ratio with time indicated the movement of composition towards congruent vaporisation. The rate of movement of O/Mn ratio towards congruency seems to be very slow. It may require a lot of time for the sample to achieve the congruency. In this series of experiments, the orifice was not clogged. But, the platinum Knudsen cell got welded to the tantalum outer cup lid. Hence, the sample could not be retrieved out of the cell for visual examination or analysis. It was clear that further experiments would require use of an appropriate strategy, which will help prevent loss of Knudsen cell or the outer cup, which will permit XRD analysis of the vaporisation residue. In the fourth series, Mn^+ was observed whereas $O2^+$ was not observed. This observation was opposite to what was seen in other cases. Hence the experiment was discontinued. Due to multiple problems, the vaporsiation studies on MnO were not pursued further. Subsequently, the vaporsiation studies on U and U-Zr were taken up to have some experience of KEMS measurements on these alloys before taking up the studies on U-Pu-Zr alloy. These systems are known to be reactive with moisture and oxygen in the atmosphere. Even though the extreme care was taken to avoid the oxidation while handling

them, their oxidation could not be avoided. In the case of uranium, it passed into the two phase region of (U-O)(l) and UO_{2-x}(s). U^+, UO^+ and UO_2^+ were ionic species observed in the mass spectrum of equilibrium vapour of uranium (oxidized) and the appearance potential measurements of these ions indicated that the corresponding neutral precursors were U(g), UO(g) and UO_2(g). Four runs of temperature dependence of ion intensities of these ions were carried out in the temperature range 1756-2018 K using electron energy of 10 eV. The mean enthalpies of vaporisation of these species were found to be in agreement with the literature values for this two phase field. U^+ and UO^+ were ionic species observed in the mass spectrum of equilibrium vapour of U-Zr system (oxidized) and the appearance potential measurements on these ions indicated that the corresponding neutral precursors were U(g) and UO(g). Six runs of temperature dependence of ion intensities of these ions were carried out in the temperature range 1645-1840 K using electron energy of 10 eV. The mean enthalpy of vaporisation of U^+ over this alloy was closer to that over the uranium system whereas that of UO^+ were very much lower than that for UO^+ over the uranium system. All the above experiments were performed under the glove box open condition. Subsequently, the box was closed with the glass panels and full arm gauntlets. U-Pu-Zr alloy are oxygen and moisture sensitive and radioactive. Hence, high purity inert atmosphere (argon) glove box is necessary for carrying out the vaporisation studies on these air sensitive and radioactive samples. The leak tightness of the box is an important parameter to certify it to take up the investigation on these kinds of samples. There is a possibility that air can enter into the box across many joints in the box and can contaminate the argon gas. If the box can be maintained as much leaktight as possible, such leak can be minimised. The leak rate of the box was evaluated by keeping it at a differential pressure of 100 mm WC (water column) negative with respect to the ambient and monitoring the pressure variation for 24 hours. It was

found to be less than 0.05 % of box volume per hour, which is the stipulated limit for a leaktight glove box. All inlets and outlets of the box were fitted with High Efficeincy Particulate Air (HEPA) filters and their trap efficiency was found out by generating the aerosols and counting the number of particles before and after the filters. They were found to be ≥99.9% efficient for the particles of 3 microns size. The impurities in argon, namely, oxygen and moisture are maintained at less than 10 ppm by recirculating it through the purification tower packed with molecular sieves and copper deoxo catalyst, which trap moisture and oxygen, respectively.

Chapter 4:

This chapter contains two parts. Part 1 deals with the high temperature mass spectrometric studies on U-Ga system whereas Part 2 discusses about the high temperature calorimetric studies on U_3Ga_5, one of the intermetallic compounds in U-Ga system.

Part 1: High Temperature Mass Spectrometric studies on U-Ga system: Thermodynamic properties over (U_3Ga_5+UGa_2) and (UGa_2+UGa_3) phase regions

Thermodynamic properties of intermetallic compounds of U-Ga system is of importance to separate uranium from the spent molten chloride salt containing it, which results from the electrorefining process. The spent molten salt consisting of uranium is equilibrated with liquid Ca-Ga alloy for the recovery of uranium. During this process, Ca, acting as a reducing agent, reduces uranium trichloride in the spent salt to uranium, which combines with gallium to form different uranium gallium intermetallic compounds and pushes the reaction in the forward direction. Thermodynamic properties of these compounds are of interest for the separation of uranium from spent molten salt.

In the present study, the high temperature mass spectrometric studies was carried out on (U_3Ga_5+UGa_2) and (UGa_2+UGa_3) two phase regions using the KEMS facility inside the glove

box. In the case of (U_3Ga_5+UGa_2) two phase region, the vaporisation studies were performed on the compositions 63 and 64 at.% Ga in the temperature range 1208-1366 K whereas in the case of (UGa_2+UGa_3) two phase region, the studies were conducted on the compositions 71 and 73 at.% Ga in the temperature range 1133-1338 K. Ga^+ was the ion observed in the mass spectrum of equilibrium vapour over both two phase regions. Ga(g) was identified to be the neutral precursor based on mass, isotopic abundance and appearance potential of the ion. Temperature dependence of ion intensity of Ga^+ was carried out with repect to the major isotope, ^{69}Ga. The measured ion intensity was converted to the partial pressure of Ga by using the pressure calibration constant obtained by using pure gallium. Logarithm values of partial pressure data obtained over the above mentioned two phase regions were plotted against the reciprocal of temperature to get the partial pressure-temperature relations and are given below:

$$\log (p_{Ga}/Pa) = (-18216 \pm 239)/(T/K)) + (12.88 \pm 0.18) \text{ [1208-1366K] for } (U_3Ga_5+UGa_2) \quad (1)$$

$$\log (p_{Ga}/Pa) = (-16225 \pm 124)/(T/K)) + (11.78 \pm 0.10) \text{ [1133-1338 K] for } (UGa_2+UGa_3) \quad (2)$$

The reactions corresponding to the above two relations are :

$$3UGa_2(s) = U_3Ga_5(s) + Ga(g) \quad (3)$$

$$UGa_3(s) = UGa_2(s) + Ga(g) \quad (4)$$

The Gibbs energies of formation of U_3Ga_5 and UGa_3 were obtained by using those of UGa_2 and Ga(g) and are given below:

$$\Delta_f G_T^o \, U_3Ga_5(s) \, (\pm 5.5) = -352.4 + 0.133 \, T(K) \text{ (kJ mol}^{-1}) \quad (5)$$

$$\Delta_f G_T^o \, UGa_3(s) \, (\pm 3.8) = -191.9 + 0.082 \, T \, (K) \text{ (kJ mol}^{-1}) \quad (6)$$

The reference states of uranium and gallium in the above two relations are γ-uranium and Ga(l). The enthalpies of reactions (3) and (4) were derived from the slopes of the the equations (1) and (2). They are 353.9 ± 6.8 kJ mol^{-1} at 1287 K and 312.7 ± 5.9 kJ mol^{-1} at 1236 K.The heat capacity

data are not available for U-Ga intermetallic compounds. Hence, the enthalpies of reactions could not be made use of to derive the enthalpies of formation of the compounds. In the case of UGa_3, the enthalpy of formation of UGa_3(s) available in the literature [4] was used along with that at 1236 K from the present study [intercept of the equation (6)] to deduce the temperature dependence relation of the enthalpy of formation by following the approach suggested by Chiotti et al. [5]. The relation is given below:

$$\Delta_f H_T^o\ (\pm 18.01) = -140.9 - 0.0412\ \mathrm{T(K)\ kJ\ mol^{-1}}\ (298.15 - 1236\ \mathrm{K}) \qquad (7)$$

Part 2: Thermodynamic data of U_3Ga_5 from calorimetric measurements

The inverse drop calorimeter was used to determine the enthalpy increments of U_3Ga_5. For the measurements, five pairs each of sample and standard (α-Al_2O_3, SRM 720, supplied by NIST, USA), each weighing about 100 mg, were dropped alternately into the sample crucible maintained at the experimental temperature. From the relative values of heat flow measured in the case of standard and sample and the known enthalpy increment data of the standard, the enthalpy increment, $H_T^0 - H_{298}^0$ of the sample was calculated. The mean of the five heat flow values for the standard and that of the sample were used to compute the enthalpy increment at that temperature. These measurements were also repeated two times at the same temperature to confirm the reproducibility of the data. For each temperature, a heat flow *(Q)* versus time (*t)* curve is obtained and subsequently the area under it was calculated. This area is proportional to the enthalpy increment of the sample dropped from room temperature to the furnace temperature. The enthalpy increment values thus obtained at different temperatures were fitted by the weighted least-squares method to obtain a non-linear expression in temperature. During the experiments, to prevent the oxidation of the U_3Ga_5 alloy samples, high pure argon gas was continuously flown over the sample.

The enthalpy increment measurements were carried out in the temperature range 793-1323 K. The measured enthalpy increments were fitted to the polynomials in temperature by using the least-squares method and the resulting expression is given below (in the temperature from 298-1400 K).

$$H_T^0 - H_{298}^0 \,/\, \text{J mol}^{-1} = 168.631T + 52.677\times10^{-3}T^2 - 12.177\times10^5 T^{-1} - 50876 \qquad (8)$$

Heat capacity was obtained by differentiating the equation (8) with respect to temperature and is given below.

$$C_p^0 \,/\text{J. mol}^{-1}\text{K}^{-1} = 168.631 + 105.364\times10^{-3}\,\text{T} + 12.177\times10^5\text{T}^{-2} \qquad (9)$$

The heat capacity determined was used to derive the enthalpy of formation of U_3Ga_5 at 298 K from that at 1287 K (intercept of the equation (5)). The value of the enthalpy of formation at 298 K thus derived is 311.3 ± 5.5 kJ mol^{-1}.

Chapter 5:

This chapter is divided into two parts. Part 1 discusses about the vaporisation studies on U-Pu-Zr alloy using the HTMS facility housed inside the glove box. Part 2 gives an account of vaporisation studies on Ru-Te system.

Part 1: Mass Spectrometric Studies on U-Pu-Zr alloy

In the case of U-Pu-Zr alloy, the high temperature mass spectrometric studies on U-18wt.%Pu-5.8 wt.%, (the nominal composition of the alloy proposed for the future Indian fast reactors is U-19wt.%Pu-6 wt.%, but the actual composition measured for the present sample was U-18wt.%Pu-5.8 wt.% [6]) were carried out over the (solid+liquid) two phase and liquid regions in the temperature ranges, 1481-1623 K and 1661-1773 K, respectively. Pu^+ and PuO^+ were the ionic species observed in the mass spectrum of the equilibrium vapour over the alloy. PuO^+ ion intensity decreased with time as the sample was heated further. From the mass, isotopic

abundance and the appearance potential, Pu(g) was established to be the neutral precursor. The measured ion intensity of Pu^+ was converted to partial pressure by using the pressure calibration constant derived from the calibration experiment with silver. Logartithmic values of partial pressures of Pu(g) were plotted against the reciprocal of temperature to get the partial pressure-temperature relations. The partial pressure–temperature relations obtained for (solid+liquid) and liquid are given below:

$\log(p_{Pu}/Pa) = -(22254 \pm 282)/T + 10.80 \pm 0.18$ for (solid+liquid) (1481-1623 K) (10)

$\log(p_{Pu}/Pa) = -(22021 \pm 1169)/T + 10.52 \pm 0.68$ for (liquid) (1661-1763 K) (11)

The apparent mean enthalpies of vaporisation of Pu(g) over (solid+liquid) and liquid regions at the mean temperature of investigation were deduced as 423.9 ± 10.2 (at 1552 K) and 425.9±12.8 (at 1712 K) kJ/mol, respectively**.** Partial pressures of Pu(g) calculated from the recommended equations over the (solid+liquid) and liquid regions at the mean temperature were 2.9×10^{-4} (1552 K) and 4.5×10^{-3} Pa (1712 K), respectively. From the measured partial pressures of Pu(g) over the alloy and that over pure Pu from literature [7], the activities of plutonium over the above phase regions were deduced as 0.03 (1552 K) and 0.05 (1712 K) respectively, indicating negative deviation from Raoult's law. In addition, the computation was performed using partial pressure data reported for uranium over U-Zr [8] and that of plutonium over Pu-Zr [9] reported in the literature, to obtain the partial pressures of uranium and plutonium for over the U-Pu-Zr alloy. The equations for activity coefficients of uranium, plutonium and zirconium given by Leibowitz et al. [10] were used to calculate their partial pressures. The above two set of values were compared with that obtained experimentally.

Part 2: Vaporisation study of the Ru-Te binary system by Knudsen effusion mass spectrometry

Ruthenium is an important fission product with significant fission yield in fast reactor for nuclear reactor safety studies [11]. The fission yields of Ru in the fast fissions of ^{235}U and ^{239}Pu are 11.8% and 23.1%, respectively and its compounds with tellurium (fission yields of Te in fast fissions of ^{239}Pu and ^{235}U : 1 at. % each) may play an important role in nuclear reactor safety studies [11]. The KEMS studies on Ru-Te system was carried out to understand the fission product-fission product interaction. The vaporisation experiments were carried out by using a VG micromass 30 BK Knudsen effusion mass spectrometer. Alumina Knudsen cells having a knife edged orifice of ≈ 0.5 mm diameter were used to contain the samples. The Knudsen cell was kept inside an outer molybdenum cup and closed with a tight-fitting lid made of tungsten and having a 3 mm diameter circular hole collinear with the Knudsen cell orifice. Heating of this whole unit ('K-cell furnace') was done by radiation and electron bombardment (EB) from two independent tungsten filaments that encircled it, one just below the top of the W lid, and the other just above the base of the Mo cup. Radiation shields, made of tantalum, were placed all around the filaments (as well as at the top and bottom) which aided the temperature stability of the K-cell furnace. The temperatures were measured by a chromel-alumel thermocouple (stainless steel sheathed) inserted through the bottom of the molybdenum cup and touching the base of the Knudsen cell. A temperature regulation of ± 1 °C could be achieved by using the provision of "thermocouple control mode", available in the EB power supply. The molecular beam effusing out of the Knudsen cell was ionized by impact of electrons emitted from a heated tungsten filament present in the ionizer of the mass spectrometer. The ions produced were accelerated to 6 kV, mass separated by a 90^{o} sector magnetic analyser, and detected by a secondary electron multiplier.

High temperature mass spectrometric measurements were conducted on the compositions, 40.0, 50.5, 69.5, and 71.5 at. % Te (referred to as S1, S2, S3, and S4, respectively). Aliquots from S1 and S2 were used for vapor pressure measurements as a function of temperature while those from S3 and S4 were used for long vaporisation experiments, isothermal at most parts, to deduce the phase boundaries of $RuTe_2$. Te^+ and Te_2^+ are the ions observed in the mass spectrum of the equilibrium vapor over (Ru + $RuTe_2$). Te(g) and Te_2(g) were ascertained to be neutral precursors of the ions based on the masses, the isotopic abundances and appearance potentials. The partial pressure-temperature relations for Te^+ and Te_2^+ were determined in the temperature range of 860 to 1030 K. The recommended p-T relation obtained by pooling together all $p(Te_2)$ values is:

$$\log [p(Te_2)/Pa] = [-(14335 \pm 148)/(T/K)] + (14.416 \pm 0.154) \quad (12)$$

The recommended *p-T* relation for Te(g) is

$$\log [p(Te)/Pa] = [-(13838 \pm 218)/(T/K)] + (12.480 \pm 0.226) \quad (13)$$

The enthalpy of formation of $RuTe_2$ was derived from the partial pressure-temperature relations for Te_2(g) using second and third law methods and is given below:

$$\Delta_f H^o_m(RuTe_2, s, 298.15\ K)/(kJ \cdot mol^{-1}) = -(121.1 \pm 16.4) \quad (14)$$

In the evaluation of reaction enthalpies, it was assumed that the composition of $RuTe_2$ phase in equilibrium with Ru(s) is stoichiometric, that is, the Ru-rich boundary is of composition 66.67 at.% Te. Having measured the homogeneity ranges of many telluride phases previously [12], we have performed similar quantitative vaporisation experiments which essentially involved measurement of $I(Te_2^+)$ all along, with aliquots of samples corresponding to ($RuTe_2$ + Te) of known composition and mass. Initially Knudsen cell with the sample was measured. At the end of the experiment, the Knudsen cell was weighed again to deduce the total mass-loss,

Δm_{total}. Since vaporisation from the Knudsen effusion cell resulted in continuous loss of tellurium as $Te_2(g)$, by making use of Hertz-Knudsen effusion equation and the relation (p=k'*I*T), the calibration constant C_{H-K} was first deduced through which Δm_{total} is related to the total area under the $I(Te_2^+)T^{0.5}$ vs. time, *t* curve:

$$(\Delta m)_t = C_{H-K} \{\Sigma [I(Te_2^+)T^{0.5}]_t \cdot \Delta t\}. \quad (15)$$

Subsequently, by using the C_{H-K} so deduced, Δm up to any desired time *t* was deduced, and in turn the sample composition also at that time of the experiment. Application of phase rule provides the basis of assigning these compositions to the time up to which the elemental tellurium was present as a coexisting phase as well as to the time from which the elemental ruthenium was present as a coexisting phase with $RuTe_2$. The above two compositions are the phase boundaries of the single phase $RuTe_2$. The compositions, 69.5, and 71.5 at. % Te (S3 and S4) were subjected to the above kind of experiments**.** Two lots of sample from each composition were used for the experiments. Te-rich boundary of $RuTe_2$ was determined at 635 and 650 K whereas Ru-rich boundary was determined at 980 K. The observation of the above experiments was that when the starting compositions were more Te-rich, the deduced Te-rich boundary compositions for the $RuTe_2$ phase were found to be more Te-rich (68.71 at.% Te at 650 K (lot 1) and 68.84 at.% Te at 635 K (lot 2) for the starting composition of 69.5 at.% Te ; 70.46 at.% Te (lot 1) and 70.17 at.% Te ((lot 2) for the starting composition of 71.5 at.% Te, respectively). The reason for this is not clear. With the large uncertainty looming on the value of Te-rich boundary, we would give credence only to the Ru-rich boundary values which did not show any particular trend with the starting composition. The observations on Ru-rich boundaries derived from four experiments indicated as follows: 1) the mean value was 66.65 ± 0.37) at. %Te and this corresponds to the nominal formula of (2.00 ± 0.03); 2) the results from

experiments with S1 and S2 evaluated by using the formula $RuTe_2$ did not require modification which would have been necessary if the Ru-rich boundary composition was to be significantly different.

Chapter 6: Conclusion

The reliability of the KEMS facilty erected inside the glove box was understood by carrying out the exploratory experiments with the elements namely, Ni, Cr and Zr. These were followed by the investigation on MnO(s). Subsequently, the vaporisation studies on U and U-Zr were taken up to have some experience of KEMS measurements on these systems prior to taking up the studies on U-Pu-Zr, the driver fuel proposed for future fast breeder reactor in India. The above experiments were conducted under the glove box open conditions. Subsequently, the glove box was closed with the glass panels and full arm gauntlets and few more modifications in the glove box and the necessary tests namely, leak rate testing and HEPA filters trap efficiency testing were carried out and the box was certified to be fit for handling radioactive and air sensitive samples.

The investigation on U-Ga and U-Pu-Zr were carried out using the above HTMS-GB facility. The Gibbs energies of formation of U_3Ga_5 and UGa_3 were determined. The data of U_3Ga_5 was reported for the first time. The enthalpy increment measurements were performed on U_3Ga_5 using an inverse drop calorimeter. These data were used to derive the enthalpy of formation of U_3Ga_5 at 298 K. Vapour pressure data of plutonium over U-18wt.%-5.8wt.% were also determined.

Using another KEMS facility (VG micromass 30 BK), the vaporisation studies on Ru-Te system was conducted. The enthalpy of formation of $RuTe_2$ at 298 K was determined. The phase boundaries of $RuTe_2$ were deduced.

Chapter 7: Scope for further work:

High temperature vaporisation studies on U-Pu-Zr of different compositions can be carried out. These data are of importance to nuclear field for fuel fabrication as well as to understand the fuel behaviour during irradiation under normal and abnormal conditions. The enthalpy increment measurements on UGa_2 and UGa_3 are not available in the literature. These data can be determined by employing the inverse drop calorimeter.

References:

1. Bhabha, H.J., Proc. Internatl. Conf. on the Peaceful uses of Atomic Energy, 1, Geneva, 1955, p-103
2. D. Darwin Albert Raj, Ph.D. Thesis, University of Madras.
3. A. Matraszek, M. Miller, L. Singheiser and K. Hilpert, J. Euro. Ceram. Soc, 24 (2004) 2649.
4. B. Prabhakara Reddy, R. Babu, K. Nagarajan, P.R. VasudevaRao, J. of Alloys and Compds. 271-273 (1998) 395.
5. P. Chiotti and J.A. Kateley, J.Nuc.Mater, 32 (1969) 135.
6. B. Seenivasulu, A. Suresh, N. Sivaraman, M. Joseph, J. Radioanal. Nucl. Chem. 311 (2017) 789.
7. C.B.Alcock, V.P.Itkin and M.K.Horrigan, Can,.Metall.Quart., 23 (1984) 309.
8. M. Kanno, M.Yamawaki, T.Koyama, N. Morika, J. Nuc. Mater. 154 (1988) 154.
9. A.Maeda, Y.Suzuki, Y. Okamoto, Toshihiko Ohmichi, J. Alloys.Compds, 205 (1994) 35.
10. L. Leibowitz, E.Veleckis, R.A. Blomquist, J. Nucl. Mater. 154 (1988) 145.
11. E. H. P. Cordfunke, R. J. M. Konings, E. F. Westrum, Jr., J. Nucl. Mater. 167 (1989) 205.

12. T.S. Lakshmi Narasimhan, R. Viswanathan, Knudsen effusion mass spectrometric study of some congruently and incongruently vaporizing systems, in: Workshop on Knudsen Effusion Mass Spectrometry (KEMS) April 23–25, 2012, Juelich. Proceedings published in ECS Transactions. 46 (1) (2013) 229. Please also see: The Open Thermodynamic Journal 7 (2013) (Suppl 1:M3) 10–20 and the references therein.

List of Figures

List of Tables

CHAPTER 1

Introduction

Energy is indispensable for our life. Per capita energy consumption is considered as an index of standard of living. It is needed for many activities starting from running the domestic electrical appliances to big industries which contribute largely to a nation's gross domestic product (GDP). In a country like ours, the demand for energy is rising steeply with increase in population. Hence, electrical energy needs to be generated out of the various possible sources available in nature. Presently the energy is tapped from different sources such as coal, water, tide, oil, wind, sun light and nuclear fuels. Some forms of energy such as wind energy, tidal energy etc., are seasonal. Hence, they would not be available continuously throughout the year. Energy obtained by burning the coal liberates huge amounts of carbon dioxide to the environment, which is one of the potential green house gases responsible for global warming. This results in many changes such as rise in sea level, acidification of ocean water etc. Also the energy derived from the coal consumes an enormous amount of fuel. Hence, the energy which can be produced from resources which do not release any green house gas is preferred. On this basis, the energy from nuclear fuel is considered to be clean. Nuclear energy results from the splitting (fission) of the nuclei of fissile or fissionable atoms which releases approximately 200 MeV of energy per fission, which is used to produce electricity. The energy produced in a fission event is immense compared to the heat released from the burning of fossil fuels. Since the irradiated nuclear fuel is highly radioactive, it needs to be handled inside the hot cell for reprocessing activities. The fresh nuclear fuel under irradiation is never fully exhausted since the depletion of fissile mass and accumulation of neutron poisons inside the fuel do not allow the chain reaction to continue incessantly. The amount of energy extractable varies from reactor

to reactor depending on the chemical form of the fuel material used and enrichment of the fissile nuclide used in the fuel.

A nuclear reactor comprises a fuel, clad material, coolant and moderator (no moderator is required for a fast reactor). The coolant extracts the heat liberated during the fissions and transfers the same to the secondary coolant (water) which boils and steam turns the turbine and generates electricity.

1.1. Three stage program of India

India follows the three stage nuclear program envisaged by Homi Jehangir Bhabha [1], the pioneer of Indian nuclear energy. In the first stage, uranium dioxide containing natural uranium is irradiated in thermal reactors where U-235 nuclei are fissioned whereas U-238 nucleus is transmuted into Pu-239 by neutron capture followed by successive emission of two beta particles. Plutonium is a manmade and highly useful fissile isotope in fast neutron spectrum. Plutonium bred in thermal reactor is used in the second stage in the form of MOX (uranium-plutonium mixed oxide) or mixed carbide in fast reactors and thorium, which is highly abundant in India, is kept in the blanket. In the fast reactor, the amount of Pu-239 produced from neutron capture of U-238 is more than that consumed in the fission events, resulting in breeding of fuel. The excess plutonium generated during the irradiation in the fast reactor can feed another reactor of the same capacity. Hence the fast reactors are generally called breeders. Uranium plutonium mixed carbide has been successfully irradiated in our Fast Breeder Test Reactor (FBTR) at Kalpakkam, India to higher burnup of 155 GWd/tonne [2]. A prototype fast breeder reactor (PFBR) of 500 MW(e) capacity located at Kalpakkam is expected to attain criticality in the near future. This PFBR uses the conventional mixed oxide as the fuel. For the future Indian fast reactors, uranium-plutonium-zirconium alloy is being considered as the driver fuels. Th-232

present in the blanket subassemblies of fast reactor will capture the neutrons escaping out of the core and get converted to U-233 which is another artificial fissile nucleus. This U-233 will be used in subsequent thermal reactors in the stage three. Since thorium is non-fissile, the fuel based on thorium needs to have other fissile atoms such as U-233, Pu-239 etc in the third stage reactors. U-233 in the form of the mixed oxide $(U,Th)O_2$ and $(Pu,Th)O_2$ will be employed as the fuels. An Advanced Heavy Water Reactor (AHWR) as proposed by Bhabha Atomic Research Centre (BARC) is expected to expedite the transition to thorium-based systems [3], so that we can exploit the most abundant thorium in India**.** The reactor fuelled with mixed oxides of thorium with uranium or plutonium is called thermal breeder since these fuels produce more U-233 nuclides than consumed even in thermal neutron energy spectrum.

1.2. Nuclear energy

Nuclear energy will play a pivotal role in future to narrow down the gap between the supply and demand in electricity which will see a huge leap with growing population in India. Nuclear energy is one of the best avenues for the production of clean energy. Hence nuclear installations will be deployed in large numbers in India to maximise the full potential of nuclear fuels.

1.3. Nuclear reactor

Nuclear reactors can be classified into many types depending on design, fuel material etc. But based on the energy of the neutrons used for fission, reactors are classified as thermal reactors, where the neutron energy is ~ 0.025 eV; and fast reactors in which neutrons possess the energy in the range of 500-600 keV.

1.3.1. Thermal reactors

Generally in thermal reactors, uranium dioxide containing natural uranium (U-235 content: 0.7%) is used as the fuel. The reactors employing such fuels along with heavy water acting as the moderator are called as Pressurised Heavy Water Reactors (PHWR). The reactors using the enriched uranium (U-235 content higher than 0.7%) and light water as both moderator and coolant are called as Pressurised Water Reactor (PWR) and Boiling Water Reactor (BWR). The enrichment of U-235 in the fuels for BWR and PWR ranges from 2 to 3%. The burnup which is a measure of energy derived from a given amount of fuel is about 0.7 at. % in PHWR and about 2-3 at. % in PWR and BWR.

1.3.2. Fast reactors

Since the core size is small for a fast reactor, it needs higher enrichment of fissile isotopes U-235 or Pu-239. Also higher enrichment helps to compensate for low fission cross section at high neutron energies. The oxide fuels $(U,Pu)O_{2-x}$ best known for ease of fabrication, higher thermodynamic stability, high melting point, higher irradiation stability, capability to undergo higher burn up and ease of reprocessing, are used as fast reactor fuels. There are some shortcomings for oxide fuels such as low heavy metal atom density and low thermal conductivity. The lower heavy metal atom density does not act favorably as far as the breeding gain is concerned. Advanced fuels such as mixed carbide (U,Pu)C and mixed nitride (U,Pu)N outweigh the oxide with respect to breeding gain. They also have higher thermal conductivity and higher heavy metal atom density. Since the fast reactors have high power density, the coolant materials to be used should have good heat transfer characteristics. Liquid sodium possessing high thermal conductivity is generally used as the coolant in fast reactor.

1.4. Reprocessing

When the fuel under irradiation can no longer sustain the chain reaction, then it is subjected to reprocessing to recover the valuable actinides. In the case of thermal reactors, reprocessing of spent fuel is entailed by accumulation of fission products, some of which are neutron poison and depletion of fissile nuclei; whereas in fast reactors, generally the clad damage due to higher neutron flux coupled with its higher speed is considered as the main reason for limiting the burnup. The spent fuel is taken out for reprocessing.

1.4.1. Aqueous process

Since India has embraced the 'closed fuel cycle' for effective utilisation of limited uranium resources, it is essential to recover the strategically valuable uranium and plutonium (collectively called as actinides) from the spent fuel (discharged from the reactor). This recovery is done by using a suitable reprocessing method. The actinides recovered from the spent fuel are converted into suitable chemical forms such as oxides, carbides and nitrides depending on the type of fuels needed for other reactors. Generally PUREX (Plutonium Uranium Redox EXtraction) process is adopted for separating the strategically valuable actinides from the spent fuel [4-6]. It is a well established process and widely followed all over the world. The spent fuel is removed from the cladding material by chemical or mechanical method. The spent fuel devoid of the clad is dissolved in concentrated nitric acid and the resulting solution termed as "Dissolver Solution" is adjusted to an acidity of 4 M HNO_3 by dilution. This solution containing uranium, plutonium, fission products, minor actinides and corrosion products is equilibrated with 30%TBP in n-dodecane. Under suitable acidic conditions of the aqueous feed, uranium and plutonium alone are extracted into organic phase. Subsequently uranium and plutonium are stripped out of the organic phase separately by appropriate treatment. The decontamination factor (ratio of β, γ activity/g of U or Pu in feed to that of U or Pu in product) achieved in PUREX process is of the

order of 10^6. This process has certain limitations like criticality while handling the dissolver solution containing higher concentration of plutonium, generation of large volume of liquid waste, aqueous solubility of organics in aqueous phase which may lead to red oil formation and radiation instability of organics which decomposes under high radiation field, proliferation probability due to the production of clean plutonium etc. Still as an established process, aqueous reprocessing method has been followed in India to reprocess the oxide fuel irradiated in thermal reactors (to < 1at% burnup) and the mixed carbide fuel irradiated in FBTR (Fast Breeder Test Reactor) to high burnup (155 Gwd/tonne). Reprocessing carbide fuel is a highly challenging task due to high plutonium content and the formation of many carboxylic acids during the dissolution of the spent fuel in the nitric acid, which can affect the extraction of the actinides by TBP adversely.

1.4.2. Non-aqueous processes

When the fuel (fast reactor fuel containing higher amounts of plutonium) is irradiated to high burn up, the fission products (FP) accumulation in the irradiated fuel will be high and the radioactivity will be immense. In this case, the irradiated fuel needs to be cooled for a longer period for the activities due to the short lived FPs to die down. To make use of the limited uranium resources, the plutonium should be produced as rapidly as possible so that many reactors can be installed in a shorter time. To achieve the above goal, the future reactors need to be fueled with the metallic fuels. The breeding ratio of metallic fuels is high compared to that of oxide. Aqueous reprocessing of spent metallic fuel is not well established. There are potential advantages to reprocess the spent metallic fuel through non-aqueous reprocessing method. In this process, inorganic chloride salts are employed as the solvents and these exhibit better thermal stability and high radiation stability. Since the salts contain no hydrogenous materials, the large

concentrations of uranium and plutonium can be accommodated in a small volume during the processes and so the process volumes are low. The final waste produced is in solid form. The lower volume of the waste makes its management less problematic.

The non-aqueous methods can be divided into the following groups:

a) Methods based on volatilities – fluoride volatility process [7] and nitrofluor process [8] belong to this group.

b) Pyrometallurgical methods – in these processes, the fuel is maintained in the metallic state throughout the process. The melt refining process [9], which was used for the processing of EBR-II fuels, belongs to this category.

c) Pyrochemical methods [10] – These methods employ oxidation-reduction reactions chemically or electrolytically to effect the separation of the fuel materials from the fission products. Salt transport process [11] and salt cycle process [12] are well known examples of pyrochemical methods of reprocessing.

Of late, non-aqueous processes involving inorganic chloride or fluoride salts are being considered as an alternate for reprocessing of the spent fuel. In this regard, several studies have been reported. These processes are applicable to metallic fuels. These can be applied to reprocessing of the oxide fuels too. In such cases, the oxide spent fuel is subjected to Direct Oxide Reduction (DOR) process to convert the oxide to metal. Subsequently, the electrorefining is performed on the metal for the separation of actinides. Generally LiCl-KCl eutectic melt is employed as the electrolytic medium. The spent fuel pin is chopped into pieces and taken in an anode basket. The cathode on which the deposition of actinides to be effected depends on whether the actinides have to be deposited separately or together. Stainless cathode is used as the

cathode for deposition of uranium alone whereas the co-deposition of uranium and plutonium is achieved by using liquid cadmium cathode. The spent fuel consists of uranium, plutonium, minor actinides, fission products etc. It is treated with some oxidizing agent such cadmium dichloride to oxidise the actinides, alkali, alkaline earth and lanthanides. Alkali, alkaline earth elements and lanthanides are very stable chloride formers whereas the thermodynamic stabilities of actinide chlorides are intermediate between those of strong chloride formers and those of noble metal elements which are retained in the anode basket.

Proliferation resistance is an added advantage of the eletrorefining since the metallic deposit that is obtained at the end of the processes is not pure with respect to plutonium and is contaminated with uranium and minor actinides. The demerits are high temperature operation (500° C), use of corrosive chloride salts and limited or no plant scale experience.

1.5. Direct oxide reduction process for the preparation of plutonium metal

High pure plutonium is used for the preparation of calibration standards which are employed in the nuclear industry and in fissile material safeguards. Metallic plutonium was first produced by reduction of PuF_4 in a sealed pressure vessel. The plutonium obtained from the above process was impure and purified by electrorefining process. PuF_4, one of the reactants in the above process posed the problem of neutron radiation hazard. ^{19}F (α,n) ^{22}Na reaction generates high neutron flux emission. Hence this fluoride had to be handled with extreme care. The above plutonium production process involved many steps like dissolution of PuO_2, precipitation of plutonium peroxide, hydrofluorination and then reduction to metal. In order to eliminate the above radiation problem and minimise the number of steps, a new method involving DOR was developed. Direct Oxide Reduction (DOR) is considered to be beneficial

and cost effective since it is a one step process. The process was developed for the preparation of ^{238}Pu metal [13].

$$PuO_2 + 2Ca_{(diss)} \xrightarrow{CaCl_2} Pu_{(l)} + 2CaO_{(diss)} \quad (1.1)$$

where 'diss' is the component (Ca or CaO) dissolved in molten calcium chloride salt and 'l' is liquid.

In the process, PuO_2 was taken in MgO crucible along with calcium and calcium chloride. The optimum temperature range for this process was fixed between 1108 and 1112 K. Above 1112 K, the reaction of Ca(l) with MgO(s) was spontaneous. It lowers the yield of metallic plutonium as some of the calcium meant for the reduction of PuO_2 is wasted. Calcium metal and calcium oxide are soluble in calcium chloride while plutonium metal is insoluble in calcium, calcium chloride and calcium oxide melt. Under heavy stirring, calcium metal dissolves into the calcium chloride flux and reacts with the suspension of plutonium dioxide particles. High pure plutonium was produced by subjecting the impure plutonium metal obtained in the above process to electrorefining in molten NaCl-KCl-PuF_3 or $PuCl_3$ at 1023 K and pure plutonium was deposited on the cathode. Using this method, large scale production of high pure plutonium [14,15] by electrorefining was carried out at Los Alamos National Laboratory, USA. Direct oxide reduction studies are carried out at the Rocky Flats Plant and Los Alamos National Laboratory [16].

1.6. Molten salt extraction process for americium removal

241-Am is used as target for producing heavier elements. Additionally it is also used in smoke detector as the radiation source material. Aged plutonium is the source of ^{241}Am since one of the isotopes of plutonium (^{241}Pu) generates ^{241}Am through the emission of beta particle. Another source of Am is the spent molten salt resulting from electrorefining of impure plutonium

metal obtained from direct oxide reduction of PuO_2 as indicated above. During electrorefining of the impure plutonium metal, americium which is more electropositive than plutonium preferentially stays in the melt. Americium (^{241}Am), which is a decay product of ^{241}Pu, should be removed from plutonium periodically so as to reduce the radiation problem to the personnel since it produces gamma radiation in small amounts during its alpha decay to ^{237}Np. Americium is separated from the plutonium metal by equilibrating it with $CaCl_2$-KCl-$MgCl_2$ at 923 K. This process is called molten salt extraction (MSE) [17] process.

1.7. Recovery of actinides from salts

The recovery of the actinides left over in the melt after electrorefining plays an important role in several ways. The recovery provides us with two important benefits. (i) increase in the percentage yield of the DOR process and (ii) the salt remaining after the removal of the actinides is highly pure and can be reused in subsequent electrorefining operations. The molten salt extraction process for plutonium-americium separation and the electrorefining process of plutonium generate a large quantity of calcium chloride based residue salts containing plutonium and americium as their chlorides. The actinide content of the waste salt, in the form of oxides/chlorides, is in the range of 0.08 to 0.14 mole/mole of calcium chloride. The actinides in the salts need to be recovered in a Salt -Scrub process before these residue salts can be discarded or recycled. Liquid Ca-Ga alloys are used for the salt-scrub process [18]. Ca-Ga alloys, in appropriate stoichiometry are added to the molten waste salts comprising calcium chloride and actinide oxide/chlorides to obtain an actinide-20 atom percent gallium alloy, based on the following reactions.

$$4MCl_3 + Ca_6Ga \rightarrow M_4Ga\downarrow + 6CaCl_2 \quad (1.2)$$

$$4MO_2 + Ca_8Ga \rightarrow M_4Ga\downarrow + 8CaO \quad (1.3)$$

where M is the actinide element. Calcium serves as the reductant, while gallium forms an alloy with the actinide to lower its activity and to facilitate the above reactions in the forward direction**.** Thus thermodynamic properties on actinide–gallium systems are of interest for the recovery of actinides from the spent molten salt as addressed in Part 1 of chapter 4 of this thesis.

1.8. Chemical state of irradiated fast reactor fuel

Before the start of irradiation, the nuclear fuel has uniform composition throughout the bulk. As the fission events get underway, the fission products formed change the composition of the fuel. The knowledge of chemical states of fission products (FPs) and their transport behaviour within the fuel will help in understanding the effect of oxygen potential in the case of oxide fuel and how the chemical states of FPs influences important physical properties such as thermal conductivity, melting point etc. Hence, it is helpful to understand the chemical state of FPs that are formed under normal operation and how it influences their release & reaction behaviour during transients and during steady operation after the fuel pin failure. The chemical state of FPs is also of importance in the dissolution of spent fuel in nitric acid.

Tellurium (Te), even though generated in low yield, is a highly corrosive fission product. The fission yields of Te in fast fissions of ^{239}Pu and ^{235}U are 1 at. % each[19]. It can form metallic phases with uranium, palladium or tin; can be a constituent of multi-component fuel-fission product oxides depending on the local oxygen potential; and can dissolve in the oxide fuels [20]. Its transport to the fuel clad gap occurs through the vapour phase co-migration with cesium [21]. Adamson et al. [22] had shown through fuel chemistry modeling and equilibrium thermodynamic calculations that cesium and tellurium present in the fuel clad gap as Cs_2Te. This compound can react with the fuel to different extent depending on the oxygen potential prevailing in the gap and increase the tellurium potential and release the tellurium. If the fuel

outer surface becomes slightly hyper-stoichiometric (O/M >2.00 where M = U or Pu or both), tellurium potential in the gap can increase to the limit where tellurium will start reacting with the clad components. In the case of uranium-plutonium mixed oxide fuel, the following are the possible reactions considered to occur in the fuel-clad gap.

$$[Cs_2Te]_{melt} + (U.Pu)O_2 + O_2(g) = Cs_2(U,Pu)O_4(s) + [Te]_{melt} \quad (1.4)$$

$$[M]_{SS} + x[Te]_{melt} = [MTex]_{melt}. \quad (1.5)$$

A small fraction of tellurium can combine with ruthenium to form $RuTe_2$. The fission yields of Ru in the fast fissions of ^{235}U and ^{239}Pu are 11.8% and 23.1% respectively [21]. The formation of ruthenium telluride can reduce the tellurium potential at the fuel-clad gap, and also alter the release behaviour of radioactive tellurium in case of clad failure.

1.9. Significance of thermodynamic data of nuclear materials obtained from vaporisation studies

With irradiation, fission products start accumulating in the lattice of the fuels and the systems become highly complex. This changes the composition, which in turn alters the thermophysical, thermochemical and mechanical properties of the fuel drastically. Also due to steep temperature gradient across the fuel pellet, there will be movement of the materials down or up the gradient and many reactions take place in the fuel matrix. If the clad breaches during irradiation, the fuel coolant interaction takes place which may further aggravate the breach, which may lead to liberation of volatile fission gases into the coolant channel. The coolant which passes over the clad to extract the heat may react with the fuel or leach the components of the clad under the conditions prevailing at the interface. Understanding of vaporisation phenomena of fuel and the compounds that are formed consequent to the above stated interactions will help to predict the mass transport of these species and the likelihood of their

formation under the reactor operating conditions. Hence, vaporisation studies on these kinds of materials are needed.

Materials evaporate at all temperatures. As temperature increases, vaporisation rate also increases and significant mass loss occurs. The knowledge of vaporisation behavior of a given material will be very useful in controlling the process parameters during its fabrication. The rate of vaporisation of pure elements is mainly decided by temperature and enthalpy of vaporization. The rate of vaporisation is also influenced by its interaction with the container material and the surrounding atmosphere. Further, the rate of vaporisation in higher order systems is affected by the factors such as the thermodynamic activities of the components, temperature and enthalpy of vaporisation. The vaporisation degrades the thermal, chemical and mechanical properties of a material in service. Hence, the knowledge of the vaporisation behavior of any material is vital to understand its applicability**.**

A simple vaporisation reaction is represented as

$$A(s) \rightleftharpoons A(g) \tag{1.6}$$

For the above reaction, the equilibrium constant can be written as follows.

$$K^{\circ} = p_A \tag{1.7}$$

where p_A is the partial pressure of A.

The magnitude of the equilibrium constant implies the extent of the vaporisation reaction. It is used to deduce many important and useful thermodynamic properties which are useful to predict the feasibility of the reaction. Additionally the thermodynamic properties derived can be used to compute the fundamental data like bond energy for a gas phase equilibrium like $A_2(g) = 2A(g)$ that exists in the gas phase above the condensed phase.

The following are the properties which can be determined by the vapour pressure measurements:

1. Vapour pressure
2. Activity
3. Enthalpy of vaporisation
4. Enthalpy of reaction
5. Enthalpy of formation
6. Free energy of reaction
7. Free energy of formation
8. Bond energy

Vaporisation phenomenon can be classified into two types, namely, congruent and incongruent.

Congruent vaporisation: The atom fractions of the elements in the vapour and the condensed phases are the same.

Examples of congruent vaporisation are

$$(1)\ H_2O(s) \rightleftharpoons H_2O(g) \tag{1.8}$$

$$(2)\ Ni(s) \rightleftharpoons Ni(g) \tag{1.9}$$

$$(3)\ MnTe(s) \rightleftharpoons Mn(g) + Te(g) \text{ or} \tag{1.10}$$

$$MnTe(s) \rightleftharpoons Mn(g) + 1/2Te_2(g) \tag{1.11}$$

$$(4)\ MnO(s) \rightleftharpoons Mn(g) + 1/2O_2(g) \text{ or} \tag{1.12}$$

$$MnO(s) \rightleftharpoons MnO(g) \tag{1.13}$$

Incongruent vaporisation: The atom fractions of the elements in the vapour and the condensed phases are not the same. In this type of vaporisation, usually the condensed phase undergoes decomposition to produce another condensed phase and a vapour. For example

$$AB(s) \rightleftharpoons A(s) + B(g) \tag{1.14}$$

Some of the examples for incongruent vaporisation are given below:

$$CaCO_3(s) \rightleftharpoons CaO(s) + CO_2(g) \quad (1.15)$$

$$UGa_3(s) \rightleftharpoons UGa_2(s) + Ga(g) \quad (1.16)$$

1.10. Objective of the present study

U-Pu-Zr alloy is considered to be the driver fuel for future Indian Fast Breeder Reactors. Hence it is essential for us to know its thermodynamic properties to understand its behaviour during irradiation. This alloy is pyrophoric and highly reactive with moisture and oxygen. Hence it needs to be handled inside the inert atmosphere glove box where oxygen and moisture levels are maintained at less than 10 ppm. Hence the commissioning of the glove box, housing a Kundsen effusion mass spectrometer (KEMS) was undertaken with the objective of carrying out the high temperature mass spectrometric experiments on plutonium based systems. Subsequent to commissioning of the KEMS facility inside the glove box, the Knudsen effusion mass spectrometric studies (also known as high temperature mass spectrometric studies) have been carried out on U-Ga system to obtain the thermodynamic data of its intermetallic compounds. These data are of interest for the recovery of uranium from the spent molten salts in the salt scrub process as indicated in section 1.7. Subsequently, Plutonium partial pressures over U-Pu-Zr alloy have been measured using KEMS facility. High temperature vaporisation behaviour of Ru-Te system has been studied by using an earlier existing Knudsen effusion mass spectrometer to understand the fission product-fission product interaction.

1.10.1. Commissioning of the Knudsen effusion mass spectrometer inside glove box

The Knudsen effusion mass spectrometer (KEMS) has been erected inside the glove box. Generally, the KEMS is suitable for the determination of the systems which are involatile or having very low vapour pressures at high temperatures. The exploratory vaporisation

experiments were conducted with the pure elements such as Cr, Ni and Zr. Subsequently, the vaporisation studies on Fe-40at.%Al was carried out to have an experience in studying metal alloy system. Then the KEMS experiments with MnO were taken up with the objective of studying a congruently vaporising oxide system. The investigation of uranium and U-Zr alloys were started to have some experience of KEMS measurements on these alloys prior to taking up ternary alloy samples of U-Pu-Zr. The above experiments with pure elements were carried out to address three important points. (i) In the case of elements, the apparent enthalpies of vaporisation derived from the KEMS experiments should be in accord with the ones reported in the literature. (ii) The pressure calibration constants calculated as a function of temperature from the measured intensities of the ions over the elements should be temperature independent. (iii) The sensitivity of the equipment (i.e., the vapour pressure measurable) should be as low as possible. The above experiments (with pure elements) were carried out with the glove box kept in open condition.

1.10.2. U-Ga system:

Buschow [23] had constructed the phase diagram of this system by using experimental methods such as X-ray diffraction, metallography, thermal analysis and reported intermetallic compounds, namely, U_2Ga_3, UGa_2 and UGa_3. He also had shown that the compound previously reported by Markarov et al. [24] as UGa, actually has the stoichiometry U_2Ga_3. Dayan et al. [25] had reported U_3Ga_5 to be the intermetallic compound with the highest uranium content in this U-Ga system. However, it had been observed by Okamoto [26] that the reactions by which the intermetallic compounds, UGa and U_3Ga_5 are formed are unknown. He had further reported that since all the three intermetalllic compounds, U_3Ga_5, U_2Ga_3 and UGa possess the same crystal structure and similar lattice parameters, they all actually could be U_2Ga_3, which had been considered as UGa and U_3Ga_5 by other investigators. Salhov et al. [27a] had reinvestigated the

uranium rich portion of U-Ga system by employing metallography, electron microscopy, X-ray diffraction and differential thermal analysis to determine the solubility of Ga in high temperature phases of uranium (β, γ) and to identify the composition of the uranium rich intermetallic compound in equilibrium with uranium. He had concluded that the composition of the compound reported earlier by different authors as U_2Ga_3 was wrong and the actual composition of the compound was U_3Ga_5. The updated phase diagram of U-Ga system comprises the four biphasic regions, U+U_3Ga_5, U_3Ga_5+UGa_2, UGa_2+UGa_3 and UGa_3+Ga [27b].

The Gibbs energies of formation of UGa_3 reported by Johnson and Feder [28] and Lebedev et al. [29] had been determined by molten salt galvanic cell measurements in the range 643-1013 K and 696-1084 K, respectively. Alcock et al. [30] had measured the vapour pressures of gallium over gallium metal as well as over U-Ga alloys by using Knudsen Effusion Mass Loss method in the range 1281-1437 K and reported the gallium partial pressure-temperature relations in the graphical form and subsequently deduced the Gibbs energies of formation of intermetallic compounds, UGa, UGa_2 and UGa_3. Chiotti et al. [31] had reviewed the thermodynamic data of the U-Ga system and computed the Gibbs energies of formation of U_2Ga_3 by considering that it coexisted with UGa_2. Gardie et al. [32] had used Knudsen cell mass spectrometric method and measured the thermodynamic activity of gallium in the U-rich region in the composition range x_{Ga} = 0.05 - 0.28 over the temperature range 1100-1670 K. They had calculated the Gibbs energy of formation of U_2Ga_3 by considering it as the most uranium rich phase instead of UGa reported previously [24]. Wang et al. [33] had done a thermodynamic calculation of phase equilibria of U-Ga system and derived the enthalpy, entropy and Gibbs energies of formation of the constituent phases at 673 K.

The thermodynamic data of intermetallic compounds in U-Ga system such as enthalpy of formation and Gibbs energy of formation determined by Knudsen effusion mass loss method by Alcock et al. over the entire composition range had been reported by themselves to be erroneous due to the contribution of gallium oxide species to the partial pressure of gallium, even though they had assumed gallium vapour to be the only evaporating species [30]. Some of the two phase regions suggested in the phase diagrams reported before Salhov et al. were irrelevant. The present phase diagram comprises, in addition to UGa_2 and UGa_3 intermetallic compounds, U_3Ga_5 which had been recently confirmed by Salhov et al [27a]. KEMS studies over gallium rich compositions of U-Ga system are not reported in the literature. In addition, heat capacity data are also not available for any of the compounds in the U-Ga system. In the present study, we have conducted the KEMS studies on two "biphasic" regions, namely, (U_3Ga_5+UGa_2) and UGa_2+UGa_3), which are gallium rich. We have also measured the enthalpy increments of U_3Ga_5 by employing the high temperature differential calorimeter in inverse drop calorimetric mode.

1.10.3. U-Pu-Zr system

O'Boyle and Dwight [34] had determined the nine isothermal sections of U-Pu-Zr system between 773 and 973 K by using electron microprobe analysis, X-ray diffraction, and optical metallography techniques. Kurata et al. [35] had carried out the thermodynamic assessment of U-Pu-Zr system by using an optimisation procedure taking into account the recently determined experimental data on the various constituent binaries. Kanno et al. [36] had conducted KEMS studies on U-Zr system over the entire composition range (X_U = 0.098, 0.285, 0.478, 0.654 and 0.860) in the temperature range 1770-2060 K and reported the partial pressure-temperature relations of uranium for the above mentioned compositions. Using the partial pressure-temperatures relations of uranium, thermodynamic activities, partial and integral molar Gibbs

energies of uranium and zirconium had been deduced. Leibowitz et al. [37], by using FACT (Facility for the Analysis of Chemical Thermodynamics) had calculated the thermodynamic data of the different phases in U-Zr system and also the phase diagram. Their calculation had suggested that the activity co-efficients of uranium is closer to unity in the liquid phase as the uranium concentration approaches one. Ogawa et al. [38] had carried out thermochemical modeling of U-Zr alloys and also proposed the phase diagram. Maeda et al. [39] had reinvestigated the U-Zr system for the two uranium rich compositions, namely, 24.4 and 39.3 at.% Zr in the temperature range 1700-1973 K and reported partial pressures and activities of uranium in these alloys. Maeda et al. [40] also had studied the vaporisation behaviour of Pu-Zr binary alloy over the entire composition range (X_{Pu} = 0.06, 0.18, 0.25, 0.40, 0.50 and 0.8) by using KEMS in the temperature range 1400-1900 K and reported the partial pressures and activities of plutonium in these alloys. Leibowitz et al. [41] had calculated the polythermal projection of solidus and liquidus of U-Pu-Zr and also the phase diagrams of the limiting binaries taking into account the thermodynamic data of the these binaries.

U-Pu-Zr alloy has been proposed as the driver fuel for the future Indian Fast Reactors. Presence of Zr in the alloy plays two major roles. (i) It increases the solidus temperature of the alloy, thereby, permitting the high temperature operation. (ii) it stabilises the alloy in bcc phase at probable reactor operating temperature like, 823-973 K (550-700°C), thereby, avoiding the anisotropic thermal expansion of U-Pu alloy [42] (iii) it prevents the Fuel Clad Chemical Interaction (FCCI) by forming a protective layer against the interdiffusion of lanthanides and clad components from the fuel to the clad and from the clad to the fuel, respectively. Thermophysical and thermodynamic properties of this fuel are important to understand its behaviour during irradiation, under normal and off normal conditions. In the present study, the

KEMS studies have been carried out on the proposed alloy composition (U-19wt%Pu-6wt%Zr) to establish the nature of vapour species formed over the alloy at high temperatures and measure their partial pressures. The details of the experiments carried out on this alloys is given in part 1 of chapter 5.

1.10.4. Ru-Te system

The phase diagram of this binary system (based on the work of Bernath et al. [43], had been reported by Hokamoto [44]. Two vaporisation studies appear in literature, one carried out by Svendsen in 1977 [45] by employing the manometric method (silica spiral gauge) and the other by Ali Basu et al. in 2003 [46] by using the forward collection method, essentially the mass-loss Knudsen effusion method. Svendsen's measurements corresponded to 1) $RuTe_x$ where x = 2.00, 1.98, 1.97, and 1.96 in the temperature range 1276-1423 K; and 2) $RuTe_y$ where y = 2.67 in the temperature range 915-1206 K. The author had observed no systematic lowering of vapor pressure with composition for $RuTe_x$ and had concluded that there is no homogeneity range on the Te-poor side of $RuTe_2$. Furthermore, the author had treated the vapor pressures measured over $RuTe_x$ as though they all correspond to ($Ru+RuTe_2$) and had reported a single Σ plot equation based on a total of 40 values of $p(Te_2)$. The values of $p(Te_2)$ deducible from the Σ plot equation given by the author, however, are by a factor of ~ 200 lower than the actually measured values; the obvious reason could be an error in the derivation of the Σ plot equation by the method of least-squares. In the case of $RuTe_y$ (liquid tellurium saturated with $RuTe_2$), the vapor pressures were nearly constant at $T > 1079$ K while the values at $T < 1079$ K did yield a very slight positive partial molar enthalpy (that is, a slope slightly higher than that for liquid tellurium). The author attributed the break at 1073 K (in the plot of $\log[p(Te_2)]$ vs. $1/T$) to formation of two liquids, but gave no reason for the break yielding only to a constancy of $p(Te_2)$

~ 46 torr from 1098 K right up to the final temperature, 1206 K, of their study with this sample. Ali Basu et al. [46] measurements corresponded to (Ru + $RuTe_2$) in the temperature range 831-1148 K with a correction for possible deviation from Knudsen flow applied for the values of vapor pressure (assumed to be entirely due to Te_2(g) species) at $T > 1026$ K. The maximum correction reportedly required at the highest temperature of 1148 K was about 38 %. We find that the value of $p(Te_2)$ obtained by Ali Basu et al., on extrapolation to the lowest temperature of Svendsen's measurements (1276 K), is higher by a factor of 5. A difference of this magnitude could arise if there is a phase transition. But non-observance by Svendsen [45] of any break in the differential thermal analysis (DTA) measurements on a two-phase sample of (Ru + $RuTe_2$), heated to 1423 K, makes us infer that the discrepancy is real. Although Ali Basu et al. [46] had not mentioned about this discrepancy in their paper, they had pointed out a difference of 20 kJ mol^{-1} that exists in the value of enthalpy of formation of $RuTe_2$ deducible from their results and that recommended by Cordfunke and Konings [47], based on Svendsen's results. On the other hand, there was good agreement reported for value of entropy of formation of $RuTe_2$.

As for the homogeneity range of $RuTe_2$, Bernath et al. [43] had estimated it to be hyper-stoichiometric and narrow: from 67.3 to 67.8 at.% Te ($RuTe_{2.06}$ to $RuTe_{2.11}$). Zhao et al. [48] had estimated it to be narrow but hypo-stoichiomtric: from 66.5 to 66.7 at. % Te. In terms of formula, however, these authors had stated it to vary from $RuTe_{2.0}$ and $RuTe_{1.9}$, which makes one suspect whether the authors had estimated that Ru-rich boundary could be down to 65.5 at. % Te (that is, well into hypo-stoichiometry).

To our knowledge, no KEMS study has ever been conducted on this system. With the above background of information on the Ru-Te system, we conducted vaporisation studies on

some Ru-Te samples with initial compositions 40.0, 50.5, 69.5 and 71.5 at.% Te, respectively by using KEMS. These details are given in part 2 of chapter 5.

Thus, this thesis present the thermodynamic data obtained for U-Ga, U-Pu-Zr and Ru-Te systems.

References:

1. H.J. Bhabha, Proc. Internatl. Conf. on the Peaceful uses of Atomic Energy, 1, Geneva, 1955, p-103
2. C.N. Venkiteswaran, N. Raghu, V. Karthik, A. Vijayaraghavan, V. Anandraj, T. Ulaganathan, T. Saravanan, V.V. Jayaraj, Shaji Kurien, John Philip, T. Johny, N.G.Muralidharan, Jojo Joseph, K.V. Kasiviswanathan, Energy Procedia, 7 (2011) 227.
3. B. Bhattacharjee, "An overview of R&D in Fuel Cycle Activities of AHWR" in: Nuclear Fuel Cycle Technologies, (Eds.,) Baldev Raj and P.R. Vasudeva Rao, BRNS, DAE, (2006), p. 3
4. D. E. Ferguson, "Chemical Reprocessing of Nuclear Fuel", 24th International Congress of Pure and Applied Chemists, Vol. 6 (London: Butterworths, 1974), p. 337.
5. W.D. Bond, Light Water Reactor Nuclear Fuel Cycle, ed. R.G. Wymer and B.L. Vondra (Boca Raton, FL: CRC Press, 1981), p. 103.
6. J.L. Swanson, Sci. and Tech. Of Tributyl Phsophate, Vol. 3, ed. W.W. Schulz, L.L. Burger, and J.D. Navratil (Boca Raton, FL: CRC Press, 1989), p. 55
7. M. J. Steindler, L.J. Anastasia, L.E. Treverrow and A.A. Chilenskas, Nucl. Mat., 15 (1969) 177.

8. G. Strickland and F.L. Horn in : Prog. In Nucl. Energy, Series III, Process Chemistry, Vol. 4, Ed. C. E. Stevenson, E. A. Mason and A. T. Gresky, Pergamon Press, Oxford, 1970, p. 399.
9. C. E. Stevenson, EBR-II Fuel Cycle Story, American Nuclear Society, 1987.
10. R. K. Steunenberg, R. D. Pierce and I. Johnson, Proc. Symp. On Reprocessing of Nuclear Fuels, Ames, Iowa, 1969, Ed. P. Chiotti, USAEC, 1969, p. 325.
11. J. B. Knighton, I. Johnson and R. K. Steunenberg in: Proc. Symp. On Reprocessing of Nuclear Fuels, Ames, Iowa, 1969, Ed. P. Chiotti, USAEC, 1969, p. 337.
12. K. M. Harmon and G. Jansen, Jr., in : Prog. In Nucl. Energy Series III, Process Chemistry, Vol. 4 Ed. Stevenson, E. A. Mason and A. T. Gresky, Pergamon press, Oxford, 1970, p. 429.
13. L. J. Mullins and C. L. Fox, Report LA-9073 (1982).
14. L. J. Mullins, D. C. Christensen and B. R. Badcock, Report LA-9154 (1982).
15. L. J. Mullins, A. N. Morgan, S. A. Apgar and D. C. Christensen, LA-9469 (1982).
16. J. L. Long, D. J. Santi, D. C. Fisher, and T.J. Humiston, Report RFP-4128, Rockwell International, Rocky Flats Plant, Golden, CO.
17. J. B. Knighton, R.G. Auge and J. W. Berry, Report RFP-2365, Rocky Flats Plant, Golden, C0, (1976).
18. B. Mishra, J.J. Moore, Metall. Trans. 25B (1994) 151.
19. E. A. C. Crouch, Atomic data and nuclear data tables: Fission product yields from neutron induced fission, Academic Press, New York and London, 19 (1977).
20. H. Kleykamp, J. Nucl. Mater. 131 (1985) 221.
21. R. Viswanathan, J. Nucl. Mater. 444 (2014) 101.

22. M. G. Adamson, J. Nucl. Mater. 130 (1985) 375.

23. K.H. J. Buschow, J. Less-Common Met., 31,(1973) 165.

24. E.S. Makarov and V.A. Levdiv, Sov. Phys. Crystallogr., 1(6) (1956) 506.

25. D. Dayan, G. Kimmel, and M.P. Dariel, J. Nucl. Mater., 135 (1985) 45.

26. H. Okamoto, J. Phase Equilibria 14(1993) 125.

27. a) ASM Alloy Phase Diagrams Center, P. Villars (Ed.), H. Okamoto and K. Cenzual, section editors; http://www1.asminternational.org/AsmEnterprise/APD, ASM International, Materials Park, OH, USA, 2006-2015

    b) S.Salhov, G.Kimmel, M.P.Dariel, J. Alloys and Compds. 444-445 (2007) 257

28. I. Johnson, H.M. Feder, in: Proceedings of the Symposium on Thermodynamics of Nuclear Materials, Vienna, IAEA, Vienna, 1962, p. 319.

29. A. Lebedev, V.N. Seregin, A.M. Poyarkov, I.F. Nichkov, S.P. Raspopin, Russ. J. Phys. Chem. 47 (1973) 402.

30. C.B. Alcock, J.B. Cornish, P. Grieveson, in: Proceedings of the Symposium on Thermodynamics, Vienna, Vol. I, IAEA,Vienna, 1966, p. 211

31. P. Chiotti, V.V. Akhachinskij, I. Ansara, M.H. Rand, in: The Chemical Thermodynamics of Actinide Elements and Compounds, Part 5, The Actinide Binary Alloys, IAEA, Vienna, 1981, p. 120.

32. P. Gardie, G. Bordier, J.J. Poupeau, J. Le Ny, J. Nucl. Mater. 189 (1992) 85.

33. J. Wang, X.J. Liu, C.P. Wang, J. Nucl. Mater. 380 (2008) 105

34. D.R. O 'Boyle and A. E . Dwight, Plutonium and Other Actinides, ed. WN. Miner, Metallurgical Soc. Of AIME, New York, 1970

35. M. Kurata,Calphad, 23 (1999) 305.

36. M. Kanno, M.Yamawaki, T.Koyama, N. Morika, J. Nuc. Mater. 154 (1988) 154.

37. L. Leibowitz and R.A. Blomquist, J.Nuc.Mater. 167 (1989) 76.

38. T.Ogawa and T.Iwai, J.Less-Common.Metals. 170 (1991) 101.

39. A. Maeda, Y. Suzuki, T.Ohmichi, J. Alloy.Comp, 179 (1992) L21.

40. A.Maeda, Y.Suzuki, Y. Okamoto, Toshihiko ohmichi, J. Alloy.Comp, 205 (1994) 35.

41. L. Leibowitz, E.Veleckis, R.A. Blomquist, J.Nuc.Mater. 154 (1988) 145

42. G. L. Hofman, L. C. Walters and T. H. Bauer, Prog. Nucl. Energy, 31 (1997) 83

43. S. Bernath, H. Kleykamp, W. Smykatz-Kloss, J. Nucl. Mater. 209 (1994) 128.

44. H. Hokamoto, J. Phase Equilibria 16 (1995) 535

45. S. R. Svendsen, J. Chem. Thermodyn. 9 (1977) 789.

46. M. Ali Basu, A. N. Shirsat, R. Mishra, A. S. Kerkar, S. C. Kumar, S. R. Bharadwaj, D. Das, J. Alloys Comp. 352 (2003) 140.

47. E. H. P. Cordfunke, R. J. M. Konings (Eds.) Thermochemical Data for Reactor Materials and Fission Products, North Holland, Amsterdam, 1990, p.324.

48. H. Zhao, H. W. Schils, Ch.J. Raub, J. Less-Common Metals 113 (1985) 75.

CHAPTER 2

Measurement of vapour pressures and derivation of thermodynamic properties

2A.0. Introduction:

All substances evaporate and the rate of vaporisation increases with temperature. In the case of a simple element, the vaporisation rate is a function of temperature and the enthalpy of vaporisation. But in a binary system, it is decided by the activities of the components in addition to temperature and enthalpy of vaporisation. Vapour pressure data are more valuable in many ways. They can be used to derive many important thermodynamic properties as indicated in chapter 1. They are used as the key input data in many industrial processes to minimise the sample loss due to vaporisation.

Vapour pressure data generated by any vapour pressure method should be highly reliable. This is possible only if the measurements of vapour pressure are conducted under equilibrium conditions. The phase rule helps in deducing the conditions for carrying out meaningful measurements of vapour pressure. In the case of vaporisation studies, normal phase rule is followed, since vapour phase is considered as one of the phases in the system. The measurements are reliable only under univariant conditions [1]. The Gibbs phase rule can be stated as follows

$$F = C-P+2 \tag{2.1}$$

where F is number of degrees of freedom, C is number of components and P is number of phases.

In a single component system, when two phases are present (one the condensed phase and the other vapour phase), the vapour pressure will get fixed when the temperature is fixed. In a two component system, there are two possibilities for doing meaningful vapour pressure

measurements. In one case, three phases (two condensed phases and one vapour phase) should be in equilibrium so that when the temperature is fixed, the pressure will get fixed. The other one is a special case in which the system contains one condensed phase and one vapour phase. In this case, the condensed phase undergoes congruent vaporisation i.e., the atom fractions of the elements are equal in condensed and vapour phases. The condition of congruent vaporisation fixes one degree of freedom. In this case, when one condensed phase and one vapour phase are in equilibrium, the pressure gets fixed when the temperature is fixed.

There are many methods reported in the literature for the measurement of vapour pressure in different pressure ranges. Some of the methods need simple apparatus while others require the sophisticated instrumentation. For generating the vapour pressure data on the materials of interest to the nuclear field, we have employed the Knudsen effusion mass spectrometry (KEMS) method also known as High temperature mass spectrometry (HTMS) for the determination of the partial pressures of the neutral vapour species in equilibrium with the condensed phases taken in a small crucible fitted with a lid having a tiny orifice. KEMS is a powerful tool to study the samples which are less volatile even at very high temperatures. In this chapter, various methods used for the determination of vapour pressure are discussed along with KEMS method, the technique used in the present study.

The available methods are able to cover the pressure range from a few atm to 10^{-9} atm. These methods are classified into two kinds, absolute and relative. The absolute methods yield the pressure data directly and require no calibration whereas the relative methods rely on the calibration using standard materials whose vapour pressures are known as a function of temperature.

2A.1.1. Manometric method

It is a simple and absolute method for the measurement of total pressure. It consists of a U tube made of glass filled with mercury which is the most preferred manometric liquid due to its high density and its non-stickiness on the glass surface. One arm of the U-tube is exposed to the sample under study whose vapour pressure is to be measured while the other arm known as the reference arm is connected to the vacuum or exposed to the atmosphere. The difference in the levels of mercury (h) in both the arms gives the pressure of the sample directly ($p=\rho gh$). The lower limit of pressure determination is 1 mm Hg or 1 torr ($1.3x10^{-3}$ atm). The pressure lower than 1 mm Hg can be measured by using a low density liquid such as water and diphenyl ether. The sample vapor should be inert with the working liquid. The liquid manometer column needs to be taller when the pressure difference to be determined is high. When low density liquids are employed, the column size needs to be increased further.

2A.1.2. McLeod gauge

In this gauge [2], the sample gas is trapped in a known large volume (V_1) at the unknown pressure (P_1). It is compressed to a small known volume (V_2) in a capillary tube. As the volume has decreased, the gas will be having sufficient pressure (P_2) to give a measurable height of Hg. Applying Boyle's law ($P_1V_1 = P_2V_2$), the unknown pressure (P_1) can be calculated. It is useful to measure the pressure down to $10^{-5} - 10^{-6}$ torr. It serves as the reference standard to calibrate low pressure gauges.

The demerits of this gauge are as follows

1. The measurements are not continuous.
2. Handling of large amounts of mercury is highly tedious.
3. It is insensitive to condensable vapours.

The above described two methods fall under the class of static methods of pressure measurement. Pressures measured by these gauges are absolute.

The thermocouple [3] and pirani gauges [4], which function on the principle of variation of thermal conductivity of the vapour which is directly related to the number density, are used to measure the residual pressures in the vacuum vessels. Ionisation gauge [5] also can also be employed to measure the pressure in the high vacuum region. Optical absorption [6] and radioactivity [7] methods have been adopted to determine the vapour density which is related to vapour pressure. The gauges such as thermocouple and ionisation gauges are the secondary gauges since they do not yield the pressures directly. These gauges needs pressure calibration.

2A.2. Dew point method:

A technique for vapour pressure measurement that is especially useful for determining the partial pressures of the more volatile components of multicomponent systems involves the measurement of the "dew point" or condensation temperature. For a single-component system consisting of vapour, the temperature at which condensation just begins as the temperature is lowered in some part of the system, is known as the dew point. However, in an alloy or other multicomponent system, the dew point or the temperature at which the vapour pressure of the pure condensable component is equal to its partial pressure over the multicomponent system is lower than the temperature of the alloy or the system because the component is present in less than unit activity.

In practice, the alloy is sealed in a long evacuated tube. One end of the tube is heated to the desired temperature while the temperature of the other end is gradually lowered until the droplets of the more volatile components condense on the inner wall. A slight increase in the temperature results in the evaporation of the condensate. By carefully narrowing the temperature

interval between condensation on and evaporation from the area of variable temperature, one may fix the dew point, the vapour pressure of the pure, more volatile component, and thus it partial pressure over the alloy. This technique is especially suitable to systems involving binary compounds which decompose to give elements whose vapour pressures are of widely differing magnitudes. An independent measurement of the vapour pressure of the pure volatile constituent must be made initially in order to establish the partial pressure over the alloy.

2A.3. Transpiration method

Transpiration is a dynamic method of vapour pressure measurement. In this method, a gas, which may be inert or reactive, is passed over a condensed sample at a flow rate sufficiently low for equilibrium conditions to be established to sweep the vapour above it. The vapour is collected at some point downstream from the sample. The vapour collected is analysed to determine the vapour or dissociation pressures of components in the sample. The volume of the gas passed is calculated from the flow rate and the duration of the experiment. From the volume of the gas and mass of the vapour collected, the vapour pressure of the sample is calculated by applying the ideal gas law. One of the limitations or of the requirements is prior knowledge of the nature, composition of vapours and their molecular weight.

For conducting meaningful vapour pressure measurements, the flow rate of the carrier gas should be optimised prior to vaporisation studies on the samples. The flow rate of the gas to be fixed for equilibrium vapour pressure measurements is determined by heating the sample to the temperature T and passing the carrier gas over the sample at different volumetric flow rates (dV/dt). The plot of pressure drawn against the flow rate shows three distinct regimes. The flow rate for the determination of equilibrium pressures can be identified from the plot. Generally the plot resembles a chair as shown in Figure 2.1. In the low flow rate regime (1) of

the carrier gas, the diffusion of the vapour species over the sample into the furnace atmosphere occurs. Consequently the gas becomes oversaturated and the pressure calculated is higher than the equilibrium pressure. In the high flow rate regime (3), the time which the gas spends with the sample vapour is too low and it comes out of the furnace undersaturated. As a result, the pressure calculated is less than the equilibrium pressure. In the intermediate flow rate regimes (2), a plateau is observed in the figure and it shows that the pressures measured are independent of the flow rate. The above flow rate dependence of pressures is performed at two to three temperatures. The flow rate for the temperature dependence of pressures is arrived at from the plateau regions of the above mentioned experiments. The pressure range in which the transpiration studies are carried out lies in the range 0.1-1atm. The lower pressure is limited by the diffusion of the sample vapours whereas the upper limit is generally determined by the apparatus which has been rarely designed for use at positive pressures.

In general, the carrier gas used for transpiration experiments is inert and mostly argon gas is used. The advantage of this method is that the experiments can be carried out under different gas atmospheres depending on the requirements. Atmospheres can be reducing or oxidising either of which is selected to control the stoichiometry of the samples which is one of the factors influencing their vap

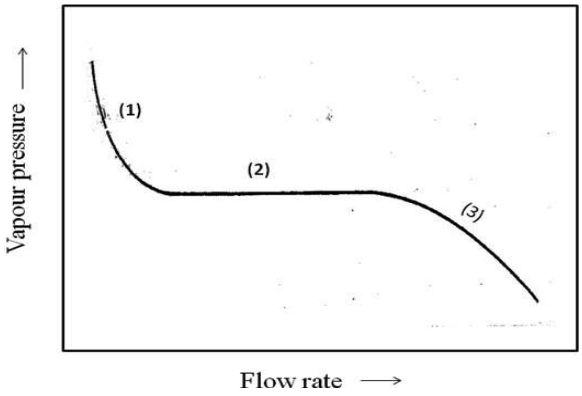

Fig. 2.1. Plot of vapour pressure vs Flow rate

2A.4. Isopiestic method

This method is based on keeping two or more samples at the same temperature equilibrating one or more volatile components in these samples. Absolute vapour pressures are calculated through a comparison with known vapour pressure systems with which the sample is in equilibrium.

A variation of the above method was used by Ipser et al. [8] for the determination of tellurium activities in the Cr-Te system. But in this method, several alloy samples along with one volatile pure element are stacked one over another in a temperature gradient furnace housed inside a closed container. The samples need not always be alloys. They may be another pure and least volatile element maintained at different high temperatures. The pure element or alloy of known composition is maintained at low temperature T_1 while the alloy samples (least volatile element samples) are kept at higher temperatures such that first sample temperature T_2 is greater than T_1, second sample temperature T_3 is higher than T_2 and so on. In this method, the vapour pressure of pure element or of alloy of known composition is equilibrated over all other samples. At equilibrium the vapour pressure of most volatile element over the samples at their respective temperatures equals that of the pure element or of alloy of known composition at low temperature. Each sample is analysed for the composition of the elements. Pressure-temperature relation for the most volatile element should be available in the literature or be measured by other techniques prior to isopiestic experiments on the samples. The activity of the most volatile pure element in each sample can be derived as follows. For a simple binary system A-B where A is the most volatile element kept at T_1, B is the less volatile element at T_2 and $T_2 > T_1$, the activity of any resulting A-B alloy can be estimated as the ratio of vapour pressure of A at T_1 to that at T_2.

2A.5. Knudsen Effusion Method

This method is well-suited for the measurement of low vapour pressures. This method is important for the determination of thermodynamic properties of vapours and condensed phases in equilibrium. This is based on the Kinetic theory of dilute gases. This is a dynamic technique based on the rate of escape of vapour molecules from an isothermal container through a small thin edged orifice into an evacuated space. A small thin edged orifice ensures that the portion of the gas in equilibrium with the sample inside the cell emanates out of it into the vacuum without disturbing the equilibrium. Effusion is the process in which gas molecules pass through a hole of diameter considerably smaller than their mean free path. Under these conditions, essentially all molecules which arrive at the hole continue and pass through the hole, since collisions between molecules in the region of the hole are negligible. The amount of molecules evaporated is much higher than that which effused out of orifice so that the equilibrium inside the container is not perturbed. The detailed discussions of these methods are reported in the literature [9-11].

2A.5.1.Hertz Knudsen equation:

This is the fundamental equation governing the effusion process. This equation is based on the kinetic theory of dilute gases according to which the flux (Z) of an ideal gas having the number density 'n', which is present inside a closed container, striking the unit area of the surface in unit time is given by the following equation.

$$Z = \frac{nc}{4} \quad \text{..... .(2.2)}$$

Where 'c' is the average velocity of the gas and 'n' is number density of gas in equilibrium with the condensed phase.

The number density 'n' is given as $$n = \frac{p}{kT} \quad \text{..... (2.3)}$$

Where ‘p’ is the pressure of gas molecules and T is the temperature in Kelvin and k is Boltzmnann’s constant.

The average velocity ‘c’ is expressed as $c = \sqrt{\frac{8kT}{\pi m}}$ ..... (2.4)

Where m is the mass of one gas atom or molecule

On substituting the expressions for ‘c’ and ‘n’ in (1), the following expression is obtained.

$$Z = p.\sqrt{\frac{1}{2\pi kTm}} \quad \text{.....(2.5)}$$

A more useful expression (2.5) for the relation between w, weight of the gas molecules striking a surface of area ‘a’ in time (t) can be obtained by multiplying both sides with (M/N) (M is the molar mass and N is the Avagadro number) and rearranging

$$w = apt\sqrt{\frac{M}{2\pi RT}} \quad \text{.....(2.6)}$$

where R is gas constant.

This equation is known as Hertz Knudsen equation or Knudsen effusion equation. This is valid for a vapour phase in equilibrium with its condensed phase as well as a mere gas phase in the container. But p (called as vapour pressure in such a case) should not be too high since the vapor cannot then be considered as an ideal gas. Also this is valid if the wall thickness of the orifice is infinitesimally thin.

If a small opening with an infinitesimal thickness is provided on the top of such a container and a high vacuum is maintained outside this opening, then all those molecules which might strike the surface of area equal to that of the opening (or orifice) can be assumed to be effusing out. Under such a situation, the measurement of this effusive flux or the weight of the

effusate can be used to calculate the equilibrium vapour pressure inside the container by using the equation (2.6). The container is called as a Knudsen cell.

2A.5.2. Molecular Flux distribution in the effusing beam

The vapour inside the cell is assumed to be isotropic, i.e., the molecules are distributed randomly in all directions and have a constant collisional rate at all surfaces. The vapour species effuse out through the orifice following the cosine distribution law [12]. Their distribution in any direction is proportional to the cosine of the angle between the normal to the orifice and the direction.

The application of cosine distribution law makes it possible to obtain the total flux from the measurement of flux in some arbitrary directions. The cosine law is a geometrical expression of the spatial distribution of molecular flux in an equilibrium system. The concept of randomness invoked in the kinetic theory of gases is also the basis of the cosine law. The relation between the total flux leaving a surface ds_i and the flux that reach another surface ds_j in a direction specified by solid angle dw_j is given by

$$Z_{ij} ds_j = Z_e ds_i (1/\pi) \cos\theta_{ij} dw_j \quad \text{.....(2.7)}$$

where θ_{ij} is the angle between the line of direction of the molecular trajectory and the normal to the surface element ds_i. In the case of effusion of molecules from a Knudsen cell, $Z_e ds_i$ denotes the total effusive flux from the orifice and the factor $(1/\pi)\ cos\theta_{ij} dw_j$ gives the fraction of the total flux having the specified direction. A portion of the emission flux may, for instance, be intercepted by a target and from the mass condensed per unit time on this target, the vapour pressure inside the Knudsen cell may be calculated by employing the above distribution equation.

2A.5.3. Free evaporation method

This is also known as Langmuir method of evaporation. In this method, the sample evaporates directly into vacuum from an open cell. Even in this case, the basic effusion equation can be used to calculate the equilibrium vapour pressures. In this method, the evaporating surface area is the sample surface area, whereas in the case of Knudsen effusion, the orifice area represents the evaporating surface area. In the case of Knudsen technique, the molecular flux effusing through the orifice of a Knudsen cell is considered whereas the molecular flux leaving the full sample surface is considered in the case of Langmuir method. The fundamental question that will come to one's mind is whether the flux from a sample surface into vacuum will be the same as in the case of a system where vapour saturation is ensured.

The pressures (p_m) measured by this method need not always be equilibrium pressures. The measured vapour pressures will be equal to the equilibrium pressures only if there is no kinetic barrier to the process of evaporation. In a kinetically hindered process, the measured pressure is less than the equilibrium pressure. The retardation in the kinetics is due to the following reasons. If the association or dissociation has to take place before evaporation, then the extra energy requirement will lower the rate of vaporisation and the measured pressure will be less than the equilibrium pressure. Most of the metals vaporises as monatomic gases and in such cases there may not be activation energy barrier and the measured pressure may be equal to the equilibrium pressure.

The pressure measured by Langmuir method (P_L) is related to the equilibrium pressure (p_e) through the vaporisation coefficient (α_V).

$$P_L = \alpha_v . p_e \quad \text{.....(2.8)}$$

α_v is different even for various crystalline forms of the same element as can be seen in the case of white and red phosphorus. White phosphorus has unit α_v whereas the value of α_v for red phosphorus is of the order of 10^{-6}. Brewer and Kane [13] ascribed the non-existence of P_4 units (which is the main gaseous species in the vapour phase) in the lattice of red phosphorus for this low value. They believed that some generalisations can be made about systems with low vaporisation coefficient: "low vaporisation coefficient can be expected whenever the main vaporising species are not present as such in the condensed phase and the atoms or molecules in the condensed phase are bound so tightly that they cannot readily reorganise to form the main gaseous species". Huang and coworkers [14] have reported the vaporisation coefficients for the various species (Se_2 to Se_9) above molten selenium as ~ 0.1.

2A.5.4. Equilibrium vapour pressures by using a Knudsen cell

Many questions regarding the vapour pressures determined by the Knudsen effusion measurements arise. How does Knudsen effusion take care of vaporisation coefficient problem? Do all the molecules striking the orifice area exit the cell? or is there a transmission loss?. What is the extent of vapour saturation in a Knudsen cell? Are the pressures determined by the Knudsen effusion equation valid irrespective of the pressures inside the Knudsen cell? If not, what is the dynamic range of vapour pressure which can be measured using Knudsen effusion method?. All these points are addressed in a brief manner in the following sections.

2A.5.4.1. Vapour pressures for substances with vaporsation coefficient < 1

The kinetics of hindered vaporisation is taken care of in the case of the Knudsen effusion method by keeping the orifice area much smaller compared to that of the evaporating sample surface area. If it is considered that the rate of effusion is the difference between that of

vaporisation and that of condensation inside the cell, the conservation of mass results in the expression given below:

$$\frac{p_k a_0}{(2\pi mkT)^{1/2}} = \frac{\alpha_v p_e a_s}{(2\pi mkT)^{1/2}} - \frac{\alpha_c p_k a_s}{(2\pi mkT)^{1/2}} \quad \text{.....(2.9)}$$

Where p_k and p_e are the vapour pressure inside the knudsen cell and the equilibrium pressure; a_o and a_s are the areas of orifice and the sample respectively; α_c is the condensation coefficient of the vapour which is defined as the fraction of the number of incident molecules which condense on striking a surface. α_c depends on the molecular flux and temperature. The above expression can be rearranged as

$$p_k = \frac{p_e}{\frac{a_0}{a_s \alpha_v} + \frac{\alpha_c}{\alpha_v}} \quad \text{.....(2.10)}$$

For a closed cell, α_c/α_v is 1. The ratio of 1 does not imply that the values of α_c and α_v are unity but equal in magnitude. Knudsen cell is a near closed cell. Hence α_c/α_v is assumed to be one. Then the above expression reduces to

$$p_k = \frac{p_e}{\frac{a_0}{a_s \alpha_v} + 1} \quad \text{.....(2.11)}$$

It is understood from the above expression that if a_o/a_c is kept much smaller, then the pressure determined will be closer to the equilibrium pressure. But there is a restriction to the values of these two factors. If the orifice area is made too low, only a small amount of effusate is collected and it affects the sensitivity of the measurement. The sample surface area also could not be too high due to the constraint in the physical dimensions of the cell. Use of sample in powder form will be helpful to some extent in increasing the surface area [15].

2A.5.4.2. Transmission of vapour phase through the orifice

In Knudsen effusion studies, the probability of a vapour molecule inside the cell to get transmitted out of the orifice is close to one if the orifice is infinitely thin. In practice, such an orifice cannot be made. Hence, one has to visualise the orifice as a cylindrical channel. The transmission loss will occur due to the inability of some molecules with velocity in certain directions to escape out of the orifice. They, while passing through such orifice, may collide with its wall and get reflected back into the Knudsen cell. Both the distribution of the effusing molecules and the extent of the transmission loss depend on the geometrical parameters of the orifice. The distribution of the effusing molecules at angles closer to the normal to the orifice will however not be affected. Therefore a correction factor needs to be incorporated in the expression (2.6) to take care of the transmission loss. This factor depends on the dimensions of the orifice (length and diameter) and gives the transmission probability of the orifice. It was Clausing who derived the correction factors for different geometrical shapes [12]. The correction factors are generally known as Clausing factors (C), which are dimensionless. After incorporating this factor, the expression (2.6) becomes

$$w = aCpt\sqrt{\frac{M}{2\pi RT}} \quad \text{..... (2.12)}$$

The quantity 'aC' may be considered the effective area of effusion.

2A.5.4.3. Extent of vapour saturation inside the cell

The extent of saturation within the Knudsen cell can never be complete since the Knudsen cell is not a completely closed system. Since the Knudsen cell is not a perfectly closed system and there is a constant passage of the molecules through the orifice, the extent of saturation can only be improved to levels close to perfect equilibrium conditions. The pressure p_k measured using the Knudsen effusion method is related to the equilibrium pressure, p_e as

$$p_k = p_e(1-X) \text{ ……..……...(2.13)}$$

The factor "X" can be brought near to zero by choosing the cell dimensions properly. Carlson [16] has performed the detailed calculations to derive the factor for cylindrical Knudsen cells. For a cell with the dimensions L/R=2 and R_o/R_c = 0.1 (the inner radius R_c, the length L and orifice radius R_o), he has computed the extent of saturation to be ~94%. If R_o/R_c is reduced to 0.01, the extent of saturation level can increase to as high as ~99%. Thus the lower value of R_o/R_c is essential to overcome the undersaturation caused by the vaporisation coefficient of less than one in some cases and the constant escape of mass through the orifice.

2A.5.4.4. Pressure range measurable using Knudsen method

The upper limit of vapour pressure is decided by the molecular flow conditions under which, there will be no collisions between the molecules as they leave the orifice. To meet these conditions, the mean free path of the molecules must be much greater than that orifice dimensions. At high vapour pressures, the mean free path becomes small compared to the orifice diameter and the flow changes from molecular to hydrodynamic flow. Then the pressure measured will be no longer closer or equal to the equilibrium.

Knudsen [17a, b] calculated that when the ratio of the mean free path ((λ) to the diameter of the orifice (d) is greater than 10, the flow through the orifice remains molecular and the pressures measured represents the equilibrium pressures inside the cell. Carlson [18] showed through the temperature dependence measurements of vapour pressures of Hg(g) over Hg(l) that the apparent pressures derived using the effusion equation matched with the equilibrium pressures up to ~9 Pa. Beyond this, the pressures measured were higher than the equilibrium pressures. An empirical relation between the maximum pressure that can be measured by the effusion studies and the radius of the orifice proposed by Boerboom [19] is given as

$$p < \frac{3.6}{r} \quad \text{.....(2.14)}$$

where the p is vapour pressure in Pa and r is the radius of the orifice in mm.

The lower limit of the range is defined by the sensitivity of the method used to analyse the vapours. Mass loss and collection methods are sensitive up to ~10^{-3} Pa. If the effusion method is coupled with a mass spectrometer with more efficient detector, then this limit can be pushed down to 10^{-7} [20] or 10^{-8} Pa [21].

2A.6. The Mass loss method

The mass loss may be obtained by weighing the Knudsen cell with the sample before and after heating to a desired temperature for a known amount of time. Alternately, the Knudsen cell may be suspended from a vacuum balance and the rate of mass loss at different temperatures may be measured. The merit of the second approach is that the mass loss is recorded simultaneously as the vapours effuse. It is possible to ensure that a steady state has reached at a given temperature from the constant rate of mass loss data obtained for different periods of time. It is also possible to make mass loss measurements at several temperatures without breaking the vacuum as in the first approach. The molar mass of the effusing species should be known to use this method. The equation to be used in both approaches is

$$p = \frac{w}{t} \frac{(2\pi RT/M)^{1/2}}{a_0 C\, 10} \quad \text{.....(2.15)}$$

where p is the vapour pressure (in Pascals), w is the weight loss (in grams), t is the period for which the sample was maintained at the desired temperature (in seconds), R is the gas constant (8.314 x 10^7 ergs/mol/Kelvin), T is the temperature (in Kelvin), M is the molar mass (in g/mol), a_0 is the orifice area (in cm^2), and C is the dimensionless Clausing factor.

2A.7. Collection technique

If the total effusate is condensed on a target, then the vapour pressure can be computed using the equation (2.15). Practically, only a portion of the effusate is collected on a small circular target which is located coaxial with and at some distance from the orifice. Since the transmission loss due to effusion is negligible in the direction close to the normal to the orifice, Clausing factor need not be applied. But the correction for the distribution of the effusate should be employed. For a target of radius r kept at a distance d from the orifice, this correction factor can be applied as

$$f = \frac{r^2}{r^2+d^2} \quad \text{.....(2.16)}$$

The factor, f, can be used in the place of Clausing factor, C, in equation (2.15). The method has the same advantage as the simultaneous weight loss measurements using a vacuum balance if collection could be carried out at different sample temperatures on different targets. But one must make sure that the condensation coefficient for the vapour on the target surface is unity. It will be possible in the collection method to know what has effused out if the chemical analysis is performed. This method may also give an idea of the relative vaporisation rates of the components of an alloy system. However, this method also demands the knowledge of the molecular weight of the effusing species to compute the vapour pressures.

2A.8. The Torsion effusion method:

The methods explained above uses the rate of effusion of the molecules through the orifice for the determination of the vapour pressures. Instead, if the momentum of the effusing molecules can be measured, vapour pressures can be calculated without using the molecular weight of the vapour species.

There are two types of measurement of momentum of the effusing molecules.

1. by suspending the Knudsen cell by using a torsion fiber. The twisting of the fiber due to the recoil force generated by the effusing molecules is measured.
2. by placing a vane on a torsional suspension in such a way that it intercepts the effusing molecular beam. The momentum transferred to it by the impinging molecules is measured.

The Torsion effusion coil method is explained in detail by Freeman **[**22**].** The Knudsen cell used in this method is in the shape of rectangular box provided with two anti-parallel effusing orifices. It is usually suspended from a massive support by using a Torsion wire of known torsion constant K_{tor}. To determine vapour pressures, a sample is placed in the cell and with the isothermal region around the cell at room temperature at which the sample has negligible vapour pressure, the orientation (rest point) of the suspension is noted. Subsequently the temperature of the sample is increased until the rate of effusion of vapour through the orifices is sufficient to produce a recoil force which rotates the cell through a conveniently measurable angle. At constant temperature of the sample, vapour pressure, the rate of effusion of vapours, the recoil force on the cell and the angle of rotation of suspension become constant.

When the angular displacement is constant, the torque produced by the recoil force due to effusion of vapour species is exactly counter balanced by restoring torque in the torsion element. The vapour pressure and the angular displacement are related by

$$p = \frac{2K_{tor}\theta}{\sum_{n=1}^{N} d_n f_n a_n} \quad \text{.....(2.17)}$$

where θ is the angular displacement, K_{tor} is the torsional constant, n is the number of orifices in the Knudsen cell, a_n is the area of the orifice, d_n is the distance between the orifice and the

suspension axis and f_n is the recoil force correction for the non-ideal orifice (something similar to Clausing factor for the normal Knudsen cell).

The angular displacement can be measured by many methods. It is generally noted through a mirror connected to a torsion fibre and a telescope to see the image developed I n the coil.

It is clear from the above equation (2.17) that the vapour pressure to be derived using this method has no dependence either on the molecular weight or on the temperature. Due to the above factors, this method is highly useful in determining the total vapour pressure of the sample. If the mass loss studies are simultaneously carried out, the mean molar weight of the effusing species can be obtained by substituting the total pressure data from this method in the equation (2.6).

2A.9. Knudsen Effusion Mass Spectrometer (KEMS) or High Temperature Mass Spectrometer (HTMS)

It is not sufficient if one measures the total vapour pressure since at high temperature, the gas phase may contain the species with unusual molecular formulae – unusual with respect to the expected or normally accepted formulae at room temperatures. For example, aluminium has the oxidation state of three in $Al_2O_3(s)$ whereas the vaporisation of $(Al(l)+Al_2O_3)$ system at high temperature [23] yielded species such as Al(g), $Al_2(g)$, $Al_2O(g)$, AlO(g), $AlO_2(g)$ and $Al_2O_2(g)$ which have aluminium in unusual oxidation states. It is impossible to identify such species in the vapour phase by employing the non-mass spectrometric methods explained previously above, which are used for the determination of the total pressure**.** There could also exist species which are polymeric – the gaseous species Te_i (i=1-7) and Se_i (1=1-9), respectively were identified in the vapour phase over Te(s) and Se(s) [24]. Some of the species may only be present as minor

species. However, to understand the nature of chemical bonding or the mechanism of a reaction, a minor species is as important as the major species. Moreover, the minor species at low temperature might become one of comparable abundance with the major species at high temperature. Brewer's view on high temperature vapours [25] are worth quoting in this connection: "At high temperatures one can just forget about the octet rule and all other valence rules that we have been taught; Anything goes".

Thus it is the complex nature of the vapour phase especially at high temperatures which makes the mass spectrometer the most powerful tool for the study of the gas phase. The sensitivity of the technique helps to identify the minor species and measure its partial pressure as a function of temperature. The determination of temperature dependence of partial pressures is important to explain many unusual phenomena occurring at high temperatures as well as to study the thermodynamics of the vapour phase and the condensed phase-vapour phase equilibria.

When Knudsen effusion method is coupled with mass spectrometer, it becomes a powerful tool for measuring the vapour pressure. In this method, the effusate is continuously mass analysed by allowing the molecular beam from the Knudsen cell into the ion source of the mass spectrometer. The advantages of coupling the Knudsen effusion method with mass spectrometer are many. While the Knudsen cell serves as a source of production of molecular beam representative of the vapour phase in equilibrium with the condensed phase at various temperatures, the mass spectrometer assists in identifying the species present in the vapour. Since mass identification is done, there is no need to know the molecular weight of the effusing species. Further, the partial pressure of each species in the vapour can be quantitatively measured whereas it is not possible by the non-mass spectrometric methods previously explained.

Mass spectrometric (MS) studies involve three steps, namely, ion formation, mass analysis of ions and collection of ions. Ions can be formed by using the methods like Electron Impact (EI) ionisation, surface ionisation, chemical ionisation, photo ionisation, laser ionisation, plasma ionisation, electro spray ionisation etc. The method applied mostly for the analysis of the gas (vapour) samples is EI, because of its ability to give the appearance and fragmentation energies with ease. The ion formation in MS is achieved by the collisions between the vapours (gas) and the electrons of well defined energy in ion source region. The ions are guided into the mass analyser, which sort out them with respect to their mass to charge ratios. Three commonly used mass analysers are the magnetic analyser, quadrupole analyser and the time-of-flight mass analyser. The ions emerging from the mass analysers are detected by suitable detectors such as Faraday cup, secondary electron multiplier (SEM) etc. More detailed information about this method is described extensively in literature [1, 9, 26].

There are different steps involved in the elucidation of the ion intensity data obtained from mass spectrum. The following are the sequences.

1. Identification of the ions
2. Identification of neutral precursors
3. Writing the chemical reactions
4. Derivation of thermodynamic properties of condensed phases and gas phase species.

2A.9.1. Identification of the ionic species

The molecular beam formed by the vapour species effusing through the orifice of an isothermal Knudsen cell entering the ion source chamber is ionised by an electron beam, at a direction perpendicular to the former, into positively charged ions. The design of the ion source configuration is usually such that the molecular, electron and ion beams are mutually

perpendicular. The ions formed are mass analysed by the mass analysers (the magnetic analyser, quadrupole analyser and the time-of-flight mass analyser) and detected by suitable detectors.

The identification of neutral species starts with indexing of the ions observed in the mass spectrum. One should look in the mass spectrum for all possible mass combinations of the elements of the condensed phase vaporised. The assignment of these masses to the actual ionic species is performed by comparing the calculated relative isotopic abundances with the observed relative peak heights. In some cases, ions of masses corresponding to metastable peaks may also be observed.

The ions corresponding to the masses of the residual gases are identified by recording a mass spectrum after isolating the ionisation chamber from the Knudsen cell chamber. For this purpose, a simple shutter is sufficient. However, one should make sure that the shutterable ions are all having their precursors which effuse from the cell-orifice only. This is particularly important if the Knudsen cell assembly is such that there exists a possibility for the molecules to condense somewhere outside the Knudsen cell and be able to evaporate at higher temperatures or if the sample creeps out of the Knudsen cell and evaporates from the surfaces outside the cell. A shutter with beam defining slits may be used to record the intensity profiles (ion intensities as a function of shutter movement). A normal intensity distribution (sharp peaks as the slits cross the molecular beam) indicates that the source of the vapour is from within the Knudsen cell whereas the distorted intensity profile indicates that the source of the vapour is mixed with that coming from sources other than the vapour in the cell [27].

2A.9.2. Identification of neutral precursors

The assignment of an ion or a group of ions to the respective neutral precursor is the most difficult task. The difficulty is due to the fact that the electron impact of the molecules results in simple as well as dissociative ionisation processes. The products of simple ionisation correspond to the masses of the parent molecules whereas those of dissociative ionisation correspond to various masses depending on which bonds are cleaved. Dissociative ionisation is primarily due to the fact that the energies of the impacting electrons are greater than the dissociation energies of the bonds. The presence of polymers in the vapour phase also can make the identification more difficult. The characterisation of the ionic species is generally carried out

1. by the use of ionisation efficiency curves
2. from the temperature dependence of ion intensities
3. from the angular distribution of species effusing through the orifice.

2A.9.2.1. Ionisation efficiency (IE) curves

An ionisation efficiency (IE) curve is a plot between ion intensity (I^+) and the energies of the impacting electrons. At low electron energies, the electrons are not energetic to cause ionisation. As the energy of the impacting electrons approaches the threshold, the sudden appearance of ion intensity is observed. Above the threshold, there exists a linear relationship between the ion intensity and the electron energies almost until the maximum ionisation efficiency is reached where the curve will flatten and at higher energies, there will be generally a decrease. The appearance potential (AP) of an ion can be obtained by extrapolation of the linear portion of the IE curve. If the ionisation potentials (IP's) are known, a good agreement of AP's with IP's will straight forward identify the parent ion. The electron impact energies should be calibrated prior to the analysis of the IE curves. The calibration is usually performed by determining the appearance potentials for the ions whose neutral precursors have known IP's.

The relation between the apparent AP and IP serves to determine the electron energy chosen in the experiment of interest accurately.

One should also look for breaks in the IE curves. An analysis of the energies at which the breaks appear as well as the nature of the breaks (upwards or downwards) would, along with the AP data, will help to figure out the fragmentation pattern. An upward break from the linear portion of the IE curve for an ion shows the onset of a fragmentation process (of some other molecules) which contributes to increased ion intensities whereas a downward break indicates the fragmentation of the ion being monitored. An excellent account of the analysis of the IE curves to identify the neutral species in the case of silver halides is given by Weil and his co-wokers [28,29].

2A.9.2.2. Temperature dependence of ion intensities

Another approach which is often adopted to assign a group of ions to a particular neutral species involves the measurement of ion intensities I^+ as a function of temperature. Apparent heats of sublimation of the ions "$\Delta_a H$" are obtained from the plots of log (I^+T) against reciprocal temperature. The word "apparent" is used to denote the fact that it does not refer to thermodynamic heat of vaporisation of an ion and to distinguish from the actual thermodynamic quantity which is the heat of sublimation of the neutral species, $\Delta_{sub}H°$. The idea of using "$\Delta_a H$"s stems from the fact that the parent ion and fragment ions originating from the same neutral species will all have similar values provided the ionisation cross section for fragmentation does not vary much as a function of temperature. Temperature dependent dissociative ionisation is not uncommon. In such cases, use of "$\Delta_a H$" data might lead to erroneous conclusions regarding the identification of parent and fragment ions. Complications will also arise if two ions originating from two different neutral species which have same $\Delta_{sub}H°$ values or if an ion is formed solely

due to fragmentation but from more than one neutral species which have different $\Delta_{sub}H°$. In the first case, one might conclude that the ion with higher mass number is a parent ion and (and that the other ion is a fragment ion). In the second case, one might think that the ion represents another neutral species. Under such circumstances, thermodynamic reasoning and the AP data would be of help in identifying the neutral species unambiguously. Thermodynamic reasoning has helped in identifying the neutral precursors for LiI^+ and $Li_2I_2^+$ in the case of vaporisation studies of Lithium iodide system [1]. The major ionic species observed were Li_2I^+, LiI^+ and Li^+. The plots of log (I+T) vs 1/T above and below the melting point were made for the ions Li_2I^+ and LiI^+. The heats of vaporisation and sublimation for the two ions were derived from the slopes. From the heats of sublimation and vaporisation of Li_2I^+, the heat of fusion (ΔH_{fus}) was found to be 37.7±2.9 kJ. This agrees well with the expected value of $2\Delta H_{fus}$ or 33.5 kJ (The calorimetrically determined value of ΔH_{fus} for LiI(s) is 16.7 kJ/mol) if we assume Li_2I^+ to be formed from Li_2I_2. The observed value of ΔH_{fus} for LiI^+ is 28.0 kJ. If LiI^+ is formed by ionisation of LiI(g) only, the observed ΔH_{fus} should be equal to the calorimetrically determined value of 16.7 kJ. On the other hand, if it is formed completely by dissociative ionisation of Li_2I^+, the observed value for ΔH_{fus} will be twice the calorimetric value. If simple ionisation and dissociative ionisation contributes to LiI^+ ion intensity, the observed ΔH_{fus} will be intermediate between ΔH_{fus}(calorimetric value) and $2\Delta H_{fus}$ (calorimetric value), depending on the relative amount of LiI^+ contributed by each process. The observed value of ΔH_{fus} for LiI^+ being higher than the calorimetrically determined value of H_{fus} indicates that the simple ionisation as well as the fragmentation also contributes to the ion intensity of LiI^+.

As much as possible, the ion intensity measurements of a polyatomic ionic species are carried out at low electron energy (in electron impact ionization) so as to minimize its

fragmentation. Higher electron energy will result in higher ion intensity for itself (polyatomic ionic species) as well as contribute to the ion intensity of another ionic species by fragmentation. Another ionic species has its origin from its own neutral precursor and the fragmentation of polyatomic species as could be seen in the above example. Then suitable correction factors involving the isotopic abundances of the polyatomic ion and its fragment ion and multiplier yield for these ions (secondary electron multiplier which will be explained later) will be used to arrive at the actual ion intensity of polyatomic ion.

2A.9.2.3. Angular distribution of the effusing species

The application of the data of angular distribution of the ions to identify the neutral species relies on the fact that each molecular species has a different angular distribution pattern. A rotary Knudsen cell is used in this method. The conventional Knudsen effusion mass spectrometry uses the static Knudsen cell unit so that the species reaching the ion source are those which effuse in a direction normal to the orifice. The use of rotary cell allows one to sample the molecular flux at various off-angles also. Whether or not an ion is formed from more than one precursor can be confirmed from the angular distribution determination of ionic species at different energies. The angular distribution will be similar for all the ionic species produced from the same neutral species even at different electron energies. Wagner an Grimley [30] identified the species over AgCl by using this technique. Measurements were made at off-axis angles upto 75°.

In addition to the above methods, there are several methods reported in the literature for identifying the neutral species.

(1). Velocity distribution of the molecules in the beam also can be used to get the angular distribution profile. Miller and Kusch [31] used a velocity selector coupled with surface ionisation detector to determine the molecular species in the vapour.

(2). Leak cell was used to detect the fragmentation processes. This cell resembles the Knudsen cell in all characteristics except a tubulation is inserted through the wall of cell by means of which permanent gases may be introduced from outside vacuum envelope. This arrangement has an advantage that the pressure of the inlet gas can be carefully controlled. The fragmentation behaviour of molecular vapour species of $Cr_2O_3(s)$ was studied by using this method [1]**.** Over pure Cr_2O_3, the species Cr^+, CrO^+, CrO_2^+, O^+ and O_2^+ were detected. The evaporation of a pure compound is commonly termed as evaporation under neutral conditions since no extraneous substance has been introduced. Under neutral condtions, the appearance potentials and the IE curves of Cr^+ and CrO^+ indicated that they were formed through simple ionsiation. Under neutral condtions, the vapour pressure of Cr(g) was greater than that of either CrO(g) or CrO_2(g). Hence, the fragmentation of a small fraction of either CrO(g) or CrO_2(g) could not be detected in the presence of large amount of Cr(g). However, when oxygen was added through the leak system, the IE curves Cr^+ and CrO^+ exhibited breaks characteristic of fragmentation. This was due to appreciable increase in the vapour pressures of CrO(g) and CrO_2(g) and decrease in that of Cr(g).

3. Double oven cell: This consists of two chambers connected to each other through a small tube. The temperatures of the chambers are independently controlled. One chamber is totally closed, used for containing the samples and kept at low temperature. The equilibrium vapour pressure developed over the sample in the closed chamber flows through the connecting channel to the other chamber operating at high temperatures. Subsequently, the gas phase dissociation reaction,

if any occurs in high temperature chamber, can be detected from the ion intensity ratios determined by using the mass spectrometer. These data are helpful to deduce the degree of fragmentation and the origin of the fragment ions.

Once the neutral species corresponding to the ions observed in the mass spectrum are identified, their measured ion intensities can be converted into the partial pressures using the relation whose derivation is explained in the following section.

2A.9.3. Derivation of the relation between ion intensity and partial pressures

The primary data that is obtained from the mass spectrometric studies are ion intensities. From this, one can get information about the number density of the molecules in the ionisation region and finally the number density of the molecules within the Knudsen cell. Therefore, a brief discussion of ion intensity measurements is given at first and subsequently the relation between the measured ion intensities and the number density of the corresponding neutral species in the ion source region is derived. Finally the relation between the measured ion intensities and partial pressures of the neutral species inside the Knudsen cell is obtained.

Relative detector response for ions of different masses:

Secondary electron multipliers (SEM) are generally employed for the measurement of ion intensities. The response of these detectors is not the same for all the ions since the multiplier factor i.e., the number of electrons generated due to the arrival of an ion on the first dynode (which are then multiplied with constant gain by each subsequent dynode) depends on the mass of the ion that is monitored. Hence, while converting the ion intensities into the partial pressures, the relative detector response should be considered. Alternately, an ion counting system can be employed as the detector. This helps is counting the number of pulses of the secondary electrons (or in other words, counting of each ion arriving at the deterctor) rather than a quantity

proportional to the number of electrons. Such a system exhibits no mass discrimination [32] and hence the counting rates recorded for each ion can directly be used. A Faraday cup detector (FCD) responds equally to all the ions, but is not sensitive enough to measure low ion currents.

If the mass spectrometer has both SEM and FCD in the collector housing, then the relative response of SEM for each ion can, in principle, be obtained if the ion intensities are measured by SEM and FCD at least at one temperature. One can utilise the ratio, I^+(FCD)/ I^+(SEM) obtained from such a measurement can be used to convert I^+(SEM) measured at other temperatures to as though they all correspond to I^+(FCD). However, the low sensitivity of FCD may not allow one to measure the ion intensity of the species with low partial pressure even at the highest temperature of the experiment. One may perhaps draw a calibration graph (a plot of the ratio, 'I^+(FCD)/ I^+(SEM)', against the mass number and resort to interpolation or extrapolation to deduce the relative response of SEM for the mass number of those ionic species for which the ratios could not be determined. In the absence of any such ratio, the relative response of SEM for each ion is assumed to be inversely proportional to the square root of the mass number of the ion that is detected.

2A.9.3.1. Number density of the molecules in ionisation region

The ion intensities, I_i^+, can be related to the number density, N_i (number of molecules per unit volume), in the ionisation volume by the equation :

$$I_i^+ = i_E^- \, l \, \sigma_i \, N_i \, \eta \, \gamma_i \quad \text{.....(2.18)}$$

where i_E^- is the electron current of energy E, l is its path length , σ_i is the ionisation cross section for the species 'i' at the electron impact energy E, η is the transmission coefficient of the

mass spectrometer (extraction efficiency from the ion source) and γ_i is the detector response for the ionic species.

The quantities, i_E^-, l and η can be grouped together into a constant since they are independent of mass. Hence the above equation becomes

$$I_i^+ = A\ \sigma_i\ N_i\ \gamma_i \quad \text{.....(2.19)}$$

Since for an ionic species, the intensity of only the isotope with the highest abundance is measured, the measured ion intensity should be corrected for isotopic abundances, n_i. If fragmentation occurs, the intensities of all the ions corresponding to a particular neutral species should be added together. If the intensity of a particular ion (parent or fragment ion) has major contributions from more than one neutral precursor, suitable correction should be incorporated.

2A.9.3.2. Partial pressure of species inside the Knudsen cell

De Maria [33] has derived, through the application of cosine law to Knudsen cell – ion source assembly, a relation between the number density N_{source} in the ion chamber and that within the Knudsen cell N_{cell} and the same is given as

$$N_{source} = N_{cell} \cdot \frac{a_0}{4\pi L^2} \quad \text{.....(2.20)}$$

where a_0 is the area of the Knudsen cell orifice and L is the distance between the orifice and entrance slit of the ion source chamber.

By combining the equations (2.19) and (2.20) and by incorporating the ideal gas law (i.e., $N_S = \frac{p}{kT}$), the relation between partial pressure, p_i, and the ion intensity, I_i^+, given below is obtained as,

$$p_i = \frac{k\, I_i^+\, T}{(\sigma_i\, n_i \gamma_i)} \quad \text{.....(2.21)}$$

where n_i is the isotopic abundance and k is constant which is commonly referred to instrument constant. It includes all the factors such as those caused by the geometry (position which influences the intensity distribution, Clausing factor etc.) and the instrumental properties (transmission coefficient of the ion source and analyser) common to all the species. The equation (2.21) demands the determination of k and the knowledge of σ_i for converting ion intensities into partial pressures.

The above equation is rewritten as

$$p_i = k'\, I_i^+\, T \quad \text{.....(2.22)}$$

where $k' = \frac{k}{(\sigma_i\, n_i \gamma_i)}$.

2A.9.4. Methods employed for determining the instrument constant k:

1. measurement of ion intensities of a reference material whose vapour pressure is known.
2. quantitative vaporisation of the sample while monitoring the ion intensities.
3. use of M^+/M_2^+ ratio provided $\Delta G°$ for the dissociation reaction is known. (M is monomer and M_2 is dimer)

2A.9.4.1. Method 1: Use of a reference substance whose vapour pressure is known for the determination of instrument constant

Partial pressure of a specie (reference) evaporating from a Knudsen cell at a constant temperature T is related to the ion intensity by the relation.

$$p_{ref} = k'_{ref}\, I^+_{ref}\, T \quad \text{.....(2.23)}$$

On rearranging, the relation (21) becomes

$$k'_{ref} = \frac{p_{ref}}{k'_{ref} T} \quad \text{.....(2.24)}$$

Hence k'_{ref} can be obtained from known vapour pressure and measured ion intensities. Similarly, the partial pressure of sample vaporsing at temperature T is related to the ion intensities by the relation.

$$p_{sample} = k'_{sample} I^{+}_{sample} T \text{.....(2.25)}$$

k'_{sample} can be computed from k'_{ref} by using the following relation.

$$k'_{sample} = \frac{k'_{ref} (\sigma n \gamma)_{ref}}{(\sigma n \gamma)_{sample}} \quad \text{.....(2.26)}$$

Such a conversion is possible if the Knudsen cell used for vaporising the sample and reference material is the same. The procedure generally followed for the determination k' is given below.

The ion intensities are measured as a function of temperature for the reference substance material before and after experiments on the sample of interest. In each of the vaporisation experiments with reference, k'_{ref} is calculated for each temperature at which ion intensity is measured and the mean of all such values are taken as the k'_{ref} for that experiment. k'_{ref} computed before and after the experiments on the sample should be constant. This ensures that the instrumental calibration constant remains unaltered during the course of these set of experiments. k' thus obtained can then be used to calculate partial pressures from the measured ion intensities.

2A.9.4.2. Method 2: Quantitative vaporisation of the sample

The most straight forward procedure of determination of k' is based on the quantitative vaporisation of the sample. The ion intensities measured at one temperature are related to the rate of mass flow through the orifice or to the total mass loss of the sample [34]. Equation (2.27), which was obtained by combining eqns. (2.12) and (2.22), can be used.

$$\Delta w_i = A_i\, k_i'\, a_0\, C\, (M_i/(2\pi R))^{0.5} \quad \text{.....(2.27)}$$

where $A_i = \int I_i^+\, T^{1/2}\, dt$ is the area under the curve $I_i^+\, T^{1/2}$ vs time (t). The ion intensities of the sample are measured as a function of time at a fixed temperature and $I_i^+\, T^{1/2}$ values are plotted against time to obtain the area. By knowing a_0 and C and using the area (A_i) and mass loss determined experimentally, the pressure calibration constant is calculated. The orifice area is generally measured by using the optical microscope and the Calusing factor is taken from the literature [35]. If the experiment is carried out at different temperatures, then the equation has to be summed over all those temperatures. Similarly, if the sample vaporises as more than one species, then intensities of all the ionic species need to be measured and the equation should be summed over.

Alternatively the term, a_0C can be determined by carrying out mass loss experiment with a vapour pressure standard like Ag. a_0C derived can be used to deduce the calibration constant for the sample.

2A.9.4.3. Method 3: From gas phase equilibria

If the monomer-dimer equilibrium of a species exists in the vapour phase over the sample, it can be used to obtain the pressure calibration constant in situ. This method requires the knowledge of the equilibrium constant of the reaction.

$$M_2(g) \rightleftharpoons 2M(g)$$

$K_{eq} = p^2(M)/p(M_2)$

$$K_{eq} = k'_M.\{(\sigma\gamma n)_{M_2}/(\sigma\gamma n)_M\}.\{I_M^{+2}/I_{M_2}^{+}\} \quad \text{.....(2.28)}$$

By using the measured ion intensities of the monomeric and dimeric ions , the ratio of ionisation cross sections and multiplier efficiencies of dimer and monomer, the pressure calibration is derived.

Once the pressure calibration constant is known, the same is substituted in the KEMS equation (2.22) to convert the measured ion intensities of ionic species to partial pressures of corresponding parent neutral species. The partial pressure data can be used to evaluate many important thermodynamic properties of the condensed and vapour phases.

Method (1) uses ratios of ionization cross sections of vapours from reference and sample under study and the vapour pressure of the reference. Hence uncertainties associated with estimated ionization cross sections of sample and reference will affect the vapour pressure of sample and this method yield less accurate vapour pressure. Method (2) uses the mass loss data i.e., mass loss incurred by a sample under study heated to and maintained at temperature 't' in time 't' and the ion intensities of all ions measured over the time 't'. It does not use the vapour pressure data of the sample. Hence this method is absolute and yields more accurate vapour pressure. Method (3) involves determination of pressure calibration constant insitu by making use of the gas phase equilibrium (dimer-monomer equilibrium) in the vapour phase over the sample under study itself. This method is also accurate. If such equilibrium exists in the vapour phase over the sample, this method is more useful. In method (1), instead of using an external reference, if we can employ the vapour over the condensed sample under investigation in pressure calibration experiment, we can obtain more accurate pressure calibration value.

2A.9.5. Evaluation of thermodynamic properties from partial pressures

2A.9.5.1. Activity of components in an alloy

The activity of a component in alloy is represented by the following equation;

$$a_i = \left[\frac{p_i}{p_i^{\circ}}\right]^{\frac{1}{n}} \quad \text{.....(2.29)}$$

where p_i is the partial pressure of the component 'i' over the sample, p_i° is the pressure of the pure component at the same temperature and n is the atomicity of the species. A twin cell or multiple cell assembly may give more accurate activity values than conventional ones [36] since measurements over the pure components and the alloys can be carried out under identical conditions. When a conventional Knudsen cell assembly (a single Knudsen cell) is used, measurements over the pure component and the alloy are performed separately and an assumption is made that the sensitivity of the instrument has not changed much during the course of the change from the pure component to the alloy system.

If the polymeric species are present in the vapour phase, then even with the conventional single Knudsen cell, activity measurements can be carried out without considering the sensitivity changes that can happen in the mass spectrometer. In such cases, the ion intensity ratio of two species, [named as M_1 (monomer) and M_2 (dimer)] are measured for the pure component and the alloy. Activity is calculated using the relation.

$$a_M = \frac{I_{M_2^+}/I_{M_1^+}}{I^{\circ}_{M_2^+}/I^{\circ}_{M_1^+}} \quad \text{.....(2.30)}$$

where I° is the ion intensity over the pure component and I is the ion intensity over the alloy.

In many cases, one of the components in a two component alloy system may be volatile and the measurement of partial pressures of that component gives its activities alone. The activities of second (least volatile) component can be estimated by applying Gibbs-Duhem equation given below.

$$(ln\, a_2)_{C_2} - (ln\, a_2)_{C_1} = -\int_{C_1}^{C_2} (N_1/N_2)\, d\, ln\, a_1 \quad \text{.....(2.31)}$$

where C_1 and C_2 refer to the compositions within which the integration is performed and N_1 and N_2 refer to the mole fractions of the components 1 and 2, respectively, at different compositions (from C_1 to C_2) at which the activities of component 1 are available. With knowledge of a_2 at least one of the compositions, a_2 at other compositions can be calculated. For a meaningful treatment of Gibbs-Duhem integration, it is essential that the activities of the component 1 should be deduced at as many temperatures as possible.

If the ion intensities corresponding to the vapour species of both the components can be measured in a two component systems at various compositions, then their activities can be derived by a Gibbs-Duhem integration of the ratio of ion intensities [37,38].

2A.9.5.2. Thermodynamic quantities for various chemical equilibria

From the partial pressures measured, reaction enthalpies are derived by using the second and third law methods.

2A.9.5.2.1. Second law method

The Gibbs energy change of reaction is related to the equilibrium constant of the reaction by the following equation:

$$\Delta_r G_T^\circ = -RT\ \ln(K) = \Delta_r H_T^\circ - T\Delta_r S_T^\circ \quad \text{.....(2.32)}$$

On rearranging the equation (2.32), it becomes

$$\ln(K) = \frac{-\Delta_r H_T^\circ}{RT} + \frac{\Delta_r S_T^\circ}{R} \quad \text{.....(2.33)}$$

On differentiating the above equation with respect to 1/T, we get

$$\frac{d\ln(K)}{d(1/T)} = \frac{-\Delta_r H_T^\circ}{R} \quad \text{..... (2.34)}$$

The above equation is known as vant Hoff's equation. If $\Delta_r H_T^\circ$ and $\Delta_r S_T^\circ$ are assumed to be constants, then from the slope of a linear plot drawn between ln K vs 1/T, one can deduce $\Delta_r H_T^\circ$ according to both equations. The enthalpy of a reaction calculated usually corresponds to the mean temperature of the investigation. If the temperature range is not large, the variation of $\Delta_r H_T^\circ$ with temperature will be smaller and hence a linear fitting of the partial pressures in the reciprocal of temperature will be valid.

The enthalpy of reaction at a reference temperature (usually 298.15 K; for the sake of convenience, this temperature will be written as 298 K in this thesis) can be further obtained by using eqn. (2.35) if the enthalpy increments data are available for the products and reactants of the reaction.

$$\Delta_r H_{298}^\circ = \Delta_r H_T^\circ - \Delta_r(H_T^\circ - H_{298}^\circ) \text{.....(2.35)}$$

One variation of the second law method known as the *Σ* plot method takes the variation of enthalpy of reaction with temperature into account. To apply this method, the heat capacities of the products and the reactants should be available in the literature. The equation (2.36) is used to derive the equation for *Σ* plot method.

$$-RT\ln(K) = \int \Delta_r C_p dT - T\int \Delta_r C_p \frac{dT}{T} \text{.....(2.36)}$$

where $\Delta_r C_p$ is the change in heat capacity of the reaction. $\Delta_r C_p$ in the form of temperature can be substituted in the above equation and on performing the integration, we get

$$-\mathrm{RT\ ln(K)} = \mathrm{f_1(T)} + \mathrm{C_1} + \mathrm{f_2(T)} + \mathrm{C_2\ T} \quad \text{..... (2.37)}$$

where $f_1(T)$ and $f_2(T)$ are new functions of temperatures and C_1 and C_2 are the integration constants. On rearranging, the above equation becomes

$$[-\mathrm{Rln(K)} - \mathrm{f_3(T)}] = \frac{\mathrm{C_1}}{\mathrm{T}} + \mathrm{C_2} \quad \text{..... ....(2.38)}$$

where $f_3(T) = [f_1(T) + f_2(T)]/T$. The quantity on the LHS is known as the Σ value. A plot between Σ and 1/T values yields a straight line with C_1 and C_2 as the slope and intercept. Since $\Delta_r H_T^\circ = \int \Delta_r C_p dT = f_1(T) + C_1$, the reaction enthalpy at any temperature 'T' can be obtained from the known values of $f_1(T)$ and C_1.

Another form of Σ plot method used by Margrave [39] and Cubicciotti [40] provides the enthalpy of reaction at 298 K directly. The equation employed by them is given as follows:

$$\Delta_r G_T^\circ = \Delta_r H_{298}^\circ + \Delta_r (H_T^\circ - H_{298}^\circ) - T(\Delta_r S_{298}^\circ + \Delta_r (S_T^\circ - S_{298}^\circ))$$

.....(2.39)

The quantities of $\mathrm{H_T^\circ - H_{298}^\circ}$ and $S_T^\circ - S_{298}^\circ$ known as the enthalpy and entropy increments are obtained from the literature. The above equation can be rearranged to get

$$-Rln(K_{eq}) - \frac{\Delta_r(H_T^\circ - H_{298}^\circ)}{T} + \Delta_r(S_T^\circ - S_{298}^\circ) = \frac{\Delta_r H_{298}^\circ}{T} + \Delta_r S_{298}^\circ$$

.....(2.40)

The expression on the LHS was referred to as Σ' by Cubicciotti and as Φ by Margrave. A plot drawn between Σ' and 1/T yields a straight line, the slope of which corresponds to the reaction enthalpy at 298 K.

An important point to be noted in the second law treatment of the partial pressure data is that it gives only one enthalpy data, which corresponds to the mid-temperature of the range, for a set of data measured at different temperatures.

2A.9.5.2.2. Third law method

In this method, the enthalpy of the reaction is directly obtained at the reference temperature (298.15 K). Substituting for $S_T^\circ = -(G_T^\circ - H_T^\circ)/T$ in equation 2.32,

$$-RT\ln(K) = \Delta_r H_T^\circ + \Delta_r\left[G_T^\circ - H_T^\circ\right] \quad \text{.....(2.41)}$$

Adding $\Delta_r H_{298.15}^\circ$ on both sides and rearranging

$$\Delta_r H_{298}^\circ = -RT\ln(K) - T\Delta_r\left[\frac{G_T^\circ - H_{298}^\circ}{T}\right] \quad \text{.....(2.42)}$$

The function $\frac{G_T^\circ - H_{298}^\circ}{T}$ is known as the free energy function. Using the eqn. (40), one can get as many $\Delta_r H_{298}^\circ$ values as the number of partial pressure data in a set. This would help to check the consistency of the partial pressure data measured at different temperatures.

2A.9.5.2.3. Comparison of second and third law methods

These laws have several merits and demerits. It will be better if we can use both the laws to derive $\Delta_r H_{298}^\circ$. In such a case, inter comparison of the enthalpies deduced from these methods can be made. A good agreement between the $\Delta_r H_{298}^\circ$ values obtained by both methods is usually considered as a reflector of the reliability of a set of partial pressure data. A

major difference between the second law value and the mean third law value may sometimes be due to only very few points which are erroneous especially at temperatures corresponding to either end of the temperature range of the measurements. Such data can be identified in the third law evaluation. A re-evaluation after eliminating such points may give a second law enthalpy in agreement in the mean third law enthalpy.

It is better to make measurements over a large temperature range to enhance the reliability of a second law value since it is obtained from the slope of ln K vs 1/T plot. It may not be possible in the case of minor species. Third law method will be of much use in such cases because, in principle, the third law can give an enthalpy data even if the pressure is measured at a single temperature. If reliable free energy functions are available, then third law gives more accurate value. The advantage of second law is that one need not plot the actual pressures. In the second law evaluation of mass spectrometric data, the enthalpy can be obtained from $\log(I^+T)$ vs 1/T plot. Hence, errors in ionisation cross section and other parameters for deducing pressures do not affect the reliability. Third law value requires absolute pressure and hence is affected by pressure calibration, ionisation cross section and detector responses.

The uncertainties in temperature measurements, especially if they are not uniform, affect the accuracy of a second law value adversely than that of a third law value. A uniform error of δT in T, in the entire range of investigation, would cause a small and roughly same relative error in the enthalpy values deduced by using both methods, if δT is not large. For example, for a reaction with an enthalpy change of 200 kJ mol^{-1}, an error if 5 K in the range of 1000 K introduces an error of ~ 2 kJ mol^{-1} in the second law value [$\Delta_r H_T^\circ \; 2\left(\frac{\delta T}{T}\right)$] and ~ 1 kJ mol^{-1} in the third law value [$\Delta_r H_T^\circ \; \left(\frac{\delta T}{T}\right)$]. If the temperature error is not uniform i.e., if there is an error

of +5 K at one end and -5 K at the other end of the temperature range of measurement or vice versa, the error of 10 K results in ΔT. If the temperature range of the measurement is ~ 100 K, then an error if ~20 kJ mol^{-1} occurs in the second law value [$\Delta_r H_T^\circ \left(\frac{\delta \Delta T}{\Delta T}\right)$] whereas the third law value may not be altered much on account of the averaging of the values at different temperatures.

While the possible errors in the second and third law are calculated, it is important to consider also the uncertainties in the pressure measurement and in the auxiliary thermodynamic quantities. Drowart and Goldfinger [41] have given the equations to compute the relative uncertainties in the enthalpies obtained by second and third laws methods. Regarding the partial pressures, the accuracy and reproducibility of the partial pressures of major species can be as high as ±20 percent whereas for minor species, the uncertainty of a factor of two or even three may exist [27]. Drowart and Goldfinger [41] have also mentioned that the third law value tends to have an absolute error of 4-20 kJ mol^{-1} and a relative error of 2 to 5 percent exists in the second law.

2A.10. Auxiliary thermodynamic quantities:

In this section, a brief discussion on how the auxiliary thermodynamic quantities are obtained is presented.

2.A.10.1. Condensed phases

Enthalpy increments are usually obtained by using drop calorimetry : In this method, the sample is dropped from room temperature to the required high temperature and the heat absorbed by it is measured. Or the sample heated in a furnace to high temperature is dropped to the calorimeter at 298.15 K and the heat released by it is measured. The data obtained are fitted to a

non-linear mathematical expression. The heat capacity equation is obtained by differentiating it with respect to temperature. Entropy increments can be evaluated from the heat capacity equation. Absolute entropy at 298.15 K is required for obtaining the Gibbs free energy function as can be seen from the equation given below:

$$[G_m^\circ(T) - H_m^\circ(298.15)]/T = \frac{[H_m^\circ(T) - H_m^\circ(298.15)]}{T} - [S_m^\circ(T) - S_m^\circ(298.15)] - S_m^\circ(298.15) \text{-------(2.43)}$$

If the heat capacity can be measured directly employing an instrument such as differential scanning calorimetry, then both enthalpy increments $\int C_p dT$ and entropy increments $\int C_p \, d\, lnT$ can be computed from them. Adiabatic calorimeter are also used for the determination of heat capacities. $S_m^\circ(298.15)$ values can be derived from low temperature heat capacity data provided there exists no uncertainty as to whether or not ordering in the sample is achieved.

If no experimental data are available, these may be estimated from the values for comparable compounds or alternately by applying Nemann Kopp's rule which says that the heat capacity of a compound is the sum of the heat capacities of constituent elements.

2.A.10.1. Gaseous phases

The auxiliary thermodynamic quantities for gases are usually computed by statistical mechanical treatment of molecular parameters. The translational, rotational, vibrational and electronic partition functions each of which expresses the distribution of gaseous molecules over possible energy states of the respective type are computed. Partition functions being a measure the probabilities, the total value Q_t is obtained is

$$Q_t = Q_{trans} \cdot Q_{rot} \cdot Q_{vib} \cdot Q_{ele} \tag{2.44}$$

For the calculation of partition functions according to equation 2.44, one needs to know the energy levels and their degeneracies.

$$Q = \sum_i P_i \, exp \, \frac{-(\epsilon_i - \epsilon^\circ)}{kT} \tag{2.45}$$

where P_i represents weighting factor (or degereracy) for the possibility that certain independent configurations have identical energies ε_i and ε^0 is the energy of the ground state.

The auxiliary thermodynamic functions for one mole of gas are derived from the following relations.

$$\frac{G_m^\circ(T) - H_m^\circ(0)}{T} = -R \ln\left(\frac{Q}{N}\right) \tag{2.46}$$

$$H_m^\circ(T) - H_m^\circ(0) = -R \ln \frac{d(\ln Q)}{dT} \tag{2.47}$$

In essence, the information needed are the mass, the vibrational frequencies and anharmonicities, geometry or the symmetry number (number of indistinguishable positions into which the molecule can be turned by simple rotation, the moment of inertia of molecules or the bond distances, the nature of electronic states and their excitation energies. Spectroscopic and electron-diffraction studies can yield the necessary information. When the experimental data are not available, they have to be estimated. The calculation of Q by using quantum statistical equations is very sensitive to the geometry and hence the estimation of them for complex molecule should be made very carefully.

Frurip and Blander [42] have discussed a dimensional analysis of classical partition functions for ionic molecules. One could derive simple expressions for the relative values of entropies and Gibbs free energy functions in terms of a universal equation for molecules of a

particular class and partition geometry. The only quantities required for calculation are the interatomic distances and atomic masses.

2A.11. Boiling point method

This is generally followed for highly volatile substances. It is based on the principle that the substance under investigation boils at a temperature at which its vapour pressure equals the ambient pressure. It can be adopted in two modes. In one mode, the boiling point of the substance is determined by noting the temperatures at which it boils while the ambient pressure is continually varied. In another mode, the boiling point is determined by varying the temperature slowly while the ambient pressure is kept constant. The temperature of onset of boiling should be detected as accurately as possible. The onset of boiling is monitored in the following ways.

1. Visual examination of bubbles appearing at boiling
2. There is a sudden fall in the temperature of the substance at boiling when it is in intimate contact with the thermocouple, since heat required for boiling is taken away from the surface of the liquid.
3. The temperature of the substance remains unaltered at boiling when the thermocouple is above it.

Even though the boiling point method is commonly used for liquid samples, solids having very low vapour pressure can also be studied using laser heating method. The vapour pressures of UO_2, SS etc are measured by using laser heating [43,44]. This boiling point method gives only the total vapor pressure and cannot give the partial pressures.

Vapor pressure data at ultra high temperatures (> 3000 K) are required for refractory materials, especially for nuclear-fuel materials, as these data are important input parameters to

carryout analysis of consequences of any off-normal events in liquid-metal-cooled fast-breeder reactors (LMFBRs) [45]. Conventional experimental techniques which are used to measure the vapor pressures below 2500K cannot be used at very high temperatures (>3000 K) because of limitations arising from the need for a suitable sample container and difficulties in generation of very high temperatures. The laser heating technique is advantageous, because the sample itself acts as a container [46].

2B.1. Calorimetry

For the present thesis, the enthalpy increments of $U_3Ga_5(s)$ have been measured by employing the temperature differential calorimeter in inverse drop method. In this connection, various calorimetric methods, which are being used for the determination of thermal properties such as heat capacity, enthalpy measurement, enthalpies of transition etc., are briefly discussed.

Calorimetry is the subject dealing with the heat changes occurring in the system under study as it is subjected to programmed heating rate. These heat changes are generally accompanied by the exothermic or endothermic events taking place in the system. These events cause in the system the change of temperature (ΔT) which can be used to derive the thermodynamic properties relevant to them. The device used in carrying out the above calorimetric experiments is known as calorimeter. Various classifications of calorimeters are available in the literature.

2B.1.1. Classification of calorimeters

Zielenkiewicz [47-49] classified the calorimeter based on the temperatures of the system and the surrounding. There are three types of calorimeters under this.

1. Adiabatic calorimeter: In this type of calorimeter, the system and surrounding temperatures are the same. No heat exchange occurs between the system and surroundings. When the system

temperature (T_{sys}) changes consequent to heat changes associated with the physical or chemical changes in the system, the surrounding temperature (T_{Surr}) is also brought to the same by external means.

2. Isothermal calorimeter: T_{sys} and T_{Surr} remain constant throughout the course of the experiment. It is otherwise known as the phase change calorimeter. Two common examples of isothermal calorimeter are ice calorimeter and diphenyl ether calorimeter. Both are used to measure the heat liberated or absorbed during the phase transformations (mainly melting) taking place in the system.

3. **Isoperibol calorimeter:** The system temperature is varied while the surrounding stays at a constant temperature.

Castanet et al. [50] had classified the calorimeters that are prevalently used in experimental thermochemisty into two types.

1. Calorimetry of non-reacting systems
2. Calorimetry of reacting systems

The first kind of calorimeters is generally suitable for carrying out heat capacity and enthalpy increment measurements and the determination of the enthalpies of phase transformations. The second kind of calorimeters finds use in measuring the heat released or taken up during the chemical reactions occurring in the calorimetric vessel (system). These are useful in the determination of partial or integral molar enthalpies of mixing of liquid alloys and the enthalpies of formation of intermetallic compounds at the ambient as well as high temperatures.

2B.2. Heat capacity measurements

Heat capacity can be measured directly by employing the differential scanning calorimeter (DSC) or indirectly by using the drop calorimeter which gives the enthalpy increment data.

2B.2.1. Differential scanning calorimeter

It is of two types. 1. Heat flux DSC 2. Power compensated DSC.

Heat flux DSC: While the reference and sample substances taken in hermetically sealed crucibles are heated at a preset heating rate, the difference in heat flow rates to the sample and reference is recorded as the signal in the DSC thermogram. The sample and reference substances are heated by a single furnace. The difference in heat flow rate is due to the difference in heat capacities between the sample and the reference. The signal can be directly transformed into the heat capacity data by using the heat capacity calibration constant obtained from the calibration studies with a calibrant like α-alumina.

Power compensation DSC: The difference in temperature between the sample and reference substances is nullified either by passage or removal of the power. The sample and reference are heated by two independent furnaces. The power passed to the sample or removed from the sample is proportional to the enthalpies of thermal events or to the heat capacity of the sample substance.

DSC has several advantages. The heat capacity data are directly obtained. The second order transitions associated with small enthalpy changes can be investigated. The DSC measurements are less time consuming. The disadvantage is that its use is limited to the temperature of ~873 K beyond which the radiation makes the measurements difficult.

2B.2.2. Drop calorimeter

This is used to measure the enthalpy increment data of the samples. It comes under isopiestic calorimetry. Generally these measurements are made with respect to the reference temperature, 298 K. The sample to be dropped into the calorimeter is heated to the known high temperature 'T'. After the temperature equilibration is attained, it is dropped into calorimetric vessel which is maintained at 298 K. As the sample attains the calorimeter temperature, an endothermic effect, proportional to the heat content, is produced. The heat contents or enthalpy increments are measured at several temperatures. They are expressed as an empirical power series in temperature. The differentiation of the resulting expression gives the equation for heat capacity.

For obtaining the accurate results, the sample must not undergo irreversible chemical change such as decomposition, reaction with container etc., when it is held at high temperature prior to its drop into the calorimeter. The success of this method is highly dependent on the complete return of the sample to a well-defined thermodynamic reference state at the end of the measurement. Sometimes, as the sample gets cooled rapidly subsequent to its drop to calorimeter, it may fail to go through some of the solid-solid transitions. Such 'freezing in' of phase transitions will lead to uncertainties in the evaluation of the heat evolved. Particularly uncertain are the drops from the liquid state, if the solid composition line is not vertical (single phase). Changes in the composition of solid phases will occur upon cooling with the resultant indefinite final state. Such problems can be overcome in 'inverse drop calorimetry' wherein the sample is dropped from a lower temperature into a calorimeter kept at a higher temperature. In this case, only rapid heating of the sample occurs during the drop and so, 'freezing in' of phase transition will not occur. The detailed description of the inverse drop calorimetry is provided in part 2 of chapter 4. The enthalpy increment measurements on a given sample are determined at

several temperatures and these are fitted to a non-linear equation in temperature of the form given below:

$$H_T^0 - H_{298}^0 = AT + BT^2 + \frac{C}{T} + D \quad (2.48)$$

The first derivative of the above equation with temperature yields the heat capacity expression shown below:

$$C_p = A + 2BT - \frac{C}{T^2} \quad (2.49)$$

Freezing-in of phase transitions are possible in samples prepared by rapid cooling. For our experiments, the samples are prepared by equilibrium methods wherein freezing -in of phase transitions are not possible and they are well characterized.

2C.1. Other thermochemical method

The EMF method

This method employs solid state galvanic or molten salt cells for the measurement of thermodynamic properties [51-53]. A cell is made up of two electrodes along with an electrolyte which acts as a medium for the movement of the ions. This method involves oxidation and reduction reactions. The main condition for successful determination of thermodynamic properties using this method is that the conduction should be purely ionic. There exists a relation between the measured cell potential and the Gibbs energy of reaction.

$$\Delta G^\circ = -nFE \quad \text{.....(2.50)}$$

where ΔG° is the Gibbs energy of reaction, n is the no of electrons involved in the redox reactions, F is the Faraday's constant and E is the EMF of the cell.

The requirements of the cell to produce the reliable thermodynamic properties are twofold. 1. Electrode reactions should be well defined and reversible. 2. The EMF should be measured between two electrodes with chemically identical electrical leads. The EMF data are recorded as a function of temperature in a small temperature range. These data are generally expressed as a linear function of temperature (E=A+BT).

The entropy of reaction is calculated from the EMF temperature relation (E-T relation) by applying the following equation.

$$\left(\frac{\partial(\Delta G^{\circ})}{\partial T}\right)_P = \Delta S^{\circ} \quad \text{.....(2.51)}$$

By taking the first derivative of E-T relation with respect to temperature and substituting the same in the above equation, we get the entropy of reaction by applying the following equation.

$$nF\frac{dE}{dT} = -\Delta S^{\circ} = \frac{-nFE - \Delta H^{\circ}}{T} \quad \text{.....(2.52)}$$

Once the entropy of reaction is known, the enthalpy of reaction can be obtained by using the above equation itself.

The heat capacity change at constant pressure of the overall reaction can be computed by using the relation given below.

$$\Delta C_p = nFT\frac{\partial^2 E}{\partial T^2} \quad \text{.....(2.53)}$$

Summary:

The detailed description of Knudsen effusion mass spectrometry was given. Other methods based on the effusion technique were also explained briefly. Other techniques namely, calorimetry and EMF method were also discussed. For the present thesis, Knudsen effusion mass spectrometry was used to generate thermodynamic properties of U-Ga, U-Pu-Zr and Ru-Te

systems and the inverse drop calorimetry was employed to measure the enthalpy increments of one of the compounds of U-Ga system, namely, U_3Ga_5.

References:

1. The Characterisation of High Temperature Vapours, Ed. J. L. Margrave, Wiley, New York, (1967), Chapter, P 20.
2. H. Mc Leod, Phil. Mag., 48 (1874) 110.
3. W. J. H. Moll and H. C. Burger, Z. Tech. Phys., 21 (1940) 199.
4. M. Pirani, Verhandl. Duet. Phys. Ges., 8 (1906) 686.
5. F.E. Pointdexter, Phys. Rev., 26 (1925) 859
6. L.L. Hirst and A.R. Olson, J. Am. Chem. Soc., 51 (1929) 2398.
7. F.S. Daiton and H.M. Kimberley, Trans. Faraday. Soc. 46 (1950) 912.
8. J.W. Hastie, D.W. Bonnell and E.R. Plante, High Temp. Sci. 13 (1980) 257.
9. Physico-Chemcial Measurements in Metal Research, Ed. R.A. Rapp, Part I, Techniques in Metal Research, Vol. IV, Series Ed. R.F. Bunshah (Wiley, New York, 1970).
10. K.D. Karlson, ref. [1], Chapter 5.
11. E.D. Cater, ref. [9], Chapter 2A.
12. K.D. Carlson, The Molecualr and Viscous Effusion of Saturated Vapours, ANL-6156 (1960).
13. L. Brewer and J.S. Kane, J. Phy. Chem. 59 (1955) 105.
14. J.Y. Huang, P.W. Gilles and J.E. Bennet, High Temp. Sci. 17 (1984) 109.
15. J. Drowart, C. Chatillon, J. Hastie and D. Bonnel, Pure & Appl. Chem., Vol.77, No.4 (2005) P.683.
16. K.D. carlson, ref. [12], Chapter 3 P. 21.

17. a. M. Knudsen, Ann. Physik 28 (1909) 75.

b. M. Knudsen, Ann. Physik 28 (1909) 999.

18. K.D. Carlson, ref. [12], Chapter 10 P. 207.

19. A.J.H. Boerboom in Mass Spectrometry, Ed. R.I. Reed Academic Press, London, (1965) P. 251.

20. D. Raj, L. Bencze, D. Kath, W.A. Oates, J. Hermann, L. Singheiser and K. Hilpert, Intermetallics 11 (2003) 1119.

21. K. Hilpert and K. Ruthardt, Ber Bunsenges. Phy. Chem. 91 (1987) 724.

22. R.D. Freeman, ref. [1], chapter 7.

23. Evan Copland, J. Chem. Therm. 38 (2006) 443.

24. R. Viswanathan, M. Sai Baba, D. Darwin Albert Raj, R. Balsubramanian and C.K. Mathews, Advances in Mass Spectrometry, 1985, Ed. J.F.J. Todd (John Wiley & Sons, 1986) Part B: p. 1087.

25. L. Brewer, Principles of High Temperature Chemistry, Proc. R.A. Welch Foundation Conf. Chem. Res., Houston, Texas, Vol VI, 1962, p. 47.

26. Introduction to Mass Spectrometry, Ed. S.K. Aggarwal and H.C. Jain, Indian Society for Mass Spectrometry (1997).

27. J. Drowart, in Mass Spectrometry, Proc. Int. School Mass Spectrom. Stefan Institute, Lubljana, 1969, Ed. J. Marsel, (1971) p. 187

28. P. Graber and K.G. Weil, Ber. Bunsenges. Phy. Chem. 76 (1972) 410.

29. O. Bernauer and K.G. Weil, Ber. Bunsenges. Phy. Chem. 78 (1974) 1339.

30. L.C. Wagner and R.T. Grimley, J. Phys. Chem. 76 (1972) 2819.

31. R.C. Miller and P. Kusch. J. Chem. Phys. 25 (1956) 860.

32. K. Hilpert, Structure and Bonding 73 (Springer-Verlag Berlin, 1990), p. 97.

33. G.De. Maria, Therochemistry and its applications to Chemical and Biochemical Systems, Ed. M.A.V. Ribeiro da silva (NATO ASI Series C, Mathematical and Physical Sciences; Vol 119, D. Reidel Publishing Company, Dordrecht, Holland (1984).

34. R. Viswanathan and K. Hilpert, Ber. Bunsenges. Phy. Cem. 88 (1984) 125.

35. E.D. Cater, in "Vapour pressure measurements" Chapter 2A: in "Techniques of Metals Research" Volume IV, Part I. Ed. R. A. Rapp, (Interscience Publishers, New York, 1970) p. 40.

36. K. A. Gingerich, J.E. Kingcade, Jr., M.J. Stickney and M.S. Chandrasekaraiah, J. Less-Common Met. 143 (1988) 373.

37. G.R. Belton and R.J. Fruehan, J. Phy. Chem. 71 (1967) 1403.

38. J. Tomiska and A. Neckel, Ber. Bunsenges. Phy. Chem. 88 (1983) 551.

39. J.L. Margrave. ref. 1.

40. D. Cubicciotti, J. Phy. Chem. 70 (1966) 2410.

41. J. Drowart and P. Goldfinger, Angew. Chem., Intl. Ed. 6 (1967) 581.

42. D.J.Frurip and M.Blander, J. Chem. Phys, 73 (1980) 509.

43. M. Boer and J. Singer, Nucl. Sci. Eng. 97 (1987) 344.

44. M. Boer and J. Singer, Report-KfK 3772, 1984.

45. M. Joseph, N. Sivakumar, P. Manoravi, Ann. Nucl. Energy. 31 (2004) 1163.

46. Chapter 15, "Laser Induced Vaporization Mass-spectrometry Studies on Refractory Materials at Ultra High Temperatures", M.Joseph, N.Sivakumar, P.Manoravi; in a book titled "Materials Under Extreme Conditions: Recent Trends and Future Prospects", Eds. Tyagi and Banerjee, Elsevier (2017), p.533-573.

47. W. Zielenkiewicz and E. Margas, Nauch. Appara. Sci. Instrum., 1 (1986) 55.

48. J. Rouquerol and W. Zielekiewicz, Thermochim. Acta, 109 (1986) 121.

49. W. Zielenkiewicz, J.Thermal Anal., 33 (1988) 7

50. R. Castanet, NATO-ASI, Kiel, August (1987) 16-27.

51. C. Wagner in; 'Advances in Electrochemistry and Electrochemical Engineering', P. Dalahay (ed), Vol (4) John Wiley, New York, (1966) P. 3.

52. T.J. Anderson, Thermodynamic and Kinetic studies of some Group III and Group V Elements and Alloys by Solid State Electrochemical Techniques, University of California, Berkeley, USA

53. A.M. Azad, Ph.D. Thesis, University of Madras.

CHAPTER 3

Commissioning of Knudsen Effusion Mass Spectrometer (KEMS) inside the glove box:

3.0. Introduction

Commissioning of a KEMS inside the glove box was one of the important activities of the chemistry program at IGCAR, for measuring vapour pressure and thermodynamic data of plutonium based systems. Quadrupole Mass Spectrometer (QMS) procured from M/s Hiden Analyticals, UK has been attached to the source chamber of the high temperature mass spectrometric set up located inside the glove box. Preliminary high temperature vaporisation studies were conducted with pure elements such as Chromium, Nickel and Zirconium. These experiments served to understand the reliability of the KEMS in conducting the meaningful vaporisation studies.

Subsequent to the experiments with the pure elements, an oxide system namely, MnO, was taken up. The studies with MnO was planned to gain experience in using the instrument to investigate the oxide system, since the actinide oxide systems need to be studied in the future. MnO was selected as it is a congruent vaporising system. Subsequently the vaporisation studies on uranium and U-Zr alloys were started to have some experience on measurements on alloys prior to taking up ternary alloy samples of U-Pu-Zr (a potential metallic alloy fuel of future FBRs in India). All the above said experiments were performed by keeping the glove box in open condition.

3.1. High purity inert atmosphere glove box system

A glove box is required for handling radioactive samples. The nuclear fuels such as U, Pu mixed carbides or nitrides and the metallic alloys (U-Pu-Zr) are sensitive to moisture and oxygen. Hence it is necessary to maintain an inert atmosphere inside the glove box. The oxygen

and moisture concentrations in the inert gas atmosphere inside the glove box should be maintained less than 10 ppm, in order to protect the samples from oxidation and hydrolysis. Generally the inert gas used is nitrogen, helium or argon [1]. Nitrogen boxes are cheap to maintain; but nitrogen will react with alkali metals. Nitrogen is also not favoured much for high purity systems since this gas will have high oxygen impurity. Helium is costly and special equipments are needed for recirculation. Argon is the ideal from all aspects like the cost, purity and ease of operation. Usually when an inert atmosphere glove box is used for handling non-radioactive materials, the pressure is maintained between 20-40 mm WC (water column) above the ambient, in order to prevent the leakage of moisture and oxygen impurities into the glove box from the ambient. However, for handling radioactive materials which are air sensitive, inert atmosphere glove box will be maintained negative with respect to ambient, so as to prevent any leak of radioactivity into the laboratory area.

The stainless steel glove box available with us was of rectangular type, erected on four legs such that the glove box floor will be at a height of ~ 1m from the ground level. It had two large ports (circular, one on each width-side) to facilitate material transfer; six glass window panels (two on the ceiling and two on each length-side); and a metal-sheet forming the floor. Our design of KEMS was such that it can be wholly housed inside a glove box. The glove box floor and the width-side walls needed to be cut open at many places to cater to and fulfill different specific purposes. The openings on the floor were made to facilitate erection of the vacuum envelope (consisting of furnace and ion-source chambers) firmly on the glove box floor. Suitable elbows and adopters were used to connect each chamber to a separate high vacuum pump, positioned below the glove box floor. The openings on the width-side walls were made to provide for ports that will permit the electrical cables and water connections to be taken through.

The window glass panels on the length-side of the glove box had circular openings (four in each panel), which were used to fix full-arm butyl rubber gauntlets. Any operation inside the glove box will be performed by using these gloves once the glove box is made 'radio-active'.

Since the glove box commissioned in our lab was erected for experiments on radioactive samples, the inert gas pressure in the box needs to be maintained negative with respect to the ambient pressure, to keep the flow of direction of air towards the box. In case of any accident in the box or the breakage or the crack in the glass panels, the negative pressure in the box will not allow the radioactive materials stored inside the box to spread out to the laboratory environment. The box should be leak tight enough to minimise the ingress of air. The stringent limit for leak rate is <0.05 vol% of the box volume per hour at a differential pressure of 100 mm WC with respect to the ambient pressure [2]. The leak rate of the box was checked, after closing it with the glass panels and full arm gauntlets in negative pressure mode with respect to the ambient and found to be within the acceptable limit.

3.1.1. Maintenance of purity of argon gas

The periodic monitoring of the purity of the gas with respect to the oxygen and moisture is necessary to avoid any reaction of the air sensitive sample with them during handling operations. Oxygen and moisture impurities are measured by suitable sensors periodically. Air ingress across the joints makes the inert gas in the box impure and increases the concentration of oxygen and moisture in the gas. Hence, the excess moisture and oxygen should be removed. For this purpose, a purification tower, made of stainless steel filled with 4A° molecular sieves and copper de-oxo catalyst, is employed. When impure argon gas is pumped through the tower, the molecular sieves trap moisture and the de-oxo catalyst removes the oxygen. Various oxygen scavengers like zirconium sponge, uranium metal, calcium etc., may also be used to remove the

oxygen [3]. But these are effective only at high temperatures and their regeneration is also not easy to carry out. But the advantage of the combination of molecular sieves and copper de-oxo catalyst is that these can be used at room temperature and their regeneration is also easy.

4A° molecular sieves and copper de-oxo catalyst get saturated with the impurities, namely, moisture and oxygen when the impure gas is continuously passed through the tower. Subsequently, the ability of the tower to purify the gas declines with time. Hence, the regeneration of the materials is necessary. The removal of moisture and oxygen is carried out by heating the tower to ~200°C and passing a mixture of Ar and H_2 (carrier gas and reducing agent). At high temperature the molecular sieves desorbs the trapped moisture whereas the hydrogen reduces the oxidised copper catalyst to release water. The water molecules liberated are carried away by argon and disposed of into the exhaust lines.

3.1.2. Glove box pressure control

The glove box pressure is maintained in the pressure range 20-40 mm WC negative with respect to the ambient, though such a condition renders maintaining the argon gas purity more difficult. Very high negative pressure is also not desirable, since it makes working with gloves very tedious and excessive negative pressure could lead to ballooning and even bursting of the gloves. A special pressure control system consisting of pressure gauge, two solenoid valves, argon supply system and control unit, is used to regulate the negative pressure in the range of 20 - 40 mm water column with respect to ambient. The control unit dictates opening and closing of these solenoid valves. The pressure of the glove box is continuously monitored using a photohelic gauge. If the negative pressure of the box exceeds 40 mm water column, the control unit actuates a solenoid valve on the argon supply line to feed argon gas to the box. If the negative pressure of the box becomes less than 20 mm water column, the control unit actuates a

solenoid valve on the argon gas exhaust line to reduce the pressure to the operating pressure range.

A stand by emergency exhaust system is provided to ensure that there is no leakage of radioactivity, in case of abnormal or sudden increase of glove box pressure due to incidents such as panel breakage, glove tearing etc. The emergency exhaust system comprises another photohelic gauge, a solenoid valve, a control unit and a blower to provide the suction.

3.2. Description of the HTMS inside the glove box

A schematic diagram of the vacuum envelope consisting of two chambers, one for housing the Knudsen cell furnace (Cell chamber) and the other for housing the QMS (Source chamber), is shown in Figure 3.1. The vacuum envelope remains wholly within the glove box and the two chambers are interconnected through a 4.0 mm diameter hole. A photograph of the HTMS facility inside the glove box is shown in Figure 3.2. A high vacuum is maintained in the cell chamber so that the probability of molecules in the effusing beam to collide with the molecules of the residual gases until they reach the ion source is extremely low. Similarly, the high vacuum maintained in the source chamber helps the ions formed in the ion source to have the mean free path several orders higher than the distance travelled by the ion so that they may not collide with the residual gases until they are collected in the collector housing. This is very much essential to get very good quality mass spectral data. Two diffusion pumps (~700 $L.S^{-1}$) are used for obtaining the high vacuum. These are backed by suitable rotary pumps. The residual pressures in the Knudsen cell furnace and ion source chambers are monitored by ionisation gauges and in the fore vacuum part by Pirani gauges (M/s Edwards, U. K). By making use of the provisions in the control electronics of these gauges, some safety interlocks necessary for smooth functioning of the equipment were incorporated.

3.2.1. Cell chamber and Knudsen cell furnace

In the cell chamber shown in Figure 3.1, the Knudsen cell furnace assembly rests on a small platform attached to an X-Y positioner through a shaft and bellows assembly as shown in

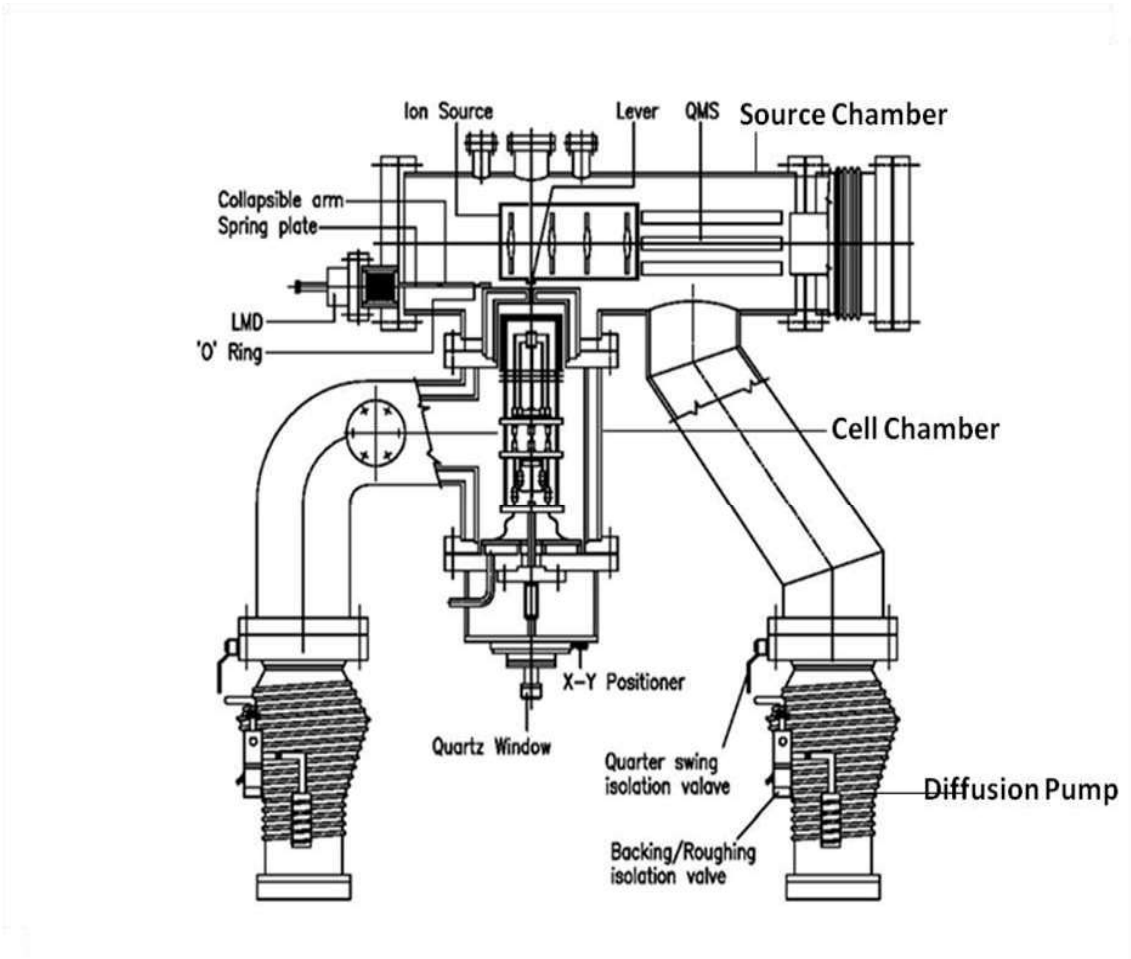

Fig.3.1 Schematic diagram of KEMS facility inside the glove box

Fig.3.2. Photograph of KEMS facility inside the glove box

A - Cell chamber; B – Source chamber; C – QMS mounted flange

Figures 3.3a and 3.3b [4]. The latter is attached to a water cooled flange having six feed-throughs for providing power to the furnace. The X-Y positioner makes it possible to align the Knudsen cell with the ion- source of the mass spectrometer. The entire chamber including the elbow that connects it to the high vacuum pump is an annular vessel so as to have water cooling. The ion-source chamber has a flange mounted QMS fixed to a conflat flange through a bellows-tie-rod device. This arrangement facilitates linear as well as angular alignment.

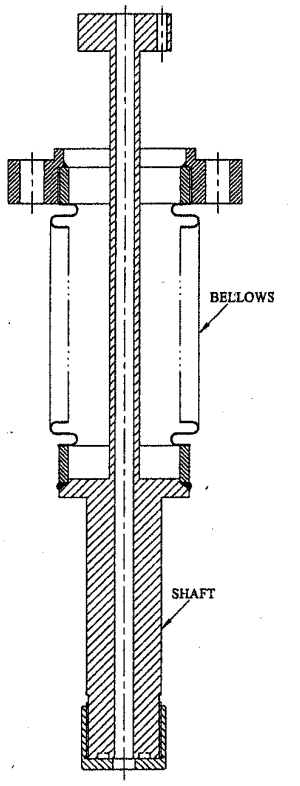

Fig.3.3a. Typical assembly of the shaft with the bellows and flange [4]

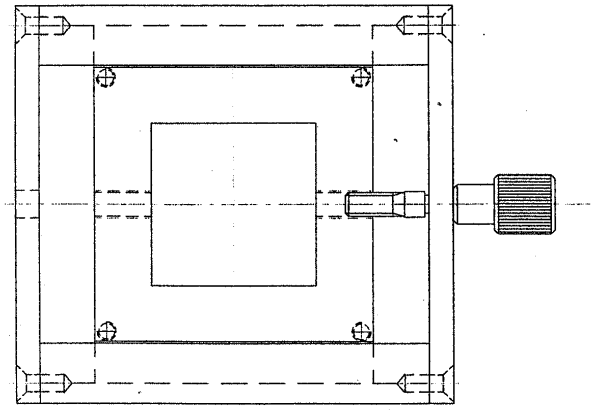

Fig.3.3b. Typical assembly of the X-Y translator [4]

The bottom end of the shaft is fixed with one quartz window. The top end of the shaft will be inside the chamber while the other end having the quartz window will be outside the chamber. The shaft is provided with a hole of 5 mm diameter to its entire length to enable the radiation from the black body hole to pass out to the pyrometer. The end of the shaft lying outside is sealed with an O-ring for achieving high vacuum in the chamber. The radiation emitted by the black body hole provided at the bottom of the crucible can be focused onto the pyrometer by deflecting it with a prism by 90º as shown in the Figure 3.4. The disappearing filament pyrometer is used for the measurement of the temperature of the black body. There are various methods of heating the sample such as the resistance heating, induction heating, electron bombardment (EB) heating etc. In the present work, EB heating was selected on the following considerations: Precise heating of the target and the attainment of the high temperatures at faster

heating rates; open and compact structure of EB furnace makes it readily compatible with the vacuum systems and good heat shielding can be given to aid in better temperature control.

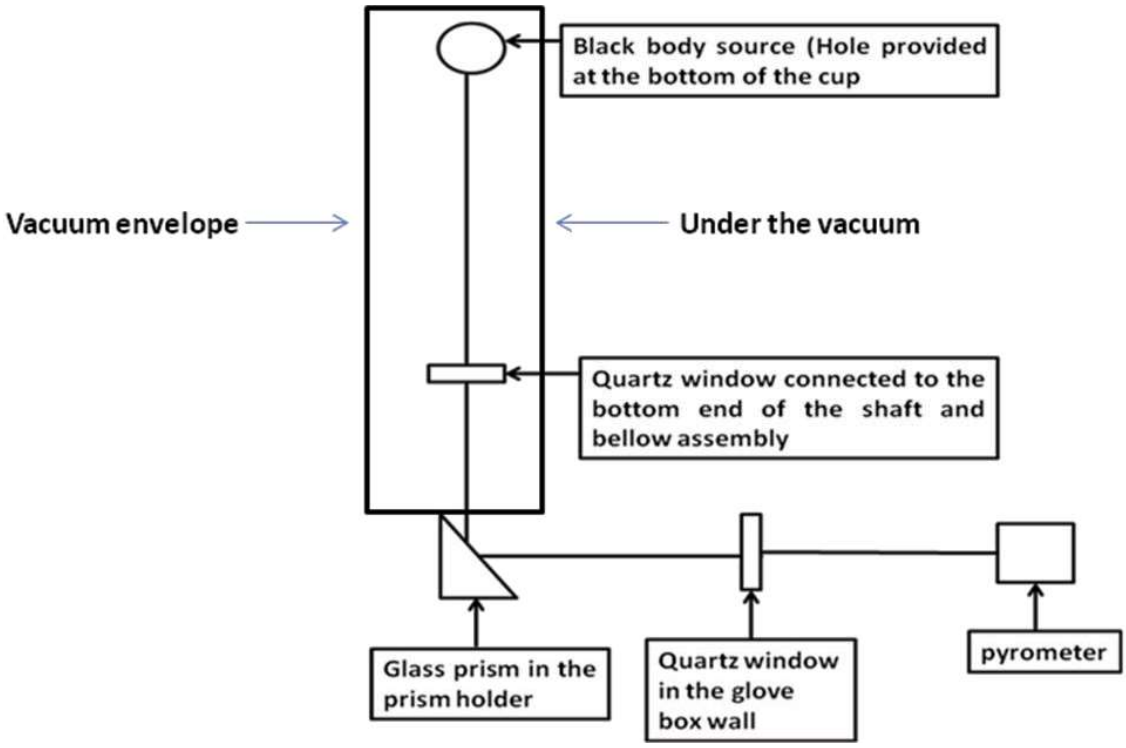

Fig. 3.4.Schematic of the alignment of prism holder with black body hole and pyrometer

A photograph of the EB furnace assembly is shown in Figure 3.5. It consists of Knudsen cell placed in an outer cup, which has three holes at the bottom such that the cup could be slid into W rods with a tripod arrangement. The cup is heated by radiation or by emission of electrons from two tungsten filaments surrounding it. It also has Ta heat shields all around. While the support rods in the EB are all mainly made of Ta and W, some components which would see $T \leq 1000$ K are made of Stainless Steel (SS). The heat shields help in maintaining the uniform temperature of the Knudsen cell keeps the power requirement less, minimises the out-gassing that would result from the heating of the surroundings otherwise, and protects the inner wall of

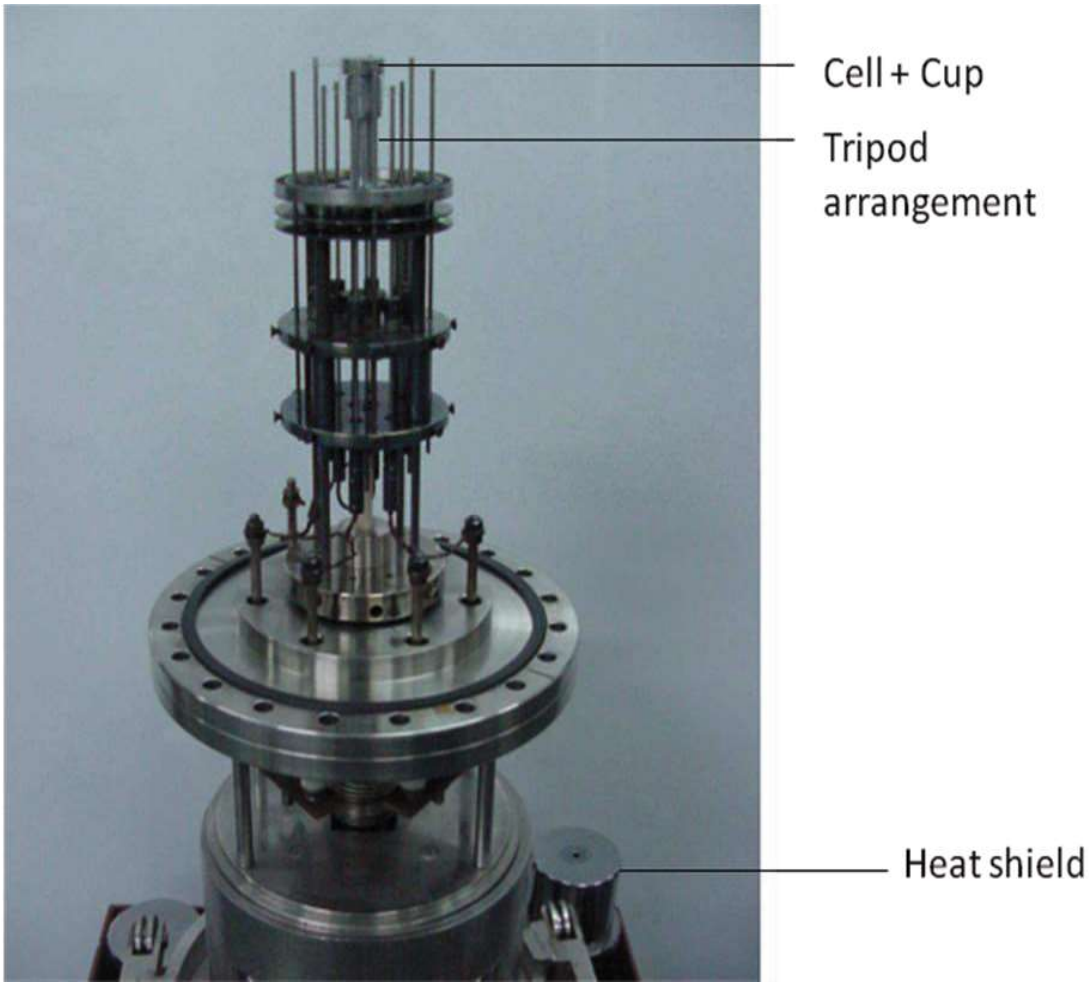

Fig. 3.5.Photograph of electron bombardment furnace [4]

the vacuum chamber from getting heated excessively. The double jacketed cell chamber is cooled by passing chilled water through the annular space. Cooling is also provided to the Knudsen cell furnace assembly flange at the bottom. The furnace could be safely heated to, and maintained at temperatures as high as ~ 2500 K. The power supply for the EB furnace is supplied

by a local manufacturer (M/s Static Power Systems, Mumbai). The filaments are heated by alternating current, and the electron bombardment of the Knudsen cell is achieved by keeping the latter at varying DC voltages depending upon the temperature requirement. A new EB power supply (M/s Autosys, Mumbai) which makes it possible to increase or decrease the filament currents and also the total power to desired values (in small increments) by touch screen control was also procured**.** In some of our earlier experiments, the power supply from M/s Static Power Systems was used. Subsequently, we have been using power supply from M/s Autosys.

The bottom flange of the Knudsen cell chamber is nearly at the level of the glove box floor. In order to take out EB furnace out of cell chamber for operations such as, to tie fresh filaments, to examine the residue of the sample after vaporisation or to load fresh sample, and even to service the whole or part of the furnace assembly, a pit was constructed on the glove box floor. The Knudsen cell furnace assembly is kept on a platform, the vertical movement of which (up and down) is accomplished by using a mechanised device, designed and fabricated in house and the device is shown in Figure 3.6 [4]. A ball screw of ~ 300 mm long and 15 mm diameter is used in order to have precise and stable movement. The nut of the assembly is connected to a base plate on which the EB furnace assembly is mounted. Effective movement of the furnace assembly is for a length of ~ 250 mm, which is sufficient for performing the above mentioned operations. The movement is fully guided with the use of two ball bearings attached to the top ring support and positioned inside the guiding grooves. The whole device is mounted on a 300 x 300 x 40 mm base. The base is connected to the glove box using a big SS bellows to take care of small deviations in the levels of the glove box base and the ground. The end flanges of the bellows are provided with leak tight ‘O’ ring joints. The rotary motion required for the screw is

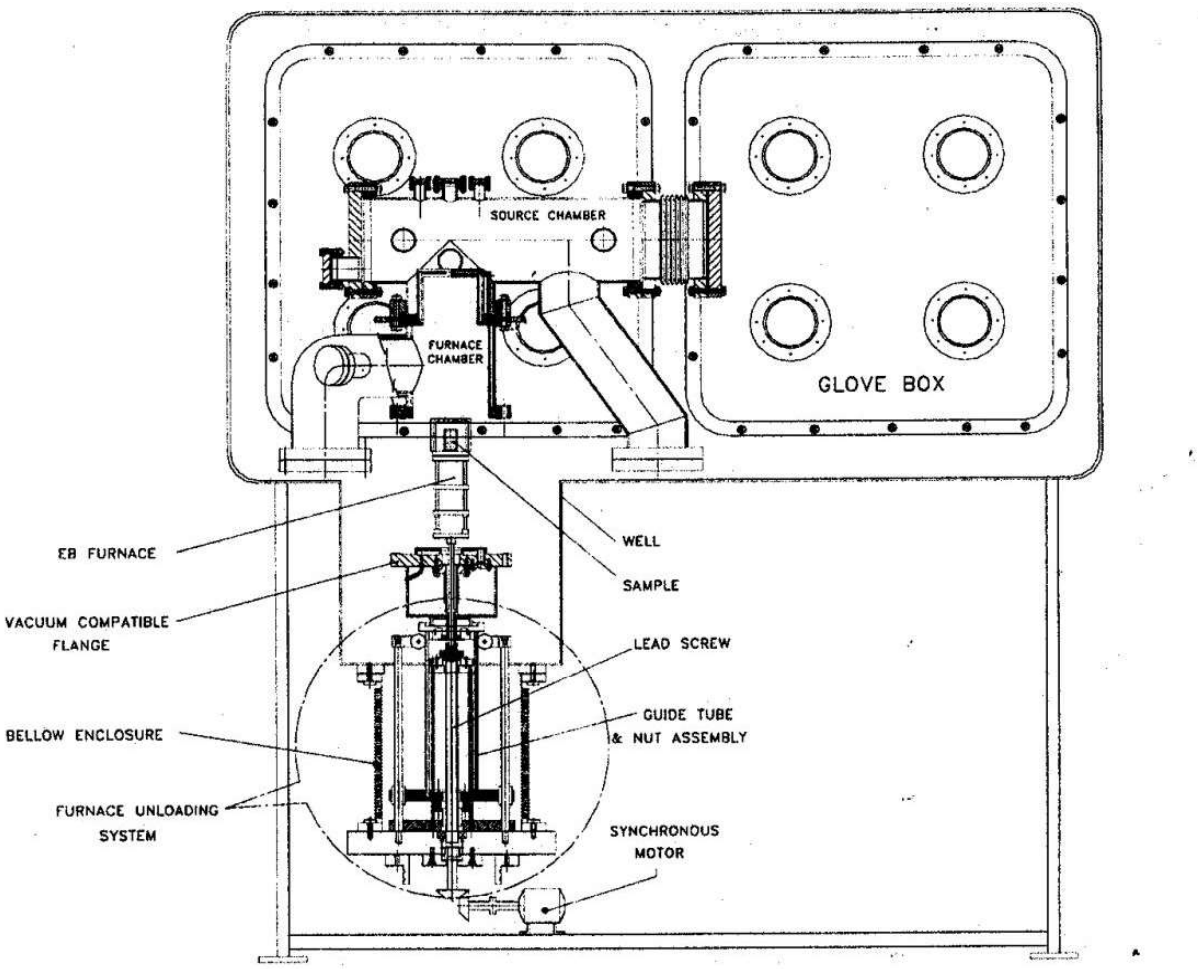

Fig. 3.6. Schematic of the vacuum chamber and Sample Change Device inside the glove box [4]

provided through a doubly sealed rotary shaft from the bottom of the thick SS base. Presently the movement is effected manually, but when connected to a stepper motor, automated movement can be achieved. Good alignment of the two flanges (one, that of the Knudsen cell chamber; and the other that of the Knudsen cell furnace assembly) could be obtained easily, as evidenced by the attainment of good vacuum within a reasonable time. Once the flange of the Knudsen cell furnace assembly is securely clutched to the flange of the Knudsen cell chamber, the platform is lowered to a height that will permit a prism stand to be slid into the base of an X-Y translator.

The furnace is placed on the top of the sample change which is moved up manually through the rotary shaft. The positioning of Knudsen cell with respect to the ion source orifice is very important to get the very high ion sensitivity. The furnace is heated to the temperature of 1000-1100 K and the alignment (perfect positioning) is achieved by looking through the prism holder kept over the window of the ion source chamber and with the help of x-y translator of the furnace assembly.

3.2.2. Source chamber

This houses Quadrupole mass spectrometer (QMS). The QMS lies just above the cell chamber and has three components, namely, ion source, mass filter and detector. The orifice of ion source, in which ionisation of the vapour species effusing from the orifice of K cell is effected, is located coaxial with that of the cell. The configuration of ion source is such that the directions of molecular beam from the cell orifice, electron emission from the ion source filaments, and the resulting positive ion beam are mutually perpendicular to each other. The positive ions generated are directed into the mass analyser (QMS) by applying suitable voltages and mass analysed according to their m/z ratio. The ions transmitted by the mass filter are detected by using a secondary electron multiplier operating in pulse counting mode.

3.3. Vacuum isolation

To be able to have the ion-source ON even when the Knudsen cell chamber is at ambient pressure (during sample changing), a specially designed vacuum isolation device was fabricated and installed and the schematics of which is displayed in Figure 3.7 [4]. The design is such that the connectivity between the Knudsen cell and the ion source chambers can be readily restored when the vacuum level in the Knudsen cell chamber is satisfactory. This essentially consists of a viton O-ring with 8.0 mm ID and 3.0 mm cross section mounted on an O-ring carrier plate. This O-ring is used for sealing off the Knudsen cell chamber from the ion source chamber. The O-ring carrier plate is fixed to a linear motion device (denoted as LMD1) of 50 mm travel length through a collapsible type arm. A spring plate keeps the collapsible arm in horizontal position leaving a small gap between the 'O' ring and the top surface of the Knudsen cell chamber, thus protecting the 'O' ring from any damage when the LMD1 is operated. During measurements, the LMD1 is kept fully retracted, in which position the O-ring carrier plate will be sufficiently away from the interconnecting hole (and thus also from the radiant energy of the high temperature furnace) that the vapor species from the Knudsen cell chamber can enter the ion-source region. When isolation of the two chambers is required, the LMD1 is operated to have it fully extended, in which position the 'O-ring carrier plate' lies exactly above the sealing surface (the top most surface of the Knudsen cell chamber). The top of the 'O-ring carrier plate' has a socket and when an appropriately dimensioned ball is placed on it and pressed hard, the collapsible arm bends in such a way that the 'O-ring carrier plate' rests on the sealing surface in a perfectly horizontal position and the sealing results. This ball is part of a lever, kept in a 90° orientation, and the lever is operated by another linear motion drive (denoted as LMD2). The ball has an 8.0 mm diameter opening which can permit unhindered flow of effusing vapor species into the ion source [4].

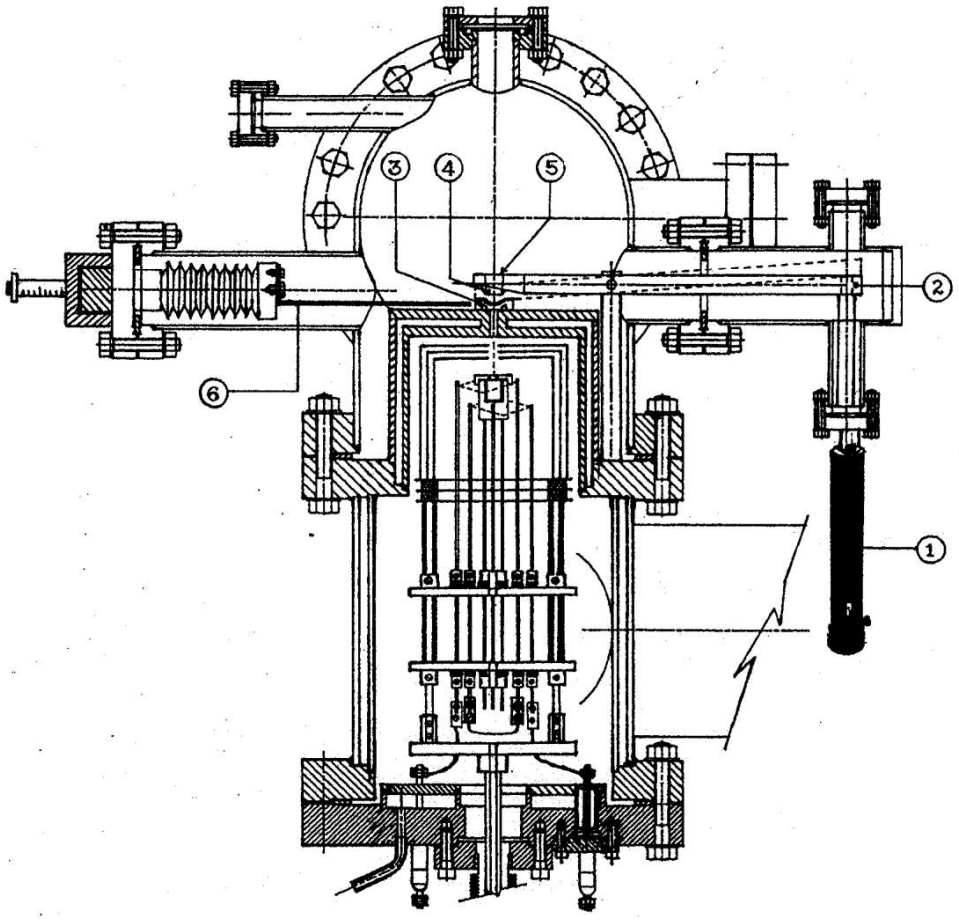

Fig.3.7.High Vacuum Isolation device [4]

1. Linear motion drive to position the lever (LMD2)
2. Lever - Bold line corresponds to normal operation position
   – Dotted line corresponds to vacuum isolation position
3. 'O' ring holder
4. Ball end of the lever
5. Hole provided inside the ball end for molecular beam passage
6. Molecular beam shutter (Linear motion drive provided for the actual operation of the molecular beam shutter is a pneumatically operated valve with 25 mm travel distance)

When the cell chamber is viewed from the front, LMD1 is located sideways and therefore can not be seen from this view, whereas LMD2 and molecular beam shutter are located opposite to each other and shown here.

3.4. Knudsen cells

Vaporisation studies involving the nuclear fuel systems are generally carried out at high temperatures (> 1000 K) for longer durations. Hence, the Knudsen cells used should exhibit high temperature stability and should not be reactive with the sample and the furnace atmosphere. The Knudsen cell material vapour pressures should be too low compared to those of the samples.

Generally the metallic cells are used for ceramic samples and ceramic cells are used for metallic samples. Suitable cells can be selected by considering the phase diagrams of the cell-sample combination.

3.5. Preliminary studies with different samples

Preliminary studies with different type of samples were carried out for gaining experience before closure of the glove box.

3.5.1. Pure elements

The main objective of carrying out the high temperature mass spectrometric studies with elements is to test the reliability of the instrument. It helped us to check: (a) its sensitivity i.e., the lowest possible pressure of vapour phase over the elements at which it can give rise to the shutterable peaks of ionic species in the mass spectrum; (b) to know whether the second law enthalpies of sublimation of the ionic species deduced by using it are in accord with the literature values or not; and (c) to examine its capability to obtain the temperature independent pressure calibration constants. The second law enthalpies and the pressure calibration constants are related to the reliability of the temperature measurements. The pressure calibration constants obtained from the above experiments are used to convert the measured ion intensities over the samples into partial pressures.

Generally, in KEMS studies, the sample taken in a suitable Knudsen cell is heated to the temperature which could be conveniently measured by the disappearing filament pyrometer. Subsequently the temperatures are raised in steps of 25 K and at each temperature, the mass spectrum of the effusing vapour phase is recorded by ionising the vapour species with electrons of fixed energy, looking for the shutterable peaks in the mass range for possible vapour species. From the mass numbers of the peaks observed in the mass spectrum of the vapour over the sample and the calculated isotopic abundances, the ionic species is identified. Ionisation efficiency (IE) curve for a given ion is obtained by plotting the measured ion intensity at the mass number of the ion against the electron energy. The appearance potential (AP) of the ion is obtained by extrapolating the linear portion of the IE curve. AP and the nature of IE curve help to establish the neutral precursor corresponding to the ionic species. Subsequently, the temperature dependence of intensity of the ionic species is measured as a function of temperature, to derive the thermodynamic properties such as vapour pressure, the enthalpy of reaction or formation of vapour species and condensed phases, Gibbs energy of reaction or formation of the vapour species and condensed phases etc.

3.5.1.1. Vaporisation studies with pure chromium

Chromium sample was taken in an alumina Knudsen cell fitted with alumina lid having the orifice of 0.5 mm diameter and placed into a tantalum outer cup with tantalum lid. From the mass numbers of the peaks observed in the mass spectrum of the vapour over the sample, the isotopic abundances and the appearance potentials, the neutral precursor was established to be Cr(g). Temperature dependence of ion intensities was carried out with respect to the major isotope, ^{52}Cr. In a given temperature dependence run, the ion intensity of $^{52}Cr^{+}$ was measured as a function of temperature. The first run of temperature dependence helped to arrive at the

temperature range over which reliable ion intensities could be recorded in the subsequent runs. The neutral species effusing out of the orifice were ionised with the electrons of energy 30 eV during the temperature dependence run. Overall, six runs of temperature dependence of ion intensity of $^{52}Cr^{+}$ were carried out in the temperature range 1287-1549 K. The logarithmic values of $I^{+}T$ of $^{52}Cr^{+}$ ion in a given run were least squares fitted linearly against the reciprocal of temperature as log ($I^{+}T$) = -A/T+B. The intensity-temperature relations obtained are provided in Table 3.1. The slope of the linear plot yielded the enthalpy of sublimation of chromium and the standard deviation of the slope was the error in the enthalpy of sublimation.

Table 3.1. Ion intensity temperature relations for Chromium

S.No	T/K	n*	log ($I^{+}T$) = -A/T +B		$\Delta_{sub}H_{app}$ (kJ/mol)	k' = p/($I^{+}T$) k'_{mean} x 10^{9} Pa/[(c/s).K]
			A	B		
chromium; log (p/Pa) = -20184/T + 12.22 [5]; 386 kJ/mol; p(min) = 3.4 x 10^{-4} Pa at 1287 K						
1	1321-1549	17	20081±226	20.72±0.16	384±4	2.69±0.20
2	1291-1531	18	20350±212	20.91±0.15	390±4	2.66±0.20
3	1287-1536	16	19971±221	20.59±0.16	382±4	2.96±0.21
4	1336-1528	13	20575±395	21.08±0.27	394±8	2.57±0.23
5	1315-1533	12	20535±304	21.06±0.22	393±6	2.53±0.20
6	1321-1549	17	20081±226	20.72±0.16	384±4	2.69±0.20

* n = no of experimental points; $\Delta_{sub}H_{app}$ = 388±7 kJ mol^{-1}; k' = 2.68±0.26 Pa/[(c/s).K]

The enthalpies of sublimation obtained for all the runs were found to be consistent with each other and in agreement with the literature data of 386 kJ/mol. The lowest measurable pressure in the case of chromium was 3.4x10^{-4} Pa at 1287 K. The pressure calibration constants

derived from all the runs were consistent with each other and the uncertainty in their values was within 10%.

3.5.1.2. Vaporisation studies with pure nickel

Similar to chromium experiments, nickel sample was taken in an alumina Knudsen cell fitted with alumina lid having an orifice of 0.5 mm diameter and placed into a tantalum outer cup with tantalum lid. From the mass numbers of the peaks observed in the mass spectrum of the vapour phase over the sample, the calculated isotopic abundances and the appearance potential, the neutral species was identified to be Ni(g). Temperature dependence of the ion intensities was performed with respect to the major isotope, ^{58}Ni. The electron energy of 30 eV was used for the ionisation of vapour species effusing through the orifice during the temperature dependence run. Overall five runs of temperature dependence of ion intensities of Ni^+ were carried out in the range 1384-1650 K. The enthalpy of sublimation was evaluated from the slope of the plot and the standard deviation of the slope was the error in the enthalpy of sublimation. The enthalpies of sublimation (419±10 kJ mol^{-1}) were found to be in agreement with the literature [5] enthalpy of sublimation of nickel (422 kJ mol^{-1}). From the experiments, the lowest pressure measurable for Nickel was found out to be $3.1x10^{-4}$ Pa at 1384 K and the variation in the values of the pressure calibration constants derived from the all the runs were within 30%.

3.5.1.3. Vaporisation studies over pure zirconium

Vaporisation studies of zirconium assisted in realising the capability of the furnace of the KEMS set up inside the glove box to reach high temperature of ~ 2250 K and gave the confidence that the KEMS set up inside the glove box can be employed for undertaking vaporisation studies on metallic alloy fuel systems.

Zirconium sample was taken in a tantalum Knudsen cell fitted with a tantalum lid having an orifice of 1 mm diameter placed inside the Knudsen outer cup. Ionic species observed in mass spectrum were Zr^+, ZrO^+ and $ZrOH^+$. Ion intensities of ZrO^+ and $ZrOH^+$ became too feeble to be detected with time. The neutral species was identified to be Zr(g) based on the mass number of the peaks observed in the mass spectrum, the calculated isotopic abundances and the appearance potential of the ion. Temperature dependence of ion intensities was carried out with respect to the major isotope, ^{90}Zr. The neutral species effusing out of the orifice were ionised with the electrons of energy 30 eV during the temperature dependence run. Vaporisation studies on zirconium were carried out both in solid and liquid regions. In the solid region, the temperature dependence of ion intensities of $^{90}Zr^+$ was carried out in the temperature range 1913-2117 K (five runs) whereas the temperature dependence runs in the liquid state were carried out in the temperature range 2129-2233 K (2 runs). The temperature range and the number of points are relatively smaller than those for earlier two elements (Cr and Ni). The enthalpies of vaporsation of zirconium corresponding to solid $\leftrightarrow$ vapour equilibrium (580±23 kJ mol^{-1}) were found to be in agreement with the literature value (590 kJ mol^{-1}). Likewise, the enthalpies of vaporisation of zirconium corresponding to liquid $\leftrightarrow$ vapour equilibrium (570±25 kJ mol^{-1}) were also found to be in agreement with the literature value (580 kJ mol^{-1}). The lowest pressure that could be measured in the case of zirconium was $9x10^{-5}$ Pa at 1913 K.

3.5.2. Measurements with MnO(s)

MnO(s) was chosen with an objective that it will provide an experience to study an oxide based system. MnO(s) is assumed to vaporise congruently [6]. However, a question arose about the congruently vaporising nature of MnO(s) when the vapour pressure data for MnO(g), Mn(g)

and $O_2(g)$ reported by Matraszek et al. [6] were analysed. The authors [6] had considered two independent equilibria which are given below:

$$MnO(s) \rightleftharpoons MnO(g)$$

$$MnO(s) \rightleftharpoons Mn(g) + 1/2O_2(g)$$

The values of O-Mn ratio in the effusate (as deduced from the pressure-temperature relations reported in that paper for MnO(g), Mn(g), $O_2(g)$ in the temperature range 1535-1782) are ~143 (1535 K) and ~2.88 (1782 K). On the other hand, the value calculated for the temperature 1700 K is ~ 3.93. Thus the values were found to be not close to 1 which is a necessary condition for congruent effusion of MnO(s). In the present study, MnO (M/s Sigma Aldrich, USA; purity 99.99 %) was used. Four different Knudsen cell combinations were used to contain the sample, each placed in a tantalum outer cup and heated by electron bombardment. Totally, four series of vaporisation experiments were performed namely, the sample contained in an alumina Knudsen cell (series 1), in an alumina cell with a platinum liner (series 2), in a platinum Knudsen cell (series 3) and in a tantalum Knudsen cell (series 4). In the first three series of experiments, O_2^+ was the principal shutterable ion to begin with, as the samples were heated from room temperature; but its variation with time as well as temperature was different in each series. This was the case with other ions Mn^+ and MnO^+ as well. This might be caused by small amounts of $Mn_3O_4(s)$ in the sample [6]. Another reason for this phenomenon could be an over-stoichiometry of O in the initial sample which was reduced under low oxygen pressure in the Knudsen cell [6].

3.5.2.1. Experiment using alumina cell (Series 1)

As the sample was freshly heated, shutterability in the intensity of O_2^+ was observed from 1500 K, but there was a steady decrease in $I(O_2^+)$ with time for every increase in temperature before becoming indistinguishable from the background (at 1700 K). In the case of Mn^+,

intensities became measurable from 1460 K, but I(Mn^+) showed a monotonic decrease after every temperature increase before becoming stable at each temperature. At one temperature, the I(Mn^+) was also measured as a function of electron energy in the range 5-25 eV to record the ionisation efficiency curve and subsequently to deduce the appearance potential of Mn^+ ion. The appearance potential derived from the IE curve was 8.87 eV and was higher by ~ 1.2 eV than the literature of 7.64 eV. From the mass and appearance potential, Mn(g) was found to be the neutral precursor of Mn^+. The ionisation efficiency curve for Mn^+ indicated the maximum ion intensity at ~ 17eV. Hence, further studies were carried out at the electron energy of 17 eV.

Temperature dependence of ion intensities of Mn^+ ions was carried out in two temperature ranges 1469 – 1591 K (four runs; set 1) and 1513-1697 K (two runs; set 2) at an electron energy of 17 eV. Ion intensity-temperature relations are shown in Table 3.2. The values of apparent enthalpies of sublimation of Mn(g) obtained in these two temperature ranges show a reasonable agreement within a particular set, but a huge difference (~128 kJ) between two sets of data. The sample after the low temperature measurements (1469 – 1591 K) was taken out and XRD analysis of the residue showed peaks corresponding to those of MnO(s). An important observation at the end of the measurements in the high temperature range 1513-1697 K was that the sample appeared to have melted, strongly stuck to the bottom of the cell, and could not be taken out for XRD analysis. Furthermore, the sample also appeared to have crept out of the Knudsen cell. What caused the melting or different apparent enthalpies in different temperature ranges remain unclear.

3.5.2.2. Experiment using platinum liner inside alumina cell (Series 2)

The next series of experiments were performed with a platinum liner placed inside the alumina cell with a reasoning that direct contact of alumina and MnO might have caused the

sample to get firmly stuck with the Knudsen cell. The experiments were conducted in the temperature range 1472- 1701 K. The electron energy of 17 eV was used for ionising the neutral species effusing from the orifice. The ion intensity-temperature data are shown in Table 3.3. Since the ion intensity of O_2^+ disappeared at the temperature of 1699 K in the experiments carried out with the sample taken in alumina Knudsen cell with alumina lid, the ion intensities of Mn^+, MnO^+ and O_2^+ were recorded at different temperatures as the sample temperature was slowly increased to 1701 K and it was maintained at that temperature for ~2.5 h to see the evolution of the O_2^+ ion intensity with time. As seen from the Table, the ion intensity of O_2^+ did not reduce to zero and those of Mn^+ and MnO^+ showed an increase. The ion signal due to O_2^+ remained the highest even at T ~ 1700 K (three times higher than Mn^+) and also shutterable. MnO^+ was also observed (~ 45 times smaller than Mn^+). Inference from series 2 was that, while

Table 3.2. Intensity-temperature relations for Mn^+ ion (series 1)

T/K	No of points	$\log (I^+T) = -A/T+B$		ΔH (kJ/mol)
		A	B	
1469-1589	9	32232±744	27.16±0.49	617±14
1480-1591	10	33274±1027	27.76±0.66	637±20
1481-1589	10	34575±1003	28.60±0.65	662±19
1477-1584	9	33122±1980	27.80±1.29	634±38
1513-1671	8	26712±981	23.29±0.62	511±19
1526-1697	10	26532±504	22.73±0.31	508±10

the Pt foil did help in prevention of disappearance of O_2^+ and also of reaction with alumina crucible, the orifice clogging did occur which was attributed to reaction of the condensate (or its liquid form) with alumina lid.

3.5.2.3. Experiment using platinum Knudsen cell (Series 3)

The third series of measurements was carried out by loading the sample in a platinum Knudsen cell. The sample was heated to relatively high temperature of 1633 K and subsequently the temperature was slowly raised in steps. The entire experiment was carried out in the temperature range 1633-1768 K. As in the previous experiments, the electron energy of 17 eV was used for ionisation of the neutral species. The pressure calibration constant derived from the vaporisation studies over pure chromium was used to convert the ion intensities into pressures. The Table 3.4 shows the variation of different ionic species with time as a function of

Table 3.3: Intensity-temperature data for Series 2 experiments

Time	T/K	I(Mn^+)	I(MnO^+)	I(O_2^+)
0 min	1472	0	0	1366
48 min	1472	0	0	1808
0 min	1511	72	0	3345
40 min	1546	120	6	4106
	1593	354	23	6387
	1621	705	38	13564
	1661	1518	56	23324
0 min	1701	2637	80	29341
168 min	1701	4436	98	29367

temperature along with O-Mn ratio. The data revealed that at a given temperature, the ion intensities of manganese containing vapour species remained approximately constant or increased marginally with time whereas the ion intensities of O_2^+ ions started diminishing with time, thereby, O-Mn ratio getting reduced towards the congruent effusion condition. The orifice was not clogged. But, the platinum Knudsen cell got welded to the tantalum outer cup lid. Hence, the sample could not be retrieved out of the cell for visual examination or analysis. The decrease in O-Mn ratio with time, as can be seen from Table 3.4, points towards congruent effusion. The rate of movement of O/Mn ratio towards congruency seems to be very slow. It may require a lot of time for the sample to achieve the congruency. It is clear that further experiments are required with an appropriate strategy, which will help prevent loss of Knudsen cell or the outer cup, which will permit XRD analysis of the vaporisation residue.

3.5.2.4. Experiment using tantalum Knudsen cell (Series 4)

Fourth series of experiment was started with the sample in a tantalum Knudsen cell. But in this case, Mn^+ ion was observed at low temperature whereas the shutterability could not be seen for O_2^+. This observation was opposite to what was seen in other cases. From all the above set of experiments on MnO, no definite conclusion could be drawn. Hence the experiment was discontinued.

3.5.3. Measurements with Fe-Al (40 at % Al) Alloy

These measurements were planned to gain experience on vaprisation studies on metal alloy based system. Earlier Darwin [4] had observed that the isotopic composition of Xe measured by the Extrel QMS was slightly different from that obtained employing the Micromass 30 BK magnetic sector mass spectrometer available in our lab. His concern was that, even for an

Table 3.4. Evolution of O/Mn ratio as a function of time at different temperatures for Series 3 experiments

	Time	T/K	I(Mn^+)	I(MnO^+)	I(O_2^+)	P(Mn)* 10^{-3} /Pa	P(O_2) /Pa	p(MnO* 10^{-4} Pa	O/Mn
Day 1	0 mins	1633	345	35	52902	1.13	3.06	1.48	6374
	46 mins	1633	385	31	48137	1.27	2.79	1.31	5292
	0 mins	1658	798	44	67021	2.66	3.94	1.88	3651
	18 mins	1658	842	45	64083	2.81	3.77	1.93	3314
	0 mins	1719	1547	94	88814	5.35	5.42	4.17	2481
	210 mins	1719	2155	95	63337	7.46	3.86	4.22	1293
Day 2	0 mins	1660	1309	55	36001	4.37	2.12	2.36	1210
	32 mins	1660	1262	48	35840	4.22	2.11	2.06	1255
	0 mins	1714	2377	104	53912	8.20	3.28	4.60	996
	333 mins	1714	2667	98	41743	9.20	2.54	4.34	693
Day 3	0 mins	1716	1862	54	34123	6.43	2.08	2.39	819
	63 mins	1716	1770	58	34510	6.12	2.10	2.57	868
	0 mins	1768	6068	217	86468	21.60	5.42	9.91	632
	26 mins	1768	7821	235	70416	27.84	4.42	10.73	402
Day 4	0 mins	1767	8357	253	76939	29.73	4.82	11.54	411
	88 mins	1767	8427	243	72299	29.98	4.53	11.09	384
	0 mins	1713	2950	77	27970	10.17	1.70	3.41	425
	31 mins	1713	3022	84	26974	10.42	1.64	3.72	400

element the isotopic composition could be slightly altered, whether there could be a serious error arising due to mass dependent transmission while dealing with two or more elements (or monomeric and polymeric species). Hence, to address the above concern, he selected Fe-Al alloy (with 40% Al) for carrying out the vaporisation studies using the KEMS with Extrel QMS. He indicated two main reasons for choosing this composition: (1) He could measure ionic species of both elements (whose mass numbers differ by a factor of two) and (2) Results for this alloy had been reported by other two groups, well known for reliable KEMS measurements.

In the present study, the vaporisation experiments on the same alloy were carried out using the KEMS presently equipped with a QMS from M/s Hiden Analyticals, UK to find out whether the results from QMS has mass dependence. Table 3.5 compares the results obtained by us over the Fe-Al alloy sample (obtained from FZ, Juelich, Germany) taken in an alumina Knudsen cell with those obtained by these groups using magnetic sector based KEMS instruments. The measured ion intensity ratio in this study agrees reasonably well with the previously measured by Darwin [4] in our lab, those measured at FZ, Juelich [7] and by Jacobson and Mehrotra [8]. The results of this study indicate that our KEMS facility is good enough to conduct the vaporisation studies on metal alloy system.

Table 3.5. Comparison of results of mass spectrometric measurements over Fe-Al alloy (40 at.% Al) with that of the reported values

$I(Al^+)/I(Fe^+)$	Reference
32.5 (at 1547 K)	Darwin et al 2002 [7]
30.0 (at 1639 K)	N. S. Jacobson [8]
33.1 (at 1481 K)	N. S. Jacobson [8]
32.6 (at 1573 K)	Darwin 2008 [4]
33±4 (1350 to 1511 K)	Present study
35 ±4 (1370 to 1503 K)	Present study

3.5.4. Measurements with pure uranium

Uranium is highly susceptible to oxidation and metallic uranium is always having a superficial layer of oxide during handling in atmospheric air. Hence, the following procedure was followed to remove any oxide layer formed. The sample stored initially in oil was cleaned with acetone. Then it was immersed in concentrated nitric acid to etch the oxide layer. The loading of the sample in the Knudsen cell and placing it under high vacuum were completed in a short time to avoid any oxidation, (subsequent to cleaning), as these processes were carried out at atmospheric condition, as the GB was kept in open condition.

For the first set of measurements, the uranium sample was taken in a tantalum Knudsen cell and then placed into the tantalum outer cup with tantalum lid. Three ions (U^+, UO^+ and UO_2^+) were observed in the mass spectrum of the equilibrium vapour over the sample. Ionisation

efficiency (IE) curves for all the three ions were obtained by measuring their ion intensities as a function of electron energy, to determine the appearance energies of all the three ions. The appearance potentials were derived (by extrapolating the linear portions of the IE curves to the X-axis [electron energy]) to be 6.8 ± 0.5, 6.6 ± 0.5 and 6.4 ± 0.5 eV for U^+, UO^+ and UO_2^+ respectively. The values obtained were slightly higher (within 1 eV) than those reported in the literature [12]. The values of appearance potentials indicated that all the three ions were formed due to simple ionization of the neutral precursors namely, U(g), UO(g) and UO_2(g). The temperature dependence of ion intensities of three ions were measured at electron energy 10 eV which is below the dissociation threshold of U-O gaseous species.

The ion intensities of UO^+ and UO_2^+ were consistently higher than that of U^+ ions. The ratios UO^+/U^+ and UO_2^+/U^+ were calculated to be 23 and 2.5 respectively at 1900 K. The above results and the ion intensities remaining stable for nearly four hours at the temperature of 2023 K indicated that the sample studied might have been actually a biphasic mixture of (U-O)(l) and UO_{2-x}(s) [11-14]. The apparent enthalpy of sublimation of the three species derived using the second law method was found to be in reasonable accord with the literature values for the two phase field, but the ratio of ion intensities were somewhat higher in our experiments. Table 3.6 shows the salient comparison. Visual observation of the furnace assembly at different times led

Table 3.6. Comparison of ΔH_{app} obtained results on vaporization studies over biphasic mixture of U(O) and UO_{2-x}

Ion (i)	ΔH_{app}/(kJ/mol)			Appearance energy /eV		$I(i^+)/I(U^+)$		
	This work[1]	Pattoret et al [11][2]	Ackermann et al[12][3]	This work	Ref.12	This work	Ref.11	Ref.12
U^+	497±42	540±8	491±6	6.8±0.5	6.1±0.3	1	1	1
UO^+	541±49	571±6	515±6	6.6±0.5	5.7±0.4	23	10	18
UO_2^+	626±56	638±6	577±6	6.4±0.5	5.5±0.4	2.3 to 2.7	1	1.4

[1] The values of enthalpy of vaporisation reported are the mean of the enthalpies of vaporisation obtained for four runs carried out at electron energy of 10 eV in the range 1756 -2018 K.

[2]Data of Pattoret et al have been reported for the reference temperature of 0 K

[3]Data of Ackermann et al have been obtained from the measurements in the range 1580-2400 K

us to following inferences: a) heating up to 1473 K (70 K above melting temperature of uranium) showed no evidence of creep of the sample or freeze of different parts –Knudsen cell, its lid, outer cup, and its lid could all be easily separated; b) when once heated to T = 1920 K, the Knudsen cell could not be opened, nor could it be taken out of the outer cup; c) keeping T = 2023 K for long time resulted in sample creeping out of the outer lid.

3.5.5. Measurements with U-5 wt. %Zr

Before loading the U-Zr sample, it was cleaned using the following procedure. The sample as received was immersed in concentrated nitric acid to remove oxide deposits on its surface. Then the sample was cleaned in distilled water. It was wiped with a tissue paper to remove the water sticking to it. The sample was loaded in a tantalum Knudsen cell placed in another tantalum outer cup and then introduced into the vacuum chamber, as immediately as possible. The ionic species observed in the mass spectrum of the equilibrium vapour were U^+, UO^+, UO_2^+, Zr^+ and ZrO^+. The intensities of ionic species of zirconium and UO_2^+ were too feeble to carry out any temperature dependence of these species.

Temperature dependence of ion intensities of U^+ and UO^+ was carried out in the temperature range 1645 – 1840 K for six days at electron energy of 10 eV. The values of apparent enthalpy of vaporisation of U^+ and UO^+ (mean of enthalpies obtained for six days) were 486 ± 27 and 266 ± 26 kJ/mol. The enthalpy of vaporisation of U^+ ions over the alloy was slightly lower than that over the pure uranium (497±42 kJ/mol). They were comparable to each other within the uncertainties in the individual values. The enthalpy of vaporisation of UO^+ ion was very much lower than that of UO^+ (541±49 kJ/mol) over two phase region. The UO^+/U^+ ratio was also much lower (~ 1 at the highest temperature and ~ 3 to 4 at the lowest temperature). On examining the Knudsen cell assembly, it was found that Knudsen cell and its lid were tightly stuck together. There was clear evidence of creep of the sample onto the Knudsen cell lid as well as the outer cup lid. That we were able to measure U^+ and UO^+ over U-Zr sample at lower temperatures than over elemental uranium leads us to suspect whether it was the sample-creep out of the lid, which was the reason for this unusual result. The creep out is not due to the temperature gradient in the Knudsen cell assembly. It was verified by carrying out the

vaporization studies on pure chromium. The enthalpy of vaporization obtained in this experiment was in accord with the literature value for pure chromium. No condensation of the vapour onto the Knudsen cell lid as well as the outer cup lid was noticed.

3.6. Summary

The results obtained from vaporisation studies on pure elements were found to be satisfactory and gave the confidence that the KEMS instrument inside the glove box can be used for generating reliable vapour pressure data of alloy systems. The vaporsiation studies on MnO could not be fully completed and no logical conclusion could be arrived at. But we have gained experience in using the KEMS for studying the oxide system. The investigation of U and U-Zr helped to gain some more experience of KEMS studies on these systems. The results also indicated that it is very important to carry out the experiments on such air sensitive sample in a high purity GB so as to avoid the oxide formation.

As indicated above, all the preliminary experiments described in this chapter were carried out under the glove box open condition. Subsequent to the above experiments, the GB was closed and the leak rate of the box was checked (i.e., after closing it with the glass panels and full arm gauntlets) at a differential pressure of 100 mm WC negative with respect to the ambient. The leak rate was found to less than the permissible limit of 0.05 vol% of the box per hour. As is necessitated for radioactive glove boxes, all the gas inlets and outlets were fitted with High Efficiency Particulate (HEPA) filters. They were tested by producing an aerosol and counting the number of particles before and after the filter. All the filters exhibited an efficiency of ≥ 99.9% for particles of 3 micron size and the glove box was certified to be fit for handling radioactivity. The box was flushed with argon gas to convert it in inert type. Oxygen and

moisture in the gas was decreased to less than 10 ppm by circulating it through the purification tower.

References

1. Selection and Design of a High Purity Inert Atmosphere System for the Plutonium Fuel Fabrication Glove Box Train, S. Majumdar, G.L. Goswami, K.C. Vas, M.S. Ramkumar and P.R. Roy, Report no: BARC/I-826 (1985).
2. Calorimetric Studies on Some Alloys of Interest in Nuclear Industry, K. Nagarajan, (1991), Ph.D. Thesis, University of Madras.
3. A Recirculating Argon Atmosphere Dry Box for Handling Pyrophoric and Hygroscopic Materials, D.D. Sood and A.V. Hariharan (1969), BARC Repot 396.
4. D. Darwin Albert Raj, Ph.D. Thesis, University of Madras (2008).
5. C. B. Alcock, V. P. Itkin and M. K. Horrigan, Can. Metall. Quart., 23, 309 (1984).
6. A. Matraszek, M. Miller, L. Singheiser and K. Hilpert, J. Euro. Ceram. Soc, 24 (2004) 2649.
7. D. Darwin Albert Raj and D. Kath, Research Record 25 June 2002, FZ, Juelich (K. Hilpert).
8. N. S. Jacobson and G. H. Mehrotra, Met. Trans. B, 24 (1993) 481.
9. A. Pattoret, J. Drowart and S. Smoes, Trans. Faraday Soc, 65 (1969) 98.
10. R. J. Ackermann, E. G. Rauh and M. S. Chandrasekaraiah, J. Phys. Chem. 73 (1969) 762.

CHAPTER 4

High Temperature Mass Spectrometric and Calorimetric Studies on U-Ga system

4.0. Introduction

In nuclear technology, pyrochemical reprocessing of spent fuel is regarded as an alternate method to aqueous processing, especially for metallic fuels. The reprocessing is generally conducted in molten salt medium (chlorides), which are known to possess high radiation and thermal stability. It is important to retrieve the valuable actinides left in the spent molten salt so as to enhance the energy derived from these precious heavy elements. One of the methods followed for extracting the actinides involves the equilibration of the spent molten salt with liquid Ca-Ga alloy [1]. Calcium acting as reducing agent, reduces the actinides in trivalent states to the metals which in turn react with gallium forming actinide-gallium alloys. Hence, it is important to study the vaporisation behaviour and derive thermodynamic properties of such actinide-gallium alloys to understand their stabilities. Accordingly, in the present work, Knudsen effusion mass spectrometer [KEMS] (also known as high temperature mass spectrometer [HTMS]) has been used to study U-Ga system to derive the thermodynamic properties of uranium-gallium intermetallic compounds.

The recent phase diagram of U-Ga binary system is shown in Figure 4.1.1 [2, 3]. According to this, there are three intermetallic compounds U_3Ga_5, UGa_2 and UGa_3 with U_3Ga_5 as the most U-rich phase. However the phase diagrams reported previously showed either U_2Ga_3 [4] or UGa [5] as the most U-rich phase. The available thermodynamic data reported in the literature were based on the phase diagrams reported in references [4] and [5]. These data had been

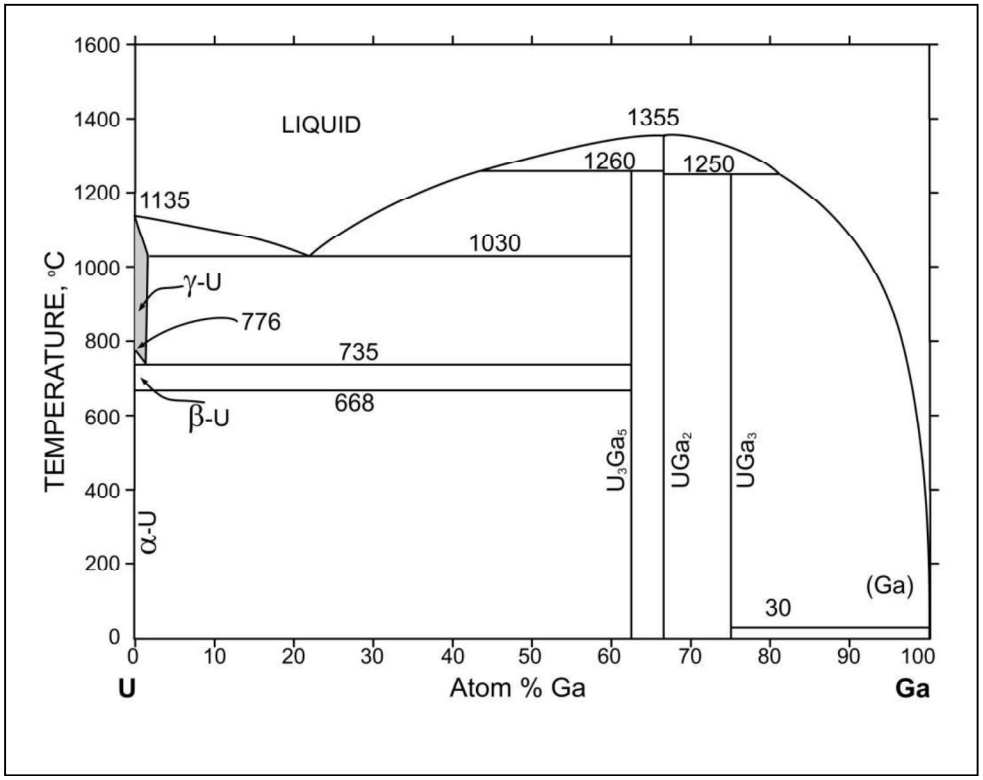

Fig. 4.1.1 Phase diagram of U-Ga system. [2, 3]

obtained by using calorimetric [6], e.m.f. [7-9] and mass loss [5] and mass spectrometric technique [10] based Knudsen effusion methods. Chiotti et al. [11] in 1981 had reviewed the thermodynamic data of U-Ga system and computed the Gibbs energies of formation of the intermetallic compounds U_2Ga_3, UGa_2 and UGa_3. Prabhakara Reddy et al. [6] had determined the enthalpies of formation of UGa_2 at 298.15 and 1563 K and of UGa_3 at 298.15 and 1038 K by employing solution and precipitation calorimetric methods, respectively. Prabhakara Reddy et al. [7] had also carried out the molten salt based e.m.f studies on U-Ga system and obtained the Gibbs energies of formation of U_2Ga_3 (800-950 K), UGa_2 (751-947 K) and UGa_3 (644-988 K).

Alcock et al. [5] have measured the total pressure over various compositions ranging from 6 to 77 at% Ga by Kundsen effusion mass loss method. They had presented their results graphically rather than giving any pressure-temperature relation. Further, they had assumed that the phase co-existing with UGa_2 is UGa and had derived the Gibbs energies of formation of UGa, UGa_2 and UGa_3 and had observed a difference in the value of Gibbs energy of formation of UGa_3 phase with those derived by e.m.f methods [8,9]. Additionally they had suspected error in their vapour pressure data due to the possible presence of gallium oxide species over the samples and suggested further work to resolve the discrepancy in the Gibbs energy data and to obtain reliable vapour pressures. Gardie et al. [10] had performed Knudsen Effusion Mass Spectrometric studies (KEMS) on the uranium rich region of the U-Ga system and reported activities of gallium in the composition range 5.3-28.0 at% Ga and in the temperature range 1100-1670 K. Subsequently the Gibbs energy of formation of U_2Ga_3(s) was derived and reported. Chiotti et al. [11] had re-evaluated the Gibbs energies of formation of various U-Ga phases reported [5,8,9] and found an excellent agreement with the values reported by Lebedev et al. [8] and Johnson and Feder [9] for the UGa_3 phase. However both these values were found to differ significantly from that reported by Alcock et al. [5] even after correcting the stoichiometry of UGa to $UGa_{1.5}$ [11]. Recently Wang et al. [12] have made a thermodynamic calculation of phase equilibria of this system and derived the enthalpy, entropy and Gibbs energies of formation of the constituent phases at 673 K. As can be seen, no reliable vapour pressure data exist in the literature on the gallium rich side of this system. Hence the present work has been undertaken to meet the objectives and aims: to carry out systematic vaporisation studies on the Ga-rich side of this system; i.e., to derive vapour pressure and other thermodynamic properties and to address the concern reported by Alcock et al. [5] regarding the vapour phase composition as indicated above.

Earlier we had conducted the preliminary investigations on U-Ga samples with compositions 63 and 64 at% Ga using alumina Knudsen cells by employing KEMS [13]. In that study, we had realised that, above 1250 K, alumina is thermodynamically unstable with U-Ga alloys, whereas yttria exhibits thermodynamically better stability as seen from the respective Ellingham diagrams [14]. Also Gardie et al. [10], based on their experimental observations, had suggested the use of yttria for uranium alloys. There are no heat capacity data available in the literature for all U-Ga intermetallic compounds. Part 1 of this chapter discusses Knudsen effusion mass spectrometric studies carried out over (U_3Ga_5+UGa_2) and (UGa_2+UGa_3) biphasic regions, which are gallium rich, by using yttria Knudsen cells and reports the vapour pressure of gallium and other thermodynamic properties obtained over these phase regions. Part 2 of this chapter deals with enthalpy increment measurements carried out on U_3Ga_5 using an inverse drop calorimeter in the temperature range 793-1323 K.

Part 1: High Temperature Mass Spectrometric studies on U-Ga system: Thermodynamic properties over (U_3Ga_5+UGa_2) and (UGa_2+UGa_3) phase regions

4.1.1. Experimental

All the samples were prepared by arc melting. About 2 g of each of the U-Ga alloys corresponding to 63 and 64 at% Ga belonging to (U_3Ga_5+UGa_2), and 71 and 73 at% Ga belonging to (UGa_2+UGa_3) were prepared by taking stoichiometric amounts of uranium (nuclear grade purity, Bhabha Atomic Research Centre, Mumbai, India) and gallium (purity: 99.99%, M/s Nuclear Fuel Complex, Hyderabad, India) required for the respective compositions and subjecting them to arc melting under argon atmosphere. Prior to the sample preparation, the uranium stored in oil was taken out and dipped in acetone to remove the oil sticking onto it. Subsequently it was dropped into 1:1 HNO_3 to dissolve the surface layer of oxide. It remained

inside the nitric acid solution until the entire mass turned metallic which was indicated by the fully shining surface. Finally it was rinsed with water and wiped with tissue paper to clear the water droplets sticking. Gallium was used as received. As an additional precaution, a freshly cleaned uranium chunk was melted, prior to melting the sample pieces of uranium and gallium, to scavenge the oxygen in the arc melting chamber. The melting was carried out thrice, turning the solidified mass upside down each time, to ensure homogeneity of the constituents. The samples thus prepared were wrapped in tantalum sheets, vacuum sealed in quartz tubes at 10^{-5} torr under argon atmosphere and annealed at 1073 K (63 and 64 at% Ga) and at 1023 K (71 and 73 at% Ga) for 14 days. The tantalum sheets used for wrapping the samples were cleaned to remove the oxide layer on the surface by immersing them in a solution of 10 vol% HF, 30 vol% HNO_3 and 60 vol% H_2SO_4. The samples prepared were characterised by X-ray diffraction (XRD) (Cu k-α Xpert pro XRD) to confirm the co-existence of the required phases. There was no evidence of presence of starting materials in these samples. In order to prevent the oxidation of alloys during handling, the samples were stored inside an argon atmosphere glove box (which houses KEMS) in which the concentrations of oxygen and moisture were maintained below 10 ppm by passing the argon gas through a purification bed filled with molecular sieves and copper deoxo catalyst to trap moisture and oxygen, respectively. Loading of the samples into the Knudsen cells were carried out inside the glove box. The levels of oxygen and moisture in the argon atmosphere glove box were monitored by appropriate sensors.

The vaporisation studies were carried out using a home-built high temperature mass spectrometric system housed inside an inert atmosphere glove box. The mass analyser used is a quadrupole mass spectrometer purchased from M/s Hiden Analyticals, UK. A schematic diagram of the experimental facility is shown in Fig 3.1 (Chapter 3). This consists of a vacuum envelope

comprising two chambers; one of which (bottom chamber or Knudsen cell chamber) accommodates the Knudsen cell furnace and another one (top chamber or ion source chamber) houses the quadrupole mass spectrometer (QMS). The Knudsen cell furnace assembly rests on a small platform attached to a X-Y positioner which makes it possible to align the Knudsen cell with the ion source of the mass spectrometer. The vacuum envelope remains wholly within the glove box and the two chambers are interconnected through a 4.0 mm diameter hole. To attain the vacuum required for the high temperature mass spectrometric experiments, each chamber is equipped with one diffusion pump (pumping speed 700 L sec^{-1}) backed by a suitable rotary pump (both the pumps were purchased from M/s Edwards, U.K) as can be seen in Figure 3.1. The residual pressures in the Knudsen cell furnace and ion source chambers are measured by using ionisation gauges (M/s SRS, U.S.A) and that in the fore-vacuum part by Pirani gauges (M/s Edwards, UK.). By making use of the provisions in the control electronics of these gauges, some safety interlocks necessary for smooth functioning of the equipment have been incorporated. To keep the ion-source ON even when the Knudsen cell chamber will be vented to ambient pressure (during sample changing), a specially designed vacuum isolation device was installed. This essentially consists of a viton O-ring having 8.0 mm ID and 3.0 mm cross section mounted on an 'O-ring carrier plate'. The design is such that the connectivity between the Knudsen cell and the ion source chambers can be readily restored when the vacuum level in the Knudsen cell chamber is satisfactory. More details are described elsewhere [15].

The samples (aliquots containing ~200 mg) were taken in yttria Knudsen cell fitted with yttria lid and this was placed inside an outer cup made of tantalum. The Knudsen cells had dimensions of i.d.: 7.0 mm; o.d.: 10.4 mm; height 7.0 mm; and the lids had an orifice (channeled) diameter of 0.7 mm. The heating of the sample was achieved by bombarding the

outer cup with the electrons emitted from two surrounding tungsten filaments. The vapour species effusing through the cell orifice were ionised in the ion source by electrons (energy = 28.8 eV; emission current = 100 μA) emitted from an oxide coated iridium filament. The ions were guided into the quadrupole field to enable their separation according to m/e ratios. The ion currents were measured by using secondary electron multiplier (SEM) operating in pulse counting mode, which generally overcomes mass discrimination effect observed in SEM detector in analog mode. A shutter inserted between the Knudsen cell chamber and the ion source aided to discriminate between the ions formed from the vapour species from the Knudsen cell and those generated due to ionisation of background molecules. The temperature of the Knudsen cell was measured by a disappearing filament pyrometer focused onto a black body hole drilled at the bottom of the cup. The pyrometer was calibrated against the melting point of silver and the electron energy scale calibration was carried out by measuring the appearance potentials of Ar^+, He^+, N_2^+, O_2^+ and H_2O^+. The error in temperature measurement was within ±5 K and that in the electron energy was ±0.5 eV.

The samples to start with, were heated slowly in steps of 100 degrees at lower temperatures (upto 800 K) and in steps of 50 degrees at higher temperatures and mass scanning was carried out at each temperature from 800 K onwards, looking for for shutterable peaks. Ga^+ was the ion observed in the mass spectra of equilibrium vapour over both the phase regions which was identified from the mass and isotopic abundances. The ion intensity data were recorded with respect to the most abundant isotope of gallium (^{69}Ga). I($^{69}Ga^+$) was measured as a function of temperature in the range of 1208-1366 K over (U_3Ga_5+UGa_2) and in the range of 1133-1338 K over (UGa_2+UGa_3). The electron energy of the emission source was kept at a value of 28.8 eV. In any given run of temperature dependence of ion intensities, the sample was

maintained at the first temperature for about 1 hour and the constancy of ion intensities during this period ensured the attainment of thermodynamic equilibrium inside the Knudsen cell. Subsequently the temperatures were changed in steps of about 20-25 K and the samples were kept at each temperature for about 30 minutes. In total, seven runs over (U_3Ga_5+UGa_2) and thirteen runs over (UGa_2+UGa_3) were carried out. Temperature changes were effected in increasing, decreasing and in cyclic modes. Moreover, the first temperature of a particular run was repeated at the end of the run to verify the reproducibility of ion intensities. Typical mass loss after temperature dependence experiments was found to be upto ~ 1 mg. Before carrying out temperature dependence experiments, preliminary isothermal experiments were performed to ensure constancy of ion intensities with time (~ 4 hrs). Pressure calibration experiments were conducted by taking pure gallium inside an inner alumina liner placed in the same Knudsen cell as was used for U-Ga samples. After each pressure calibration experiment, the Knudsen cell was thoroughly degassed at ~1600 K, so that ion intensity of gallium was not detectable or insignificant. The samples after KEMS studies were subjected to XRD analysis to confirm the co-existing phases [16]. Figure 4.1.2 shows the XRD of samples before and after KEMS experiments over 64 at% Ga (U_3Ga_5+UGa_2) and 71at% Ga (UGa_2+UGa_3).

4.1.2. Results and Discussion

Figure 4.1.3 shows the ionisation efficiency curve of $^{69}Ga^+$ ion obtained over (U_3Ga_5+UGa_2); (similar curve was obtained over other phase region as well); From the curve, the appearance energy of Ga^+ was derived by linear extrapolation method. That the value obtained (6.2 eV) is comparable with the literature value of 6.0 eV [17] indicates that the ions formed are due to simple ionisation of neutral vapour species. From mass, isotopic abundances and the appearance

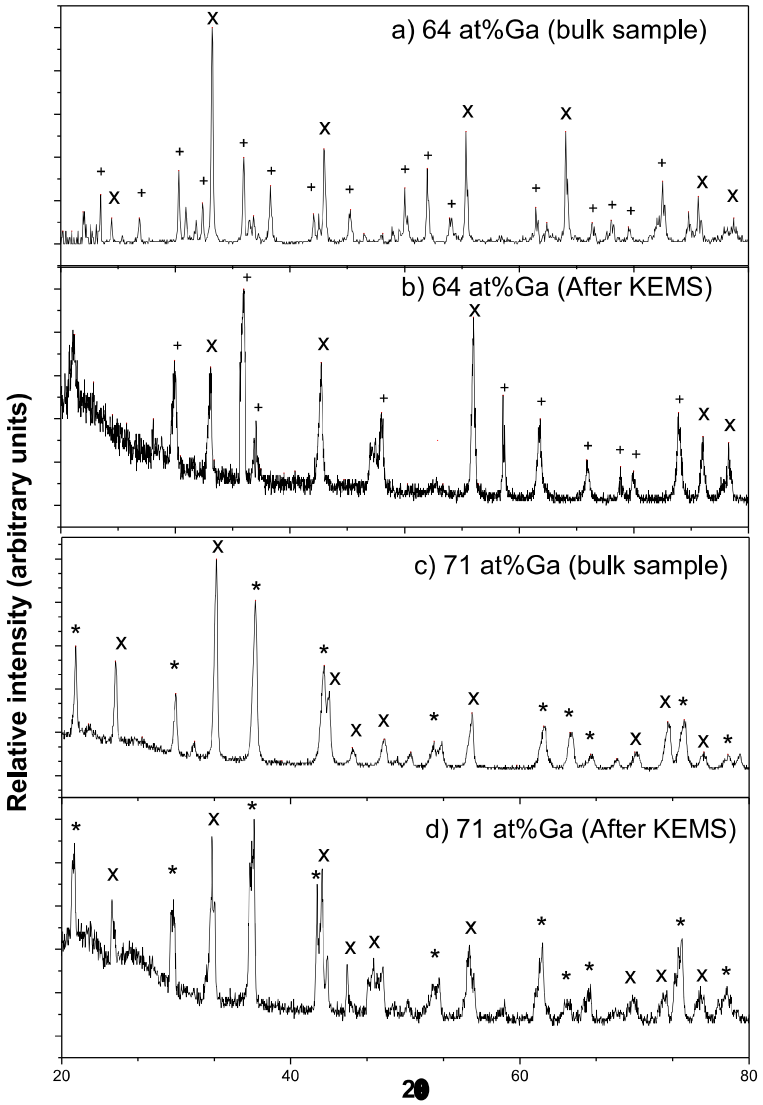

Fig. 4.1.2. XRD results of U-Ga samples, (+) – peaks due to U_3Ga_5 ; (x) – peaks due to UGa_2 ; (*)– peaks due to UGa_3

energy, the neutral species was established to be Ga(g). Alcock et al. [5] had carried out the Knudsen-effusion mass loss studies and had reported that the mass loss in their experiments could have been increased due to the co-evaporation of volatile gallium oxide species along with gallium vapour. However, we carried out the measurements with two types of Knudsen cells,

initially using alumina cell in our preliminary studies over (U_3Ga_5+UGa_2) [13] and subsequently yttria cell in the present work. In both the instances, we did not observe any detectable signal at masses corresponding to gallium-oxide bearing species even at the highest temperature of the measurement. Additionally, that the samples could be detached easily from the Knudsen cell at the end of each set of measurements, indicated that no interaction had occurred between the sample and the container material. The intensities of gallium ions measured were converted into partial pressure by using the relation given below.

$$p_{Ga} = k'_{Ga} I_{Ga^+} T \qquad (4.1.1)$$

where $k'_{Ga} = k/(\sigma n)_{Ga}$ is the pressure calibration constant; k is the instrument calibration constant; I_{Ga^+} is the ion intensity of gallium; σ is the ionisation cross section; and n is the isotopic abundance. Since liquid gallium was used for performing pressure calibration experiments, k'_{Ga} from the latter measurements was used directly for deriving partial pressures of gallium over the alloys. The partial pressure-temperature relations for Ga(g) obtained from the individual data points over different compositions are provided in Tables 4.1.1 and 4.1.2 for (U_3Ga_5+UGa_2) and (UGa_2+UGa_3), respectively. The overall p-T relations were obtained by least-squares fitting of all the individual partial pressure data (77 points in the case of (U_3Ga_5+UGa_2) and 159 points in the case of (UGa_2+UGa_3)) from the individual runs and the resulting equation are given as

$\log (p_{Ga}/Pa) = (-18216 \pm 239)/(T/K)) + (12.88 \pm 0.18)$ [1208-1366K] for (U_3Ga_5+UGa_2) (4.1.2)

$\log (p_{Ga}/Pa) = (-16225 \pm 124)/(T/K)) + (11.78 \pm 0.10)$ [1133-1338 K] for (UGa_2+UGa_3) (4.1.3)

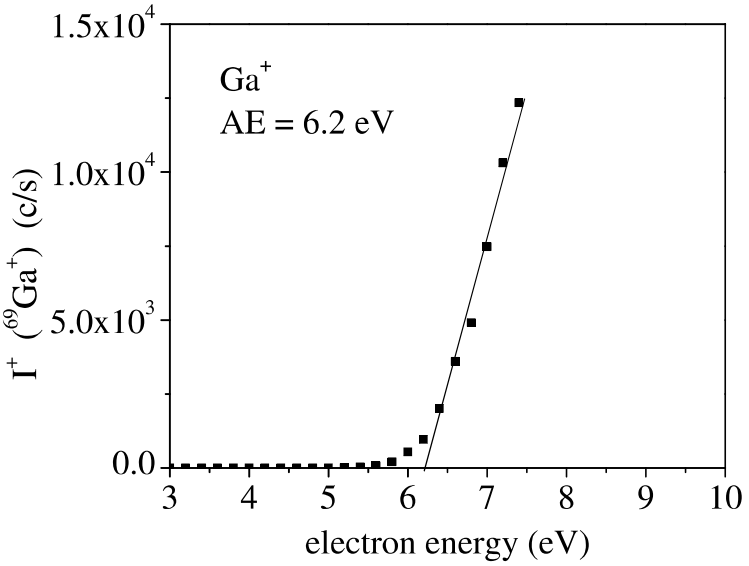

Fig. 4.1.3. Ionisation efficienecy curve of $^{69}Ga^+$ over (U_3Ga_5+UGa_2)

4.1.2.1. Comparison of vapour pressures

Figure 4.1.4 compares the vapour pressures obtained in the present work with those reported by Alcock et al. [5]. Since Alcock et al. had reported their data only in the form of figure e, the pressure and temperature points were extracted from the same and were least-squares fitted by us. As observed, there is a very good agreement in the values of p_{Ga} between these two studies over (U_3Ga_5+UGa_2) and an agreement within 50% over (UGa_2+UGa_3). It needs to be stated that for least-squares fitting of Alcock et al.'s data over (U_3Ga_5+UGa_2), we used the data points corresponding to the composition (65 at% Ga) which lies within the (U_3Ga_5+UGa_2) two phase region. However, Alcock et al., in their evaluation, used data points corresponding to the composition 52 at% Ga, as this was within (UGa+UGa_2) region of the phase diagram reported at that time [5], in addition to the data points of the composition 65 at% Ga. The p(Ga) obtained in our earlier work [13] using alumina cell are higher by a factor of 2.6 than that obtained in the present work. We are not able to attribute the exact reason for the difference in the values of

partial pressures. However as mentioned in the introduction (section 4.0), alumina is less compatible with uranium at temperatures above 1250 K and hence any reaction between the cell and sample could have caused an increase in vapour pressure. Since subsequent experiments were carried out with yttria cells, which were found to be compatible with U-Ga alloys [10, 14], the partial pressures obtained in the present work can be considered more reliable. The p-T relations given in equations 4.1.2 and 4.1.3 are the recommended ones over (U_3Ga_5+UGa_2) and (UGa_2+UGa_3) phase regions, respectively.

4.1.3. Thermochemical quantities

4.1.3.1. Thermodynamic data of U_3Ga_5 from p-T relation over U_3Ga_5+UGa_2 two phase region

4.1.3.1.1. The Gibbs energy of formation of U_3Ga_5

The vaporisation reaction corresponding to equation 4.1.2 can be written as follows:

$$3UGa_2(s) \rightleftharpoons U_3Ga_5(s) + Ga(g) \qquad (4.1.4)$$

The equilibrium constant (K°) – temperature relation for the above reaction is the same as the pressure-temperature relation, since K° = p_{Ga}/Pa. The Gibbs energy of reaction $(\Delta_r G_T^\circ)$ – temperature relation was arrived at by substituting the K°-T relation in the following equation.

$$\Delta_r G_T^\circ = -RTln(K^\circ) = -RTln(p_{Ga}/atm) \qquad (4.1.5)$$

$\Delta_r G_T^o$ (±4.6) = 348.8 – 0.1507 T(K) (kJ mol^{-1}) for (U_3Ga_5+UGa_2) (4.1.6)

The Gibbs energy of reaction 4.1.4 can also be derived by employing the following relationship also.

$$\Delta_r G_T^\circ = \Delta_f G_T^\circ(U_3Ga_{5(s)}) + \Delta_f G_T^\circ(Ga_{(g)}) - 3\Delta_f G_T^\circ(UGa_{2(s)}) \qquad (4.1.7)$$

Table 4.1.1. Partial pressure – temperature relations over (U_3Ga_5+UGa_2)

Sample composition	No of points	Temperature range (K)	log(p_{Ga}/Pa)=−A/T+B A	B	p_{Ga}/Pa at 1287 K[a]	$\Delta_r H_T^o$ (kJ mol^{-1})
63 at%Ga						
Run 1	9	1232-1345	18759±325	13.34±0.25	5.8×10^{-2}	359.2±6.2
Run 2	14	1223-1359	18334±231	12.95±0.18	5.1×10^{-2}	351.0±4.4
Run 3	12	1230-1321	18457±576	13.07±0.45	5.4×10^{-2}	353.4±11
64 at%Ga						
Run 4	8	1221-1351	18243±75	12.97±0.06	6.2×10^{-2}	349.3±1.4
Run 5	11	1208-1361	18429±347	13.03±0.27	5.1×10^{-2}	352.9±6.6
Run 6	11	1257-1366	18531±399	13.03±0.30	4.3×10^{-2}	354.8±7.6
Run 7	12	1229-1364	18627±224	13.19±0.17	5.2×10^{-2}	356.7±4.3
Recommended	77	1208-1366	18216±239	12.88±0.18	5.3×10^{-2}	353.9±6.8[b]

[a] middle temperature of investigation

[b] Standard deviation of the mean

Table 4.1.2. Partial pressure-temperature relations over (UGa_2+UGa_3)

Sample composition	No of points	Temperature range (K)	$\log(p_{Ga}/Pa)=-A/T+B$		p_{Ga}/Pa at 1236 K[a]	$\Delta_r H_T^o$ (kJ mol^{-1})
			A	B		
71at%Ga						
Run 1	13	1133-1296	16232±355	11.86±0.29	5.3×10^{-2}	310.8±6.8
Run 2	12	1145-1322	16114±209	11.75±0.17	5.2×10^{-2}	308.5±4.0
Run 3	10	1146-1318	16181±305	11.77±0.25	4.8×10^{-2}	309.8±5.8
Run 4	10	1146-1331	16236±196	11.73±0.16	3.9×10^{-2}	310.9±3.8
Run 5	13	1156-1334	16192±227	11.71±0.18	4.1×10^{-2}	310.0±4.3
Run 6	13	1152-1334	16358±276	11.81±0.22	3.8×10^{-2}	313.2±5.3
Run 7	10	1159-1338	16322±331	11.79±0.27	3.8×10^{-2}	312.5±6.3
73at%Ga						
Run 8	14	1158-1331	16288±293	11.88±0.23	5.0×10^{-2}	311.9±5.6
Run 9	13	1156-1325	16448±320	11.96±0.26	4.5×10^{-2}	314.9±6.1
Run 10	13	1151-1330	16321±106	11.84±0.09	4.3×10^{-2}	312.5±2.0
Run 11	12	1150-1325	16546±110	12.05±0.09	4.6×10^{-2}	316.8±2.1
Run 12	14	1141-1326	16761±400	12.22±0.32	4.6×10^{-2}	320.9±7.7
Run 13	12	1140-1324	16332±190	11.86±0.15	4.4×10^{-2}	312.7±3.6
Recommended	159	1133-1338	16225±124	11.78±0.10	4.5×10^{-2}	312.7±5.9[b]

[a] middle temperature of investigation

[b] Standard deviation of the mean

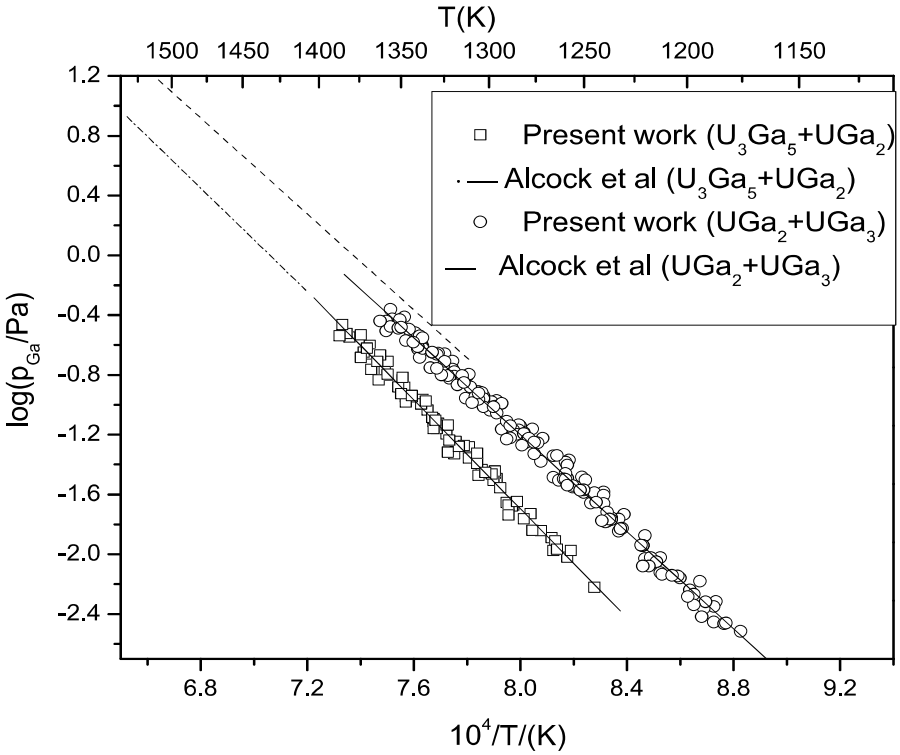

Fig.4.1.4. Comparison of log (p_{Ga}/Pa) vs. 1/T(K) plots.

The equations (4.1.6) and (4.1.7) were used to derive the Gibbs energy of formation of U_3Ga_5. The required Gibbs energy of formation value for UGa_2(s) was taken from the reference [7]. Since the temperature range of measurements of Prabhakara Reddy et al. [7] is lower (751-947 K) compared to that of present work (1208-1366 K) for (U_3Ga_5+UGa_2) two phase region, the data obtained by them were recalculated to the temperature range of present work, taking into consideration the appropriate reference states [18]. For Ga(g), the values of the Gibbs energy of formation given as a function of temperature in JANAF thermochemical tables [19] in the range 1100-1500 K were fitted into a linear relation and these expressions are given below.

$$\Delta_f G_T^o \text{ UGa}_2\text{(s) } (\gamma\text{-U and Ga(l)}) \ (\pm 3.0) = -145.6 + 0.059 \text{ T(K) (kJ mol}^{-1}) \qquad (4.1.8)$$

$$\Delta_f G_T^o \text{ Ga(g)} = 264.4 - 0.1076 \text{ T(K)} \text{ (kJ mol}^{-1}\text{)} \quad (4.1.9)$$

The Gibbs energy of formation of U_3Ga_5 (s) thus obtained is given as

$$\Delta_f G_T^o \text{ } U_3Ga_5(s) \text{ } (\pm 5.5) = -352.4 + 0.133 \text{ T(K)} \text{ (kJ mol}^{-1}\text{)} \quad (4.1.10)$$

In the above expression, the reference states are γ-uranium and Ga(l), which are the stable phases in the temperature range of the present investigation.

Gardie et al. [10] had measured the thermodynamic activity of gallium assuming most uranium rich phase as U_2Ga_3 and reported Gibbs energy of formation of this phase. However as can be seen from Figure 4.1.1, the most uranium rich phase is U_3Ga_5. Hence, by using the activity of gallium reported by Gardie et al. [10], we re-evaluated the Gibbs energy of formation (in the range 1100-1292 K) considering that their experimental pressure points would correspond to (U_3Ga_5+UGa_2) two phase region according to the present phase diagram, since the compositions covered in their studies lie within the above two phase region. Accordingly the Gibbs energy of formation of U_3Ga_5 is given as

$$\Delta_f G_T^o \text{ } U_3Ga_5(s) \text{ } (\pm 12.7) = -318.4 + 0.1023 \text{ T(K)} \text{ (kJ mol}^{-1}\text{)} \quad (4.1.11)$$

The reference states are γ-uranium and Ga(l). The Gibbs energies of formation of U_3Ga_5 computed from equations (4.1.10) and (4.1.11) at the middle temperature of our investigation (1287 K) are −186.5 and −190.5 kJ mol^{-1}, respectively. The Gibbs energy of formation with respect to α-uranium (the phase which is stable at room temperature) and Ga(l) was also computed and the same is given as

$$\Delta_f G_T^o \text{ } U_3Ga_5(s) \text{ } (\pm 5.5) = -329.6 + 0.109 \text{ T} \text{ (kJ mol}^{-1}\text{)} \quad (4.1.12)$$

The Gibbs energy of formation of U_3Ga_5 has been experimentally determined for the first time.

4.1.3.1.2. The enthalpy of formation of U_3Ga_5

The enthalpy of the above reaction calculated from the slope of the equation (4.1.2) is 353.9±6.8 kJ mol^{-1} at 1287 K. No enthalpy of formation data is available in the literature for U_3Ga_5 and heat capacity data are not available for both the condensed phases represented by equation (4.1.4). Hence, the reaction enthalpy as obtained above could not be made use of further to deduce the enthalpy of formation of U_3Ga_5.

4.1.3.2. Thermodynamic data of UGa_3 from p-T relation over UGa_2+UGa_3 two phase region

4.1.3.2.1. The Gibbs energy of formation of UGa_3

The vaporisation reaction corresponding to equation (4.1.3) can be written as follows:

$UGa_3(s) \rightleftharpoons UGa_2(s) + Ga(g)$ (4.1.13)

The Gibbs energy of reaction $(\Delta_r G_T^\circ)$-temperature relation for this two phase region was derived as it was done for the other two phase region as discussed above and the relation obtained is written as

$\Delta_r G_T^\circ$ (±2.4) = 310.7 – 0.130T (K) (kJ mol^{-1}) (U_3Ga_5+UGa_2) (4.1.14)

The Gibbs energy of reaction given by equation (4.1.13) can also be given as

$$\Delta_r G_T^\circ = \Delta_f G_T^\circ(UGa_{2(s)}) + \Delta_f G_T^\circ(Ga_{(g)}) - \Delta_f G_T^\circ(UGa_{3(s)}) \quad (4.1.15)$$

By using the equations (4.1.14) and (4.1.15), the Gibbs energy of formation of UGa_3 was obtained. The equation (4.1.8) was used as the input for the Gibbs energy of formation of UGa_2 since the temperature range of 1133-1338 for (UGa_2+UGa_3) two phase region in the present study corresponds to γ-uranium and Ga(l). The equation (4.1.9) was used as the input for the value of the Gibbs energy of formation of Ga(g). The expression for the Gibbs energy of formation of UGa_3 is given as

$\Delta_f G_T^o$ UGa_3(s) (±3.8) = −191.9 + 0.082 T (kJ mol^{-1}) (4.1.16)

The reference states are γ-uranium and Ga(l). The Gibbs energy of formation of UGa_3 computed from equation (4.1.16) at the middle temperature of our investigation (1236 K) is −90.9 kJ mol^{-1}. This value along with those available in the literature is tabulated in Table 4.1.3. In general, there is a good accord in the values determined by the experiments, though the value of Alcock et al. [5] is very much lower. One possible reason could be that they used the Gibbs energy of formation of UGa(s) determined by themselves in the same study for deriving the values for UGa_2 and subsequently that of UGa_3. However, in the present study, the value of Gibbs energy of formation of UGa_2(s) reported by Prabhakara Reddy et al. [7] was used to arrive at the Gibbs energy of formation of UGa_3(s). The value of Wang et al. [12] derived from thermodynamic calculations is more negative.

We also computed the Gibbs energy of formation of UGa_3 with respect to α-uranium (the phase which is stable at room temperature) and Ga(l) and the same is given as

$$\Delta_f G_T^o \, UGa_3(s) \, (\pm 3.8) = -184.3 + 0.0737 \, T(K) \, (kJ \, mol^{-1}) \qquad (4.1.17)$$

4.1.3.2.2. The enthalpy of formation of UGa_3

The enthalpy of the above reaction calculated from the slope of the equation (4.1.3) is 312.7±5.9 kJ mol^{-1} at 1236 K. Heat capacity data is also not available in the literature for UGa_3. Hence, the enthalpy of reaction derived from the experiments could not be used further to derive the enthalpy of formation of UGa_3. However, a relation for the enthalpy of formation of UGa_3 as a function of temperature was derived by adopting the procedure used by Chiotti et al. [20] which was used to evaluate the Gibbs energies of formation of uranium aluminides. Using Kirchoff's equation [21],

$$\Delta_f H_{T_2}^o = \Delta_f H_{T_1}^o + \Delta C_p [T_2 - T_1] \qquad (4.1.18)$$

Table 4.1.3. Comparison of Gibbs energies of formation of UGa_3(s)

Compound	$\Delta_f G_T^o$ (kJ mol^{-1})	Method	T/K	Reference
	−122.4+0.060 T	KEML	1280-1530	Alcock et al [5]
	−184.0+0.072 T(±4.0)	e.m.f	644-988	Prabhakara reddy et al [7]
UGa_3	−176.0+0.064 T	e.m.f	693-942	Lebedev et al [8]
w.r.t γ-U	−178.0+0.064 T	e.m.f	643-942	Johnson et al [9]
and liq.Ga	−177.2+0.064 T	Assessment	298-942	Chiotti et al [11]
	−142.2+0.01024 T	Calculation		Wang et al [12]
	−191.9+0.0817 T(±3.8)	KEMS	1133-1338	Present work
	−48.2	KEML[a]	1236	Alcock et al [5]
UGa_3	−95.0(±4.0)	e.m.f	1236	Prabhakara reddy et al [7]
w.r.t γ-U	−96.9	e.m.f	1236	Lebedev et al [8]
and liq.Ga	−98.9	e.m.f	1236	Johnson et al [9]
	−98.1	Assessment	1236	Chiotti et al [11]
	−129.54	Calculation	1236	Wang et al [12]
	−90.9(±3.8)	KEMS	1236	Present work

ΔC_p was deduced between 298 and 1236 K, the middle temperature of the present work over (UGa_2+UGa_3). The required $\Delta_f H^o_{298.15K}$ with respect to U(α) and Ga(s), −153.2±17.6 kJ mol^{-1} was taken from the reference [6]. The above was obtained by Prabhakara Reddy et al. by employing the solution calorimetry [6]. The intercept of equation (4.1.16), −191.9±3.8 kJ mol^{-1} is $\Delta_f H^o_{1236K}$ with respect to U(γ) and Ga(s). ΔC_p thus obtained was used in the Kirchoff's equation along with the enthalpy of formation at 298.15 as another input to derive a temperature dependence relation for the $\Delta_f H^o_T$ of UGa_3 valid in the range 298.15-1236 K and the same was given as

$$\Delta_f H^o_T\ (\pm 18.01) = -\ 140.9 - 0.0412\ \mathrm{T(K)}\ \text{kJ mol}^{-1}\ (298.15\text{-}1236\mathrm{K}) \qquad (4.1.19)$$

For comparing the value of enthalpy of formation of UGa_3 derived above with that reported by Prabhakara Reddy et al. [6] determined by precipitation calorimetry at 1038 K ($\Delta_f H^o_{1038K}$ (U(β) and Ga(l)) = −162.4 kJ mol^{-1}) , the same was obtained by interpolating the equation (15) to 1038 K. The value thus obtained is −183.7 kJ mol^{-1}. Similarly, to compare with the data of Wang et al. [12] ($\Delta_f H^o_T$ (U(α) and Ga(l)) = −152.0 kJ mol^{-1} (673 K)), the enthalpy of formation at 673 K was calculated using equation 4.1.19. The value thus obtained was -168.6 kJ mol^{-1}.

4.1.4. The error calculation

The estimated uncertainty (u) in the measured partial pressure of Ga(g) is u(p) =0.2p. This was based on considering Ga(g) as the major species in the mass spectra. As pure gallium, one of the components of the U-Ga system was used in pressure calibration experiments, errors due ionisation cross sections would cancel out. Since ion counting was used for intensity measurements, error due to mass dependent discrimination by the detector does not exist. The

uncertainties quoted in the enthalpies of reactions (4.1.4) and (4.1.13) (Tables 4.1.1 and 4.1.2) were deduced from the standard deviation of the mean. The errors in the Gibbs energies of reactions (equations (4.1.4) and (4.1.13)) were computed from the statistical errors associated with the slopes of the fitted equations (4.1.2) and (4.1.3) for the experimental temperature and pressure data points. The errors quoted for Gibbs energy of formation for U_3Ga_5(s) and UGa_3(s) were computed by error propagation due to errors in the Gibbs energies of equations (4.1.6) and (4.1.14) and to the errors in the literature data for the other phases involved in the reactions (4.1.4) and (4.1.13)**.** In a similar way, error in the enthalpy of formation of UGa_3(s) (equation (4.1.18)) was computed.

4.1.5. Conclusion

Vaporisation studies over (U_3Ga_5+UGa_2) and (UGa_2+UGa_3) two phase regions were carried out by Knudsen effusion mass spectrometry and partial pressures of gallium as a function of temperature have been reported for the first time. Vapour phase consisted of only Ga(g), removing doubts raised by Alcock et al. [5] for the possible presence of Ga-O bearing species. The p-T relation over (U_3Ga_5+UGa_2) in the range 1208-1366 K is given as $\log(p_{Ga}/Pa) = (-18216\pm239)/(T/K)+(12.88\pm0.18)$ and that over (UGa_2+UGa_3) in the range 1133-1338 K is given by $\log(p_{Ga}/Pa) = (-16225\pm124)/(T/K)+(11.78\pm0.10)$. The reaction enthalpies were computed from the slopes of log (p) vs. 1/T plots as 353.9±6.8 and 312.7±5.9 kJ mol^{-1} at 1287 and 1236 K, the respective middle temperatures of the investigations. Using the vapour pressure data and the required information from literature, the Gibbs energies of formation of U_3Ga_5(s) and UGa_3 (s) were deduced as $\Delta_f G_T^o$ U_3Ga_5(s) (±5.5) = −352.4+0.133 T(K) (kJ mol^{-1}) and $\Delta_f G_T^o$ UGa_3(s) (±3.8) = −191.9 +0.082 T(K) (kJ mol^{-1}). The data for the U_3Ga_5 phase is being

reported for the first time. The enthalpy of formation of UGa_3 as a function of temperature in the range 298.15-1236 K was also deduced.

Part 2: Thermodynamic data of U_3Ga_5 from calorimetric measurements

4.2.1. Preparation of samples

Nuclear grade uranium (Bhabha Atomic Research Centre, Mumbai, India) and gallium (Purity, 99.99% M/s Nuclear Fuel Complex, Hyderabad, India) were used for the preparation of U_3Ga_5. Stoichiometric amounts of uranium and gallium were taken and subjected to arc melting. The melting was done thrice, flipping the solidified molten mass each time. The samples prepared were wrapped in tantalum sheet, vacuum sealed in quartz tube at 10^{-5} Torr under argon atmosphere and annealed at 1073 K for 14 days. The samples were handled inside an argon atmosphere glove box in which the levels of moisture and oxygen were maintained below 10 ppm by circulating the argon gas through the purification bed filled with copper deoxo catalyst and molecular sieves which remove oxygen and moisture, respectively.

4.2.2. Characterisation by X-ray diffraction

X-ray diffraction (XRD) characterization of the sample was carried out using a PANalytical X'PertPro MPD system with Cu K_α radiation and secondary beam curved graphite monochromator. XRD patterns for the sample were recorded in the range 2θ = 25 to 80° with step size of 0.02° and a counting time of 5 s per step.

4.2.3. Enthalpy increment measurements

4.2.3.1. Calorimeter

In the present study, a high temperature differential calorimeter (Model HT 1500 of M/s. SETARAM, France) was employed for the enthalpy increment measurements. The calorimeter, method of measurement, the procedure adopted for enthalpy increment measurements and the

analysis of the measured data to compute thermodynamic functions have been described elsewhere [22]. For the sake of clarity, a brief description of the instrument is given here. The instrument functions as an isoperibol calorimeter and employs a thermopile detector for measuring the heat flow between two alumina crucibles. The thermopile detector shown in Figure 4.2.1 is made of 18 Pt-Rh thermocouples arranged in such a way that the two sets of junctions form two rings each supporting a crucible. The crucibles are either half filled with alumina powder or kept empty. The crucibles are positioned inside the constant temperature zone of a graphite resistance furnace. When the two crucibles are at the same temperature, there will not be any heat flow between them. However, when a process occurs in the sample crucible, the associated thermal effect produces a differential temperature or temperature difference between the two crucibles, causing a heat flow between them. The integrated output of the thermopile measures the thermal effect. An automatic data acquisition system has been provided to measure the thermo e.m.f. values at constant intervals and to store the data and to simplify the operation of computations. PC based data acquisition is enabled by using HP-34812A Bench Link data acquisition software (Version 1.0) through a HP-34810A 6½-digit multimeter (data acquisition system). Subsequent data evaluation was carried out by using Microcal Origin (Version 5.0) to generate $\Delta T - t$ curves for the measurements and to calculate the area of the $\Delta T - t$ curves.

Two types of thermopiles are used as detectors in this calorimeter. One made of Pt/Pt-10%Rh thermocouples (for below 1573 K) and the other made of Pt-30%Rh/Pt-6%Rh thermocouples (for above 1573 K).

4.2.3.2. Method of measurement

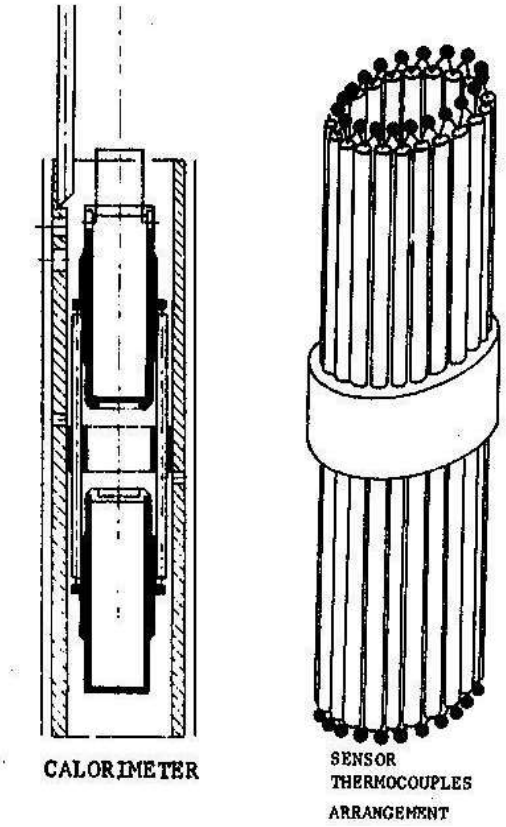

Fig. 4.2.1. Thermopile arrangement in the calorimeter

In a typical experiment, five pairs each of sample and standard (α-Al_2O_3, SRM 720, supplied by NIST, USA) [23], each weighing about 100 mg, are dropped alternately into the sample crucible maintained at the experimental temperature. From the relative values of heat flow measured in the case of standard and sample, and the known enthalpy increment data of the standard, the enthalpy increment, $H_T^0 - H_{298}^0$ of the sample was calculated. The mean of the five heat flow values for the standard and that of the sample were used to compute the enthalpy increment at that temperature. These measurements were also repeated two times at the same temperature to confirm the reproducibility of the data. A typical heat flow signal obtained at a particular temperature (1008 K) is displayed in Figure 4.2.2. From this, the area under the heat flow *(Q)* versus time *(t)* curve was calculated. This area is proportional to the enthalpy increment of the sample dropped from room temperature to the furnace temperature. The enthalpy increment values thus obtained at different temperatures were fitted by the weighted least-squares method to obtain a non-linear expression in temperature. During the experiments, to prevent the oxidation of the U_3Ga_5 alloy samples, high pure argon gas was continuously flown over the sample.

4.2.4. Results and discussion

The X–ray diffraction (XRD) pattern of U_3Ga_5 is shown in Figure 4.2.3, which is in good agreement with that reported in literature {JCPDS, ICDD card number: 04-001-1065} [24]. Neither uranium nor gallium was observed in the X-ray diffraction pattern. The enthalpy increment measurements using the calorimeter were standardised by carrying out the drop experiments on ThO_2. The overall error in these measurements was ascertained to be ± 2.5% by

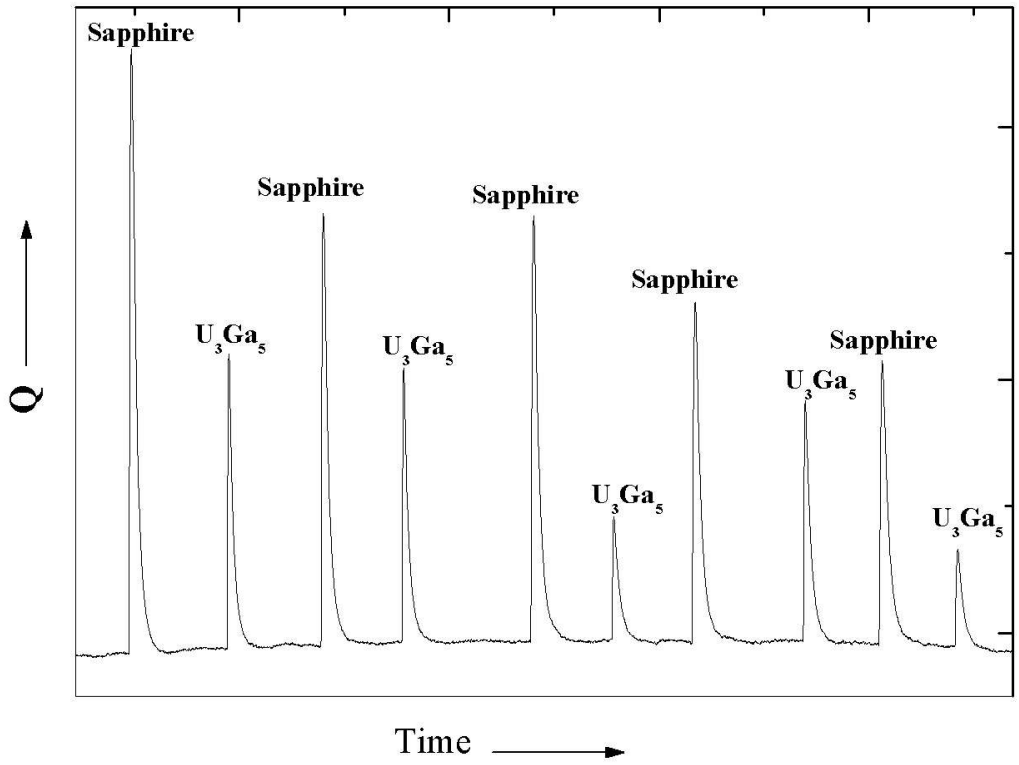

Fig. 4.2.2. Typical calorimetric signal obtained for U_3Ga_5 at 1008 K

comparing the results with the assessed data of Godfrey *et al.* [25]. The temperature of the sample was measured with an accuracy of ± 0.5 K. The experimental values of enthalpy increments of U_3Ga_5 are given in Table 4.2.1 along with those computed from equation (4.2.1). The measured enthalpy increments were fitted to the polynomials in temperature by using the least-squares method and the resulting expression is given below (in the temperature from 298-1400 K).

$$H_T^0 - H_{298}^0 \,/\, \text{J mol}^{-1} = 168.631T + 52.677\times10^{-3}T^2 - 12.177\times10^5\,T^{-1} - 50876 \qquad \text{--- (4.2.1)}$$

The standard error and standard deviation of the fit were 0.39 % and 725 J mol^{-1}, respectively.

The constraints used for fitting are: (a) $H_T - H_{298} =$ 0 at 298 K and (b) the derivative of the function at 298 K is equal to the value of heat capacity of the U_3Ga_5 at 298 K(213.74 J mol^{-1} K^{-1}). Since heat capacity data at 298.15 K is not available in the literature for U_3Ga_5, it was calculated from the heat capacity data of pure U and Ga [26] by applying the Neumann-Kopp's molar additivity rule. The standard error between the experimental data and the smoothened enthalpy values from the fit equation was computed using the following expression

$$Standard\ error = \sqrt{\frac{\sum (Residual)^2}{(No.\ of\ observations - No.\ of\ coefficients)}} \qquad (4.2.2)$$

Using the fitted equation (4.2.1), heat capacity, entropy and Gibbs energy function were computed and are given in Table 4.2.2. The S^0_{298} value of U_3Ga_5 needed for the computation of the entropy and Gibbs energy functions were estimated from the literature data of S^0_{298} values of the respective components by applying Neumann-Kopp's rule(S^0_{298} of U_3Ga_5 =354.76J $K^{-1}mol^{-1}$) [26]. Heat capacity was obtained by differentiating the equation (4.2.1) with respect to temperature and is given below.

$$C_p^0 \text{ /J. mol}^{-1}\text{K}^{-1} = 168.631 + 105.364\times10^{-3}\,T + 12.177\times10^{5}\,T^{-2} \qquad (4.2.3)$$

The measured enthalpy increment values of U_3Ga_5 along with the fitted values as well as those computed by Neumann-Kopp's law using the enthalpy data of the elements from the literature [26] are shown in Figure 4.2.4. The values from the fits are within ± 1 % of the measured values. The present enthalpy increment values are in good agreement within 3% with the values calculated using Neumann-Kopp's rule. In Figure 4.2.5, heat capacity values computed from

present enthalpy increments for U_3Ga_5 are compared with the values calculated using Neumann-Kopp's rule. As can be seen from the Figure 4.2.5, the present heat capacity data are lower than but within 4% of the values calculated using Neumann -Kopp's rule.

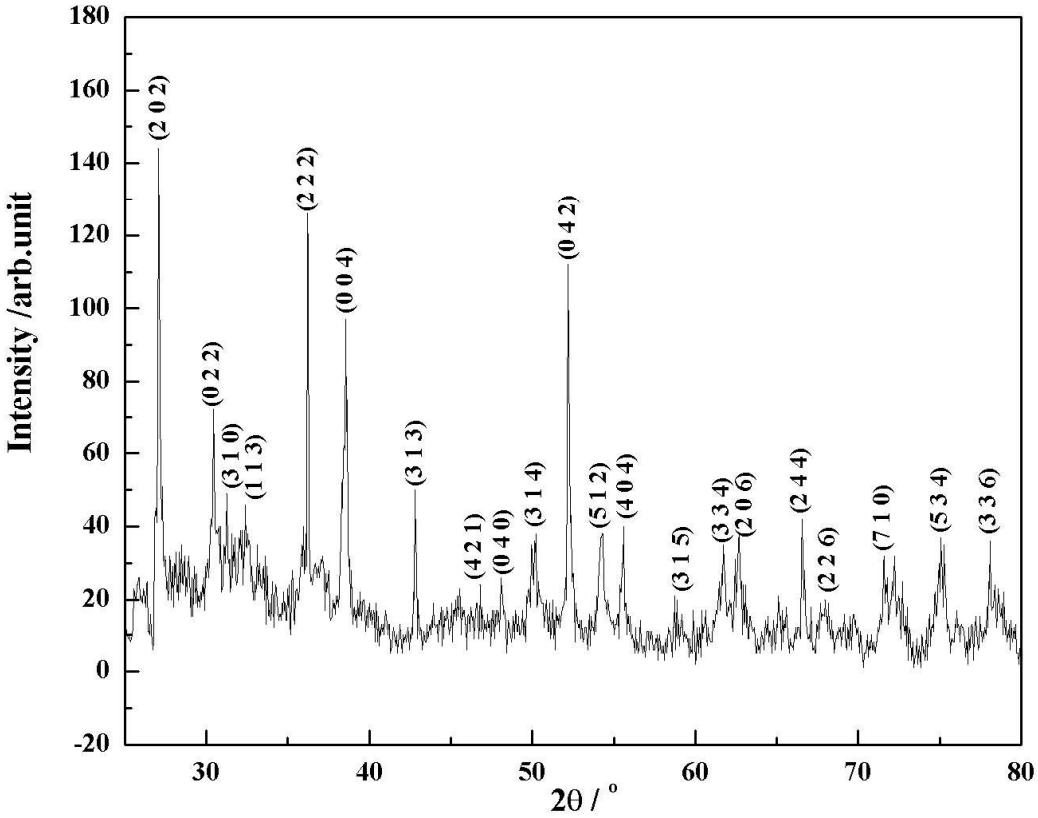

Fig. 4.2.3. XRD pattern of U_3Ga_5

4.2.5. Calculation of enthalpy of formation of U_3Ga_5 at 298 K

The temperature dependence of Gibbs energy of formation of U_3Ga_5 was recently reported by us [27] as,

$$\Delta_f G_T^o, U_3Ga_5\ (\pm 5.5) = -352.4 + 0.133\ T\ (K)\ (kJ\ mol^{-1}) \quad (4.2.4)$$

Table 4.2.1. Measured enthalpy increments and fit values of U_3Ga_5 (s)

T/K	ΔH^T_{298} Measured	ΔH^T_{298} Fit	((ΔH^T_{298} Fit - ΔH^T_{298} Measured)
	kJ mol^{-1}		/ ΔH^T_{298} Fit)*100 %
793	115.097	114.439	-0.58
841	127.447	126.752	-0.55
899	140.876	141.943	0.75
957	158.191	157.476	-0.45
1008	171.251	171.419	0.10
1060	185.311	185.912	0.32
1113	200.503	200.971	0.23
1165	216.325	216.029	-0.14
1219	231.811	231.962	0.07
1272	247.641	247.896	0.10
1323	264.077	263.505	-0.22

Table 4.2.2. Thermodynamic functions of U_3Ga_5(s)

T/K	$(H_T^o - H_{298}^o)$ / $kJmol^{-1}$	$Jmol^{-1}K^{-1}$		
		C_p^0	S_T^0	$-(G_T^o - H_{298}^o/T)$
298	0	213.74	354.76	354.76
300	0.395	213.77	356.08	354.76
400	21.961	218.38	418.09	363.19
500	44.173	226.18	467.62	379.28
600	67.237	235.23	509.65	397.59
700	91.238	244.86	546.63	416.29
800	116.220	254.82	579.97	434.70
900	142.207	264.95	610.57	452.56
1000	169.214	275.20	639.01	469.80
1100	197.250	285.53	665.73	486.41
1200	226.322	295.90	691.02	502.41
1300	256.432	306.31	715.11	517.86
1400	287.585	316.75	738.19	532.78

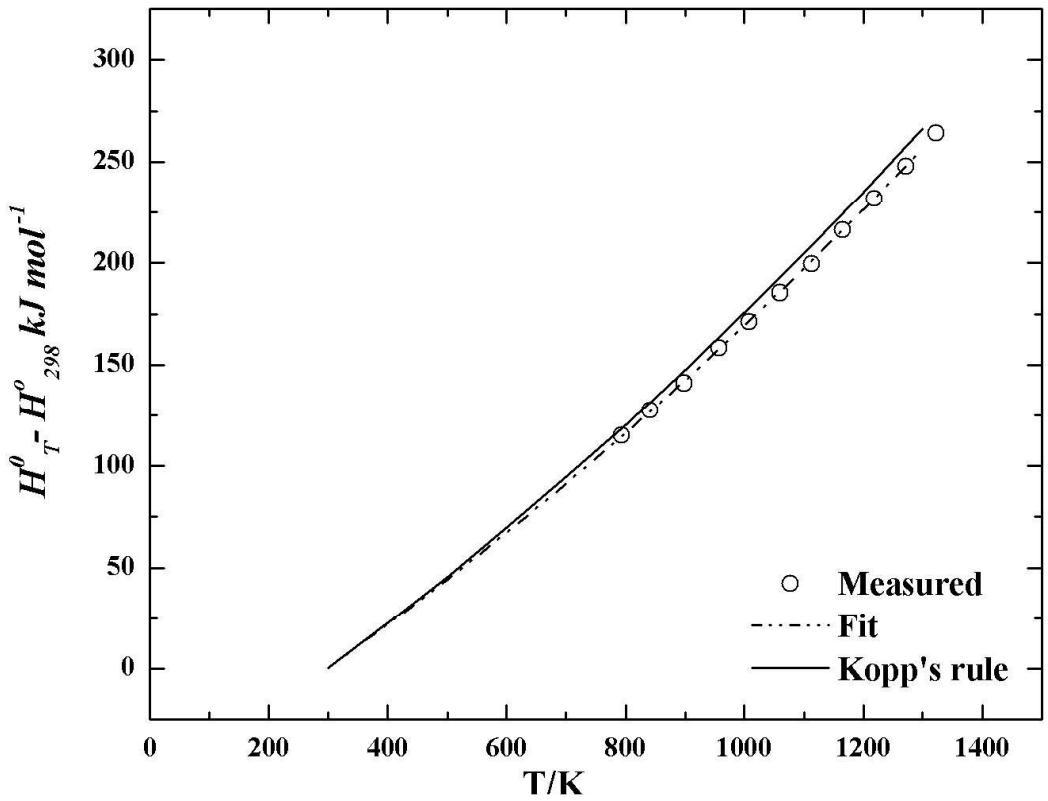

Fig. 4.2.4. Enthalpy increments of U_3Ga_5

The above expression corresponds to reference states of γ-uranium and liquid gallium, the stable phases in the temperature range 1208-1366 K. Using the intercept from the above equation (the enthalpy of formation of U_3Ga_5 at 1287 K, the middle temperature of the above temperature range) and the heat capacity data of U_3Ga_5 deduced from enthalpy increment measurements of the present study, the enthalpy of formation at 298 K was calculated by applying the Kirchoff's equation [21],

$$\Delta_f H^o_{T_2} = \Delta_f H^o_{T_1} + \int_{T1}^{T2} \Delta C_p dT \qquad (4.2.5)$$

The procedure is described below.

$$\Delta_f H_{298K,U_3Ga_5} = \Delta_f H_{1287K,U_3Ga_5} - \int_{1049}^{1287} \Delta C_p dT + 3*\Delta_{\beta-\gamma} H^{\circ}{}_{1049K,U}$$

$$- \int_{942}^{1049} \Delta C_p dT + 3*\Delta_{\alpha-\beta} H^{\circ}{}_{942K,U} - \int_{303}^{942} \Delta C_p dT + 3*\Delta_{s-l} H^{\circ}{}_{303K,Ga} - \int_{298}^{303} \Delta C_p dT$$

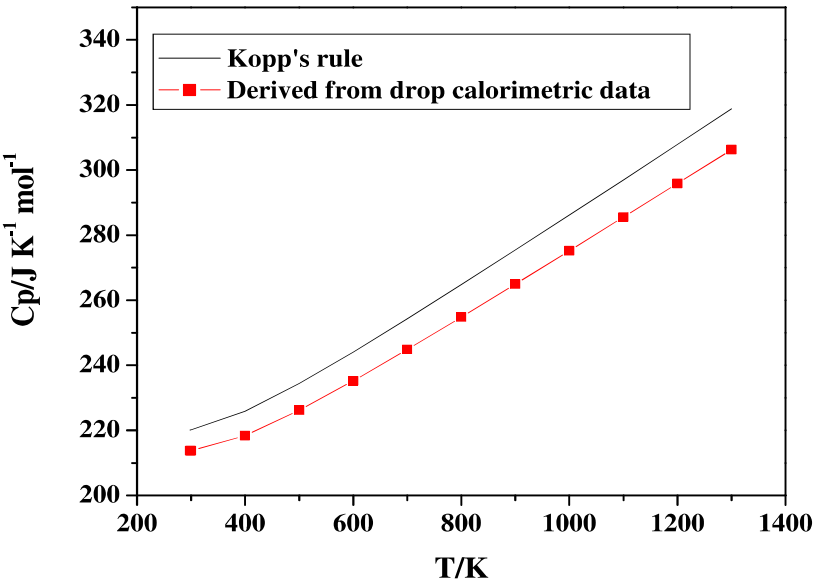

Fig. 4.2.5. Heat capacity of U_3Ga_5

The heat capacity data and the enthalpies of transitions of uranium (α – β and β – γ) and gallium (s-l) required for the computation were taken from the reference [26] and are given in Table 4.2.3. $\Delta_f H^o_{298}$, U_3Ga_5 thus derived is given as -311.3 ± 5.5 kJmol^{-1}. This value is less negative than that ($\Delta_f H^o_{1287}$ = -352.4 ± 5.5 kJmol^{-1}) obtained at 1287 K [27]. As seen from the above equation, the difference of -41.06 kJ mol^{-1} is just not due to the difference in the heat capacities of products and reactants alone, but also includes enthalpies of phase transitions of the reactants,

namely, uranium ($\alpha - \beta$ and $\beta - \gamma$) and gallium (s-l) as well. The contribution of the latter calculated from the enthalpies of $\alpha - \beta$ and $\beta - \gamma$ transitions for uranium [26] and the enthalpy of melting of solid gallium [26] is +50.6 kJ.

4.2.6. Conclusion

The high temperature enthalpy increment of U_3Ga_5 was measured for the first time by employing the method of inverse drop calorimetry in the temperature range 793-1323 K. Subsequently other thermodynamic functions, namely, heat capacity, entropy and Gibbs energy functions were computed in the temperature range 298-1400K. Using the heat capacity data, the enthalpy of formation of U_3Ga_5 at 298 K has been computed as -311.3 ± 5.5 $kJmol^{-1}$ and the same is reported for the first time.

References:

1. B. Mishra, J.J. Moore, Metall. Trans. 25B (1994) 151.
2. ASM Alloy Phase Diagrams Center, P. Villars (Ed.), H. Okamoto and K. Cenzual, section editors; http://www1.asminternational.org/AsmEnterprise/APD, ASM International, Materials Park, OH, USA, 2006-2015
3. S.Salhov, G.Kimmel, M.P.Dariel, J. Alloys and Compds. 444-445 (2007) 257.
4. T. B. Massalski, Binary Alloy Phase Diagrams: 2nd edition, ASM, Ohio, 1990.
5. C.B. Alcock, J.B. Cornish, P. Grieveson, in: Proceedings of the Symposium on Thermodynamics, Vienna, Vol. I, IAEA,Vienna, 1966, p. 211
6. B. Prabhakara Reddy, R. Babu, K. Nagarajan, P.R. VasudevaRao, J. of Alloys and Compds. 271-273 (1998) 395.

Table 4.2.3. Values of heat capacities and enthalpy of transitions used for computing enthalpy of formation of U_3Ga_5

Species	Heat capacities $C_p = a+bT+CT^{-2}$ (J mol^{-1} K^{-1})			Reference
	a	$B*10^3$	$C*10^{-5}$	
U_3Ga_5	168.63	105.36	12.17	Present study
U(α)	13.01	35.33	3.66	[26]
U(β)	42.91			[26]
U(γ)	38.28			[26]
Ga(s)	27.18	83.7		[26]
Ga(l)	25.10	1.05	2.81	[26]
Enthalpy of transitions $\Delta H°$ (kJ mol^{-1})				
U(α) = U(β) (T=942 K)		2.79		[26]
U(β) = U(γ) (T =1049 K)		4.78		[26]
Ga(s) =Ga(l) (T= 303 K)		5.59		[26]

7. B. Prabhakara Reddy, R. Kandan, K. Nagarajan, P.R. VasudevaRao, Thermochim. Acta. 366 (2001) 37.
8. A. Lebedev, V.N. Seregin, A.M. Poyarkov, I.F. Nichkov, S.P. Raspopin, Russ. J. Phys. Chem. 47 (1973) 402.
9. I. Johnson, H.M. Feder, in: Proceedings of the Symposium on Thermodynamics of Nuclear Materials, Vienna, IAEA, Vienna, 1962, p. 319.
10. P. Gardie, G. Bordier, J.J. Poupeau, J. Le Ny, J. Nucl. Mater. 189 (1992) 85.

11. P. Chiotti, V.V. Akhachinskij, I. Ansara, M.H. Rand, in: The Chemical Thermodynamics of Actinide Elements and Compounds, Part 5, The Actinide Binary Alloys, IAEA, Vienna, 1981, p. 120.
12. J. Wang, X.J. Liu, C.P. Wang, J. Nucl. Mater 380 (2008) 105.
13. P. Manikandan, T.S. Lakshmi Narasimhan, M. Joseph and K. Nagarajan, Proceedings of the Sixteenth National Symposium on Thermal Analysis, BARC, Mumbai, Dec 19-21, 2013, P.59
14. C.W. Bale, E. Bélisle, P. Chartrand, S.A. Decterov, G. Eriksson, K. Hack, I.-H. Jung, Y.-B. Kang, J. Melançon, A.D. Pelton, C. Robelin, S. Petersen, CALPHAD, 33 (2009) 295.
15. D. Darwin Albert Raj, R. Viswanathan, and P. Manikandan ECS Transactions, 46 (1) (2013) 77.
16. JCPDS-ICDD (PDF-4+-2014). (Indexing numbers: U_3Ga_5: 04-001-1065; UGa_2: 04-003-6156; UGa_3: 04-006-7493)
17. C. E. Moore, Ionisation Potentials and ionisation limits derived from the analysis of Optical Spectra, NSRDS-NBS 34 (Nat. Stand. Ref. Data Ser., Nat. Bur. Stand., 34) (1970).
18. R. Hultgren, P.D. Desai, D.T. Hawkins, M.Gleiser, K.K. Kelly, "Selected values of the thermodynamic properties of the elements", John Wiley and Sons, Newyork, 1963.
19. JANAF Thermochemical Tables, 3rd ed., J. Phys. Chem. Ref. Data 14 Suppl. No. 1 (1985).
20. P. Chiotti and J.A. Kateley, J. Nuc. Mater, 32 (1969) 135.

21. O. Kubaschewski and C.B. Alcock, Metallurgical Thermochemistry, 5th edition, 1979. Pergamon press, Oxford, UK.

22. K. Nagarajan, Rita Saha, R. Babu, C. K. Mathews CK. Thermochim Acta, 90 (1985) 297.

23. Synthetic Sapphire Al_2O_3, Certificate of Standard Reference Materials 720, 1982. (NBS, U.S.Department of Commerce, Washington, DC 20234, USA).

24. Powder diffraction files (Inorganic Phases), Joint Committee on Powder Diffraction Data (JCPDS), International Centre for Diffraction Data (2015) (ICDD card number: 04 – 001 - 1065)

25. T.G. Godfrey, J.A. Woodley, J.M. Leitnaker, Thermodynamic Functions of Nuclear Materials, UC, UC_2, UO_2, ThO_2 and UN.ORNL-TM-1596 (Rev); 1966.

26. L.B. Pankratz, Thermodynamic properties of elements and oxides, Bull. US. Bur. Mines, 1982.

27. P. Manikandan , V.V. Trinadh, Suranjan Bera, T.S. Lakshmi Narasimhan, M. Joseph , J. Nucl. Mater, 475 (2016) 87.

Chapter 5

Part 1: Mass Spectrometric Studies on U-Pu-Zr alloy

5.1.1. Introduction

Metallic U-Pu-Zr fuel is considered as an advanced fast reactor fuel because of its superior properties such as high burn up potential, thermal response, inherent safety etc [1,2]. U-Pu-Zr alloy with composition U-19wt%Pu-6wt%Zr is being considered to be the driver fuel for the future Fast Reactors in India. Vaporisation behaviour and thermodynamic properties of this fuel are important to understand its behaviour during irradiation and under transient conditions. Studies on the vaporisation of the fuel also would help in identifying the vapour species present as well as in deriving their partial pressures. Kurata et al. [3] have re-evaluated the thermodynamic data pertaining to U-Pu-Zr system by using the CALPHAD method, incorporating recently determined experimental data on the various limiting binaries. O'Boyle and Dwight [4] had determined the nine isothermal sections of U-Pu-Zr system between 773 and 973 K by using electron microprobe analysis, X-ray diffraction, and optical metallographic techniques. The calculated phase diagram at 1500 K is shown in Figure 5.1.1 [3]. Kanno et al. [5] have carried out Knudsen Effusion Mass Spectrometric [KEMS] studies on U-Zr system in the temperature range 1770-2060 K for the compositions X_U = 0.098, 0.285, 0.478, 0.654 and 0.860 and reported the partial pressures of U(g) over these alloys. Subsequently, thermodynamic activities and partial molar Gibbs energies of uranium in the alloys were derived, and the same for zirconium were deduced by employing the Gibbs-Duhem integration. Using these data, integral molar Gibbs energies of the alloys were computed. Maeda et al. [6] had reinvestigated the U-Zr system by Knudsen effusion mass spectrometry for two uranium rich compositions, 24.4 and 39.3 at% Zr in the temperature range 1700-1973 K and reported vapour pressures of

uranium over these alloys and activities of uranium in these alloys. Leibowitz et al. [7] had derived the thermodynamic functions for all existing uranium-zirconium phases and also based on calculations given the phase diagram of the U-Zr system. Ogawa et al. [8] had carried out the thermochemical modeling of U-Zr alloys and described the thermochemical properties of the solution phases. Maeda et al. [9] had also studied the vaporisation behaviour of Pu-Zr binary alloys covering the entire composition range (X(Pu) = 0.06, 0.18, 0.25, 0.40, 0.50, and 0.80) by using Knudsen effusion mass spectrometry in the temperature range 1400-1900 K and reported the partial pressures and activities of plutonium in the alloys. Leibowitz et al. [10] have also carried out thermodynamic and phase diagram evaluation of U-Pu-Zr and the limiting binaries. However, there are no experimentally determined vapour pressure and other thermodynamic data available in the literature on U-Pu-Zr alloys. Even though the nominal fuel composition is U-19 wt%Pu-6 wt%Zr, the actual alloy sample composition used in this study was found to be U-18 wt%Pu-5.8 wt%Zr [11]. In the present work, the Knudsen effusion mass spectrometric studies on the composition U-19 wt%Pu-6.0 wt%Zr was undertaken. We deduced the vapour pressure and enthalpy of vaporisation by KEMS and also the vapour pressure values based on calculations assuming ideal solution model.

5.1.2 Experimental:

The U-Pu-Zr with the composition U-19 wt%Pu-6 wt%Zr was obtained from Bhabha Atomic Research Centre (BARC), Mumbai, India). It was prepared by gravity casting method [12]. In order to prevent the oxidation of this alloy, the samples were handled inside an argon atmosphere glove box (which houses KEMS; see below) in which the levels of oxygen and

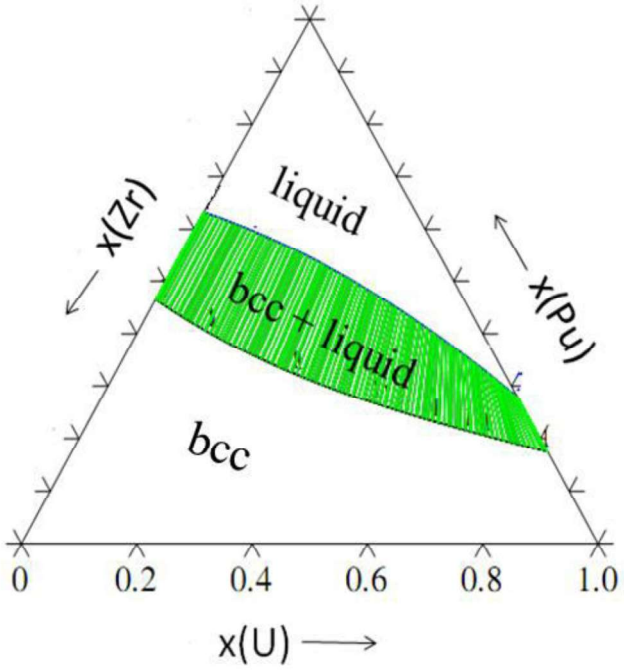

Fig 5.1.1. Isothermal section of the system U-Pu-Zr at 1500 K computed by using Kurata's data [3]

moisture were maintained below 10 ppm by passing the argon gas through a purification bed filled with molecular sieves and copper deoxo catalyst that trap moisture and oxygen, respectively. The levels of oxygen and moisture in the argon atmosphere glove box were measured by appropriate sensors.

5.1.3. Mass Spectrometric measurements

5.1.3.1 High Temperature Mass Spectrometry

The vaporisation studies were carried out by using a home built high temperature mass spectrometric system housed inside an inert atmosphere glove box. A schematic diagram of the vacuum envelope consisting of two chambers, one housing the Knudsen cell furnace assembly and the other housing the quadrupole mass spectrometer (QMS), is shown in Figure 3.1 of chapter 3 and detailed description of the instrument is given in that chapter.

Totally three sets of experiments were conducted, taking a fresh lot of sample each time. The samples were contained in an yttria Knudsen cell fitted with yttria lid (channeled orifice 0.7 mm dia) and this was placed in a tantalum outer cup fitted with tantalum lid. A hole drilled at the bottom of the tantalum cup serves as black body source for measuring the temperature using an a disappearing filament pyrometer. The tantalum cup containing the sample was heated (under a vacuum of 10^{-7} Torr) by electrons emitted from two surrounding tungsten filaments. The vapour effusing from the Knudsen cell was ionised by electron bombardment (electron energy = 28.8 eV; emission current 100 μA) and the ions produced were mass analysed using a quadrupole mass filter. The ion intensities were measured using a secondary electron multiplier operating in pulse counting mode. A shutter interposed between the Knudsen cell chamber and the ion source helped to discriminate the ions that emanated from the Knudsen cell and those produced due to the ionisation of the background molecules. The temperature of the Knudsen cell was measured

by focusing the pyrometer onto a black body hole provided at the bottom of the cell. The pyrometer was calibrated against the melting point of silver and the electron energy calibration was carried using the first ionisation energies of Ar^+, He^+, N_2^+, O_2^+ and H_2O^+. The error in temperature measurement was within ±5 K and that in the electron energy was ±0.5 eV.

In the first set of experiments, about 100 mg of sample was taken. This was used as preliminary experiments for ascertaining the ions, neutral species and temperature range of experiments and for obtaining the ionisation efficiency curve. The sample did not last long for carrying out any temperature dependence measurements. Subsequently about 300 mg of sample was used in the experiments 2 and 3 that were carried out over (solid +liquid) and liquid regions, respectively. The temperature of the sample was slowly increased from room temperature in steps of 50 degrees and at each temperature above 1400 K, the mass scanning was carried out looking for shutterable peaks. Pu^+ and PuO^+ were the ions observed in the mass spectra (from 1650 K onwards) over the alloy. PuO^+ was identified from mass number of the peak and the isotopic abundance. The intensities of PuO^+ vanished quickly as the sample was heated further. The intensities of $^{239}Pu^+$ were measured as a function of electron energy (in order to obtain ionisation efficiency curve) to deduce its appearance energy. The measurements over (solid+liquid) region were carried out in the temperature range 1481-1623 K, and that over the liquid phase in the range 1661-1763 K, respectively. The partial pressure data obtained for the temperatures above 1643 K corresponds to the liquid region of the alloy [14]. In a given run, the sample was kept at the first temperature for about an hour and the constancy of ion intensities during the period ensured the thermodynamic equilibrium inside the Knudsen cell. Subsequent temperature changes were made in steps of 10-20 K and the sample was kept at each successive temperature for about 30 minutes. Measurements of ion intensities were carried out with thermal

cycling in order to ensure reproducibility in the values measured. In all, four runs of temperature dependence of ion intensities of $^{239}Pu^{+}$, were carried out - two in the (solid+ liquid) two phase region and two in the liquid region. Pressure calibration experiments were carried out by taking pure silver in an alumina liner kept inside the same yttria Knudsen cell that was used in the measurements on U-Pu-Zr.

5.1.3.2. Thermal Ionisation Mass Spectrometry

The isotopic composition of U, Pu and Zr were obtained by using a magnetic sector-multi collector thermal ionisation mass spectrometer (Model: ISOPROBE-T, M/S ISOTOPX, UK). It is equipped with a 20 sample turret and multi detector array with 9 faraday cups and an axial secondary electron multiplier. The instrument uses a 90^0 sector magnet designed with 26.5^0 oblique incidences to provide a better mass dispersion. U-Pu-Zr sample dissolved in 12M HNO_3 was subjected to ion exchange separation to collect individual elements separately and to avoid isobaric interference at mass 238 from U and Pu. Dowex 1x8, 200-400 mesh anion exchange resin was loaded in glass column (~5.0 cm bed height). It was preconditioned with 10 bed volume of 7.5 M HNO_3. A known quantity of sample was taken in a teflon boat and evaporated under IR lamp. Before complete evaporation, sample was mixed with 7.5M HNO_3. After washing the column with 7.5M HNO_3, the preconditioned sample was loaded in the column. Two bed volumes of 7.5M HNO_3 were added to the column and the eluted solution was collected and analysed for Zr. Similarly four bed volume of 3.5 M HNO_3 was passed through this column to collect uranium. Finally five bed volume of 0.35M HNO_3 was passed through the column to elute plutonium. The above collected fractions were evaporated to dryness with an IR lamp. The samples were re-dissolved in a minimum quantity of the solvent (0.75 M HNO3) and loaded onto the filaments for analysis by TIMS. U and Pu samples were loaded on Ta outer filament in Ta-

Re-Ta triple filament configuration. Similarly Zr samples were loaded onto an outgassed rhenium filament in Re-Re-Re triple filament system.

TIMS analysis was carried out by using static multi collection mode and the collector gain calibration required for this purpose was carried out prior to the analysis of samples. More details are described elsewhere [15]. The samples were slowly heated to 4.5 A and 1.2 A using heating ramps of 0.002 A/s and 0.001 A/s for central (ionization) and side (vaporization) filaments respectively. At this stage, Re^+ signal was measured and the the focussing conditions were optimised with respect to this ion. Subsequently, the currents of side and center filaments were slowly increased to 1.9 A and 5.4 A respectively, to get minimum ion intensity for the peaks of interest. Once the ion of interest started appearing, "flat topped" isotopic peaks were obtained by proper focusing. Also, all the peaks were checked for "coincidence" which ensured each and every isotope fell on to a specific detector that was assigned to it. In general, the central filament and the side filaments were heated by using a current of 5.4 A and 2.3 A, respectively, for a satisfactory analysis of U and Pu. The isotope ratios were obtained by comparing the ion intensities. During the experiments, vacuum of around 5×10^{-8} Torr at the ion source and 4×10^{-9} Torr at the analyzer was maintained by using turbo molecular and ion pumps respectively. The isotopic abundances of uranium, plutonium and zirconium are given in table 5.1.1.

5.1.4. Computation Procedures

The partial pressures and activities of plutonium, uranium and zirconium were computed by using the partial pressure data reported over the binaries U-Zr [5] and Pu-Zr [9] and assuming ideal solution approach as given below.

Case 1: $U_pPu_qZr_{(1-p-q)}$ considered as an ideal solution of U-Zr and Pu-Zr alloys

Step-1: Formulation of equation

Table 5.1.1. Results of TIMS analysis for U-Pu-Zr alloy sample

Element,	Mass no of the Isotope	Relative Isotopic abundance (%)
Uranium	233	0.0066 ± 45.29
	234	0.0112 ± 50.99
	235	0.7304 ± 0.60
	236	0.0064 ± 48.86
	238	99.25 ± 0.008
Plutonium	238[a]	0.1851 ± 2.0
	239	70.18 ± 0.02
	240	25.41 ± 0.06
	241	2.577±0.36
	242	1.642 ± 0.61
Zirconium	90	48.78 ± 3.66
	91	10.52 ± 2.52
	92	18.29 ± 7.69
	94	17.39 ± 5.68
	96	5.26 ± 29.11

[a]Deduced by combining mass spectrometric and alpha spectrometric results.

$U_pPu_qZr_{(1-p-q)} \equiv x_1[U_{y1}Zr_{(1-y1)}] + (1-x_1)[Pu_{y2}Zr_{(1-y2)}]$ (5.1.1)

To solve for the three variables, x1, y1 and y2, two expressions, y1=p/x1 and y2 = q/(1- x1) were used. Obviously a range of values are possible which will satisfy the condition that $0 < y1 < 1$ and $0 < y2 < 1$. Two extreme ternary alloy combinations were selected, one in which the U-Zr alloy will have the highest possible U atomic fraction and the other in which the Pu-Zr alloy will have the highest possible Pu atomic fraction. Thus, for the ternary alloy of U75% Pu19% Zr6% (wt.%), two combinations represented by equations (2) and (3) will encompass the composition range:

$U_{0.684}Pu_{0.173}Zr_{0.143} \equiv 0.69\ [U_{0.991}Zr_{0.009}] + 0.31\ [Pu_{0.558}Zr_{0.442}]$ (5.1.2)

$U_{0.684}Pu_{0.173}Zr_{0.143} \equiv 0.82\ [U_{0.834}Zr_{0.166}] + 0.18\ [Pu_{0.961}Zr_{0.039}]$ (5.1.3)

Step-2: Calculation of vapour pressures for U-Zr alloys and Pu-Zr alloys of compositions given in equations (5.1.2) & (5.1.3).

At $T \leq 2000$ K, partial pressure of zirconium over U-Zr and Pu-Zr alloys can be neglected because even over elemental zirconium, the vapor pressure at T = 2000 K is only 4.6×10^{-4} Pa. Partial pressures over U-Zr and Pu-Zr alloys corresponding to the above mentioned compositions were deduced from the mass spectrometric results of Kanno et al. [5] for U-Zr system and of Maeda et al. [9] for Pu-Zr system. p(U) over any required composition of $U_{(1-x3)}Zr_{x3}$ is deduced from known values of p(U) over $U_{(1-x2)}Zr_{x2}$ and $U_{(1-x1)}Zr_{x1}$ by assuming that $[\Delta p(U)/\Delta x(U)]$ is constant between the two adjacent values of x(U). Values of activity of uranium and thus p(U) are available in the literature [5] for x(U) = 1, 0.86, 0.654, 0.478, 0.285. Similarly, p(Pu) over any required composition of $Pu_{(1-x3)}Zr_{x3}$ is deduced from the known values of p(Pu) over $Pu_{(1-x2)}Zr_{x2}$ and $Pu_{(1-x1)}Zr_{x1}$ by assuming that $[\Delta p(Pu)/\Delta x(U)]$ is constant between the two

adjacent values of x(Pu). Values of activity of Pu and thus p(Pu) are available in the literature [9] for x(Pu) = 1, 0.8, 0.5, 0.4.0.25, and 0.18.

Step 3: Calculation of vapor pressures over $U_pPu_qZr_{(1-p-q)}$

Vapour pressures were calculated using the combinations that have the most U-rich U-Zr alloy composition and also most Pu-rich Pu-Zr alloy composition.

(a) the combination that has the most U-rich U-Zr alloy composition (as per equation 5.1.2) $U_{0.684}$ $Pu_{0.173}$ $Zr_{0.143}$ is considered as an ideal solution of 0.69 [$U_{0.991}$ $Zr_{0.009}$] + 0.31 [$Pu_{0.558}Zr_{0.442}$]. The total vapor was deduced as sum of 0.69 × p(U) over $U_{0.991}$ $Zr_{0.009}$ and 0.31 × p(Pu) over $Pu_{0.558}Zr_{0.442}$.

(b) the combination that has the most Pu-rich Pu-Zr alloy composition (as per equation 5.1.3) $U_{0.684}Pu_{0.173}Zr_{0.143}$ is considered as an ideal solution of 0.82 [$U_{0.834}Zr_{0.166}$] + 0.18 [$Pu_{0.961}Zr_{0.039}$]. The total vapor pressure is the sum of 0.82 x p(U) over $U_{0.834}Zr_{0.166}$ and 0.18 x p(Pu) over $Pu_{0.961}Zr_{0.039}$.

Case-2: $U_pPu_qZr_{(1-p-q)}$ as an ideal solution of U, Pu, and Zr.

The total vapor pressure is the sum of $p^o(U) + q\ p^o(Pu) + (1-p-q)\ p^o(Zr)$ where p^o denotes the vapor pressure over pure element. The required vapour pressure data over pure elements were taken from reference [16].

5.1.5. Results and discussion

Figure 5.1.2 shows the ionisation efficiency curve (plot of ion intensity vs. electron energy) of $^{239}Pu^+$. From the curve, the appearance energy was derived by linear extrapolation method. The value of 6.3±0.5 eV deduced from the plot agrees well with the value of 6.02 eV reported in the literature [17]. The neutral precursor for the ion detected in the mass spectra were ascertained to be Pu(g) based on the mass, isotopic abundance and appearance energy. The

measured ion intensities of Pu were converted to partial pressures by the following relation

$$p_{Pu} = k'_{Pu}\, I_{Pu^+}\, T \qquad (5.1.4)$$

where $k'_{Pu} = k'_{Ag}\,(\sigma n)_{Ag} / (\sigma n)_{Pu}$ is the pressure calibration constant; I_{Pu^+}, the ion intensity of plutonium; σ, the ionisation cross section; n, the isotopic abundance. The plutonium ion intensities were measured with respect to the major isotope, Pu-239. The value of isotopic abundance of ^{239}Pu measured by using TIMS was used in computing the plutonium partial pressures. The mean pressure calibration constant derived from the calibration experiments with pure silver was used to convert the measured ion intensities of $^{239}Pu^+$ to partial pressures. Tables 5.1.2 and 5.1.3 give respectively, the least-square regression analysis of the dependence of vapour pressure on temperature along with the partial pressures for Pu(g) computed at the mean temperature of the investigation over (solid+liquid) and liquid regions. Figure 5.1.3 shows a typical plot of log (p_{Pu}/Pa) vs. 1/T (K^{-1}) obtained over the above phase regions. The equations 5.1.5 and 5.1.6 were obtained by least-squares regression analysis of all the data obtained from individual runs.

$\log(p_{pu}/Pa) = -(22254\pm282)/T + 10.80\pm0.18$ for (solid+liquid) (1481-1623 K) (5.1.5)

$\log(p_{pu}/Pa) = -(22021\pm1169)/T + 10.52\pm0.68$ for (liquid) (1661-1763 K) (5.1.6)

The apparent mean enthalpies of vaporisation of Pu(g) over (solid+liquid) and liquid regions at the mean temperature of investigation were deduced as 423.9 ± 10.2 (at 1552 K) and 425.9±12.8 (at 1712 K) kJ/mol, respectively. Partial pressures of Pu(g) calculated from the recommended equations over the (solid+liquid) and liquid regions at the mean temperature were

Table 5.1.2. Temperature dependence of partial pressure over (U-19 wt%Pu-6 wt%Zr) (solid+liquid)

Sample	Runs	Temp. range (K)	log(p_{Pu}/Pa) = -A/T+B		p_{Pu}/Pa at 1552 K	$\Delta_v H°_T$ (kJ.mol^{-1})
			A	B		
U-19Pu-6Zr	Run1	1544 - 1623	22113±809	10.71±0.51	2.9×10^{-4}	423.4±15.5
	Run2	1481-1593	22134±133	10.72±0.09	2.9×10^{-4}	423.8±2.6
	Combined	1481-1623	22254±282	10.80±0.18	2.9×10^{-4}	[a]423.6±9.1[b]
Pure Pu [16]		912-2500	16658	8.67	8.6×10^{-3}	318.9

[a]Mean $\Delta_v H_T^{\circ}$ of the two runs; [b]uncertainty estimated by error propagation method

Table 5.1.3. Temperature dependence of partial pressure over (U-19 wt%Pu-6 wt%Zr) liquid region

Sample	Runs	Temp. range (K)	log(p_{Pu}/Pa) = -A/T+B		p_{Pu}/Pa at 1712 K	$\Delta_v H°_T$ (kJ.mol^{-1})
			A	B		
U-19Pu-6Zr	Run1	1668-1763	22284±959	10.72±0.56	5.0×10^{-3}	426.7±18.4
	Run2	1661-1761	22206±378	10.58±0.22	4.0×10^{-3}	425.2±7.2
	Combined	1661-1763	22021±1169	10.52±0.68	4.5×10^{-3}	[a]425.9± 12.8[b]
Pure Pu [16]		912-2500	16658	8.67	8.7×10^{-2}	318.9

[a]Mean $\Delta_v H_T^{\circ}$ of the two runs; [b]uncertainty estimated by error propagation method

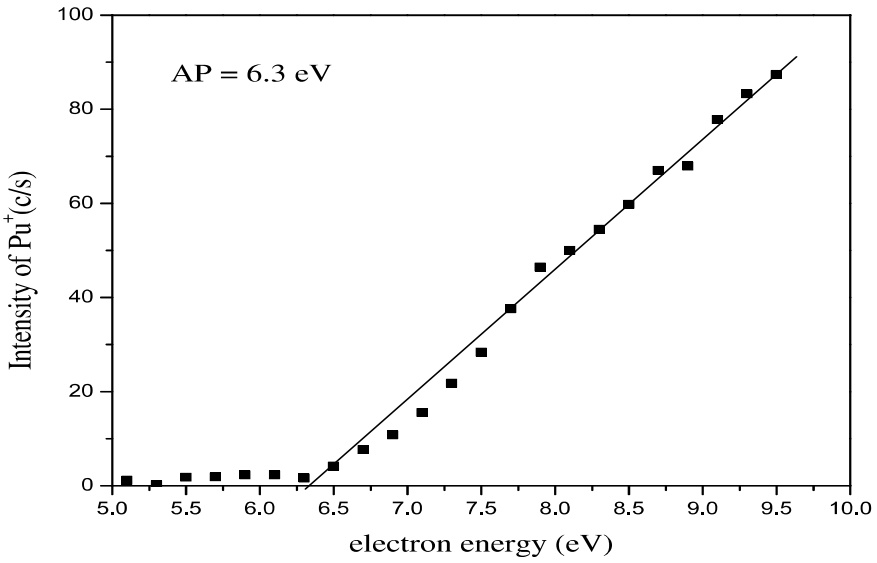

Fig 5.1.2. Ionisation Efficiency Curve of $^{239}Pu^{+}$

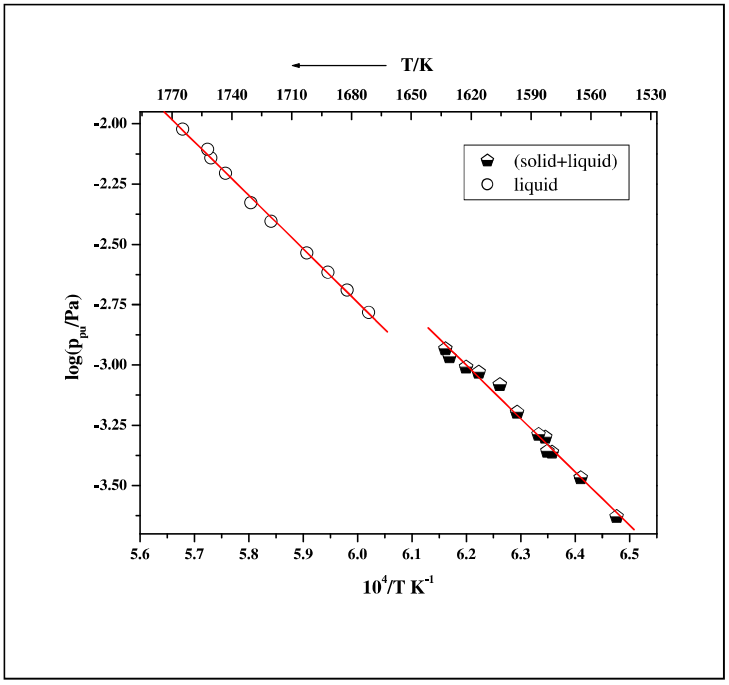

Fig 5.1.3: A typical plot of log (p_{Pu}/Pa) Vs 1/T (K^{-1}) over U-Pu-Zr alloy

2.9×10^{-4} Pa (1552 K) and 4.5×10^{-3} Pa (1712 K), respectively. From the measured partial pressures of Pu(g) over the alloy and that over pure Pu from literature [14], the activities of plutonium over the above phase regions were deduced as 0.03 (1552 K) and 0.05 (1712 K) respectively, indicating a negative deviation from Raoult's law.

The partial pressure data obtained by computation for case-1 and case-2 described in Section 2 are given in Table 5.1.4. The calculations were carried out essentially to compare the values obtained with experimental data and also with those computed from the equations proposed by Leibowitz et al. [10] and Joseph et al. [18] for the ternary U-Pu-Zr liquid solutions. The activities of Pu, U, and Zr and thus vapour pressures computed from the equations given by Leibowitz et al. [10] are given in Table 5.1.5. For the purpose of comparison, from the data given in Tables 5.1.4 and 5.1.5, pressure-temperature relations were deduced for uranium and plutonium. These relations are given in table 5.1.6 along with those obtained experimentally in the present study. As can be seen, the computed data for p(Pu(g) show a fair agreement amongst each other and the activities show a slight negative deviation from Raoult's law. A comparison of partial pressures of plutonium at 1700 K derived from the computation in the present work and those of Leibowitz et al. [10] with the experimental values from the present work indicate that the computed data are higher than the experimentally measured values by a factor of about 20. Joseph et al. [18] have reported a vapour pressure equation for this alloy composition based on a semi empirical method using the principle of corresponding state. The total pressure computed at 1700 K based on this equation gives a value of 2.29×10^{-2} Pa which is about 4.8 times higher than what has been experimentally obtained over liquid region.

Table 5.1.4: Partial pressures of U and Pu and total vapor pressure (in Pa) over [U-19 wt%Pu-6 wt%Zr] (i.e.) $U_{0.684}Pu_{0.173}Zr_{0.143}$ obtained from computations.

T/K	Case-1-Partial pressures as per equation 5.1.2[a]			Case-1- Partial pressures as per equation 5.1.3[b]			Case-2 [c] Ideal solution		
	p(U)	p(Pu)	P(tot)	p(U)	p(Pu)	P(tot)	p(U)	p(Pu)	P(tot)
1500	2.8×10^{-7}	4.2×10^{-3}	4.2×10^{-3}	3.2×10^{-7}	3.3×10^{-3}	3.3×10^{-3}	2.7×10^{-7}	3.4×10^{-3}	3.4×10^{-3}
1600	3.1×10^{-6}	2.1×10^{-2}	2.1×10^{-2}	3.2×10^{-6}	1.6×10^{-2}	1.6×10^{-2}	3.0×10^{-6}	1.8×10^{-2}	1.8×10^{-2}
1700	2.5×10^{-5}	8.4×10^{-2}	8.4×10^{-2}	2.4×10^{-5}	6.9×10^{-2}	6.9×10^{-2}	2.5×10^{-5}	7.8×10^{-2}	7.8×10^{-2}
1800	1.7×10^{-4}	2.9×10^{-1}	2.9×10^{-1}	1.4×10^{-4}	2.4×10^{-1}	2.5×10^{-1}	1.7×10^{-4}	2.9×10^{-1}	2.9×10^{-1}
1900	9.0×10^{-4}	9.0×10^{-1}	9.0×10^{-1}	7.2×10^{-4}	7.6×10^{-1}	7.6×10^{-1}	9.1×10^{-4}	9.4×10^{-1}	9.4×10^{-1}
2000	4.1×10^{-3}	2.5	2.5	3.0×10^{-3}	2.1	2.1	4.2×10^{-3}	2.7	2.7

[a] p(U) = 0.69 p(U) over $[U_{0.991}Zr_{0.009}]$; p(Pu) = 0.31 p(Pu) over $[Pu_{0.558}Zr_{0.442}]$

[b] p(U) = 0.82 p(U) over $[U_{0.834}Zr_{0.166}]$; p(Pu) = 0.18 p(Pu) over $[Pu_{0.961}Zr_{0.039}]$

[c] p(U) = 0.68 p(U) over elemental uranium; p(Pu) = 0.17 p(Pu) over elemental plutonium. That is a(U) = x(U) = 0.68, and a(Pu) = x(Pu) = 0.17.

Table 5.1.5. Activities for a liquid solution of [U-19 wt%Pu-6 wt%Zr] (i.e.) $U_{0.684}Pu_{0.173}Zr_{0.143}$, as computed from the equations proposed by Leibowitz et al. [10]; partial pressures deduced from the activity values.

T/K	U		Pu		Zr		P(tot)/Pa
	a(U)	p(U)/Pa	a(Pu)	p(Pu)/Pa	a(Zr)	p(Zr)/Pa	
1500	0.7363	2.96×10^{-7}	0.1560	3.04×10^{-3}	0.2342	7.40×10^{-10}	3.04×10^{-3}
1600	0.7329	3.26×10^{-6}	0.1571	1.63×10^{-2}	0.2271	1.40×10^{-8}	1.63×10^{-2}
1700	0.7300	2.72×10^{-5}	0.1580	7.15×10^{-2}	0.2210	1.87×10^{-7}	7.15×10^{-2}
1800	0.7273	1.79×10^{-4}	0.1588	2.67×10^{-1}	0.2157	1.87×10^{-6}	2.67×10^{-1}
1900	0.7250	9.64×10^{-4}	0.1595	8.65×10^{-1}	0.2111	1.47×10^{-5}	8.66×10^{-1}
2000	0.7229	4.39×10^{-3}	0.1601	2.50×10^{0}	0.2070	9.32×10^{-5}	2.50×10^{0}

Table 5.1.6. p-T relations for U, Pu, and total vapor pressure over U-19 wt%Pu-6 wt%Zr:

ln p/Pa = -A/T + B; p(tot) = p(Pu); $\Delta_v H^o$/(kJ/mol) = A*8.3143e-3

Method	$\log(p_{Pu}/Pa) = -A/T+B$		$\Delta_v H^o$ (kJ.mol^{-1})	P_{pu}/Pa at 1700 K
	A	B		
Present study (Experimental)	**Pu(g)**			
Solid+Liquid	22254±282	10.80±0.18	424	5.1×10^{-3}
Liquid	22021±1169	10.52±0.68	426	3.7×10^{-3}
Calculation				
Case 1[a]	16611	8.70	318	8.5×10^{-2}
Case 1[b]	16855	8.75	323	6.8×10^{-2}
Ideal solution (case 2)	17401	9.13	333	7.8×10^{-2}
Leibowitz et al. [10]	17488	9.14	335	7.1×10^{-2}
	$\log(p_U/Pa) = -A/T+B$			P_U/Pa at 1700 K
	U(g)			
	A	B		
Calculation				
Case 1[a]	24997	10.11	479	2.6×10^{-5}
Case 1[b]	23823	9.39	456	2.4×10^{-5}
case 2	25159	10.20	482	2.5×10^{-5}
Leibowitz et al. [10]	25030	10.15	479	2.7×10^{-5}

[a]Pressure temperature relation for $U_{0.684}Pu_{0.173}Zr_{0.143} \equiv 0.69\ [U_{0.991}Zr_{0.009}] + 0.31\ [Pu_{0.558}Zr_{0.442}]$

[b]Pressure temperature relation for $U_{0.684}Pu_{0.173}Zr_{0.143} \equiv 0.82\ [U_{0.834}Zr_{0.166}] + 0.18\ [Pu_{0.961}Zr_{0.039}]$

From the activity data given in Table 5.1.5, it can be seen that there is a slight negative deviation for Pu and positive deviations for U and Zr. We do not know the reason for this. However, we find in the equations pertaining to the calculation of activity coefficients given in reference [10] for Pu, a negative sign is present whereas for U and Zr, the negative sign is missing.

5.1.5.1. Calculation of uncertainty in the values of thermodynamic quantities

The estimated uncertainty (u) in the measured partial pressure of Pu(g) is u(p) =0.2p. The errors shown for the enthalpy of vaporisation were calculated from the standard deviation of the mean and the mean of the errors associated with individual values by using error propagation method.

5.1.6. Conclusion

Knudsen Effusion Mass Spectrometric experiments have been carried out on U-Pu-Zr alloy with the composition U-19 wt%Pu-6 wt%Zr. These measurements were carried out in two temperature ranges namely, 1481-1623 K (two phase region of solid + liquid) and 1661-1763 K (liquid). Pu(g) was the vapour species observed over the alloys. The pressure – temperature relations thus obtained over the (solid+liquid) and liquid phase regions were found to be:

$$\log(p_{Pu}/Pa) = (-22254\pm282)/T+(10.80\pm0.18) \text{ and}$$

$$\log(p_{Pu}/Pa) = (-22021\pm1169)/T+(10.52\pm0.68),$$

respectively. The enthalpies of vaporisation of plutonium over the (solid+liquid) and liquid phase regions were derived as: 423.9 ± 10.2 at 1552 K and 425.9 ± 12.8 kJ/mol at 1712 K respectively. All these data have been obtained for the first time. Partial pressures of U, Pu and Zr calculated based on ideal solution have also been deduced.

References:

[1] A. Riyas and P. Mohanakrishnan, Ann. Nucl. Energy, 35 (2008) 87. 11.

[2] G. L. Hofman, L. C. Walters and T. H. Bauer, Prog. Nucl. Energy, 31 (1997) 83

[3] M. Kurata,Calphad, 23 (1999) 305.

[4] D.R. O 'Boyle and A. E. Dwight, Plutonium and Other Actinides, ed. WN. Miner, Metallurgical Soc. Of AIME, New York, 1970

[5] M. Kanno, M.Yamawaki, T.Koyama, N. Morika, J. Nuc. Mater. 154 (1988) 154.

[6] A. Maeda, Y.Suzuki, Y. Okamoto, Toshihiko Ohmichi, J. Alloys.Compds, 205 (1994) 35.

[7] L. Leibowitz and R.A. Blomquist, J. Nucl. Mater. 167 (1989) 76.

[8] T. Ogawa and T. Iwai, J. Less-Common. Metals. 170 (1991) 101.

[9] A. Maeda, Y. Suzuki, T.Ohmichi, J. Alloys. Compds, 179 (1992) L21.

[10] L. Leibowitz, E. Veleckis, R.A. Blomquist, J. Nucl. Mater. 154 (1988) 145.

[11] B. Seenivasulu, A. Suresh, N. Sivaraman, M. Joseph, J. Radioanal. Nucl. Chem. 311 (2017) 789.

[12] Randall S. Fielding and Douglas L. Porter, J. Nucl. Mater, 441 (2013) 530

[13] P. Manikandan, V. V. Trinadh, Suranjan Bera, T. S. Lakshmi Narasimhan, M. Joseph, J. Nucl. Mater. 475 (2016) 87.

[14] P. Puthiyavinayagam, 'Progress in Fast Reactor Programme of India: April 2014 – March 2015', presented at 48th annual meeting of TWGFR IPPE, Obninsk, Russian Federation, 25-29 May 2015

[15] S. Bera, R. Balasubramanian, Arpita Datta, R. Sajimol, S. Nalini, T. S. Lakshmi Narasimhan, M. P. Antony, N. Sivaraman, K. Nagarajan, P. R. Vasudeva Rao, Int. J. *Anal* Mass. Spectrom. Cromatogr, 1 (2013) 55.

[16] C.B. Alcock, V.P. Itkin and M.K. Horrigan, Can,.Metall.Quart., 23 (1984) 309.

[17] J.E. Sansonetti and W.C. Marin, Handbook of Basic Atomic Spectroscopic Data, American Institute of Physics, 2005.

[18] M. Joseph, N. Sivakumar, P. Manoravi, Annals of Nuclear Energy. 31 (2004) 1163.

Part 2: vaporisation study of the Ru-Te binary system by Knudsen effusion mass spectrometry

5.2.1. Introduction

Thermodynamic information on binary systems of tellurium, a volatile and reactive element generated during fission in nuclear reactors, is of practical importance - to gain an understanding of the chemical interaction of tellurium with the fuel-cladding or with the fellow fission products [1]. Ruthenium is an important fission product with significant fission yield for nuclear reactor safety studies [2]. Its compounds with tellurium may play an important role in nuclear reactor safety studies [2]. KEMS study carried out on (Ru + Te) system is discussed in this chapter.

The only condensed phase known to exist in (Ru + Te) system is ruthenium ditelluride, $RuTe_2$ [3]. The phase diagram of this binary system (based on the work of Bernath et al. [3], as shown by Hokamoto [4] is given in figure 5.2.1. To our knowledge, no KEMS study has been conducted on this system. However, two vaporisation studies exist in literature, one performed by Svendsen in 1977 [5] using manometric method (silica spiral gauge) and the other by Ali Basu et al. in 2003 [6] by using forward collection method, essentially the mass-loss Knudsen effusion method. Svendsen's measurements corresponded to 1) $RuTe_x$ where x = 2.00, 1.98, 1.97, and 1.96 in the temperature range 1276-1423 K; and 2) $RuTe_y$ where y = 2.67 in the temperature range 915-1206 K. The author observed no systematic lowering of vapor pressure with composition for $RuTe_x$ and concluded that there is no homogeneity range on the Te-poor side of $RuTe_2$. Furthermore, the author treated vapor pressures measured over $RuTe_x$ as though all correspond to (Ru+$RuTe_2$) and reported a single Σ plot equation based on 40 values of $p(Te_2)$. The values of $p(Te_2)$ deducible from the Σ plot equation given by the author, however, are by a factor of ~ 200 lower than the actually measured values, the obvious reason could be an error in

the derivation of the Σ plot equation by the method of least-squares. In the case of $RuTe_y$ (liquid tellurium saturated with $RuTe_2$), the vapor pressures were nearly constant at $T > 1079$ K while

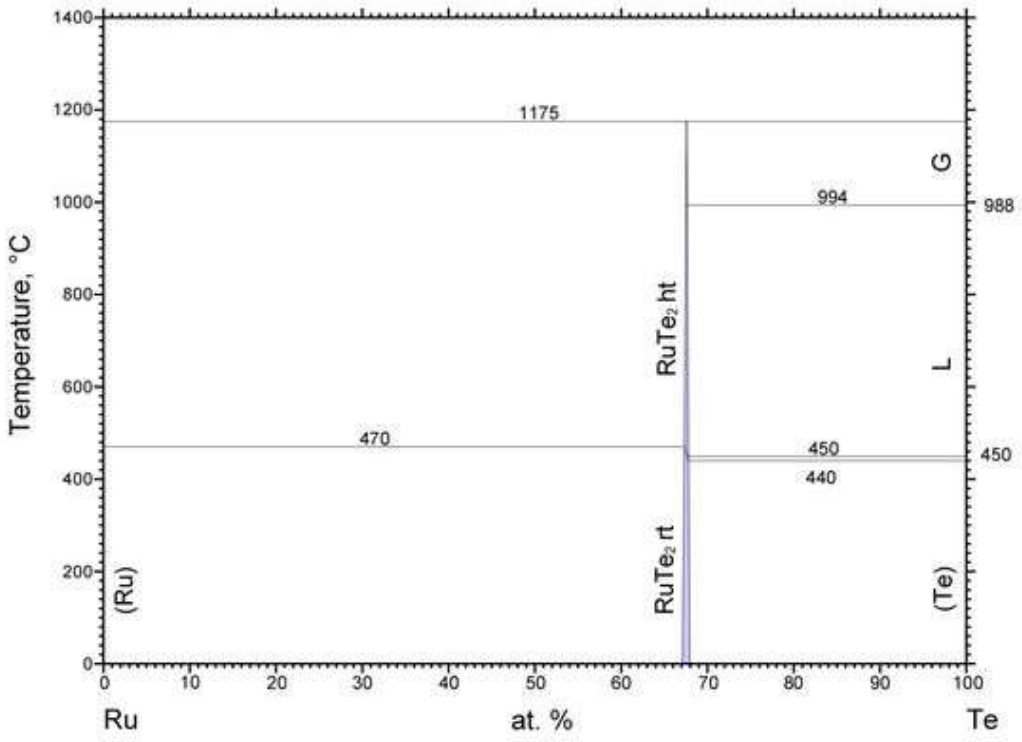

Fig. 5.2.1. Phase diagram as given by Hokamoto[4].

rt - room temperature; ht - high temperature

the values at T < 1079 K did yield a very slight positive partial molar enthalpy (that is, a slope slightly higher than that for liquid tellurium). The author attributed the break at 1073 K (in the plot of log[p(Te_2)] vs. 1/T) to formation of two liquids, but gave no reason for the break yielding only to a constancy of p(Te_2) ~ 46 torr from 1098 K right up to the final temperature, 1206 K, of their study with this sample. Ali Basu et al. [6] measurements corresponded to (Ru + $RuTe_2$) in the temperature range from 831 to 1148 K with correction for the possible deviation from Knudsen flow applied for the values of vapor pressure (assumed to be entirely due to Te_2(g) species) at T > 1026 K. The maximum correction reportedly required at the highest temperature of 1148 K was about 38 %. We find that the value of p(Te_2) obtained by Ali Basu et al., on extrapolation to the lowest temperature of Svendsen's measurements (1276 K), is higher by a factor of 5. A difference of this magnitude could arise if there is a phase transition, but non-observance by Svendsen [5] of any break in the differential thermal analysis measurements on a two-phase sample of (Ru + $RuTe_2$), heated to 1423 K, makes us infer that the discrepancy is real. Although Ali Basu et al. [6] did not mention about this discrepancy in their paper, they did point out the difference of 20 kJ mol^{-1} that exists in the value of enthalpy of formation of $RuTe_2$ deducible from their results and that recommended by Cordfunke and Konings [7], based on Svendsen's results. On the other hand, there was good agreement reported for value of entropy of formation of $RuTe_2$.

As for the homogeneity range of $RuTe_2$, Bernath et al. [3] estimated it to be hyper-stoichiometric and narrow: from 67.3 to 67.8 at.% Te ($RuTe_{2.06}$ to $RuTe_{2.11}$). Zhao et al. [8] also estimated it to be narrow but hypo-stoichiomtric: from 66.5 to 66.7 at. % Te. In terms of formula, however, these authors stated it to vary from $RuTe_{2.0}$ and $RuTe_{1.9}$, which makes one suspect

whether the authors estimated that Ru-rich boundary could be down to 65.5 at. % Te (that is, well into hypo-stoichiometry).

With the above background of information on the Ru-Te system, vaporisation studies were conducted on Ru-Te samples with initial compositions 40.0, 50.5, 69.5 and 71.5 at.% Te, respectively by using KEMS. The experiments with the first two compositions had the objective of determining the partial pressures of gaseous species over the two-phase field (Ru + $RuTe_2$) while the experiments with the latter two compositions had the objective of deducing the homogeneity range of $RuTe_2$ by making use of preferential vaporisation of tellurium from the sample, initially corresponding to the two-phase field ($RuTe_2$ + Te). The chapter describes these measurements.

5.2.2. Experimental

Four samples were prepared such that two each would lie on either side of $RuTe_2$ in the Ru-Te phase diagram [3] (see figure 5.2.1) - by direct reaction of ruthenium and tellurium (both from Leico, U. S. A; and purity: 0.999 mass fraction), the compositions of the samples being 40.0, 50.5, 69.5, and 71.5 at. % Te deduced basically from the masses of Ru and Te taken for preparation. The samples will be henceforth referred to as S1 (40.0 at. %) , S2 (50.0 at. %), S3 (69.5 at. %) and S4 (71.5 at. %), respectively. Sample preparation essentially consisted of the following steps: i) taking appropriate amounts of Ru and Te: ii) homogeneous mixing of the two powders with a mortar and pestle: iii) pelletising; iv) placing the pellets in the one end closed quartz tubes, a few times of flushing with argon followed by evacuation; v) sealing the quartz tubes under a residual pressure of 10^{-5} torr; vi) finally heating vacuum-sealed quartz tubes at appropriate temperatures in an horizontal furnace. At the end of the first cycle of heating (S1 and S2 at 700 °C for 7 days; S3 and S4 at 400 °C for 18 days), the quartz tubes were broken

open, the pellets were ground, and the whole operation was repeated for a second cycle of heating for similar duration. The heating as well cooling cycles involved keeping the samples at different temperatures (steps of 100 °C for a minimum duration of about 30 minutes). The samples prepared were subsequently characterized by XRD to confirm that S1 and S2 belonged to the (Ru + $RuTe_2$) two-phase region while S3 and S4 belonged to the ($RuTe_2$ + Te) two-phase region. Aliquots from S1 and S2 were used for vapor pressure measurements as a function of temperature while those from S3 and S4 were used for long vaporisation experiments, isothermal at most parts, to deduce the phase boundaries of $RuTe_2$. Pressure calibration experiments were performed before as well as after the experiments with S1 and S2 by using Te(s), and sometimes additionally with Ag(s) also, although, only the values from Te(s) pressure calibrations were finally used. In the case of runs with S3 and S4, since the starting mixture itself had excess tellurium, it was possible to have the pressure calibration with Te(s) performed in situ.

The vaporisation experiments were carried out by using a VG micromass 30 BK Knudsen effusion mass spectrometer. Alumina Knudsen cells having a knife edged orifice of ≈ 0.5 mm diameter were used to contain the samples. The Knudsen cell was kept inside an outer molybdenum cup and closed with a tight-fitting lid made of tungsten and having a 3 mm diameter circular hole collinear with the Knudsen cell orifice. Heating of this whole unit ('K-cell furnace') was done by radiation and electron bombardment (EB) from two independent tungsten filaments that encircled it, one just below the top of the W lid, and the other just above the base of the Mo cup. Radiation shields, made of tantalum, were placed all around the filaments (as well as at the top and bottom) which aided the temperature stability of the K-cell furnace. The temperatures were measured by a chromel-alumel thermocouple (stainless steel sheathed) inserted through the base of the molybdenum cup and touching the base of the Knudsen cell. A

temperature regulation of ± 1 °C could be achieved by using the provision of "thermocouple control mode", available in the EB power supply. The molecular beam effusing out of the Knudsen cell was ionized by impact of electrons emitted from a heated tungsten filament in the ionization chamber. The ions produced were accelerated to 6 kV, mass separated by a 90^{o} sector magnetic analyzer, and detected by a secondary electron multiplier/ Faraday cup. In this work, only the secondary electron multiplier detector (with discrete dynodes) was used to measure the ion currents. A 'molecular beam' shutter (a stainless steel plate), positioned just below the entrance slit of the ion-source block and operated by means of a linear motion drive, provided the means of measuring the ion intensities under 'shutter open' condition (that is, with the shutter withdrawn) and under 'shutter close' condition (that is, with the shutter moved horizontally across so as to block the effusing molecular beam from entering into the ion-source). Thus the ion intensities measured under shutter close condition result from the ionization of residual gas in the ion-source while those measured under shutter open condition result from the ionization additionally of vapor species effusing from the Knudsen cell.

Periodically, calibration of thermocouple and ionising electron energy scale was performed - the thermocouple calibration against the melting temperature of silver and by checking the temperature dependence of ion intensity of Ag^{+} over Ag(s); and the electron energy calibration by determining the apparent appearance energies (AE) for In^{+}, Hg^{+}, Ag^{+}, Ar^{+} and He^{+} and by checking the linear relationship between AE and the known first ionization energies (IE).

With S1 and S2, many experiments of different types were performed, but, for obtaining the partial pressure-temperature relations corresponding to (Ru + $RuTe_2$), only six runs were chosen, two runs with one aliquot of S1 (61.6 mg) and four runs, two with each of two aliquots

of S2 (80.1 and 84.3 mg). The ion intensities of Te^+ and Te_2^+, the only ionic species detected, were measured at different electron energies, viz., 29.6, 26.6, and 11.6 eV, the contribution to $I(Te^+)$ through dissociative ionization of $Te_2(g)$ expected to be relatively very low at 11.6 eV. With S3 and S4 also, many experiments were performed, but, for reporting the phase boundaries of $RuTe_2$, only four runs were chosen, two runs with two aliquots of S3 (78.9 and 21.9 mg) and two runs with S4 (77.8 and 79.9 mg). Results from S1 and S2 showing Te(g) to be < 5 % of the vapor phase, measurements on S3 and S4 were restricted to only $I(Te_2^+)$ and at high electron energies to have high intensity. At the end of each of run with S3 and S4, the container was weighed to deduce the mass loss and thus the final composition as well. Furthermore, the residues from S3 and S4 were also subsequently subjected to temperature dependence experiments to examine whether the results are similar to those with S1 and S2.

5.2.3. Results and Discussion

5.2.3.1. Pressure calibration with Te(s)

With the information available in literature on (Ru + $RuTe_2$) [5, 6] pointing towards preferential vaporisation of tellurium, mainly as $Te_2(g)$, we first took up experiments with elemental tellurium to obtain pressure calibration constant $k(Te_2)$, according to the relation:

$$k(Te_2) = [p^o(Te_2)]/[I^o(Te_2^+)\cdot T], \quad (5.2.1)$$

where $p^o(Te_2)$ is the known partial pressure of $Te_2(g)$ over Te(s) [9] and $I^o(Te_2^+)$ is the measured ion intensity of Te_2^+ at temperature T. Usually, $k(Te_2)$ was determined at least at three temperatures and a mean value was computed. $k(Te_2)$ was also determined at two electron impact energies E_1 and E_2, chosen after determining the ionisation efficiency curves for Te^+ and Te_2^+ such that at E_1, $I(Te_2^+)$ would be around the maximum value and at E_2, fragmentation of $Te_2(g)$ would be negligibly low. Similar pressure calibration was once again performed at the

end of the experiments with (Ru + $RuTe_2$). A mean value from both pressure calibrations was employed to deduce the partial pressures of Te(g) and Te_2(g) over (Ru + $RuTe_2$), as described below.

5.2.3.2. Partial pressure measurements over (Ru + $RuTe_2$) for samples S1 and S2

Te^+ and Te_2^+ are the ions observed in the mass spectrum of the equilibrium vapor over (Ru + $RuTe_2$) at T ~ 1030 K, at which, the vapor pressure as deducible from previous studies (0.6 Pa [5] and 4.1 Pa [6]), would be within that which would ensure Knudsen flow conditions. These ions were identified by comparison of intensities at different m/z values from 120 to 130 (for Te^+) and from 250 to 260 (for Te_2^+) with the relative isotopic abundances known for Te^+ and computed for Te_2^+. Subsequent measurements were restricted to the isotope that has the highest relative abundance. Thus, in the whole paper, I(Te^+) corresponds to m/z = 130 and I(Te_2^+) corresponds to m/z = 256. Measurement of I(Te^+) and I(Te_2^+) as a function of electron impact energy (at a constant vaporisation temperature of ~ 1030 K) was then performed which led to obtain ionisation efficiency curves for the two ions. Figure 5.2.2 shows the ionisation efficiency curves for both Te^+ and Te_2^+ (corresponding to the linear portion) over Te(s) (figure 5.2.2a and 5.2.2b) and over (Ru + $RuTe_2$) (figure 5.2.2c and 5.2.2d). Since the appearance of Te^+ over Te(s) (Figure 5.2.2b) is known to be only due to fragmentation [9] and since appearance of Te^+ over (Ru + $RuTe_2$) is at much lower energy (Figure 5.2.2d), one can infer that in the case of latter, I(Te^+) contribution from fragmentation is negligible at the electron energy E2 (≈ 11.6 eV). I(Te^+) and I(Te_2^+) were measured as a function of Knudsen cell temperature, at high and low electron impact energies. The maximum temperature change covered was from 860 to 1030 K in the two runs with an aliquot from S1, and from 910 to 1030 K with an aliquot from S2, and from 920 to 1030 K with another aliquot from S2. Optimization of I(Te_2^+) with respect to Knudsen

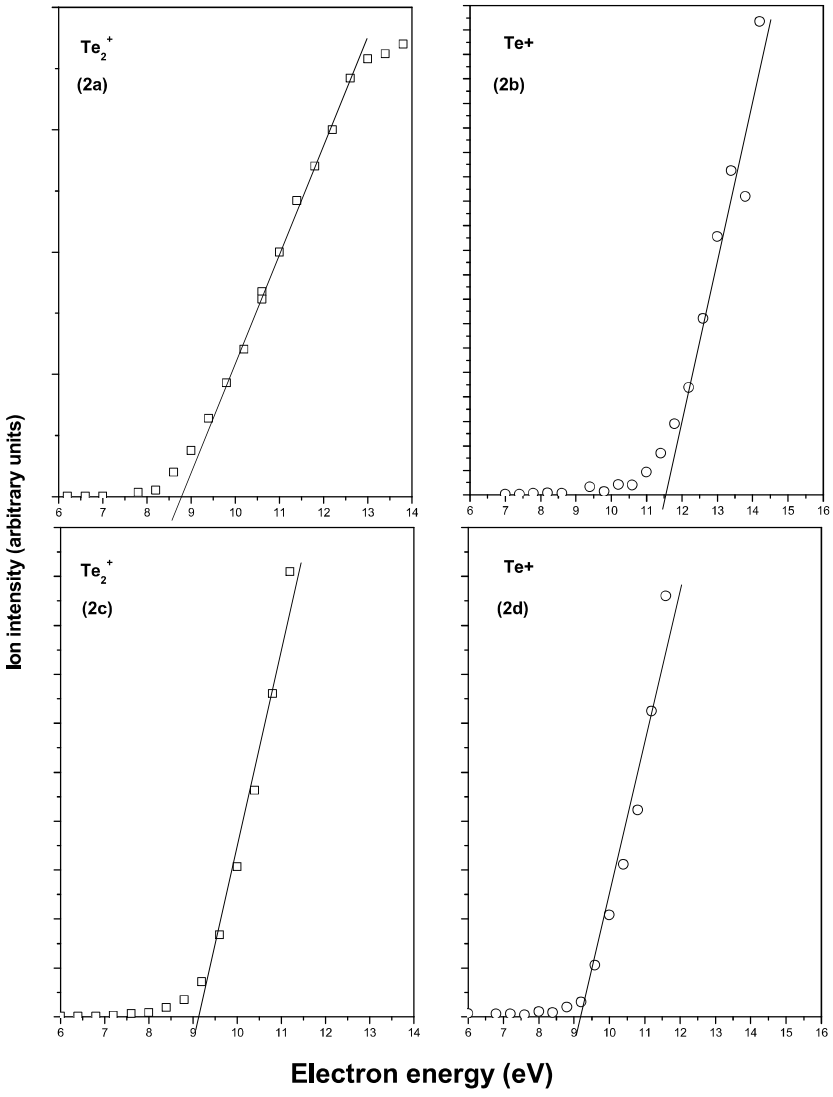

Fig.5.2.2. Ionisation efficiency curves over Te(s) (2a and 2b), and over (Ru + $RuTe_2$) (2c and 2d).

cell position was done mostly at high electron energy, but with respect to focusing conditions, it was done at low electron energy in all runs. Table 5.2.1 gives $I(Te^+)$ and $I(Te_2^+)$ measured over S1 and S2 in six runs. These are net intensities, computed from the intensities measured first with the 'molecular beam shutter' open, then with the 'molecular beam shutter' close, and again with the 'molecular beam shutter' open. For some inexplicable reason, measurement of $I(Te^+)$ in runs 5 and 6 was afflicted with instability which forced us to ignore as unreliable even those measured at a few temperatures. Partial pressures $p(Te_2)$ and $p(Te)$ were computed from the ion intensities according to relations:

$$p(Te_2) = k1 \cdot I(Te_2^+) \cdot T \tag{5.2.2}$$

$$p(Te) = k1 \cdot I(Te^+) \cdot T \cdot k2 \tag{5.2.3}$$

where $k1 = k(Te_2)$, the pressure calibration constant for $Te_2(g)$ obtained in pressure calibration runs over elemental tellurium (see equation 5.2.1). k2 is just another constant (as defined in equation 5.2.4 given below) , employed to account for the differing values of σ (the ionization cross sections for the gaseous species Te_2 and Te), γ (the relative detector gain for the ionic species Te_2^+ and Te^+), and η (the relative abundance of the measured isotope of Te_2^+ and Te^+).

$$k2 = [\sigma(Te_2)/\sigma(Te)] \cdot [\gamma(Te_2^+)/\gamma(Te^+)] \cdot [\eta(Te_2^+)/\eta(Te^+)] \tag{5.2.4}$$

Since $\sigma(Te_2)$ was assumed as 1.44 times $\sigma(Te)$, absolute value of $\sigma(Te)$ was not required to be used at any electron energy. The selection of $\sigma(Te_2)/\sigma(Te) = 1.44$ was prompted by its usage by us previously in our measurements on elemental tellurium [9] and tellurium and selenium clusters [10], and by Rosinger et al.[11] in their measurements on sulfur clusters. The value of γ was assumed to be inversely proportional to square root of the mass of the ion. The value of η for $^{130}Te^+$ was taken from literature (33.799%) [12] while that of $^{256}Te_2^+$ was computed. The

Table 5.2.1

Ion intensities (arbitrary units, I/I^{θ}) measured as a function of temperature at high (E1) and low electron energies (E2) over (Ru + $RuTe_2$).

T/K	I^+ at E1		I^+ at E2		*T*/K	I^+ at E1		I^+ at E2	
	$I(Te_2^+)$	$I(Te^+)$	$I(Te_2^+)$	$I(Te^+)$		$I(Te_2^+)$	$I(Te^+)$	$I(Te_2^+)$	$I(Te^+)$
S1(aliquot1): Run 1; E1=29.6 eV; E2=11.6 eV					S1(aliquot1): Run 2; E1=29.6 eV; E2=11.6 eV				
860	6.7×10^{-5}		1.5×10^{-5}		860	3.5×10^{-5}		1.7×10^{-5}	
870	9.7×10^{-5}		3.5×10^{-5}		880	1.0×10^{-4}	4.8×10^{-5}	5.2×10^{-5}	7.6×10^{-6}
885	1.9×10^{-4}	8.3×10^{-5}	5.6×10^{-5}	4.4×10^{-6}	900	2.5×10^{-4}	1.1×10^{-4}	1.3×10^{-4}	1.8×10^{-5}
900	3.3×10^{-4}	1.3×10^{-4}	1.3×10^{-4}	1.5×10^{-5}	920	5.6×10^{-4}	2.6×10^{-4}	2.9×10^{-4}	3.4×10^{-5}
915	6.9×10^{-4}	2.7×10^{-5}	2.3×10^{-4}	2.4×10^{-5}	940	1.3×10^{-3}	5.3×10^{-4}	6.7×10^{-4}	7.4×10^{-5}
930	1.4×10^{-3}	5.4×10^{-4}	4.6×10^{-4}	4.6×10^{-5}	960	2.7×10^{-3}	1.1×10^{-3}	1.4×10^{-3}	1.5×10^{-4}
945	2.6×10^{-3}	9.8×10^{-4}	7.7×10^{-4}	8.0×10^{-5}	960	3.0×10^{-3}	1.2×10^{-3}	1.4×10^{-3}	1.5×10^{-4}
960	4.5×10^{-3}	1.7×10^{-4}	1.4×10^{-3}	1.4×10^{-4}	980	5.9×10^{-3}	2.2×10^{-3}	2.9×10^{-3}	2.6×10^{-4}
975	8.3×10^{-3}	3.0×10^{-4}	2.7×10^{-3}	2.4×10^{-4}	1000	1.5×10^{-2}	4.6×10^{-3}	6.7×10^{-3}	5.5×10^{-4}
990	1.4×10^{-2}	5.2×10^{-3}	4.6×10^{-3}	4.1×10^{-4}	1018	2.6×10^{-2}	8.6×10^{-3}	1.2×10^{-2}	9.7×10^{-4}
1010	3.0×10^{-2}	1.0×10^{-3}	8.9×10^{-3}	8.7×10^{-4}	1030	3.9×10^{-2}	1.3×10^{-2}	1.8×10^{-2}	1.5×10^{-3}
1030	5.8×10^{-2}		1.2×10^{-2}						
S2(aliquot1): Run 3; E1=26.6 eV; E2=11.6 eV					S2(aliquot1): Run 4; E1=26.6 eV; E2=11.6 eV				
975	7.5×10^{-3}	3.4×10^{-3}	2.8×10^{-3}	2.7×10^{-4}	910	4.0×10^{-4}	2.1×10^{-4}	1.3×10^{-4}	2.1×10^{-5}
990	1.3×10^{-2}	5.6×10^{-3}	4.4×10^{-3}	4.3×10^{-4}	930	8.3×10^{-4}	3.8×10^{-4}	2.7×10^{-4}	5.3×10^{-5}
1005	2.2×10^{-2}	8.9×10^{-3}	7.3×10^{-3}	6.7×10^{-4}	950	1.9×10^{-3}	1.1×10^{-3}	6.9×10^{-4}	7.9×10^{-5}
1020	3.8×10^{-2}	1.5×10^{-2}	1.3×10^{-2}	9.2×10^{-4}	960	3.8×10^{-3}	1.7×10^{-3}	1.3×10^{-3}	1.2×10^{-4}
1030	5.1×10^{-2}	1.9×10^{-2}	1.8×10^{-2}	1.2×10^{-3}	975	6.1×10^{-3}	3.0×10^{-3}	2.3×10^{-3}	2.1×10^{-4}
960	3.5×10^{-3}	1.6×10^{-3}	1.2×10^{-3}	1.2×10^{-4}	990	1.1×10^{-2}	5.1×10^{-3}	3.5×10^{-3}	3.3×10^{-4}
945	1.8×10^{-3}	1.0×10^{-3}	6.2×10^{-4}	7.2×10^{-5}	1005	1.9×10^{-2}	8.0×10^{-3}	6.5×10^{-3}	5.9×10^{-4}
930	9.7×10^{-4}	5.6×10^{-4}	3.3×10^{-4}	5.1×10^{-5}	1020	2.5×10^{-2}	1.3×10^{-2}	1.0×10^{-2}	9.1×10^{-4}
910	3.3×10^{-4}	3.4×10^{-4}	1.2×10^{-4}	2.9×10^{-5}	1030	3.8×10^{-2}	1.7×10^{-2}	1.4×10^{-2}	1.1×10^{-3}
S2(aliquot2): Run 5; E1=26.6 eV; E2=11.6 eV					S2(aliquot2): Run 6; E1=26.6 eV; E2=11.6 eV				
920	5.3×10^{-4}		3.3×10^{-4}		920	5.3×10^{-4}		3.1×10^{-4}	
930	9.1×10^{-4}		5.0×10^{-4}		930	6.8×10^{-4}		4.6×10^{-4}	
950	1.9×10^{-3}		1.1×10^{-3}		950	1.8×10^{-3}		1.0×10^{-3}	
965	3.0×10^{-3}		2.1×10^{-3}		965	3.0×10^{-3}		2.0×10^{-3}	
980	6.5×10^{-3}		4.1×10^{-3}		980	6.2×10^{-3}		3.9×10^{-3}	
1000	1.1×10^{-2}		7.4×10^{-3}		1000	1.1×10^{-2}		7.2×10^{-3}	
1015	1.9×10^{-2}		1.2×10^{-2}		1015	1.9×10^{-2}		1.2×10^{-2}	
1030	3.3×10^{-2}		2.1×10^{-2}		1030	3.1×10^{-2}		1.9×10^{-2}	

values of $p(Te_2)$ and $p(Te)$ so obtained were subjected to second- and third-law evaluation of following vaporisation reactions:

$$RuTe_2(s) \rightleftharpoons Ru(s) + (2/i)Te_i(g) \; (i = 2 \text{ or } 1) \qquad (5.2.5)$$

Tables 5.2.2 and 5.2.3 give the results evaluated for $Te_2(g)$ and Te(g), respectively. The *p-T* relations (log [p(i)/Pa] = (-A/T) + B) were deduced by the method of least-squares and $p(i)$ for each run at $T = 975$ K was computed subsequently from these relations. The equations used for the second-and third-law evaluations are:

$$[\Delta_r H_m^o(T_m)]_{II\ law} = (-R) * 2.3026 * A*(2/i) \qquad (i = 2 \text{ or } 1) \qquad (5.2.6)$$

$$[\Delta_r H_m^o(298.15\ K)]_{II\ law} = [\Delta_r H_m^o(T_m)]_{II\ law} - \Delta_r[H^o(T_m) - H^o(298.15\ K)] \qquad (5.2.7)$$

$$[\Delta_r H_m^o(298.15\ K)]_{III\ law} = [(-T)\cdot R\cdot \ln(K^o)] - [T\cdot \Delta_r\{[G^o(T) - H^o(298.15\ K)]/T\}] \qquad (5.2.8)$$

where T_m is the mean temperature of a run taken as $[(T_1 + T_2)/2]$ where T_1 is the lowest temperature and T_2 is the highest temperature in the run, R is the universal gas constant, $[H^o(T_m) - H^o(298.15\ K)]$ is the enthalpy increment for each participant in the reaction, K^o, the equilibrium constant = $\{[p(Te_i)/Pa]/[101325\ Pa]\}^{(2/i)}$ for the reaction, and $\{-[G^o(T) - H^o(298.15\ K)]/T\}]$ is the Gibbs free energy function for each participant in the reaction.

Table 5.2.4 gives the auxiliary thermal functions [7] (enthalpy increments and Gibbs free energy functions) used in these evaluations for $RuTe_2(s)$, Ru(s), $Te_2(g)$, and Te(g).

From Table 5.2.2 where results for $Te_2(g)$ are shown, one infers that while there is reasonably good agreement between the partial pressures of $Te_2(g)$, $[p(Te_2)]$, measured at high and low electron energies, the agreement between second and third law enthalpies was not that good at both electron energies, the second-law values being ≈ 30 kJ·mol^{-1} consistently higher in

Table 5.2.2 Evaluation of $p(Te_2)$ with measured $I(Te_2^+)$[a] over (Ru+$RuTe_2$). Reaction: $RuTe_2(s) = Ru(s) + Te_2(g)$.

Run No.	Temperature Range		Log(p/Pa) = -[A/(T/K)] + B		P/Pa at T = 975 K	$\Delta_r H_m^o(T)$/ (kJ·mol^{-1})		
						Second-law		Third-law
	T_1/K	T_2/K	-A	B		at $T_m = (T_1+T_2)/2$	at 298.15 K	at 298.15 K
At high electron energy (29.6 eV or 26.6 eV) [b]								
1	860	1030	15992 ± 137	16.16 ± 0.15	0.57	306.2 ± 2.6	312.8 ±2.6	280.9 ± 0.6
2	860	1030	16196 ± 139	16.17 ± 0.15	0.36	310.1 ± 2.7	316.7 ± 2.7	284.2 ± 0.6
3	910	1030	17367 ± 370	17.48 ± 0.38	0.47	332.5 ± 7.1	338.9 ± 7.1	281.5 ± 0.8
4	910	1030	16078 ±429	16.09 ±0.44	0.39	307.9 ± 8.2	314.3 ± 8.2	282.7 ± 0.6
5	920	1030	15604 ± 301	15.70 ± 0.31	0.49	298.8 ± 5.8	305.1 ±5.8	280.9 ± 0.4
6	920	1030	15883 ± 318	15.96 ± 0.33	0.47	304.1 ± 6.1	310.5 ±6.1	281.4 ± 0.5
At low electron energy (11.6 eV)[c]								
1	860	1030	15678 ± 309	15.77 ± 0.33	0.49	300.2 ± 5.9	306.8 ± 5.9	281.8 ± 0.5
2	860	1030	15936 ± 128	16.05 ± 0.14	0.51	305.1 ±2.5	311.7 ± 2.5	281.3 ± 0.6
3	910	1030	17336 ± 412	17.45 ± 0.42	0.46	332.0 ± 7.9	338.3± 7.9	281.5 ± 0.8
4	910	1030	16650 ± 382	16.68 ± 0.39	0.40	318.8 ± 7.3	325.2 ± 7.3	282.7 ± 0.7
5	920	1030	16016 ± 220	16.11 ± 0.23	0.48	306.7 ± 4.2	313.0 ± 4.2	281.1 ± 0.5
6	920	1030	16096 ± 253	16.17 ±0.26	0.45	308.2 ± 4.8	314.6 ± 4.8	281.6 ± 0.5

[a] Measured $I(Te_2^+)$ are given in Table 1. $p(Te_2) = k1 \cdot I(Te_2^+) \cdot T$

[b] k1 = 0.0717 for run 1; 0.070 for run 2; 0.0716 for runs 3 and 4; 0.1061 for runs 5 and 6.

[c] k1 = 0.210 for runs 1; 0.2052 for run 2; 0.2051 for runs 3 and 4; 0.164 for runs 5 and 6.

Table 5.2.3 Evaluation of p(Te) with measured I(Te^+)[a] over (Ru+$RuTe_2$). Reaction: $RuTe_2$(s) = Ru(s) + 2 Te(g).

Run No.	Temperature Range		Log(p/Pa) = -[A/(T/K)] + B		P/Pa at T = 975 K	$\Delta_r H_m^o(T)$/ (kJ·mol^{-1})		
						Second-law		Third-law
	T_1/K	T_2/K	-A	B		at T_m = (T_1+T_2)/2	at 298.15 K	at 298.15 K
At high electron energy (29.6 eV or 26.6 eV)[b]								
1	900	1010	15938 ± 152	15.51 ±0.16	0.15	610.4 ± 5.8	616.1 ±5.8	507.3 ± 1.6
2	880	1030	14992 ± 103	14.34 ± 0.11	0.09	574.1 ± 3.9	579.8± 3.9	513.4 ± 1.2
3	910	1030	14786 ± 390	14.36 ± 0.40	0.16	566.2 ± 14.9	571.9 ±14.9	503.9 ± 1.2
4	910	1030	15734 ± 396	15.26 ± 0.41	0.13	602.5 ± 15.2	608.2 ± 15.2	506.6 ± 1.6
At low electron energy (11.6 eV); Case 1: with normal k1[c]								
1	900 [d]	1010	15063 ± 198	13.996 ± 0.21	0.035	576.8± 7.6	582.6 ± 7.6	529.1 ± 0.9
2	880	1030	14106 ± 166	13.005 ± 0.17	0.034	540.2 ± 6.4	545.9 ± 6.4	528.5 ± 0.5
3	910	1030	13708 ± 467	12.58 ± 0.48	0.033	525.0 ± 17.9	530.6± 17.9	529.0 ± 0.7
4	910	1030	13879 ± 354	12.70 ± 0.36	0.029	531.5 ± 13.6	537.1 ± 13.6	530.9 ± 1.5
At low electron energy (11.6 eV); case 2: with modified k1[e] [f]								
1	900 [d]	1010	15063 ± 199	13.78 ± 0.21	0.021	576.8 ± 7.6	582.6 ± 7.6	536.9 ± 0.8
2	880	1030	14106 ± 166	12.79 ± 0.17	0.021	540.2 ± 6.4	545.9 ± 6.4	536.3 ± 0.4
3	910	1030	13708 ± 467	12.35 ± 0.48	0.020	525.0 ± 17.9	530.6 ± 17.9	537.3 ± 0.7
4	910	1030	13879± 354	12.48 ± 0.36	0.018	531.5 ± 13.6	537.1 ± 13.6	539.2 ± 0.5

[a] Measured I(Te^+) are given in Table 5.2.1. p(Te) = k1· I(Te^+) ·T·k2. k2 for all runs = 0.6952

[b] k1 = 0.0717 for runs 1; 0.070 for run 2; k1 = 0.0716 for runs 3 and 4.

[c] k1 = 0.210 for run 1; 0.2052 for run 2; k1 = 0.2051 for runs 3 and 4.

[d] The lowest temperature point (T = 885 K) was neglected.

[e] k1 = 0.1282 for run 1; 0.1254 for run 2; k1 = 0.1228 for runs 3 and 4 (see text and table 5.2.5 for modified k1).

[f] Recommended p-T relation (see eq. 10) was obtained by treating all p(Te)s from runs 2, 3, and 4 as though they constitute a single run. Recommended $\Delta_r H_m^o$ (298.15 K) was obtained by taking mean of mean second- law value (537.9 ± 24.6) kJ·mol^{-1} and third-law value (537.6 ± 1.8) kJ·mol^{-1} from runs 2, 3, and 4.

Table 5.2.4. Thermal functions used in the present study for all evaluations[a)].

T/K	$RuTe_2$(s)	Ru(s)	Te_2(g)	Te(g)
$[H^o(T) - H^o(298.15\ K)]/(kJ \cdot mol^{-1})$				
298.15	0	0	0	0
800	38.5	13.2	19.9	10.4
900	46.5	16.0	24.2	12.5
1000	54.5	19.0	28.6	14.6
1100	62.7	22.0	33.0	16.8
1200	71.0	25.2	37.5	18.9
1300	79.5	28.4	41.9	21.1
1400	88.1	31.7	46.3	23.3
1500	96.8	35.1	50.7	25.5
$\{-[G^o(T) - H^o(298.15\ K)]/T\}/(J \cdot mol^{-1} \cdot K^{-1})$				
298.15	95.0	28.6	258.8	182.6
800	122.6	37.7	272.6	190.1
900	128.5	39.7	275.6	191.7
1000	134.1	41.7	278.6	193.2
1100	139.4	43.5	281.4	194.6
1200	144.4	45.3	284.0	195.9
1300	149.2	47.0	286.6	197.2
1400	153.8	48.7	289.0	198.4
1500	158.2	50.2	291.3	199.6

[a)] Taken from Reference [7].

all runs. The results given in Table 5.2.3 shows that the values of partial pressures of Te(g), *p*(Te), deduced for different runs at low electron energy are mutually consistent while those deduced at high electron energy are not so, and also are at least three times relatively higher, fragmentation contribution from $Te_2(g)$ being the most plausible reason. Also, the second law value corresponding to measurements at high electron energy were about 65 to 100 $kJ.mol^{-1}$ higher than the third-law value for each run. As for the evaluation corresponding to measurements at low electron energy, one might state that considering the low abundance of Te(g) relative to that of $Te_2(g)$, the agreement between second and third law values is comparatively better in the sense that at least in two runs (runs 3 & 4), it was fairly good and that in run 2, it was only slightly higher while in run 1, the second-law value was too high.

The consistently higher second-law enthalpy for $Te_2(g)$ was very disconcerting to us which made us first to examine whether this discrepancy could have arisen due to an error in temperature measurement. We deduced that to have ~ 30 $kJ{\cdot}mol^{-1}$ higher value as second-law enthalpy, the error in temperature should have been ~ 50 K. The first proof that our temperature measurement is correct within ± 5 K was obtained through heating a few silver pieces inside a Knudsen cell across two temperatures T_1 and T_2 ($T_2 > T_1$) and subsequent visual examination of the residue (upon cooling to ambient temperature) as to whether the residue remained as separate pieces or got transformed to a single globule, the latter happening in case T_2 was above the melting temperature of silver (1235 K). A more concrete proof was obtained when the apparent second-law enthalpy of sublimation of Ag^+, determined periodically during our study of Ru-Te system, agreed well with the known value of enthalpy of sublimation of Ag(g). With the doubt on temperature measurement thus removed, we then performed a critical analysis of the intensities measured over solid silver and over (Ru + $RuTe_2$) samples. It led us to infer that the

higher second-law values over (Ru + $RuTe_2$) might have been caused by the build-up of background in the ion-source region with tellurium vapor species in the case of (Ru + $RuTe_2$), the kind of build-up that was not discernable in the case of silver. The background build-up of tellurium appeared to depend on sample temperature (that is, vapor pressure) and also on time for which the shutter was kept open. For instance, with vaporisation of silver which involved measurements in the temperature range from 1120 to 1220 K, the 'shutter open' counts at 1220 K was 8.6 times that at 1120 K whereas the 'shutter close' counts at 1220 K was only 1.7 times that at 1120 K. On the other hand, with vaporisation of (Ru + $RuTe_2$) which involved measurements in the temperature range from 920 to 1030 K, the 'shutter open' counts at 1030 K was 47 times that at 920 K whereas the 'shutter close' counts at 1030 K was also as high as 40 times that at 920 K. Although it is only the net counts (difference between shutter open and shutter close counts) that are used for partial pressure computations, it is very likely that the build-up of shutter close counts can make the net intensity somewhat underestimated at all temperatures, the effect very likely to be relatively greater at lower temperature than at higher temperature (due to higher signal strength at higher temperature). This could in return affect the second-law enthalpy more than the third-law enthalpy. An empirical equation was sought to be applied to account for this background build-up: corrected net intensity, $[I(Te_2)^+]_c = [I(Te_2)^+]^{0.9}$. Such an equation when applied in the case of run 5, for example, gave $[I(Te_2)^+]_c = 1.5 \cdot [I(Te_2)^+]$ at 1030 K and $[I(Te_2)^+]_c = 2.2 \cdot [I(Te_2)^+]$ at 920 K. Table 5.2.5 gives the results of re-evaluation for $Te_2(g)$. A new set of $k(Te_2)$ values, computed from $[I^o(Te_2)^+]_c=[I^o(Te_2)^+]^{0.9}$ in pressure calibration runs with solid tellurium were used. A comparison of tables 5.2.2 and 5.2.5 reveal that while the $p(Te_2)$ values at T = 975 K remained practically unaltered, the mean third-law values also remaining nearly the same (with reduced standard deviations), the agreement

between second- and third-law values became very good. We seek to recommend values deduced from corrected intensities at low eV. Accordingly, the recommended p-T relation obtained by pooling together all $p(Te_2)$ values from all six runs is:

$$\log [p(Te_2)/Pa] = [-(14335 \pm 148)/(T/K)] + (14.416 \pm 0.154) \quad (5.2.9)$$

The errors quoted for the coefficients are standard deviations. The recommended enthalpy change for the incongruent reaction involving $Te_2(g)$ is (284.3 ± 16.4) kJ·mol^{-1} at T = 298.15 K. It is the mean of 'mean second-law' and 'mean third-law' values from six runs. While the uncertainties in the mean second- and third-law values are standard deviations, that in the recommended value is deduced by error propagation of the two uncertainties.

Having chosen the results at low electron energy for $Te_2(g)$ (despite the fact that the high energy results were also reasonably consistent), the task would be relatively simpler in the case of Te(g) - that only the measurements at low electron energy would need to be considered; and furthermore, unlike for $Te_2(g)$, no correction in I(Te^+) due to background build-up of $Te_2(g)$ in the ion-source would be required, since fragmentation would be negligibly low at low electron energy. The results given in Table 5.2.3 at low electron energy correspond to two cases: one with normal k1 and the other with modified k1. The p(Te) values with normal k1 (Case 1) are slightly higher than those with modified k1 (Case 2), but the discrepancy of this level (a factor of 1.6) is not something considered serious for a minor vapor species. Since for the major vapor species $Te_2(g)$ itself, we chose to recommend the results with modified k1, we would select the case 2 evaluations for Te(g). As for the reaction enthalpies, there is a large discrepancy (≈ 40 kJ·mol^{-1}) between second- and third-law enthalpies for run 1, while for other three runs, the agreement is fairly good. Accordingly, only the results from runs 2 to 4 were considered for obtaining the recommended p-T relation for Te(g) :

Table 5.2.5. Evaluation of $p(Te_2)$ with corrected $I(Te_2^+)$[a] over ($Ru+RuTe_2$). Reaction: $RuTe_2(s) = Ru(s) + Te_2(g)$.

Run No.	Temperature range		Log(p/Pa) = -[A/(T/K)] + B		P/Pa at T = 975 K	$\Delta_r H_m^o(T)$/ (kJ mol^{-1})		
						Second-law		Third-law
	T_1/K	T_2/K	-A	B		at $T_m=(T_1+T_2)/2$	at 298.15 K	at 298.15 K
At high electron energy (29.6 eV or 26.6 eV) [b]								
1	860	1030	14433 ± 124	14.60 ± 0.13	0.63	276.4 ± 2.4	282.9 ± 2.4	279.1 ± 0.1
2	860	1030	14617 ± 125	14.61 ± 0.13	0.42	279.9 ± 2.3	286.4 ± 2.3	282.3 ± 0.2
3	910	1030	15672 ± 333	15.78 ± 0.34	0.51	300.1 ± 6.4	306.5 ± 6.4	280.6 ± 0.4
4	910	1030	14513 ± 386	14.53 ± 0.40	0.44	277.9 ± 7.4	284.3 ± 7.4	281.8 ± 0.3
5	920	1030	14086 ± 271	14.18 ± 0.28	0.54	269.7 ± 5.2	276.1 ± 5.2	280.2 ± 0.2
6	920	1030	14337 ± 286	14.41 ± 0.30	0.51	274.5 ± 5.5	280.9 ± 5.5	280.6 ± 0.2
At low electron energy (11.6 eV)[c] [d]								
1	860	1030	14151 ± 278	14.25 ± 0.30	0.55	271.0 ± 5.3	277.5 ± 5.3	279.9 ± 0.3
2	860	1030	14383 ± 115	14.51 ± 0.13	0.57	275.4 ± 2.2	282.1 ± 2.2	279.8 ± 0.1
3	910	1030	15645 ± 370	15.75 ± 0.38	0.51	299.6 ± 7.1	306.0 ±7.1	280.6 ± 0.4
4	910	1030	15028 ± 344	15.06 ± 0.35	0.44	287.7 ± 6.6	294.1 ± 6.6	281.8 ± 0.3
5	920	1030	14456 ± 198	14.55 ± 0.20	0.53	276.8 ± 3.8	283.2 ± 3.8	280.4 ± 0.2
6	920	1030	14528 ± 227	14.60 ± 0.23	0.50	278.2 ± 4.4	284.5 ± 4.4	280.8 ± 0.2

[a] $[I(Te_2^+)]_c = [I(Te_2^+)]^{0.9}$ and $p(Te_2) = k1 \cdot I(Te_2^+)_c \cdot T$; modified k1, deduced with $[I^o(Te_2^+)]^{0.9}$ used here.

[b] k1 = 0.0490 for run 1; 0.0479 for run 2; 0.0476 for runs 3 and 4; 0.0676 for runs 5 and 6.

[c] k1 = 0.1282 for run 1; 0.1254 for run 2; 0.1228 for runs 3 and 4; 0.0998 for runs 5 and 6.

[d] Recommended p-T relation (see eq. 5.2.9) was obtained by treating all $p(Te_2)$s from all runs as though they constitute a single run. Recommended $\Delta_r H_m^o$ (298.15 K) was obtained by taking mean of mean second-law value (287.9 ± 16.4) kJ·mol^{-1} and third-law value (280.6 ± 0.8) kJ·mol^{-1}.

$$\log [p(\mathrm{Te})/\mathrm{Pa}] = [-(13838 \pm 218)/(T/\mathrm{K})] + (12.480 \pm 0.226) \quad (5.2.10)$$

The errors quoted for the coefficients are standard deviations. The recommended enthalpy change for the incongruent reaction involving Te(g) was deduced to be (537.7 ± 24.7) $kJ \cdot mol^{-1}$ at T = 298.15 K, which is the mean of 'mean second-law' and 'mean third-law' values, once again corresponding to runs 2 to 4. The uncertainty is deduced by error propagation of uncertainties in the mean second- and third-law values, which are standard deviations.

Just for academic interest, we performed the evaluation of $I(Te^+)$ at high electron energy as two additional cases (besides that which is given in Table 5.2.3): a) by subtracting from measured $I(Te^+)$, the fragmentation contribution from $Te_2(g)$ by using $[I^o(Te^+)/I^o(Te_2^+)]$ ratio obtained over elemental tellurium - the correction for fragmentation applies more for monomer than for dimer, because $k(Te_2)$ obtained from calibration run over pure tellurium (where Te^+ is wholly due to fragmentation) inherently takes into account of fragmentation loss for dimer; b) by applying the empirical correction as applied for Te_2^+, that is, by taking $[I(Te)^+]_c=[I(Te)^+]^{0.9}$ – emphasising the fact that the background build-up correction applies for Te^+ at high electron energy, mainly because $Te_2(g)$ being the major species (and causing the build-up), its fragmentation will manifest as background build-up for Te^+ also. As stated already, at low electron energy, due to absence of fragmentation, background build-up does not apply for Te^+. These results are given in Table 5.2.6. If one compares these results with those given in Table 5.2.3, following inferences can be made: 1) although the p(Te) values deduced at high electron energy after fragmentation correction (case 1 in Table 5.2.6) are much lower than the p(Te) values deduced without such a correction and are in accord with those deduced at low electron energy (case 1 in Table 5.2.3), the discrepancy between second- and third-law values remained rather large still; and 2) evaluation with $I(Te^+)_c = [I(Te^+)]^{0.9}$ (case 2 in Table 5.2.6) decreased the

discrepancy between second-and third-law values significantly, but the p(Te) values remained rather very high. We believe that the unusually high [$I^o(Te^+)/I^o(Te_2^+)$] ratios observed over elemental tellurium pressure calibration runs (≈ 0.3 unlike previous measurements of < 0.05) contributed to the whole exercise of the correction procedure (either for fragmentation or for ion-source background build-up) not being so effective or fruitful for Te(g) at high electron energy as was for Te_2(g). It would be useful to restate here that the recommended p-T relations for both Te_2(g) and Te(g) involved the use of modified k(Te_2) at low electron energy, which implies that background build-up was considered for elemental tellurium also. Although the temperature dependence effect was not that readily discernable over elemental tellurium because the temperature range accessed for pressure calibration was very small (30 K), wherever it was discernable, it got decreased by the use of $[I^o(Te_2^+)]_c = [I^o(Te_2^+)]^{0.9}$. As stated already, no build-up of background effect was revealed in our previous studies of M-Te systems [13] or over elemental tellurium [9], as evidenced by consistent observation of a good agreement between second-and third-law enthalpies for elemental tellurium and for the binary systems as well.

The relative mole fraction of Te(g) and Te_2(g) deducible from the recommended p-T relations (equations 5.2.9 and 5.2.10) for these two species are: 0.042 and 0.958, respectively at T = 860 K; and 0.034 and 0.966, respectively at T = 1030 K. That is, the vapor is composed mainly of Te_2(g) and the p(Te)/p(Te_2) ratio is < 0.05. The equilibrium constant, K_p, for the dissociation reaction $Te_2(g) \rightleftharpoons 2\ Te(g)$, as deduced from the present study are in excellent agreement with the values recommended by us in 1994 [14] based on the results of similar KEMS studies on Fe-Te, Cr-Te, Ni-Te, and Mo-Te systems in which the p(Te)/p(Te_2) ratios varied from as low as 0.02 (Fe-Te system) to as high as ~ 1.0 (Cr-Te system). In the two terminal temperatures 860 K and 1030 K, for instance, the K_p values deduced from the p-T relations from

this study are: 1.2 x 10^{-5} Pa and 3.8 x 10^{-3} Pa, respectively; and the corresponding values from our previous paper [14] are: 8.4 x 10^{-6} Pa and 3.8 x 10^{-3} Pa, respectively. This aspect together with reasonably good agreement between second- and third-law enthalpies for the two vaporisation reactions lend reliability to the results recommended in the present study.

To compare our recommended results with those reported for Ru+$RuTe_2$ in previous two studies of Svendsen [5] and Ali Basu et al. [6], we have given in Table 5.2.7 $p(Te_2)$ values at 6 temperatures from 900 to 1400 K, deduced from the *p-T* relations obtained in all three studies. Two sets of values are shown for Svendsen, one (column 2) corresponding to the Σ plot equation reported in the paper and the other (column 3) corresponding to the normal least-squares fit *p-T* relation deduced by us from the $p(Te_2)$s reported in the same paper. The two sets of $p(Te_2)$ data differ by a factor of ~ 200 which prompted us to check the Σ plot equation given by the author, by deducing it ourselves from the basic principle of the Σ plot method [15] and the heat capacity equations given by Svendsen. The discrepancy is traced to a missing constant (10.715) on the right hand side of the equation given in the paper [5], which probably is the typographical error. With this correction done, the discrepancy between the measured $p(Te_2)$ values and the Σ plot equation practically vanished. Table 5.2.7 shows that the $p(Te_2)$ obtained in the present study lies within those obtained in the other two studies, but are very close to that of Ali Basu et al. [6]. For instance, in the temperature range of the study by Ali Basu et al., which envelopes that of the present study, we observe that the $p(Te_2)$ obtained by us is ~ 35 % less than those obtained by Ali Basu et al.; and in the temperature range of the study by Svendsen, which is beyond that of the present study as well Ali Basu et al, we observe that the $p(Te_2)$ obtained by Svendsen [5] is 4 times lower than our values and 5 times lower than Ali Basu et al.s' values. Figure 5.2.3 shows the measured $p(Te_2)$ values of all three studies as a plot of log[$p(Te_2)$] vs. 1/T.

Table 5.2.6 Evaluation of *p*(Te) with corrections applied to measured I(Te^+) over (Ru+$RuTe_2$) at high electron energy of 29.6 eV or 26.6 eV [a]. Reaction: $RuTe_2(s) \rightleftharpoons Ru(s) + 2Te(g)$.

Run No.	Temperature Range		log(*p*/Pa) = -[A/(*T*/K)] + B		P/Pa at *T* = 975 K	$\Delta_r H_m^o(T)$/ (kJ mol^{-1})		
	T_1/K	T_2/K	-A	B		Second-law		Third-law
						at $T_m = (T_1+T_2)/2$	at 298.15 K	at 298.15 K
Case 1: $[I(Te^+)]_c = \{[I(Te^+)] - k_{fc} \cdot [I(Te_2^+)]\}$ [b) c)]								
1	900	1010	14936 ± 193	13.963 ± 0.20	0.044	572.0 ± 7.4	577.7 ±7.4	525.5 ± 0.8
2	880	1030	12621 ± 417	11.363 ± 0.44	0.026	483.3 ± 16.0	489.1 ± 16.0	532.0 ± 1.1
3	910	1030	10748 ± 672	9.715 ± 0.69	0.049	411.6 ± 25.7	417.3 ± 25.7	522.4 ± 1.8
4	910	1030	15088 ±784	14.130 ±0.81	0.045	577.8 ± 30.0	583.5 ± 30.0	523.9 ± 1.5
Case 2: $[I(Te^+)]_c = \{[I(Te^+)]^{0.9}\}$ [d)]								
1	900	1010	14386 ± 137	14.01 ±0.14	0.18	550.9 ± 5.2	556.7 ± 5.2	502.8 ± 0.8
2	880	1030	13534 ±93	12.95 ±0.10	0.12	518.3 ± 3.6	524.1 ±3.6	508.6 ± 0.3
3	910	1030	13349 ±351	12.95 ± 0.36	0.18	511.2 ± 13.4	516.8 ± 13.4	501.2 ± 0.6
4	910	1030	14202 ± 356	13.77 ±0.37	0.16	543.9 ±13.6	549.5 ± 13.6	503.6 ±0.9

[a] $p(Te) = k1 \cdot [I(Te^+)]_c \cdot T \cdot k2$; k2 for all runs = 0.6952. Correction applied for fragmentation (case 1) and for ion-source background build-up (case 2).

[b] Normal k1:0.0717 for run 1; 0.070 for run 2; 0.0716 for runs 3 and 4.

[c] $k_{fc} = [I(Te^+)/ I(Te_2^+)]$ over elemental tellurium pressure calibration runs. $k_{fc} = 0.255$ for runs 1 and 2; $k_{fc} = 0.311$ for runs 3 and 4.

[d] Modified k1: 0.0490 for run 1; 0.0479 for run 2; 0.0476 for runs 3 and 4.

Table 5.2.7 Comparison of [p(Te$_2$)/Pa] over (Ru + RuTe$_2$)[a].

T/K	Svendsen [5]		Ali Basu et al. [6]	This work
	From the eq. given in the reference[b]	From the eq. deduced by us[c] using p(Te$_2$)	From the eq. given in the refrence[d]	Eq. (5.2.9)
900	1.69 x 10^{-5}	4.44 x 10^{-3}	3.86 x 10^{-2}	3.01 x 10^{-2}
1000	8.54 x 10^{-4}	2.11 x 10^{-1}	1.55	1.21
1100	2.09 x 10^{-2}	4.96	3.18 x 10^{1}	2.42 x 10^{1}
1200	2.98 x 10^{-1}	6.91 x 10^{1}	3.94 x 10^{2}	2.95 x 10^{2}
1300	2.80	6.41 x 10^{2}	3.31 x 10^{3}	2.45 x 10^{3}
1400	1.89 x 10^{1}	4.32 x 10^{3}	2.06 x 10^{4}	1.50 x 10^{4}

[a] Svendsen: 1276 to 1422 K; Ali Basu et al.: 831 to 1148 K; This work: 860 to 1030 K.

[b] $[(\Delta H_I/T) - I] = -1.9872 \ln\{p(Te_2)/atm.\} - 10.715 \ln(T/K) + 1.2469 \times 10^{-2} (T/K)$

$- 0.1398 \times 10^{-3} (T/K)^{3/2} + 121589 (K/T)^2$.

$\Delta H_I = (75127 \pm 581)$ cal$_{th}$ mol^{-1} and $I = (104.029 \pm 0.428)$ cal$_{th}$ K^{-1} mol^{-1}.

[c] $\log (p/Pa) = - [15091/(T/K)] + 14.415$

[d] $\ln (p/Pa) = - [33231.2/(T/K)] + 33.67$

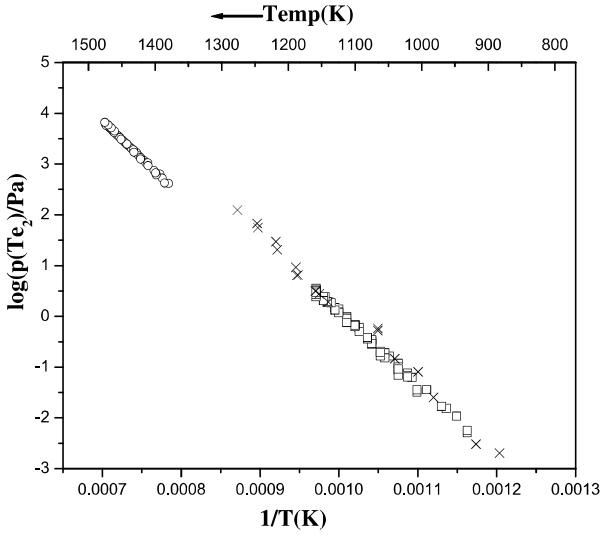

Fig.5.2.3. Comparison of p(Te_2) over (Ru + $RuTe_2$) : (□) Present work; (o) Svendsen [5]; (×) Ali Basu et al. [6].

In order to show how the third-law values varied with temperature in different modes of evaluation, results from run 2 was selected, and given in table 5.2.8. For the principal vaporisation reaction, $RuTe_2(s) \rightleftharpoons Ru(s) + Te_2(g)$, four cases were chosen, while for the vaporisation reaction involving the minor species Te(g) and for the homogeneous reaction involving dissociation of $Te_2(g)$, three cases were chosen. For the vaporisation reaction involving $Te_2(g)$, when no correction was applied in $I(Te_2^+)$, there is a clear temperature dependence at both high and low electron energy. When the correction according to the empirical equation $[I(Te_2^+)]_c = [I(Te_2^+)]^{0.9}$ and modified $k(Te_2)$ were employed, the temperature dependence practically vanished. Results of a least squares analysis, performed according to $\Delta_r H°(298.15) = A*T + B$ revealed some interesting features. While the values of slope (A) represent temperature dependence behaviour of third-law values, the values of intercept are all close to the

Table 5.2.8 Third-law enthalpies for reactions $RuTe_2(s) \rightleftharpoons Ru(s) + 2/i\ Te_i(g)$ (i = 2 or 1) and $Te_2(g) \rightleftharpoons 2\ Te(g)$ at different temperatures for run 2.

T/K	$RuTe_2(s) \rightleftharpoons Ru(s) + Te_2(g)$				$RuTe_2(s) \rightleftharpoons Ru(s) + 2Te(g)$			$Te_2(g) \rightleftharpoons 2Te(g)$		
	1[a]	2[b]	3[c]	4[d]	1[a]	2[b]	3[e]	1[a]	2[b]	3[f]
	III law $\Delta_rH°(298.15)$/kJ· mol^{-1}				III law $\Delta_rH°(298.15)$/kJ· mol^{-1}			III law $\Delta_rH°(298.15)$/kJ· mol^{-1}		
860	287.4	284.9	282.8	280.6	-	-	-	-	-	-
880	286.1	283.0	282.1	279.4	518.6	529.8	537.0	232.4	246.7	257.6
900	285.4	282.3	282.1	279.3	517.5	528.5	535.8	232.0	246.2	256.5
920	285.3	282.1	282.5	279.7	515.4	530.0	537.6	230.1	247.9	257.9
940	284.7	281.4	282.4	279.6	515.0	529.0	536.7	230.3	247.5	257.1
960	284.6	281.3	282.9	279.9	513.9	528.5	536.4	229.2	247.2	256.4
960	283.8	281.3	282.2	279.9	512.5	528.5	536.4	228.7	247.2	256.4
980	283.9	280.9	282.8	280.2	512.8	530.1	538.1	228.9	249.2	258.0
1000	281.6	279.4	281.3	279.3	510.6	528.0	536.2	228.9	248.6	256.9
1018	281.8	279.2	281.9	279.6	508.7	527.5	535.8	227.0	248.3	256.2
1030	281.4	278.8	281.9	279.6	507.4	525.9	534.4	225.9	247.1	254.7
Mean III	284.2±1.9	281.3±1.8	282.3±0.5	279.7±0.4	513.2±3.6	528.6±1.3	536.4±1.0	229.4±2.0	247.6±0.9	256.8±1.0
LS fit[g]	$\Delta_rH°(298.15) = A·T + B$				$\Delta_rH°(298.15) = A·T + B$			$\Delta_rH°(298.15) = A·T + B$		
A	− 0.034	−0.031	−0.004	−0.002	−0.072	−0.018	−0.010	−0.039	0.010	−0.011
B	316.3	310.9	286.0	281.2	581.9	546.0	546.0	266.3	238.3	267.6
R^2	0.94	0.94	0.21	0.05	0.97	0.50	0.23	0.91	0.29	0.35

[a] $[I(Te_i]^+$ (i = 2 or 1) and normal k1 at high electron energy (E1) used.

[b] $[I(Te_i]^+$ (i = 2 or 1) and normal k1 at low electron energy (E2) used.

[c] $[I(Te_2^+]^{0.9}$ and modified k1 at high electron energy (E1) used.

[d] $[I(Te_2^+]^{0.9}$ and modified k1 at low electron energy (E2) used.

[e] $[I(Te)^+]$ and modified k1 at low electron energy (E2) used.

[f] $[I(Te_2^+]^{0.9}$ and $[I(Te)^+]$, and modified k1 at low electron energy (E2) used.

g) Least-squares analysis according to III law $\Delta_r H°(298.15) = A*T + B$ along with R^2

second-law values. A low value of slope and a low value of R^2 for the case 4 can be taken to support the validity of the approach adopted by us to obtain recommended p-T relation and $\Delta_r H°(298.15)$ value. Similarly, for the vaporisation reaction involving Te(g), results shown for case 3, accord support to our recommendations. That for the dissociation of $Te_2(g)$ also, it is the case 3 that gave the best results in terms of low slope and R^2, while both second- and third-law values are in reasonable agreement with the known value [14] gave additional support to our methodology. Table 5.2.9 compares the thermodynamic properties pertinent to incongruent vaporisation of $RuTe_2(s)$ and also those to formation of this phase, obtained in this study with those reported previously. The value of $[\Delta_r H_m^o\ (298.15\ K)]$ for the incongruent vaporisation reaction equation (5.2.5) (i=2), deduced from the results of Svendsen [5] or attributed to the author by Cordfunke and Konings [7] is slightly on the higher side compared to that obtained in this study or by Ali Basu et al. [6]. Consequent to this is the reason for the value of $[\Delta_f H_m^o\ (298.15\ K)]$ of $RuTe_2(s)$ by Svendsen being higher, too. However, if one considers the uncertainties associated with the results from the three vaporisation studies, each of different type, all results seem to have some consistency. In Table 5.2.9, we chose to give $\Delta_f S_m^o\ (298.15\ K)$ values, although Svendsen [5] as well as Ali Basu et al. [6] reported only $S_m^o\ (298.15\ K)$ values for $RuTe_2(s)$, and so did Cordfunke and Konings [7] and Mills [17]. The value of $[S_m^o\ (298.15\ K)]/(J{\cdot}mol^{-1}{\cdot}K^{-1})$ deducible from the present study is 87.2 ± 10.4, while those reported previously are: 89.5 ± 2.5 [6], 90.5 ±7.0 [7], and those selected in the two assessments are:100.4 ± 12.6 [17], 95.0 ± 2.5 [8].

A useful method of comparing the vapor pressures data from different studies is that suggested by Paule and Mandel [18]. This method is similar to the sigma method [15] in that it will yield $\Delta_f H_m^o\ (298.15\ K)$ as slope, but an intercept which should be zero for an ideal case if both measured $p(Te_2)$ values and the thermal functions, $\Delta_r\{-[G^o(T) - H^o(298.15\ K)]/T\}$, are accurate.

The following equation was employed to evaluate $p(Te_2)$ values obtained in the present study and in the

Table 5.2.9 Thermodynamic properties pertinent to vaporisation or formation of $RuTe_2$(s).

Reference	Method	$\Delta_r H^o_m$(298.15 K)/ (kJ·mol^{-1})	$\Delta_r S^o_m$(298.15 K)/ (J·mol^{-1}·K^{-1})	Remarks
Reaction 1: Incongruent vaporisation to Te_2(g): $RuTe_2$(s) ⇌ Ru(s) + Te_2(g)				
This work	KEMS	287.9 ± 16.4	200.2 ± 10.4	Mean of second-law values from six runs. The uncertainties are standard deviations.
		280.6 ± 0.8		Mean of third-law values from six runs.
		284.3 ± 16.4	200.2 ± 10.4	Recommended values in the present study.
Svendsen [5]	Silica spiral gauge	299.9 ± 2.4	197.2 ± 1.8	Deduced by us from the basic equations of the Σ plot .
		288.9 ± 12.4[a)]	180.2 ± 1.7[a)]	From the normal least-squares fit *p*-T relation deduced by us.
		306.9 ± 2.5		Calculated by Cordfunke and Konings [7] .
Ali Basu et al.[6]	mass-loss Knudsen effusion	276.3 ± 6.0 [b)]	183.8 ± 6.0 [b)]	Second-law values reported in the paper. $\Delta_r S^o_m$(298.15 K) deduced by us from $\Delta_r S^o_m(T_m)$.
		283.2 ± 7.0	196.9 ± 6.0	
		278.6 ± 4.0		Third-law value reported in the paper.
Reaction 2: Incongruent vaporisation to Te(g): $RuTe_2$(s) ⇌ Ru(s) + 2 Te(g)				
This work	KEMS	537.9 ± 24.6	155.0 ± 4.3	Mean of second-law values from three runs.
		537.6 ± 1.8	-	Mean of third-law values from three runs.
		537.7 ± 24.7	155.0 ± 4.3	Recommended values in the present study.
Reaction 3: Formation from the constituent elements: Ru(s) + 2 Te(s) ⇌ $RuTe_2$(s)				
This work	KEMS	– (121.1 ± 16.4)	– (39.8 ± 10.4)	Deduced from the recommended values for reaction 1 and the literature values[c)] for Te_2(g) [7,16].
Svendsen [5]	Silica spiral gauge	– (136.7 ± 2.4)	– (36.8 ± 1.8)	Deduced by us from the Σ plot values for reaction 1 and the literature values[c)] for Te_2(g) [7,16]. The value reported by the author [5] for $\Delta_f H^o_m$: – (140.2 ± 2.9) kJ·mol^{-1}
Ali Basu et al.[6]	mass-loss Knudsen effusion	– (120.0 ± 8.0)	– (36.5 ± 6.0)	Deduced by us from the second-law values for reaction 1 and the literature values[c)] for Te_2(g) [7,16].
Mills [17]	Estimation	– (108.8 ± 25.1)		Estimated from the selected values for RuS_2 and $RuSe_2$ and other Group VIII chalcogenides [17]
Cordfunke and Konings [7].	Calculation	– (141.7 ± 2.6)		Calculated from $\Delta_r H^o_m$(298.15 K) for reaction 1 and by combining with the selected value for Te_2(g) [7].

[a)] at T_m = 1349 K, the mean temperature range of measurements.

[b)] at T_m = 990 K, the mean temperature range of measurements.

[c)] $\Delta_f H^o_m$(Te_2(g), 298.15 K) = (163.2 ± 0.5) kJ·mol^{-1} [16]; $\Delta_f S^o_m$(Te_2(g) 298.15 K) = 160.4 J·mol^{-1}·K^{-1}, computed from S^o_m(298.15 K) values given in reference [8] for Te_2(g) (258.8 J·mol^{-1}·K^{-1}) and Te(s) (49.2 J·mol^{-1}·K^{-1}

previous two studies by Svendsen [5] and Ali Basu et al. [6]:

$$\Delta_r\{-[G^o(T) - H^o(298.15\ K)]/T\} - \{R \ln [(p/Pa)/(101325\ Pa)]\} = \{[\Delta_r H_m^o(298.15\ K)]/T\} + B \quad (5.2.11)$$

Table 5.2.10 gives the results of such an evaluation. It confirms the good agreement for the values of $\Delta_r H_m^o$ (298.15 K) obtained in the present study and that by Ali Basu et al. As for the intercept, the value is the lowest for the present study and the highest for that by Ali Basu et al. [6], though.

Table 5.2.10. Vapor pressure evaluation by a second-law method which employs the Gibbs free energy functions (eq. 5.2.11).

Reference	Method	Temperature Range/ K	No. of points	Slope = $\Delta_r H^o_m$(298.15 K)/ (kJ·mol^{-1})	Intercept
Present work	KEMS	860 to 1030	58	280.7 ± 2.8	– (0.0002 ± 0.002)
Svendson [6]	Silica Spiral gauge	1276 to 1422	40	298.5 ± 2.4	– (0.003 ± 0.002)
Ali Basu et al.[7]	Mass-loss Knudsen effusion	831 to 1148	19	282.0 ± 6.7	– (0.004 ± 0.007)

5.2.3.3. Composition range of existence of $RuTe_2$

In the evaluation of reaction enthalpies, it was assumed that the composition of $RuTe_2$ phase in equilibrium with Ru(s) is stoichiometric, that is, the Ru-rich boundary is of composition 66.67 at.% Te. Having measured the homogeneity ranges of many telluride phases previously in our lab [13], we have performed similar vaporisation experiments which essentially involved measurement of $I(Te_2^+)$ all along, with aliquots of samples corresponding to ($RuTe_2$ + Te) and of known composition and mass. At the end of the experiment, we weighed the Knudsen cell again to deduce the total mass-loss, Δm_{total}. Since vaporisation from the Knudsen effusion cell resulted in continuous loss of tellurium as $Te_2(g)$, by making use of Hertz-Knudsen effusion equation and the basic KEMS equation, we first deduced the calibration constant $C_{H\text{-}K}$ through which Δm_{total} is related to the total area under the $I(Te_2^+)T^{0.5}$ vs. time, t curve:

$$(\Delta m)_t = C_{H\text{-}K} \{\Sigma [I(Te_2^+)T^{0.5}]_t * \Delta t\}. \quad (5.2.12)$$

This equation is same as 2.27 ($\Delta w_i = A_i\, k_i'\, a_0\, C\, (M_i/(2\pi R))^{0.5}$) given in chapter 2.

$k_i'\, a_0\, C\, (M_i/(2\pi R))^{0.5}$ and A_i in the equation (2.27) corresponds to $C_{H\text{-}K}$ and $\{\Sigma\ [I(Te_2^+)T^{0.5}]_t * \Delta t\}$ in equation 5.2.12, respectively.

Subsequently, by using the $C_{H\text{-}K}$ so deduced, Δm up to any desired time t was deduced, and in turn the sample composition also at that time of the experiment. Application of phase rule provides the basis of assigning these compositions to the time up to which the elemental tellurium was present as a coexisting phase as well as to the time from which the elemental ruthenium was present as a coexisting phase with $RuTe_2$. These two compositions respectively are the phase boundaries of the single phase $RuTe_2$. Figure 5.2.4 shows the plot of $\log[I(Te_2^+)\cdot T^{0.5}]$ vs. time corresponding to one of the four experiments, while Table 5.2.11 gives the phase boundary compositions deduced in all four experiments.

Figure 5.2.4 reveals that while the cross over from ($RuTe_2$+Te) into $RuTe_2$ was effected at 635 K, that from $RuTe_2$ into (Ru + $RuTe_2$) was effected at 980 K. This was because as long as the sample composition corresponded to that of ($RuTe_2$+Te) two phase region, $p(Te_2)$ was high and constant, but once excess tellurium was exhausted off and the sample was single phase $RuTe_2$, the $p(Te_2)$ would decrease monotonically with time at each temperature to so low values that one cannot visualize effecting the cross over to (Ru + $RuTe_2$) in reasonable time. Therefore, temperatures were regularly increased. The value of $p(Te_2)$ at 980 K was nearly the same as at 635 K. Once it was confirmed that the sample indeed was a two-phase mixture (by the constancy of $p(Te_2)$ or $I(Te_2^+)\cdot T$ with time), decrease or increase in temperatures were made to ascertain that the corresponding changes in $p(Te_2)$ were in accord with those deducible from the recommended $p(Te_2)$-T relation for (Ru + $RuTe_2$). In the inset of figure 5.2.4, it is shown that a temperature cycle imposed on the sample after it exited the $RuTe_2$ single phase region revealed that $I(Te_2^+)$ at 980 K was consistent in both decreasing (from 1000 K) or increasing (from 960 K) temperature directions. Thus these experiments in addition to yielding

phase boundaries also served to confirm our $p(Te_2)$ values obtained over the samples S1 and S2 as indicated in Fig 5.2.3.

Table 5.2.11 shows that the values of the Te-rich boundary compositions given in this table appear to indicate a trend - the more Te-rich the initial compositions are, the more Te-rich are the deduced Te-rich boundary compositions for the $RuTe_2$ phase. While the reason for this is not clear, observation of this kind of trend might raise a doubt as to whether the homogeneity range of $RuTe_2$ could be even smaller than that

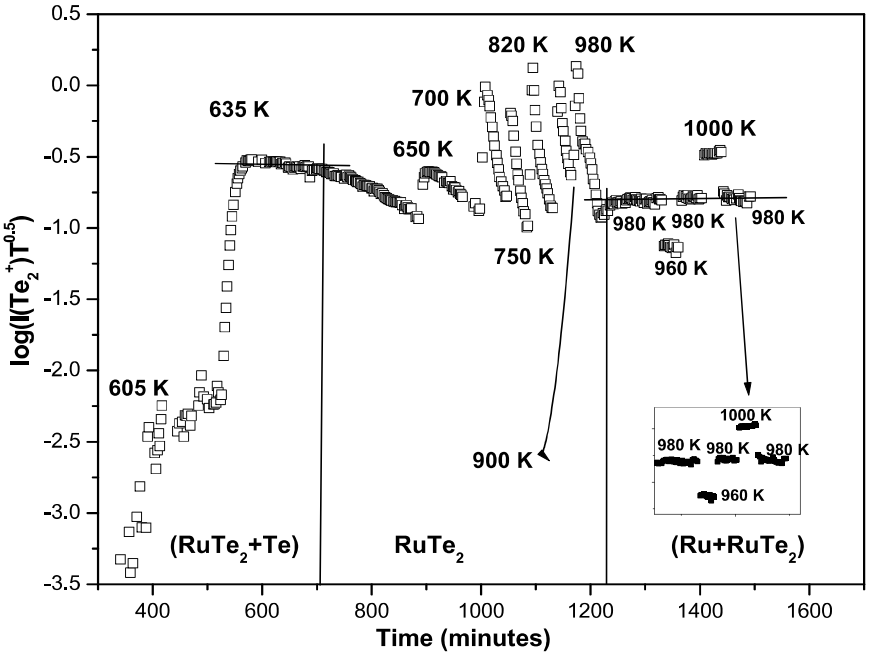

Fig.5.2.4. Variation of $\log[I(Te_2^+)\cdot T^{0.5}]$ with time as the condensed phase initially in the two phase field ($RuTe_2$ + Te) traversed across the single-phase region of $RuTe_2$ to finally reach another two-phase field (Ru + $RuTe_2$).

Table 5.2.11. Salient results from the $RuTe_2$-homogeneity range experiments

Run	*T*/K	Te-rich boundary (at. % Te)	*T*/K	Ru-rich boundary (at.% Te)
S3: Starting composition: 69.50 at. % Te				
1	650	68.71	980	66.57
2	635	68.84	980	66.71
S4: Starting composition: 71.50 at. % Te				
3	635	70.46	980	66.24
4	635	70.17	980	67.08

obtained from S3, if, for instance, the starting composition were to be of even less tellurium content than S3. Such a doubt especially is valid since in no previous study [3,8] was the width reported as large as that obtained in the present study (≥ 2.1 at. % Te). However, being aware that unless we obtain a clear evidence for the sample having been in ($RuTe_2$+Te) -by an observation of the constancy of $I(Te_2^+)$ for reasonable time, delineating the Te-rich boundary of $RuTe_2$ would involve great uncertainty, we did not plan similar experiments with samples containing relatively lower tellurium percentage than S3. Thus, with the uncertainty looming large on the value of Te-rich boundary, we would give credence only to the Ru-rich boundary values which did not show any particular trend with the starting composition. Furthermore, since the mean value, (66.65 ± 0.37) at. %Te, from the four experiments corresponds to the nominal formula of (2.00 ± 0.03), the results from experiments with S1 and S2 evaluated by using the formula $RuTe_2$ did not require modification which would have been necessary if the Ru-rich boundary composition was to be significantly different.

5.2.4. Conclusion

Knudsen effusion mass spectrometric study of the Ru-Te binary system was conducted for the first time. The direct confirmation of incongruent vaporisation of $RuTe_2$ was obtained - primarily to $Te_2(g)$ and to a very small extent to Te(g), the relative compositions of the two

species in conformity with our previous studies on other M-Te binary systems. The *p-T* relations were determined in the temperature range of 860 to 1030 K, and thermodynamic quantities for the vaporisation reactions and as well as the formation of $RuTe_2(s)$ were deduced. The Ru-rich phase boundary was confirmed to be essentially the stoichiometric composition.

References

[1]. M. G. Adamson, E. A. Aitken, T. B. Lindemer, J. Nucl. Mater. 130 (1985) 375.

[2]. E. H. P. Cordfunke, R. J. M. Konings, E. F. Westrum, Jr., J. Nucl. Mater. 167 (1989) 205.

[3]. S. Bernath, H. Kleykamp, W. Smykatz-Kloss, J. Nucl. Mater. 209 (1994) 128-131.

[4]. H. Hokamoto, J. Phase Equilibria 16 (1995) 535-536.

[5]. S. R. Svendsen, J. Chem. Thermodyn. 9 (1977) 789-800.

[6]. M. Ali Basu, A. N. Shirsat, R. Mishra, A. S. Kerkar, S. C. Kumar, S. R. Bharadwaj, D. Das, J. Alloys Comp. 352 (2003) 140-142.

[7]. E. H. P. Cordfunke, R. J. M. Konings (Eds.) Thermochemical Data for Reactor Materials and Fission Products, North Holland, Amsterdam, 1990, p.324-325.

[8]. H. Zhao, H. W. Schils, Ch.J. Raub, J. Less-Common Metals 113 (1985) 75-82.

[9]. R.Viswanathan,Ph.D Thesis, University of Madras, 1991.

[10]. R. Viswanathan, M. Sai Baba, D. Darwin Albert Raj, R. Balasubramanian, C.K. Mathews, A High Temperature Mass Spectrometric Study of Tellurium and Selenium Clusters in: Advances in Mass Spectrometry, Ed. J.F.J. Todd, John Wiley & Sons., 10 (1985) 1087-1088.

[11]. W. Rosinger, M. Grade, W. Hirshwald, Ber. Bunsenges. Phys. Chem. 87 (1983) 536-542.

[12]. IUPAC Technical report, Pure Appl. Chem. 74 (2002) 1987-2017.

[13]. T.S. Lakshmi Narasimhan, R. Viswanathan, Knudsen effusion mass spectrometric study

of some congruently and incongruently vaporizing systems, in: Workshop on Knudsen Effusion Mass Spectrometry (KEMS) April 23–25, 2012, Juelich. Proceedings published in ECS Transactions. 46 (1) (2013) 229. Please also see: The Open Thermodynamics Journal 7 (2013) (Suppl 1:M3) 10–20 and the references therein.

[14]. R. Viswanathan, M. Sai Baba, D. Darwin Albert Raj, R. Balasubramanian, T. S. Lakshmi Narasimhan, C. K. Mathews, Spectrochim. Acta 49B (1994) 243-250.

[15]. K. K. Kelley, Contributions to the Data on Theoretical Metallurgy XV, Bulletin 601, Burea of Mines, A Reprint of Bulletins 383, 384, 393, and 406, United States Government Printing Office, Washington, 1962. p3 of Bulletin 383 (III. The Free Energies of Vaporisation and Vapor Pressures of Inorganic Substances).

[16]. F. Gronvold, J. Drowart, E. F. Westrum, Jr., The Chemical Thermodynamics of Actinide Elements and Compounds. Part 4. The Actinide Chalcogenides (Excluding Oxides), IAEA, Vienna, 1989.

[17]. K. C. Mills, Thermodynamic Data for Inorganic Sulphides, Selenides and Tellurides. Butterworths, London, 1974.

[18]. R. C. Paule, J. Mandel, Analysis of Interlaboratory Measurements on the Vapor Pressures Of Cadmium and Silver, NBS Special Publication, 1971, pp. 221-260.

CHAPTER 6

Summary

The Knudsen effusion mass spectrometry (KEMS) (also known as High temperature mass spectrometry [HTMS]) was the basis of this thesis. The preliminary experiments on pure elements and an oxide system was conducted using the KEMS facility housed inside an inert atmosphere glove box but under 'box-open' conditions. Vaporisation studies on U-Ga and U-Pu-Zr systems were carried out using KEMS inside the Ar atmosphere glove box whereas the vaporisation studies on Ru-Te was performed employing the High temperature mass spectrometer equipped with 90° magnetic sector. The enthalpy increment measurements on U_3Ga_5(s) were carried out using the inverse drop calorimeter.

The KEMS equipped with QMS as the mass analyser was housed inside the glove box to take up the high temperature vaporisation studies on plutonium based systems. Such systems require an inert atmosphere (Argon gas) glove box with the impurities such as moisture and oxygen maintained at less than 10 ppm. The experiments on pure elements (Nickel and Chromium) were carried out with the glove box kept open with the following three objectives: 1. To know the sensitivity of the KEMS i.e., the lowest pressure that can be measured. 2. To examine whether the second law enthalpies of sublimation of the ionic species deduced by using experimental facility are in agreement with the literature values or not. 3. To examine its capability to give the temperature independent pressure calibration constants. The enthalpies of sublimation obtained with chromium and nickel were found to be in agreement with the literature values and the pressures as low as 3.1 $x10^{-4}$ Pa at 1384 (Ni) and $3.4x10^{-4}$ Pa at 1287 K (Cr) could be measured. These studies confirmed that this KEMS facility is completely suitable for vaprisation and mass spectrometric studies.

The vaporisation studies on pure Zr helped to realise the high temperature capability of the electron bombardment furnace. The temperature as high as ~ 2250 K could be attained and maintained by the furnace. Further, the vaporisation studies on MnO(g) was taken up to gain an experience in using the instrument to investigate the oxide system. Following which, vaporisation studies on U and U-Zr were carried out to have some KEMS studies on theses alloys before taking up the studies on U-Pu-Zr alloy. All the above experiments were performed under glove box open condition.

Subsequently, the box was closed with glass panels and full arm gauntlets. All the gas inlets and outlets were fitted with HEPA filters. All the filters were tested for the trap efficiency by producing aerosol particles and counting them before and after the filters. The efficiency was found to be ≥ 99.9% for particles of 3 micron size and the glove box was certified to be fit for handling radioactivity. The leak tightness of the glove box was tested at a differential pressure of 100 mm water column negative with respect to the ambient and the leak rate was found to be less than the prescribed limit of < 0.05 vol% of the box volume per hour. The box was flushed with argon gas to convert the atmosphere into inert type. The impurities (moisture and oxygen) in the gas is being maintained at less than 10 ppm by circulating Ar through the purification tower packed with molecular sieves and copper deoxo catalyst. The vaporisation studies on U-Ga and U-Pu-Zr systems were performed in the certified glove box.

Thermodynamic properties of U-Ga intermetallic compounds are important to understand the reduction of actinide tri-chlorides left over in spent chloride molten salt, resulting from the electrorefining operation. Intermetallic compounds of uranium and gallium may be formed when uranuium chlorides in spent molten a salt is equilibrated with the liquid Ca-Ga alloy. Calcium reduces uranium chlorides into uranium whereas gallium combines with uranium to form

intermetallic compounds and pushes the reduction process in the forward direction. In this regard, the Gibbs energies of formation of U_3Ga_5 and UGa_3 were obtained in the present study by carrying out vaporisation studies on (U_3Ga_5+UGa_2) and (UGa_2+UGa_3) two phase regions using the KEMS facility inside the glove box. Ga(g) was identified to be the neutral species. The vaporisation studies on these two phase regions were carried out in the temperature range 1208-1366 K and 1133-1338 K. The measured gallium vapour pressures were used to derive the Gibbs energies of formation of U_3Ga_5 and UGa_3. The data for U_3Ga_5 was determined for the first time.

There are no heat capacity data for all the U-Ga compounds. Hence, the high temperature data of U_3Ga_5 and UGa_3 could not be converted to the reference temperature (298 K). In the present study, yet another experiment was carried out to measure the enthalpy increment measurements on U_3Ga_5 using the method of inverse drop calorimetry in the temperature range 793-1323 K. The enthalpy of formation of this compound at 298 K was derived using the data obtained KEMS and the enthalpy increments measured.

Alloy of U-19 wt%Pu-6 wt%Zr is the proposed fuel for the future Indian fast breeder reactors. Hence, vaporisation studies on this composition were conducted in (solid+liquid) and liquid regions using HTMS inside the glove box in the temperature range 1481-1623 K and 1661-1773 K, respectively. Pu(g) and PuO(g) were ascertained to be the neutral species in the vapour phase over the sample. Vapour pressure of plutonium over this alloy will be useful in the preparation of alloy and to understand its behaviour during the irradiation and the radioactivity release in case of severe nuclear reactor accident.

Tellurium is a volatile and reactive fission product. Thermodynamic information on binary systems of tellurium is of practical importance - to gain an understanding of the chemical interaction of tellurium with the fuel-cladding or with the fellow fission products. Ruthenium is

an important fission product with significant fission yield for nuclear reactor safety studies. In the present study, the vaporisation studies on Ru-Te system was taken up to get the thermodynamic data of $RuTe_2$. These data will be useful in predicting the release behaviour of tellurium in case of nuclear reactor accident. Partial pressures of Te_2 and Te over the compositions ($Ru+RuTe_2$) were determined by employing a VG micromass 30 BK Knudsen effusion mass spectrometer equipped with 90° magnetic sector. The pressure temperature relations of $Te_2(g)$ were used to derive the enthalpy of formation of $RuTe_2$ at 298 K. Tellurium rich and ruthenium rich phase boundaries of $RuTe_2$ were obtained.

CHAPTER 7

Scope for further work

High temperature vaporisation studies on U-Pu-Zr of different compositions can be carried out to generate the vapour pressure data. For U-Pu system, no vapour pressure data has been reported in the literature. This binary alloy is considered as a potential fuel for the mechanically bonded pin configuration, as the breeding ratio for this fuel will be much better than the sodium bonded U-Pu-Zr alloy fuel. Hence, the KEMS measurements on different compositions of this U-Pu system will be very vital. These data are of importance to nuclear field for fuel fabrication as well as to understand the fuel behaviour during irradiation under normal and off-normal conditions. The enthalpy increment measurements on UGa_2 and UGa_3 are not available in the literature. These data can be determined by employing the inverse drop calorimeter.